



# University of HUDDERSFIELD

## University of Huddersfield Repository

Motara, Hasina

Isothermal Titration Calorimetric Studies of Complexation Reactions

### Original Citation

Motara, Hasina (2011) Isothermal Titration Calorimetric Studies of Complexation Reactions. Doctoral thesis, University of Huddersfield.

This version is available at <http://eprints.hud.ac.uk/id/eprint/10779/>

The University Repository is a digital collection of the research output of the University, available on Open Access. Copyright and Moral Rights for the items on this site are retained by the individual author and/or other copyright owners. Users may access full items free of charge; copies of full text items generally can be reproduced, displayed or performed and given to third parties in any format or medium for personal research or study, educational or not-for-profit purposes without prior permission or charge, provided:

- The authors, title and full bibliographic details is credited in any copy;
- A hyperlink and/or URL is included for the original metadata page; and
- The content is not changed in any way.

For more information, including our policy and submission procedure, please contact the Repository Team at: [E.mailbox@hud.ac.uk](mailto:E.mailbox@hud.ac.uk).

<http://eprints.hud.ac.uk/>

# Isothermal Titration Calorimetric Studies of Complexation Reactions

By

Hasina Motara

February 2011



*University of*  
**HUDDERSFIELD**

The University of Huddersfield  
Department of Chemical and Biological Sciences

A thesis submitted to the University of Huddersfield in partial  
fulfilment of the requirements for the degree of Doctor of  
Philosophy

## Abstract

The objective of this work has been to study the binding of metal ions to complex ligands expressing two or more metal binding sites, in terms of the thermodynamics of the binding events, and to use this information to contribute to the understanding of both the metal binding processes and the properties of the metal/ligand complexes. Two ligands have formed the basis of the study, one a naturally occurring enzyme and the other a newly synthesised ligand with two distinct binding sites (to form supramolecular complexes). The principle technique used to determine thermodynamic parameters has been isothermal titration calorimetry (ITC).

The first system studied involved the enzyme  $\beta$ -lactamase II from *Bacillus cereus* 569/H/9 (BcII). The binding of zinc (II), cobalt (II) and cadmium (II) was investigated in aqueous solution at pH's from 5.2 to 7.2. By using three or more buffers at each pH it has been possible to determine not only the binding constants of the metal ions at these pH's but also the molar enthalpies of binding (and hence molar entropies). In addition, the dissociation of hydrogen ions from the enzyme on metal binding was also observed. In the case of all three metal ions, one metal ion per enzyme appears to bind at low pH and two metal ions at high pH (within the pH 5.20-7.20 range). In the case of zinc and cobalt ions two metal ions seem to bind per mole of enzyme in a cooperative mechanism. In contrast two cadmium ions appear to bind to the active sites of the enzyme non-cooperatively. For all three metal ions, models have been developed to describe the two binding sites and the sources of H<sup>+</sup> ions that dissociate on metal ion binding.

The second system studied involved the supramolecular synthesised ligand bipy-aza-crown-4. This ligand has two metal binding sites, one at the 2,2'-bipyridine and the other at the aza-crown-4. The objective was to compare the way copper (II) binds in acetonitrile solution with the way in which the copper (II) complex with this ligand is crystallised from methanol solution with

progressively increased copper (II) concentration, as revealed by single crystal x-ray diffraction.

Smaller ligands that represent the two individual complexation regions of the synthesised ligand were also used for comparison. Both ITC and solution spectroscopic measurements were used to compare the binding model that was proposed in methanol solution. It was demonstrated in acetonitrile solution that copper (II) binds to the 2,2-bipyridine site first in a 1:2 ( $\text{Cu}^{2+}:\text{L}$ ) ratio, then binds to the aza-crown site in a 1:1 ( $\text{Cu}^{2+}:\text{L}$ ) ratio. So it was demonstrated that the overall stoichiometric ratio of copper ion to bipy-aza-crown-4 in the fully formed complex is 3:2 ( $\text{Cu}^{2+}:\text{L}$ ). Possibly the main conclusion drawn is that the order in which the binding sites are occupied in acetonitrile solution is different to that in which they are occupied in methanol.

## Acknowledgments

At first, I would like to express my sincere gratitude to my supervisors; Prof Robert Brown and Prof Michael Page, without whom I would not have started on this journey and for their constant guidance and encouragement during the course of this research and the considerable contribution towards this project. Rob, a special thanks to you for all the help and advice and dealing with me especially, during the difficult times.

I would like to thank Dr Craig Rice and Dr Cara Sutton for supplying the supramolecular ligands for me to work with and for sharing useful suggestions on supramolecular chemistry and the valuable knowledge on the ligand.

I would also like to thank Dr Adriana Badarau, for her help in the beginning of the BcII work with the production of the BcII enzyme and also thank you so much for replying to the numerous emails from me.

Thank you to all the technicians from University of Huddersfield but special thanks goes Felix who was always there to give me help when required.

At last, but no way means the least, I would like to thank my Husband, Moosa, with his patience and support over this last year. A special thanks goes to my family (my brothers and sister), Mum and Dad what can I say. Without you I don't think I would be here where I am now, you have given me all the support and encouragement and provided me with everything, you are the best parents.

# Table of Contents

Overall Objective of the Project.....	1
<b>Chapter 1: Thermodynamics and Calorimetry.....</b>	<b>1</b>
1.1-Introduction .....	2
1.1.1- Laws of Thermodynamics .....	2
1.1.1.1 - First Law of Thermodynamics.....	2
1.1.1.2 - Second Law of Thermodynamics.....	5
1.1.2 - Enthalpic and Entropic Properties from Isothermal Titration Calorimetry.....	7
1.1.2.1 - Significance of $\Delta H_m^0$ .....	7
1.1.2.2 - Significance of $\Delta S_m^0$ .....	7
1.1.3 - Calorimetry .....	8
1.1.3.1 - Isothermal Titration Calorimetry (ITC).....	8
1.1.3.2 - Power Compensation Calorimeter .....	9
1.1.4 - Isothermal Titration Calorimeter.....	10
1.1.5 - C- Values and Curve Shapes .....	14
1.1.6 - ITC Calibration.....	15
1.1.7 - Heat of Dilution .....	16
1.2- References .....	17
<b>Chapter 2 : Metallo-<math>\beta</math>-lactamase .....</b>	<b>18</b>
2.1 - Introduction .....	19
2.1.1- Bacteria and Antibiotics .....	19
2.1.1.1 - The Mode of Action of $\beta$ -lactam Antibiotics.....	21
2.1.1.2 - Bacteria Cell Wall Structure and Synthesis.....	21
2.1.1.3 - Peptidoglycan .....	23
2.1.2 - $\beta$ -lactamases .....	27
2.1.3 - Serine $\beta$ -lactamases .....	29
2.1.4 - Class B $\beta$ -lactamases .....	31
2.1.5 – BclI from Bacillus Cereus 569/H/9 Metallo- $\beta$ -lactamase .....	33
2.1.6 - Crystal Structure of Metallo- $\beta$ -lactamases .....	35
2.1.7 - Zinc Coordination to Metallo- $\beta$ -lactamases.....	37

2.1.8 Role of Zinc ion in Metallo- $\beta$ -lactamases .....	38
2.1.9 – Mechanisms for Metallo- $\beta$ -lactamases.....	40
2.1.10 – Different Metal ions Used to Bind the Active Sites of Metallo- $\beta$ - lactamases.....	43
2.1.11 - Research Aims .....	46
2.2 - Metallo- $\beta$ -lactamase - Experimental .....	47
2.2.1 - Enzyme Preparation .....	47
2.2.1.1 - Materials .....	47
2.2.1.2 - Instrumentation .....	48
2.2.2 – Production of Competent Cells .....	49
2.2.3 - Production of BcII .....	50
2.2.4 - Isolation and Purification of <i>Bacillus Cereus</i> 569/H/9 (BcII) Metallo- $\beta$ - lactamase. ....	51
2.2.4.1 - Isolation .....	51
2.2.4.2 - Purification .....	51
2.2.4.3 - General Procedure to Determine the Enzyme Concentration .....	53
2.2.4.4 - Determination of Enzyme Activity Towards Hydrolysis of Benzylpenicillin .....	53
2.2.4.5 - Determination of Rate Constant.....	54
2.2.4.6 - Removal of Zinc ion from ZnBcII by Dialysis.....	54
2.2.4.7 - Determination of Zinc Concentration in ApoBcII and Buffers .....	55
2.2.4.8 - Determination of EDTA Concentration in ApoBcII .....	55
2.2.5 - Settings for Isothermal Titrations .....	58
2.2.6 - Estimation of Experimental Error .....	59
2.3: Results.....	18
2.3.1 - Part One: Zinc ion Titrated into ApoBcII.....	60
2.3.1.1 - Dissociation of Acid Groups on BcII when Zinc ion Binds.....	80
2.3.2 - Part two: Cobalt ion Titrated into ApoBcII .....	85
2.3.2.1 - Dissociation of Acid Groups on BcII when Cobalt ion Binds ....	100
2.3.3 - Part Three: Cadmium ion Titrated into ApoBcII .....	106
2.3.3.1 - Dissociation of Acid Groups on BcII when Cobalt ion Binds ....	113
2.4 - Discussion .....	118
2.4.1 - Amino Acids.....	118
2.4.2 - Ionisation and Binding of Metal ions to Ligands.....	119

2.4.3 - Number of Metal ions Bound .....	122
2.4.4 - Buffer Effect .....	129
2.4.5 - Binding Constants.....	130
2.4.6 - Enthalpies and Entropies of Binding .....	134
2.4.7 - Number of Protons Released.....	136
2.4.8 - Possible Models to Explain Metal ion Binding Results.....	141
2.5 - Conclusion .....	148
2.6 - References .....	150
<b>Chapter 3 : Supramolecular Complexes .....</b>	<b>158</b>
3.1 - Introduction .....	159
3.1.1 - Supramolecular Chemistry.....	159
3.1.2 - Host and Guest Chemistry .....	160
3.1.3 - Binding: Chelate and Macrocyclic Effects .....	161
3.1.4 - Selectivity of Metal ions Binding to Ligands .....	162
3.1.5 - Allosteric Effects .....	163
3.1.6 - Crown Ethers .....	164
3.1.7 - Aza-Crown Ethers.....	167
3.1.8 - Single Crystal X-ray Diffraction Results.....	169
3.1.9 - Objective of this Work .....	174
3.2 - Experimental.....	175
3.2.1 – Instrumentation .....	175
3.2.2 - Solutions for ITC .....	175
3.2.3 - ITC Setting.....	176
3.2.4 - UV-Vis Analysis .....	177
3.2.5 – Electron Spin Resonance (ESR).....	177
3.2.6 - Synthesis of Ligand: Bipy-aza-crown-4.....	178
3.3 - Results and Discussion.....	179
3.3.1 - Copper ion Binding to Bipy-aza-crown-4.....	179
3.3.2 - Experimental Errors for the Data .....	180
3.3.3 - Titrations: Copper ion into Ligands .....	181
3.3.3.1 - Copper ion Binding to 2,2-bipyridine (bipy) .....	181
3.3.3.2 - Copper ion Binding to 3,3'-diamino-2,2'-bipyridine (diaminobipy) .....	184

3.3.3.3 - Copper ion Binding to 1, 4, 8, 11-tetraazacyclodecane (aza-crown-4).....	186
3.3.3.4 - Copper ion Binding to Fused 2,2'-bipyridine aza-crown-4 (bipy-aza-crown-4).....	189
3.3.4 – UV-Vis Spectral Analysis .....	193
3.3.4.1 - Spectral Titration of Copper ion into Bipy-aza-crown-4.....	193
3.3.5 - Electron Spin Resonance (ESR).....	203
3.4 - Conclusion.....	208
3.5 - References .....	210
<b>Chapter 4 - .....</b>	<b>213</b>
Overall Conclusions .....	213
Future Work.....	216
Appendix.....	217

## Abbreviations

Ala	Alanine
Asn	Asparagine
ATP	Adenosine triphosphate
Bipy	2,2-bipyridine
Cacodylate	Dimethylarsinic acid
Conf	Conformation
Cys	Cysteine
EDTA	Ethylenediaminetetraacetic acid
Enz	Enzyme
Equivs	Equivalents
ESR	Electron Spin Resonance
EXAFS	Extended X-ray Absorption Fine Structure
FPLC	Fast Protein Liquid Chromatography
Glu	Glutamic acid
HEPES	N-[2-hydroxyethyl]piperazine-N'-[2-ethane sulfonic acid]
His	Histidine
Int	Intrinsic
ion	Ionisation
ITC	Isothermal Titration Calorimetry
$K_b$	Binding Constant
$K_d$	Dissociation Constant
$K_a$	Association Constant
LMCT	Ligand to Metal Charge Transfer
MeCN	Acetonitrile
MES	2-[N-morpholino]ethanesulfonic acid
MOPS	3-[N-morpholino]propanesulfonic acid
N	Molar Ratio of Metal to Enzyme/ligand (stoichiometric ratio)
n	Number of Protons Released
NAG	N-acetylmuramic acid
NAM	N-acetyl-D-glucosamine
NMR	Nuclear Magnetic Resonance
NQI	Nuclear Quadrupole Interaction

obs	Observed
PAC	Perturbed Angular Correlation
PIPES	Piperazine-N,N'-bis[2-ethanesulfonic acid]
TEAP	Tetraethyl-ammonium Perchlorate
Sec/S	seconds
UV-Vis	Ultra-Violet Visible
$\Delta H$	Change in Enthalpy
$\Delta H^\circ$	Molar Change in Enthalpy
$\Delta H^\circ_m$	Enthalpy of Reaction
$\Delta S$	Change in Entropy
$\Delta S^\circ$	Molar Change in Entropy
$\Delta G$	Change in Gibbs Free Energy
$\Delta G^\circ$	Molar change in Gibbs Free energy
$^\circ\text{C}$	Degrees Celsius
$\mu\text{cal}$	Micro-calories

## **Overall Objective of the Project**

The project is a study of the energetics of the binding of metal ions to chelating ligands. Two types of ligands have been studied. The first are enzymes in which metal ions are naturally present and so require them to be removed to enable the binding process to be studied. The second are synthetic ligands, often with more than one binding site, which may be informative mimics of the enzymatic system. The objective of the work has been to characterise the thermodynamics of these binding events (stoichiometries, binding constants, enthalpies and entropies) as a way of contributing to the understanding of the mechanisms of metal ion binding to enzymes and other ligands, and the structures of the resultant complexes.

# **Chapter 1**

# **Thermodynamics and Calorimetry**

## 1.1-Introduction

### 1.1.1- Laws of Thermodynamics

#### 1.1.1.1 - First Law of Thermodynamics

The First Law of Thermodynamics states that energy cannot be destroyed or created but it can be converted from one form into another. Therefore this law is equivalent to the law of conservation of energy.

Firstly, it is helpful to consider a system and its surroundings. The energy of a system is usually defined as its internal energy  $U$ , and the First Law states that the internal energy of a system can only be changed if heat is added or removed or work done on or by the system.

This is summarised in equation 1:

$$\Delta U = q + w \qquad \text{Equation 1}$$

where  $\Delta U$  is the change in internal energy,  $q$  is the heat absorbed by the system from the surrounding and  $w$  is the work done on the system.

We are only going to consider pressure/volume work when a chemical change takes place in a system. The pressure/volume work done is generally very small unless a gas is produced or consumed. In each case (Equation 2):

$$w = - P\Delta V \qquad \text{Equation 2}$$

## Chapter 1.1 – Thermodynamics and Calorimetry - Introduction

where  $P$  is the pressure in the system (taken as constant) and  $\Delta V$  is the change in volume of the system.

$$\text{So} \quad \Delta U = q - P\Delta V \quad \text{Equation 3}$$

If there is no change in volume, then no work is done (Equation 4) and:

$$\Delta U = q \quad \text{Equation 4}$$

The heat added,  $q$ , is relatively easy to measure so, when there is no change in volume,  $\Delta U$  can quite easily be determined.

However, if  $P/V$  work is done, then  $q$  does not equal  $\Delta U$ . To help in dealing with this situation, a second state function is defined called the enthalpy  $H$  (Equation 5).

$$H = PV + U \quad \text{Equation 5}$$

The change in enthalpy is (Equation 6):

$$\Delta H = \Delta (PV) + \Delta U \quad \text{Equation 6}$$

or

$$\Delta H = P\Delta V + V\Delta P + \Delta U.$$

If pressure/volume work is done but pressure is constant, then (Equation 7):

$$\Delta H = P\Delta V + \Delta U \quad \text{Equation 7}$$

And so, by substitution of equation 3:

$$\Delta H = P\Delta V + q - P\Delta V .$$

Therefore:

$$\Delta H = q. \qquad \text{Equation 8}$$

Since measuring  $q$ , the heat changes associated with a process, is precisely what is done in a calorimeter, the basic information gathered from the calorimetric measurement for a process when the pressure of the system is held constant is  $\Delta H$ .

### 1.1.1.2 - Second Law of Thermodynamics

The Second Law of Thermodynamics introduces entropy where in one form states that the entropy of a system and its surroundings increases through any spontaneous process,<sup>1</sup> or more strictly:

$$\Delta S_{\text{uni}} \geq 0.$$

If a reaction is then spontaneous according to the Second law of thermodynamics, the  $\Delta S_{\text{uni}}$  must then increase. This change in entropy can be made of two segments, the entropy change of the system and the entropy change of the surroundings (Equation 9), and so for a spontaneous process:

$$\Delta S_{\text{uni}} = \Delta S_{\text{sys}} + \Delta S_{\text{surr}} \quad \text{Equation 9}$$

Both the entropy changes of the system and the surroundings are required to determine if a reaction is spontaneous or not and, conversely, a spontaneous process can only occur if the total entropy change (system plus surroundings) is positive.

Whether or not a process is spontaneous can be described in terms of properties of the system only, if we define a new term, the Gibbs Free Energy  $G$  (Equation 10), this is defined as:

$$G = H - TS \quad \text{Equation 10}$$

All the terms in Equation 10 refer only to the system under study. The spontaneous nature of a reaction is determined from Equation 11. When any process is at constant pressure and temperature, the change in Gibbs free energy of the system is:

$$\Delta G = \Delta H - T\Delta S \quad \text{Equation 11}$$

and under standard conditions:

$$\Delta G^{\circ} = \Delta H^{\circ} - T\Delta S^{\circ} \quad \text{Equation 12}$$

The equilibrium constant for a reaction is related to  $\Delta G^\circ$  as follows:

$$\Delta G^\circ = -RT \ln K \quad \text{Equation 13}$$

If  $\Delta G^\circ$  is negative, the reaction or process is spontaneous, whereas if  $\Delta G^\circ$  is positive the reaction occurs spontaneously in the opposite direction. Shown below in **Table 1.1** is how  $\Delta H$  and  $\Delta S$  work together to give spontaneous and non-spontaneous reactions.<sup>2</sup>

**Table 1.1** - shows how  $\Delta H$  and  $\Delta S$  can vary together for a reaction to give a net free energy change.<sup>2</sup>

$\Delta H$	$\Delta S$	$\Delta G = \Delta H - T\Delta S$
<b>Negative</b>	<b>Positive</b>	Both enthalpically (exothermic) and entropically favoured. Spontaneous at all temperatures
<b>Negative</b>	<b>Negative</b>	Enthalpically favoured but entropically unfavourable. The reaction is spontaneous only at temperatures below $T = \Delta H/\Delta S$
<b>Positive</b>	<b>Negative</b>	Enthalpically unfavourable (endothermic) and entropically unfavourable.
<b>Positive</b>	<b>Positive</b>	This reaction is enthalpically unfavourable and entropically favourable. So only occurs when $T > \Delta H/\Delta S$ .

## 1.1.2 - Enthalpic and Entropic Properties from Isothermal Titration Calorimetry

The heat output from a typical isothermal titration calorimetry experiment when a titrant (in our case a solution of a metal ion) is added to a solution of a chelating ligand (or chelating enzyme) provides directly a binding constant (equilibrium constant) for the reaction between metal ion and ligand and the molar enthalpy of the binding reaction  $\Delta H^\circ$ . From these,  $\Delta G^\circ$  and then  $\Delta S^\circ$  can be directly calculated, as will be explained later.

### 1.1.2.1 - Significance of $\Delta H^\circ_{rn}$

The molar enthalpy of reaction will broadly reflect the strength of the metal-ligand interactions relative to those interactions which are lost when binding occurs (between metal ion and solvent for example). In the particular case of metal ions introduced to metal-binding enzymes, other bond making and bond breaking events can occur. For example, it is possible that metal binding to a ligand changes the  $pK_a$  of one or more protons on an enzyme and that the metal binding event is accompanied by proton loss or gain. There may also be ligand conformational changes that accompany metal binding.<sup>3</sup> The overall heat measured is a combination of all these processes.

### 1.1.2.2 - Significance of $\Delta S^\circ_{rn}$

Entropy changes measured for binding of a metal to a ligand or enzyme can be determined from the output of an isothermal titration calorimetry experiment. They can give useful information on the binding reaction taking place. The entropy changes may be due to quite complex combinations of events: solvation, desolvation, conformational changes, reduction and increase in modes of translational freedom through changes in the number of individual particles in solution.<sup>3-5</sup>

### 1.1.3 - Calorimetry

There are several types of calorimeter. The calorimeter that has been used for this research is a power compensation calorimeter.

#### 1.1.3.1 - Isothermal Titration Calorimetry (ITC)

Isothermal titration calorimetry is titration calorimetry performed at constant temp.<sup>6</sup> The instrument used for the research is a VP-ITC from Microcal (**Figure 1.1**). The ITC technique provides the thermodynamic parameters from a single experiment: the enthalpy ( $\Delta H^\circ$ ), the reaction stoichiometry (N), the binding constant ( $K_b$ ), and hence the entropy changes ( $\Delta S^\circ$ ).

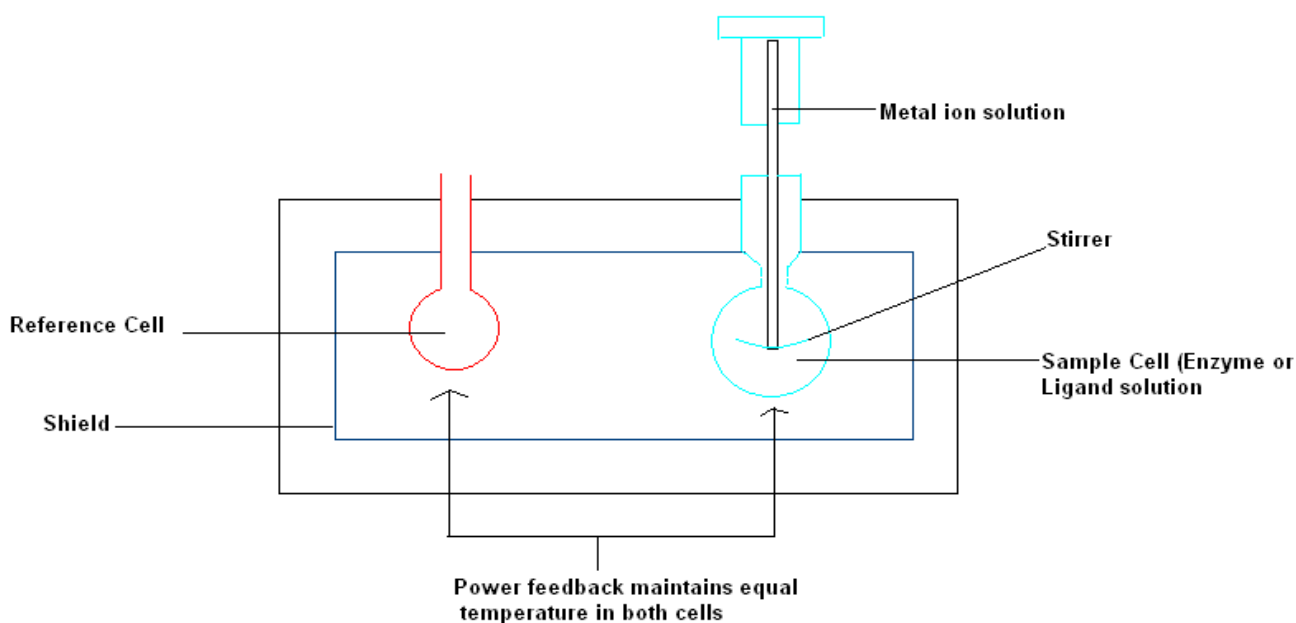


**Figure 1.1:** The Sample and Reference cell in a VP-ITC

### 1.1.3.2 - Power Compensation Calorimeter

The main principle of ITC is to monitor the enthalpy change associated with a chemical event brought about by titrating one solution into another. The VP-ITC measures the heat absorbed or released.

There are two cells, a sample cell and a reference cell. The ligand or enzyme solution is loaded into the sample cell and the reference cell is loaded with water or solvent and these cells initially are at a much lower temperature to the titration temperature and heat is provided to the cells to maintain the temperature of reaction. The metal ion solution is titrated into the ligand solution (or enzyme) in small aliquots and the heat released or observed on addition of each aliquot ( $q$ ) is monitored over a period of time.

ITC has a feedback mechanism where it measures the heat released or absorbed by the sample cell. During the titration, temperature difference between the reference and the sample cell is monitored and power is supplied to both cells to maintain a constant temperature difference. Any change in the temperature difference between sample and reference cells results in either more or less power being added to the sample cell,<sup>6</sup> and it is the power that is needed to maintain this that is recorded when you collect the signal. Exothermic reactions will only allow a small decrease in the feedback power, whereas endothermic reactions will produce an increased power feedback.

Both cells are in contact with a large thermal reservoir so, after a thermal event accompanying addition of titrant, the power required to maintain the steady temperature difference quickly returns to its previous value. The ITC output is essentially the power/ time plot for the sample cell.

### 1.1.4 - Isothermal Titration Calorimeter

The ITC instrument output is in the form of a power versus time plot. This appears as positive or negative peaks, each one corresponding to addition of an aliquot of titrant, and the direction of the peaks depend on whether the process occurring in the cell is exothermic or endothermic (the calorimetric output in **Figure 1.2** is exothermic). After calibration the power/time plot is integrated and the heat ( $q$ ) values are then plotted against time, and then re-plotted against the molar ratio of added titrant (usually the metal ion) to the ligand or enzyme in the cell. This plot typically takes the form shown in **Figure 1.2**.

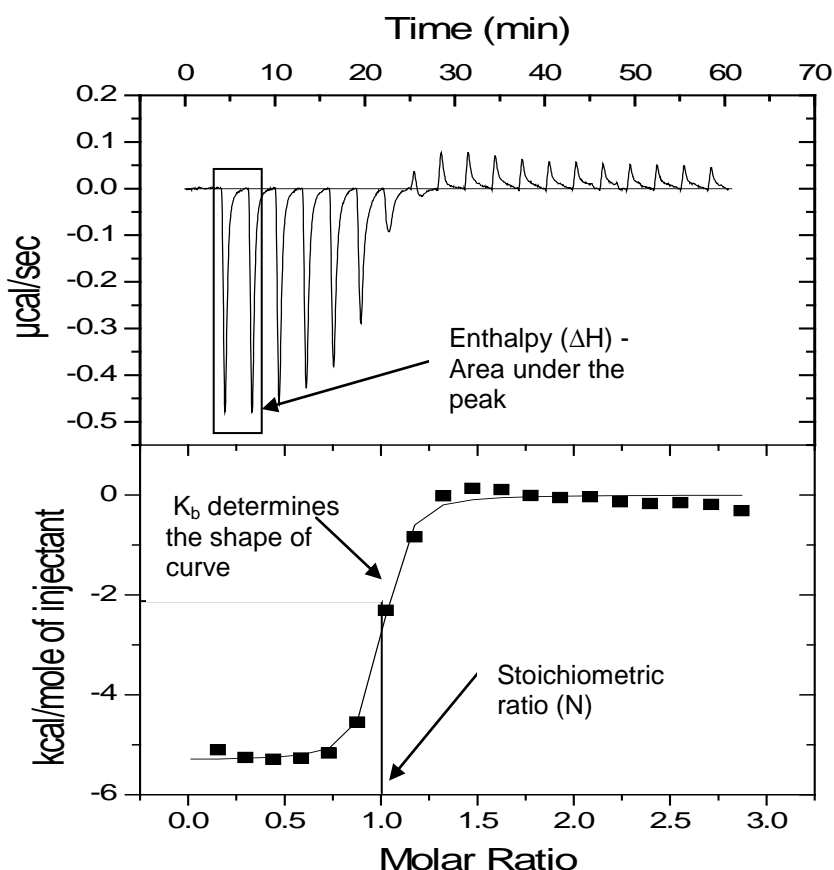


**Figure 1.2:** A typical calorimetric output from an ITC titration experiment for an exothermic reaction.

The second plot is a typical differential molar enthalpy output shown as a function of the amount of titrant added. In the early stages all the titrant added in each aliquot reacts with the ligand in the cell so the heat output is relatively high. As the end point or equilibrium point of the titration is approached, the amount of titrant from each aliquot that reacts falls (controlled by the equilibrium constant of the reaction). Beyond the end point the extent of reaction falls further, eventually to zero or to heat of dilution which is assumed to be constant through the titration.

Roughly speaking, the molar enthalpy of the reaction can be judged from the first points in the titration. The stoichiometry of the reaction is determined from the position of the equivalence point. The binding constant controls the shape of the curve, the greater the  $K_b$  (depending on Equation 14), the steeper the drop in the plot as the equivalence point is passed.

The position of the equilibrium in Equation 14 is defined by the equilibrium constant  $K_b$ . This is then calculated as shown below as the concentration of the product is divided by the reactants.



$$K_b = \frac{[ML]}{[M][L]}$$

Equation 14

So to calculate the binding constant and the other parameters from the ITC titration data involves simulating the data generated using Origin version 7 software to simulate the resultant enthalpy / extent of reaction to determine the molar enthalpy of reaction ( $\Delta H^\circ$ ), the ratio of metal ion to ligand (N) at the equivalence point and the binding constant for the reaction between metal ion and ligand ( $K_b$ ). From the  $K_b$ ,  $\Delta G^\circ$  is calculated and, knowing the reaction temperature,  $\Delta S^\circ$  (molar entropy of reaction) is also calculated.<sup>7-9</sup>

For every injection in the titration, either heat is absorbed or released and this is proportional to the change in concentration of bound metal ion, so this is expressed as:

$$q = V \cdot \Delta H^{\circ} \cdot \Delta[M]_{\text{bound}}$$

Where  $V$  is the volume of reaction and  $\Delta H^{\circ}$  is the observed enthalpy of binding. The cumulative heat  $Q$  is then expressed in terms of the total metal ion concentration  $[M]_t$  to give Equation 16 which is used to perform the simulation, in this equation,  $E$  is the enzyme or ligand and  $M$  is the metal ion.

$$\frac{dQ}{d[M]_t} = \frac{\Delta H^{\circ} V^{\circ}}{2} \left[ 1 + \frac{1 - [M]_t/[E]_t - N/K_b[E]_t}{(1 + [M]_t/[E]_t + K_b[E]_t)^2 - 4[M]_t/[E]_t} \right]$$

**Equation 16.<sup>9</sup>**

The  $[M]_t$  and  $[E]_t$  are the concentration of metal ion and ligand (or enzyme) solution.<sup>9</sup>  $V^{\circ}$  is the active volume of solution in the calorimetric cell, and  $dQ/d[M]_t$  is the differential heat output on addition of metal ion.  $\Delta H^{\circ}$  and  $K_b$  are determined from the simulation of the  $dQ/d[M]_t$  versus molar ratio plot.

Equation 16 uses the data obtained from the titration by plotting and fitting with an incremental heat signal which is the first derivative of heat with respect to the total concentration of metal ion bound to ligand, is plotted against the molar ratio, which yields a sigmoidal titration curve. The titration curve produced is a plot of differential heat output on addition of metal ion versus the molar ratio of metal ion added to the ligand.

The enthalpy ( $\Delta H^{\circ}$ ) tends to influence the intercept on the y-axis (**Figure 1.2**) and the stoichiometry ( $N$ ) controls the position of the inflection point.  $K_b$  is determined from the overall shape of the curve.

It turns out that the shape of the titration curve, and the sharpness of the inflection at the equivalence point can be shown to depend on a newly defined

parameter, the Wiseman c-parameter:<sup>7, 10, 11</sup> Wiseman isotherm relates to the stepwise change in heat of the system with respect to the number of moles of titrant added per injection to the ratio of metal ion to ligand concentration at a given point during the titration. The importance of this is that the precision with which a titration curve can be simulated depends on the value of c.

$$c = N [E] K_b.$$

A high value of c can result from a high concentration of enzyme/ligand and/or a high value of  $K_b$ . Typical curves showing the influence of values of  $K_b$  are shown in **Figure 1.3**.

**Note** the cell has an active cell volume of 1.4 ml. This is the volume of the coin shaped cell that is inside the thermal core. To access the cell, there is a stem that needs to be filled with the sample as well. The stem volume is 0.4 ml, so the actual sample volume needed is 1.8 ml. Where the stem and the overflow compartment meet on top, there is a ledge where the filling syringe should be positioned when taking off the excess. The same applies for the reference cell. The ledge has a function of ensuring that the sample and the reference cell have the same amount of liquid in order to match the heat capacity.

The volume needs to be at least 1.8 ml as this is also considered when analyzing the data and the dilution of the ligand injected and the cell material expelled. The volume of measurement is constant but as the injections proceed, liquid is expelled.

### 1.1.5 - C- Values and Curve Shapes

Curves are shown in **Figure 1.3**, for c-values between 0.1 and 500.<sup>7</sup>

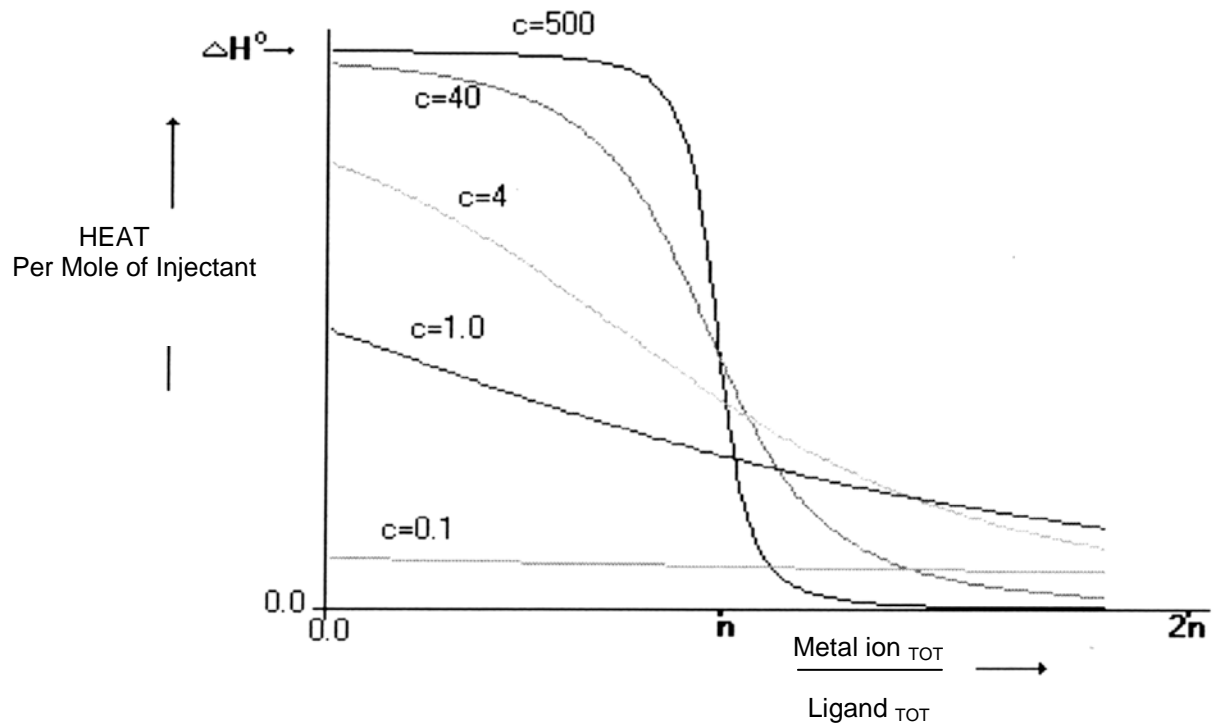


**Figure 1.3:** C-values curve.<sup>7</sup>

In general, for c-values between 10 and 50, good simulation is possible but for c-values 1-5 and 100-1000 the binding constant is harder to simulate precisely. Therefore, in ITC, the concentration of ligand or enzyme in the cell should be chosen, if possible, so that the c-value falls in the range where simulation is most precise.

### **1.1.6 - ITC Calibration**

The calorimeter has to be calibrated regularly to convert the electrical signal to power output. The calorimeter was calibrated electrically using an internal heater every month. A chemical calibration, based on a titration of aqueous barium chloride into 18-crown-6 solution, was carried out every year.<sup>12</sup>

Electrical calibration was performed where both the syringe and the sample cell were filled with degassed water and a known power was achieved through an electrical heater in the cell. Each pulse was 1  $\mu\text{cal}/\text{sec}$  power for 300 sec, the instrument specification requires that the percentage error on measuring the energy on electrical calibration should be less than 1%.

### 1.1.7 - Heat of Dilution

The ITC data from a titration can require some correction before simulation. The most common factor that has to be corrected for is the additional heat either released or absorbed as a result of the dilution of the titrant and the analyte as the titrant is added.

The heat of dilution has to be subtracted from each peak in the heat versus time plot. This can be done in a variety of ways. The simplest way to do this is to measure the heat output for aliquots of titrant added well after the end point and to make the assumption that these heats are due to dilution only. The heats of dilution can then be subtracted from all the peaks in the titration. This has been the approach used in the work reported in this thesis.

A more rigorous determination of the contributions due to dilution can be determined by separately determining the heats associated with:

- Solvent into solvent
- Metal ion solution into solvent
- Solvent into ligand or enzyme solution

Firstly the addition of solvent into solvent blank is performed to see if there is any interaction between the solvents that may occur in the reaction.

Then the metal ion solution is added to the solvent and the solvent added to the ligand solution are performed to measure heats of dilution of these components to check the change in heat is uniform throughout the whole titration. In this work reported here, it was established that this level of correction of heats of dilution was not necessary.

## 1.2- References

1. Atkins, P.W., Depaula, J.J. Atkins' Physical Chemistry. Oxford University Press (UK), 8<sup>th</sup> ed. **2006**, pg 81-83.
2. Voet, Voet, Pratt. Fundamentals of Biochemistry. John Wiley & sons Ltd. (UK). **1999**.
3. Ladbury, S.E. *Biotechniques*, **2004**, 37, 885-887.
4. Holdgate, G., Fisher, G., Ward, W. In Biocalorimetry 2 Ladbury, J.E., Doyle, M.L., Eds. John Wiley, Chicester, **2004**, 59-79.
5. Wadso, I., Isothermal Microcalorimetry for the characterisation of interactions between drugs and biological materials, *Thermochimica Acta*, **1995**, 267, 45-59.
6. Wadso, I., Goldberg, R.N. Standards in Isothermal Microcalorimetry: IUPAC Technical Report. *Pure. Appl. Chem*, **2001**, 73, No 10, 1625-1639.
7. Harding, S.E. and Chowdry, B. Protein-Protein Ligand Interactions: Hydrodynamics and Calorimetry. Oxford University Press, **2000**.
8. Wiseman, T., Williston, S., Brandts, J.F. and Lin, L.N. Rapid Measurements of Binding Constants and Heats of Binding using a new Titration Calorimetry, *Anal. Biochem*, **1989**, 179, 131-137.
9. Indyk, L., Fisher, H.F. Theoretical Aspects of Isothermal Titration Calorimetry, *Methods. Enzy*, **1998**, 295, 350-365.
10. Pierce, M., Raman, C.S. and Nall, B.T. Isothermal Titration Calorimetry of Protein-Protein Interactions. *Methods. Enzy*, **1999**, 19, 213-221.
11. Turnball, W.B. and Daranas, A.H. On the value of C: Can Low Affinity System is studied by Isothermal Titration Calorimetry, *J.Am.Chem.Soc*, **2003**, 125, 14859-14866.
12. Gherrau, A., Buschmann, H.J. and Schollmeyer, E. Complex Formation of Crown Ethers and Cryptands with Ba<sup>2+</sup> in the Biphasic System Chloroform/water Studied by Titration Calorimetry, *Thermochimica Acta*, **2005**, 425, 1-5.

# Chapter 2:

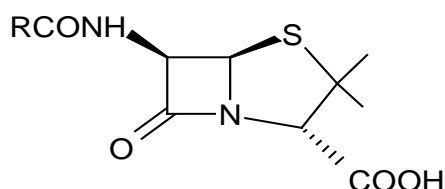
# Metallo- $\beta$ -lactamase

## 2.1 –Introduction

### 2.1.1- Bacteria and Antibiotics

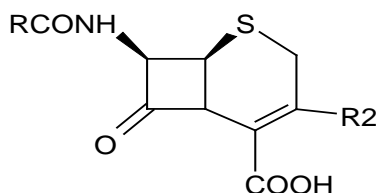
Antibiotics are substances produced by microorganisms such as bacteria or fungi, which are released from cells to harm or kill other microorganisms. Therefore antibiotics are used by bacteria and fungi to kill or inhibit the growth of other microorganisms.

The first antibiotic discovered was penicillin (**Scheme 2.1**) in 1929 by Sir Alexander Fleming. He observed the inhibition of *Staphylococci* on an agar plate contaminated with penicillium mould,<sup>1</sup> but was unable to isolate and characterise the individual antibacterial substances. However, during the early 1940's Ernst Chain and Howard Florey isolated and characterised the substance, and they suspected penicillin had a four membered  $\beta$ -lactam ring fused to a five membered thiazolidine ring. But this was left unconfirmed, until Crowfoot in 1949 confirmed the structure of penicillin by x-ray crystallography.<sup>2</sup>



**Scheme 2.1:** Structure of Penicillin.

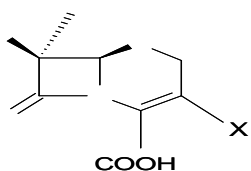
Penicillin is the parent compound of many other  $\beta$ -lactam antibiotics. After the discovery of penicillin, cephalosporin (**Scheme 2.2**) was later found to be a related antibiotic having a  $\beta$ -lactam ring, but this time fused to a six membered dihydrothiazine ring.



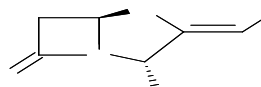
**Scheme 2.2:** Structure of Cephalosporin.

## Chapter 2.1 - Metallo- $\beta$ -lactamase - Introduction

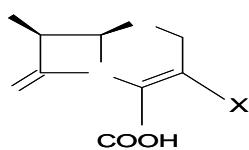
The number of different antibiotics discovered continues to grow and represents a large family of compounds which can be divided into different groups according to their structure.<sup>3</sup> The antibiotics show similarities in their structure, having a  $\beta$ -lactam ring which is often fused to another ring structure through the nitrogen and the adjacent tetrahedral carbon atom of the  $\beta$ -lactam ring. There are many  $\beta$ -lactam antibiotics (**Scheme 2.3**) that have been either isolated from fermentation of microbial culture or synthesised in the laboratory.



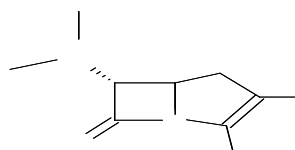
Cephameycins



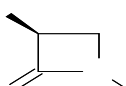
Oxapenamams



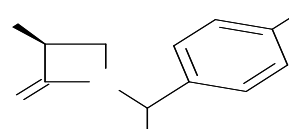
Oxacephemams



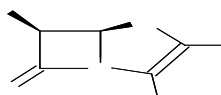
Carbapenamams



Monobactams



Norcardicins



Carbapenamams

**Scheme 2.3:** Examples of some  $\beta$ -lactam antibiotics.

#### 2.1.1.1 - The Mode of Action of $\beta$ -lactam Antibiotics

$\beta$ -Lactam antibiotics are relatively rare in nature and the chemical reactivity of the  $\beta$ -lactam is the common focus of their biological reactivity.<sup>4</sup>  $\beta$ -Lactam antibiotics interfere with the formation of the bacterial cell wall, and eventually cause the death of the bacterium by cell lysis.

#### 2.1.1.2 - Bacteria Cell Wall Structure and Synthesis

The cell wall is a major structure in bacterial cells. It is made up of several layers,<sup>5</sup> which protect the cell from osmotic lysis. The cell wall also determines the shape of the cell.

Cell wall structure is unique in prokaryotes and bacterial cell wall structures are divided into two types: Gram-positive and Gram-negative bacteria characterised by staining with Gram's stain.

Gram-positive bacteria are less complex than Gram-negative bacteria. Gram-positive bacteria have a thick multiple layer of peptidoglycan with a smooth appearance which stains the cell purple with Gram's stain. Gram negative bacteria however, consist of three layers: the cytoplasmic membrane, a thin peptidoglycan layer and an outer membrane. This thin layer of peptidoglycan is sandwiched between the inner and the outer lipid bilayers and stains the cell red with Gram's stain (**Figure 2.1**).

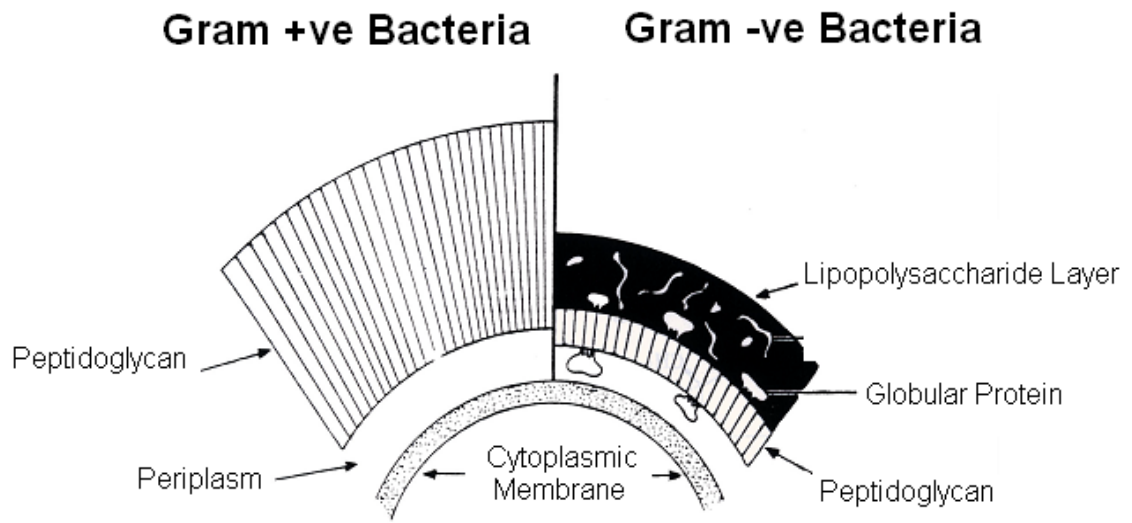
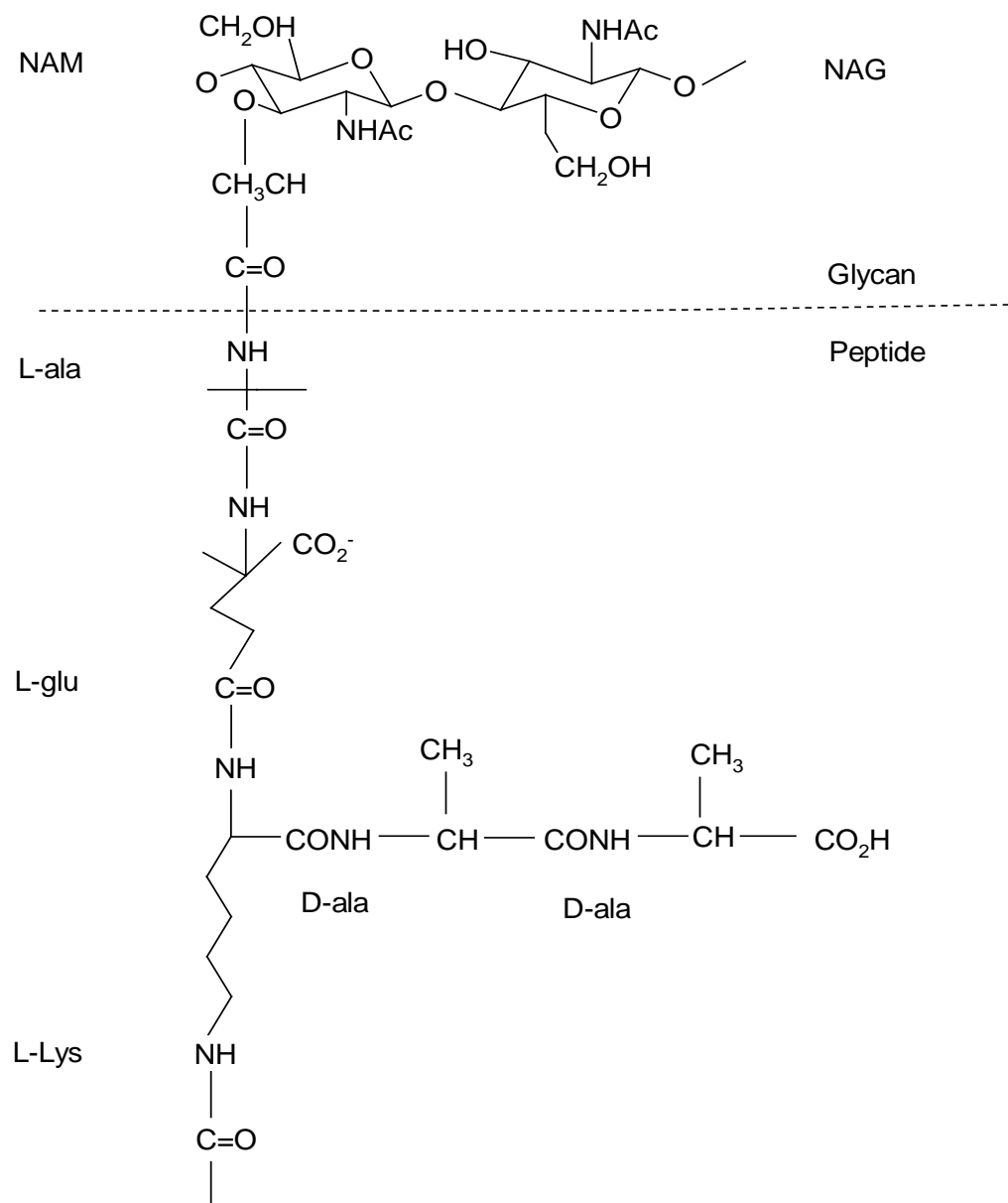


**Figure 2.1:** Gram positive and Gram negative bacterial cell wall structures.

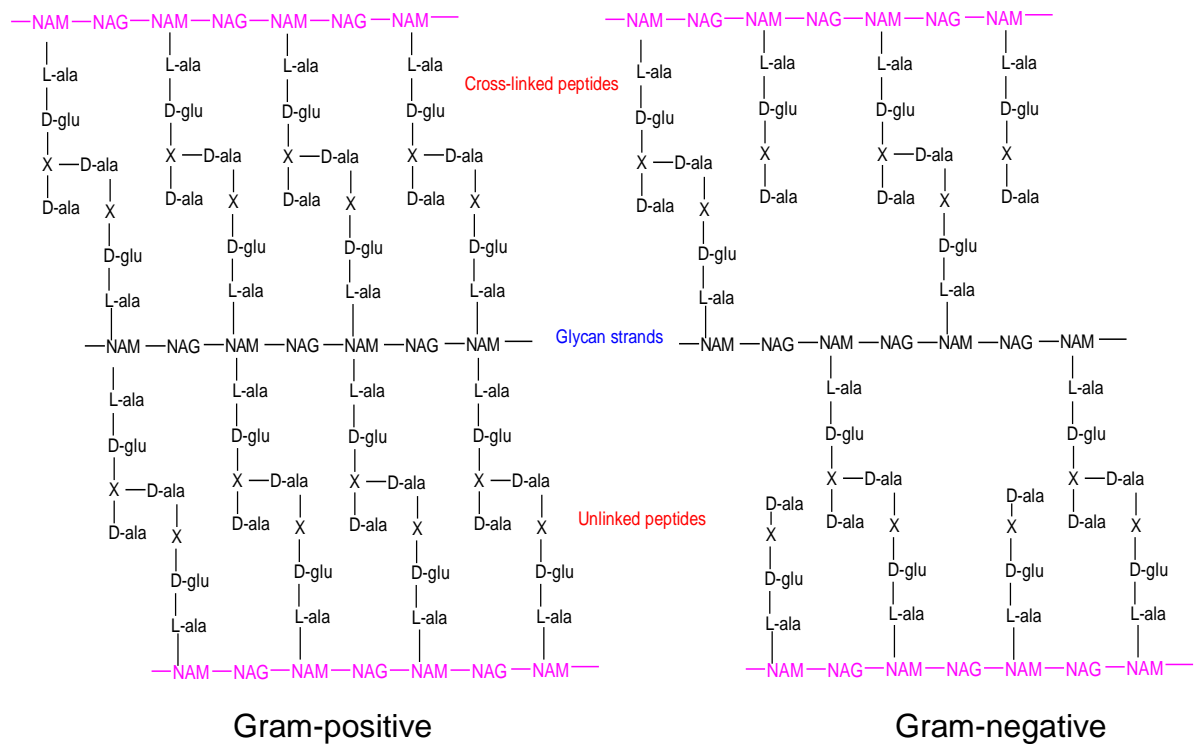
## 2.1.1.3 - Peptidoglycan

Gram-negative and Gram-positive bacterial cell wall structures both contain peptidoglycan. Peptidoglycan is a rigid structure made up of polysaccharide or glycan strands that are covalently cross-linked by peptide chains which are branched (**Scheme 2.4**). The glycan strands consist of alternating units of  $\beta$ -1,4 linked residues of N-acetyl-D-glucosamine (NAG) and N-acetylmuramic acid (NAM).



**Scheme 2.4:** Chemical structure of Peptidoglycan.

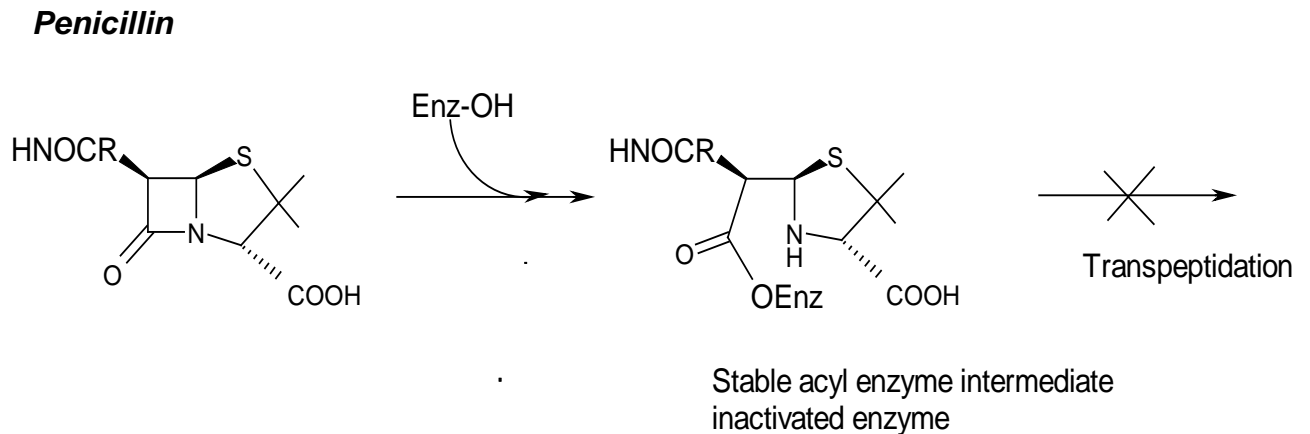
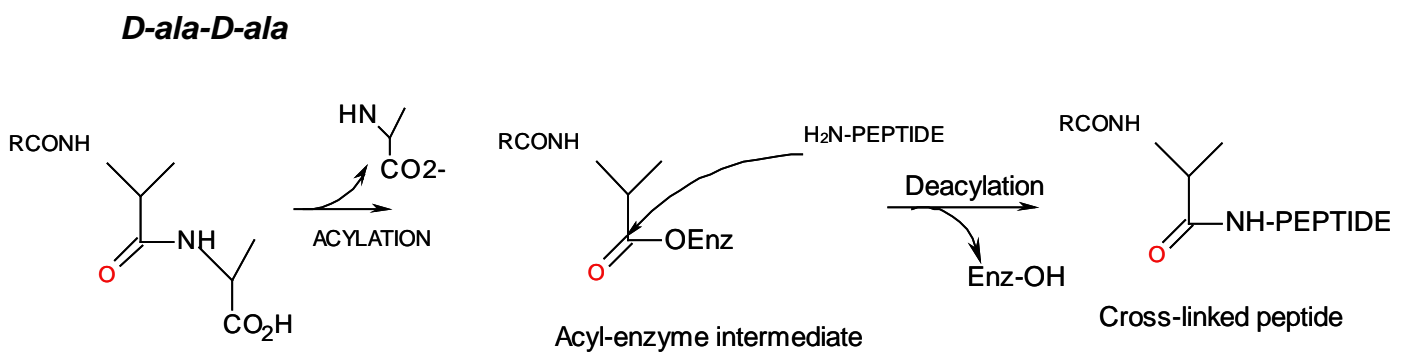
During biosynthesis of the bacterial cell wall, the peptidoglycan carries pentapeptides, these commonly have a sequence of NAG-NAM-L-ala-D-glu-X-D-ala-D-ala (**Scheme 2.5**). In this sequence the X is an amino acid residue such as L-lysine or meso-diamino-pimelic acid. The cross-linking of NAG-NAM occurs by a transpeptidation reaction that displaces the D-alanine residue with the free amino acid group on the adjacent pentapeptides.



**Scheme 2.5:** Pentapeptides sequence carried in peptidoglycan.

The cell wall is produced in three stages, the final one of which forms a rigid cell wall and involves the cross-linking of peptidoglycan strands catalysed by a transpeptidase enzyme. Penicillin interferes with this final step by destroying the synthesis of cross-linked peptidoglycan.

The transpeptidase enzyme uses an active site serine to displace the terminal D-ala residue and form an acyl-enzyme intermediate which is then deacylated by nucleophilic attack from a peptide amine (**Scheme 2.6**).



**Scheme 2.6:** Transpeptidation reaction of D-ala-D-ala compared with the  $\beta$ -lactam antibiotic reaction catalysed by serine transpeptidase enzymes.

The structure of penicillin resembles the structure of D-alanyl-D-alanine residues that are involved in the cross-linking of peptidoglycan. Similar to the reaction with D-ala-D-ala the serine residue attacks the  $\beta$ -lactam carbonyl carbon causing the ring to open and forming an acyl-enzyme. However, with  $\beta$ -lactam antibiotics the acyl-enzyme is not turned over, as it is relatively stable as the amine leaving group blocks the active site against nucleophilic attack.

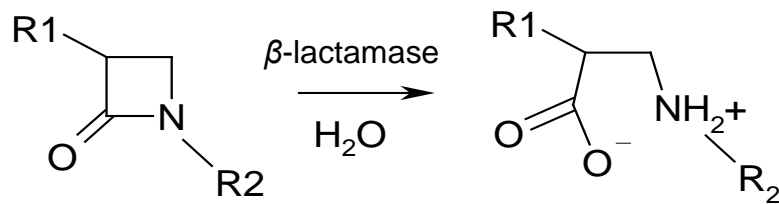
In modern society there is a serious need to challenge bacteria that have acquired resistance to antibiotics.<sup>3</sup> There are a number of ways in which bacteria can become resistant and these can be done using the following:

- Enzyme modification of the antibiotic to make it inactive.
- Preventing the antibiotic from binding by modifying the antibiotic target and this can be done by modification of the ribosomes or the enzymes that are responsible for the cell wall synthesis.
- Or by expression of efflux pumps<sup>6</sup> that can transport the antibiotic out of the cell using pumps.<sup>3</sup>

$\beta$ -Lactam antibiotics are effective and widely used compounds in the treatment of pathogenic bacterial infections,<sup>7</sup> but as mentioned above, there are mechanisms through which the bacteria can develop  $\beta$ -lactam resistance. The main reason for resistance to antibiotics in a large number of clinically important pathogens is the inactivation of antibiotics by the action of  $\beta$ -lactamases.<sup>1</sup>

### 2.1.2 - $\beta$ -Lactamases

$\beta$ -Lactamases are extracellular or periplasmic enzymes synthesised by bacteria<sup>8</sup> and represent the most widely spread mechanism of bacterial resistance to the therapeutic action of the  $\beta$ -lactam antibiotics. They catalyse the hydrolysis of the amide bond of the  $\beta$ -lactam ring causing the ring to open (**Scheme 2.7**).



**Scheme 2.7** - Hydrolysis of the  $\beta$ -lactam ring.

$\beta$ -Lactamases are divided into two categories: serine  $\beta$ -lactamases and metallo-  $\beta$ -lactamases. Serine  $\beta$ -lactamases are subdivided into three classes A, C and D.<sup>6</sup> Metallo-  $\beta$ -lactamases are a separate class and are assigned to class B (**Figure 2.2**).

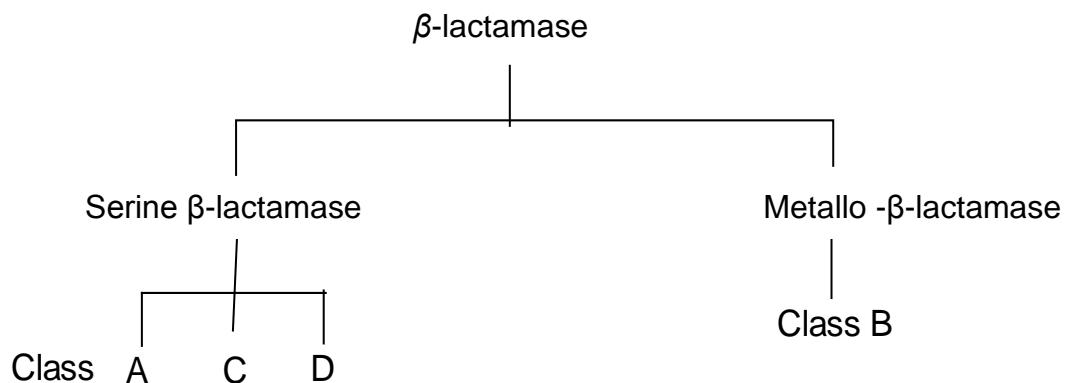
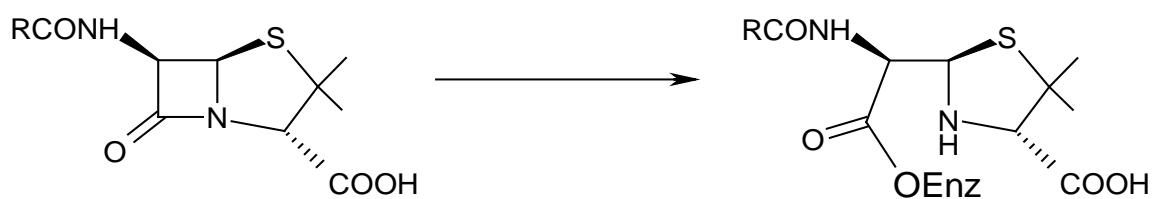


**Figure 2.2** – Divisions of  $\beta$ -lactamase.

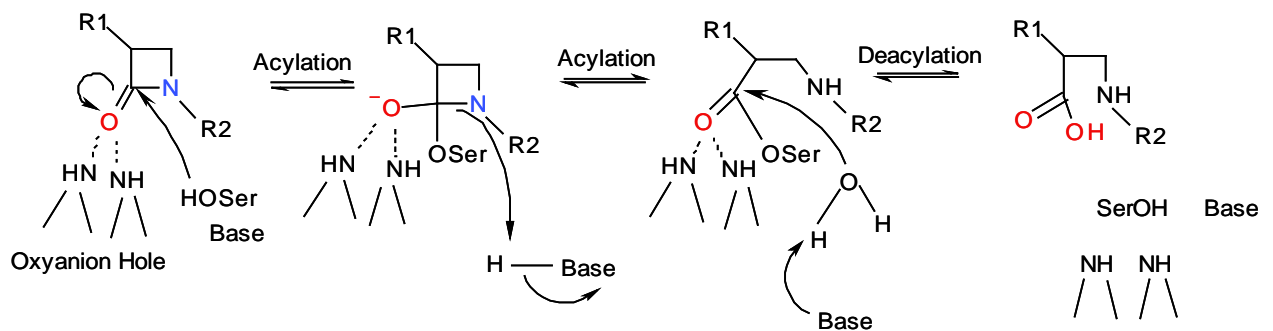
Serine  $\beta$ -lactamases have a serine residue at their active site, the hydroxyl group of which allows nucleophilic attack on the carbonyl carbon atom of the  $\beta$ -lactam ring <sup>7</sup> forming an acyl-enzyme intermediate (**Scheme 2.9**). Class B enzymes require metal ions for their catalytic activity and these enzymes catalyse the hydrolysis of a wide range of  $\beta$ -lactam antibiotics, but with no detectable intermediate.



**Scheme 2.9:** Formation of an acyl-enzyme intermediate.

### 2.1.3 - Serine $\beta$ -lactamases

Serine  $\beta$ -lactamases have probably evolved from D,D-peptidases. The cleavage of the  $\beta$ -lactam ring by serine  $\beta$ -lactamases occurs in the same way as the reaction with the D,D-peptidases, by a double displacement mechanism of acylation and deacylation (**Scheme 2.10**).<sup>9</sup>



**Scheme 2.10**– Serine  $\beta$ -lactamases double displacement mechanism.

The acylation of the active site serine hydroxyl group involves its deprotonation, using a general base, and nucleophilic attack on the carbonyl carbon of the  $\beta$ -lactam by the serine oxygen to give a tetrahedral intermediate. The carbonyl oxygen becomes negatively charged in the tetrahedral intermediate and is stabilised by an oxyanion hole.<sup>10-12</sup> The oxyanion hole of the enzyme donates two peptide hydrogen bonds to the  $\beta$ -lactam carbonyl oxygen by polarising the carbonyl group of the substrate. Cleavage of the C-N bond in the tetrahedral intermediate to give the acyl-intermediate requires nitrogen protonation. Once the C-N bond is cleaved and the acyl-intermediate formed, it then goes through the deacylation step, which requires nucleophilic attack by a water molecule. This can be activated by the same general base used to activate the serine nucleophile, or by another general base<sup>9</sup> as shown in **Table 2.1**.

**Table 2.1:** General Bases.<sup>9</sup>

Class	Oxyanion hole	Base <sub>1</sub>	H <sup>+</sup> donor	Base <sub>2</sub>
A	Ser <sub>70</sub> & Ala <sub>237</sub>	Ser <sub>130</sub> -Lys <sub>73</sub> -Glu <sub>166</sub> -H <sub>2</sub> O Ser <sub>130</sub> -Lys <sub>73</sub> -NH <sub>2</sub>	Ser <sub>130</sub> -OH	Glu <sub>166</sub> -CO <sub>2</sub> <sup>-</sup>
C	Ser <sub>64</sub> & Ser/Ala <sub>318</sub>	Lys <sub>315</sub> -Tyr <sub>150</sub> -O <sup>-</sup>	Tyr <sub>150</sub> -OH	Tyr <sub>150</sub> -O <sup>-</sup>
D	Ser <sub>67</sub> & Phe <sub>208</sub>	Lys <sub>150</sub> -NH-CO <sub>2</sub> <sup>-</sup>	-	Lys <sub>150</sub> -NH-CO <sub>2</sub> <sup>-</sup>

Class A  $\beta$ -lactamase enzymes are found in both Gram-positive and Gram negative bacteria.<sup>13</sup> They are sometimes described as penicillinases as they can efficiently hydrolyse penicillin.

Class C  $\beta$ -lactamase enzymes are often described as cephalosporinases as they have a larger  $k_{cat}$  value than that of penicillin for the hydrolysis of cephalosporins. The structures of class C are very similar to those of class A.

Class D  $\beta$ -lactamase enzymes also consist of a serine group at the active site, but are structurally very different from class A and C serine  $\beta$ -lactamases. Class D  $\beta$ -lactamases have the ability to hydrolyse oxacillins and are therefore usually considered as oxacillinases, they are always plasmid encoded<sup>14,15</sup> and their kinetics are complex with some substrates.<sup>16</sup>

### 2.1.4 - Class B $\beta$ -Lactamases

Class B  $\beta$ -lactamases are metallo-  $\beta$ -lactamases and require zinc ions for their activity.<sup>17</sup> They require either one or two zinc ions for the hydrolysis of  $\beta$ -lactam antibiotics.<sup>18</sup> The first metallo-  $\beta$ -lactamase was discovered in 1966 from an innocuous strain of *Bacillus cereus*.<sup>18</sup>

Metallo-  $\beta$ -lactamase mediated resistance has appeared in many pathogenic strains of bacteria, and are being rapidly spread by horizontal transfer, which involves both plasmid and integron-borne genetic elements.<sup>19</sup>

Metallo-  $\beta$ -lactamases are sub-divided into B1, B2 and B3 according to their amino-acid sequences, substrate profile and metal ion requirement.<sup>20</sup> Subclass B1 is the largest group. This class is well studied and contains  $\beta$ -lactamases that hydrolyse a wide range of substrates, such as penicillin, cephalosporin and carbapenems. Subclass B1 enzymes have four main well-studied  $\beta$ -lactamase enzymes,<sup>21-23</sup> these are: BcII from *Bacillus cereus* (the enzyme used in this research),<sup>24</sup> CcrA from *Bacteroides fragillis*,<sup>25-27</sup> IMP-1 from *Pseudomonas aeruginosa* and BlaB from *Cryseobacterium meningosepticum*.<sup>28</sup>

Subclass B2 enzymes usually hydrolyse carbapenems but have poor activity against other substrates such as penicillin and cephalosporin.<sup>29, 30</sup> The subclass B2 enzymes are CphA from *Aeromonas hydrophilia*<sup>31</sup> and ImiS from *Aeromonas veronii*.<sup>32</sup>

Finally, subclass B3 enzymes are characterised by a broad substrate profile and are known as tetrameric zinc  $\beta$ -lactamases. The B3 enzymes include L1 from *S.maltophilia*<sup>33</sup> and FEZ-1 enzyme from *Legioneilla gormanii*. Both of these enzymes hydrolyse a wide range of  $\beta$ -lactam antibiotics.<sup>32</sup>

Metallo-  $\beta$ -lactamase enzymes have either one or two zinc ions bound to their active sites. The zinc ion in site one is usually bound in the histidine (3H) site,

which is tetra-coordinated, whereas the second zinc ion binds to site two (DCH) in the cysteine site (Cys) that is penta-coordinated.

**Table 2.2** shows how the three subclasses B1, B2 and B3 differ in the residues used as ligands for the zinc ions. Subclass B1 and B2 enzymes use almost the same residues to coordinate zinc ions in site one, but the coordination of zinc two is different. The only difference in coordination is that B2 enzymes uses an asparagine (Asn) residue at position 116 instead of histidine (His) at this site in B1. In subclass B3 zinc ion in site 2 is coordinated by His 121 instead of cysteine (Cys) 221 and in B3 enzymes the His 116 is replaced by glutamine (Gln) 116.

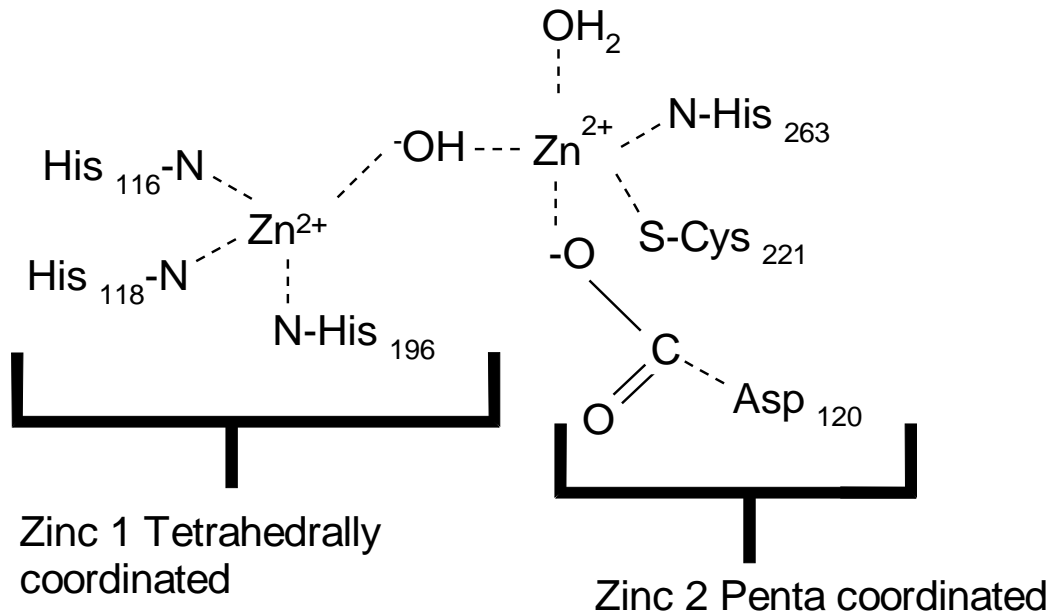
**Table 2.2** - Zinc ligands in class B  $\beta$ -lactamases.<sup>34</sup>

Sub class	Zinc ion in site one (3H)			Zinc ion in site two (DCH)		
B1	His <sub>116</sub>	His <sub>118</sub>	His <sub>196</sub>	Asp <sub>120</sub>	Cys <sub>221</sub>	His <sub>263</sub>
B2	Asn <sub>116</sub>	His <sub>118</sub>	His <sub>196</sub>	Asp <sub>120</sub>	Cys <sub>221</sub>	His <sub>263</sub>
B3	His/Gln <sub>116</sub>	His <sub>118</sub>	His <sub>196</sub>	Asp <sub>120</sub>	His <sub>121</sub>	His <sub>263</sub>

### 2.1.5 – BclI from *Bacillus Cereus* 569/H/9 Metallo- $\beta$ -lactamase

BclI was the first metallo- $\beta$ -lactamase to be isolated from an innocuous strain of *Bacillus cereus*.<sup>35</sup> BclI is from the subclass B1 and zinc ion binding is crucial for its activity. There have been many reports on the structure of BclI, indicating that when metal ions bind, they either occupy both sites or only the histidine site. **Scheme 2.11** shows how the metal ion binds to its individual amino acid side chains. Zinc one is tetrahedrally coordinated to the imidazole groups of three His residues (His116, 118 and 196) and a bridging water molecule or a hydroxide-ion. Zinc two is penta-coordinated to His263, Asp120, Cys221, the bridging water or hydroxide-ion and a water molecule/bicarbonate ion.

Some metalloenzymes appear as mono-zinc (where one zinc ion is bound to the enzyme) and others have been shown to be di-zinc (when two zinc ions are bound to the enzyme).<sup>36</sup> For example, reports on the structure of metallo- $\beta$ -lactamase from *B. fragilis* are shown to have two zinc ions, both of which are tightly bound,<sup>37,38</sup> but the loss of a single zinc ion has been claimed not to be important for  $\beta$ -lactamase activity.<sup>39</sup> The metallo- $\beta$ -lactamase BclI from *B. cereus*, equally, has been shown to exhibit maximum catalytic activity with one bound metal ion,<sup>10</sup> although two metal ions are observed in one of the crystal structures. However, the stoichiometric ratio of the number of metal ions bound to the metallo- $\beta$ -lactamase from *B-cereus* has been shown to vary as a function of pH.<sup>1</sup> At low pH only one metal ion has been shown to be bound to BclI according to X-ray crystallography, while at pH 7.5 in a structure of BclI two metal ions are bound.<sup>1</sup> However it is still very unclear the number of metal ions required for activity.



**Scheme 2.11:** How zinc ions coordinate to the amino acids in BclI.

The two metal ions are arranged in close proximity to each other with a distance between them of 3.4-4.4 Å.<sup>37,38,40-43</sup> Reports on the crystal structure for the mono-zinc form of BclI at pH 5.7 show the metal ion is chelated by three histidines and a water molecule. Some of the studies using PAC (perturbed angular correlation), EXAFS (extended X-ray absorption fine structure) spectra and kinetic analysis suggested that in the mono-form of zinc at neutral pH, the metal ion is shared between site one and site two.<sup>44</sup> However, at low pH the structure shows the solvent molecule to be strongly associated to zinc ion in site one.<sup>1</sup>

The mono-zinc form of BclI has been thought to be catalytically active but it has been suggested that the binding of second zinc ion gives a more catalytically active enzyme,<sup>45,46</sup> because the  $k_{cat}$  value, determined using benzylpenicillin as a substrate, is approximately two-fold lower for the mono-zinc form than the di-zinc form of BclI. According to the equilibrium studies, the zinc ions at the active site have different dissociation constants for the two binding events. There has been different dissociation constants reported as for the mono-zinc form ranging from 0.6 nM to 120  $\mu$ M and for the di-zinc form ranging between 1.5  $\mu$ M to 24 mM of BclI.<sup>21, 45, 47, 48</sup> The different values reported could be due to different strains of BclI used.

### 2.1.6 - Crystal Structure of Metallo- $\beta$ -lactamases

There are many crystal structures reported for metallo- $\beta$ -lactamases,<sup>23</sup> mainly from subclass B1 and B3. The crystal structures reported from B1 are BclI from *Bacillus cereus*, CcrA from *Bacillus fragillis* and IMP-1 from *P.aeruginosa*.<sup>23</sup> The crystal structures from B3 reported are L1 from *S. maltophilia* and FEZ-1 from *F. gormanii*. All these metallo- $\beta$ -lactamase enzymes have the same fold of  $\alpha\beta\beta\alpha$ , where the  $\beta$ -sheets are packed against each other to form the core of the enzyme; this is where the active sites are situated, at the bottom of the wide shallow groove between the two  $\beta$ -sheets (**Figure 2.3**).<sup>49, 50</sup> The  $\alpha$ -helices are then packed on the surface of each  $\beta$ -sheet. The fifth  $\alpha$ -helix is located between the last two  $\beta$ -strands on the *N*-terminal sheet.<sup>23</sup> This  $\alpha$ -helix and two  $\beta$ -strands form the bridge of the C-terminal domain. So the *N*-terminal half represents the first  $\alpha\beta$  unit and the second  $\alpha\beta$  unit is formed by the C-terminal, where the zinc cluster and active sites are positioned at the top of the interface between the two domains.<sup>23</sup>

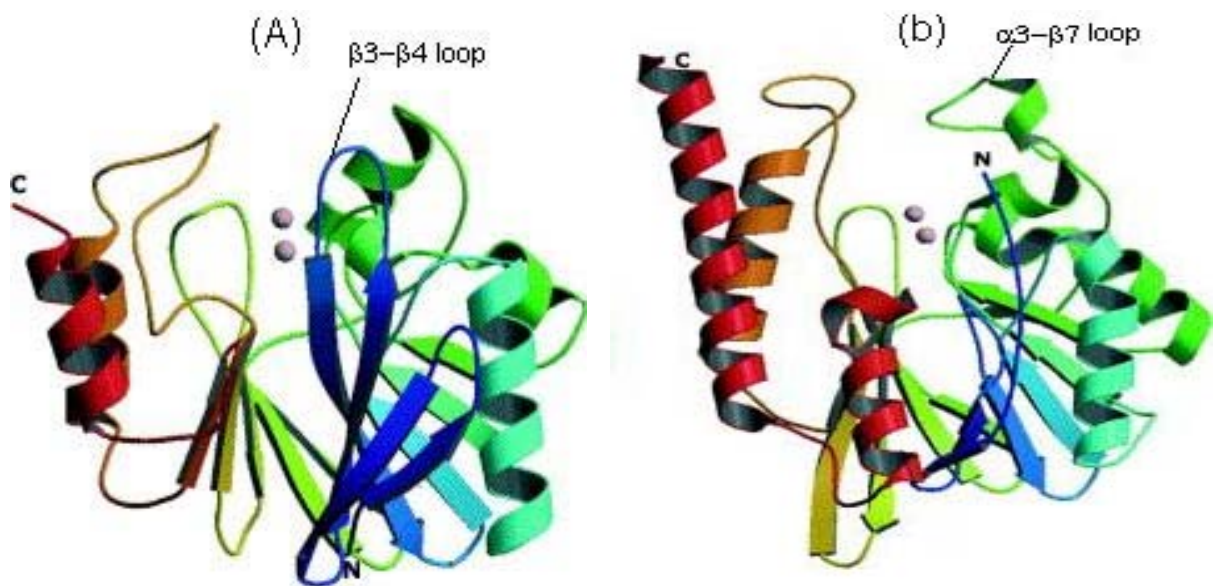


**Figure 2.3** - A ribbon representation of the overall fold of metallo- $\beta$ -lactamases of B1 (*B.cereus*) and B3 (FEZ from *F.gormaii*). The blue ribbons are the  $\beta$ -strands, the red ribbons are  $\alpha$ -helices and the grey spheres are zinc ions. Adapted from ref 51.

**Figure 2.3** shows the overall ribbon representation of metallo- $\beta$ -lactamase from subclass B1 (BclI) and B3 (FEZ). The structures are similar, but there are differences between the two, in B1 the secondary element interacts directly with bound inhibitors but in subclass B3 enzymes this does not occur. B3 enzymes contain a disulfide bond that is not present in B1 and the disulfide bridge is between two cysteine residues.<sup>52</sup> In B1 the  $\beta$ 3- $\beta$ 4 loop allows the hydrophobic side chains to interact with the bound inhibitors,<sup>53, 54</sup> whereas in B3 it contains mainly hydrophilic residues and the  $\beta$ 3- $\beta$ 4 loop is much smaller.

### 2.1.7 - Zinc Coordination to Metallo- $\beta$ -lactamases

Different metallo- $\beta$ -lactamases have different metal ion affinities and metal ion requirements for catalysis for each binding site. Three enzymes *B.fragillus*, *B.cereus* and *S.maltophilia*, are compared for their coordination environments of dinuclear zinc centres in **Figure 2.4**.<sup>54</sup>

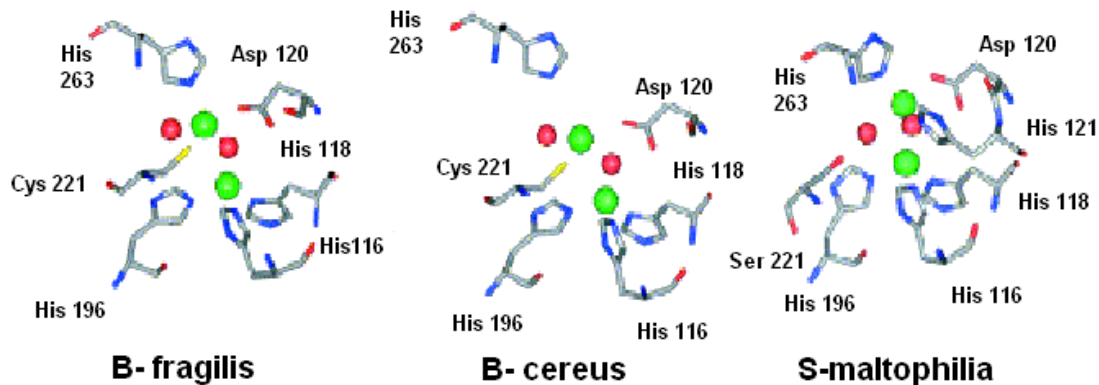


**Figure 2.4:** Comparison for the coordination environments in *B.fragillus*, *B.cereus* and *S.maltophilia*.<sup>16</sup>

The structures for both the *B.fragillus* and *B.cereus* can be superimposed but the distance between zinc ion one and zinc ion two in *B.cereus* is between 3.4-4.4 Å, which is greater than that in *B.fragillus*<sup>55</sup>. In *B.fragillus* (B1) zinc ion one is tetrahedrally coordinated with three histidine residues and a water molecule (solvent),<sup>23</sup> zinc ion two is pentacoordinated by three ligands (Cys, His and Asp) and two solvent molecules (water). One of the solvent molecules coordinates to both the zinc ion atoms. The side chain asp interacts with zinc ion two and the shared solvent water molecule makes a bridging ligand between the two sites.<sup>33</sup> The second solvent water molecule only interacts with zinc ion two giving itself a position in site two to become pentacoordinated.<sup>23</sup>

### 2.1.8 Role of Zinc ion in Metallo- $\beta$ -lactamases

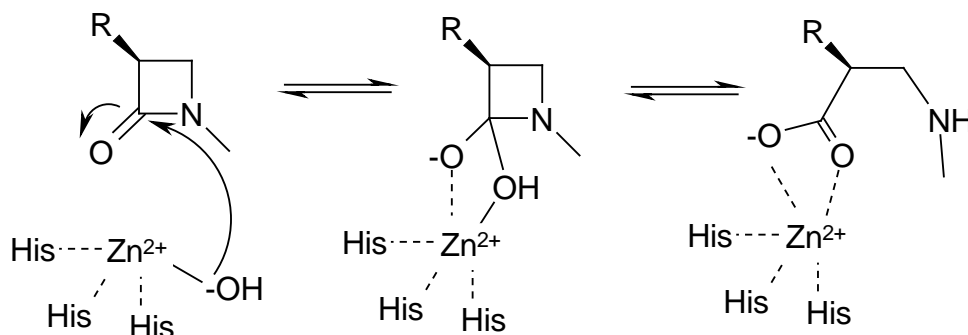
Zinc ions are a vital element required in metallo- $\beta$ -lactamases for the catalytic activity of the enzyme. Zinc ion is a component that is essential in many cellular processes, and is the most abundant transition metal ion found in the human body. The element usually loses two electrons and combines chemically in the 2+ oxidation state. For metallo- $\beta$ -lactamase enzymes, other metal ions can be used as a replacement to the zinc ion but the zinc enzyme complex is usually the most efficient.

The importance of zinc ion has been long recognised, and has been reported previously. It is described as being essential in a structural role as well as in the catalysis of  $\beta$ -lactamases. The zinc ion, according to x-ray structures, is coordinated to three amino acid residues (three histidines in BclI) and a water molecule in the mono-nuclear metallo-  $\beta$ -lactamases, in the dinuclear metallo- $\beta$ -lactamase, the second zinc ion is pentacoordinated.

The role of the zinc ion, as some studies have suggested, is to act as a Lewis acid, polarising the  $\beta$ -lactam carbonyl group and stabilising oxyanion formation in the tetrahedral intermediate. The water molecule bound to zinc ion can ionise and its  $pK_a$  value can be determined from kinetic studies, the electronic properties of the metal complex or by calculation using the electrostatic contributions from nearby residues.<sup>22, 56-59</sup> Theoretical studies have been performed using carbonic anhydrase II and show that the amino acid residues are responsible for the electrostatic stabilisation of the hydroxide-ion and the negatively charged transition state. They further indicate that the charged ligands are responsible for lowering the  $pK_a$  of the zinc-bound water molecule. Therefore the zinc ion complex lowers the  $pK_a$  of the bound water molecule and makes it available as a nucleophilic hydroxide-ion for the catalysis at neutral pH.<sup>57 21, 58,59</sup>

The lower the  $pK_a$  of the zinc bound water molecule presumably indicates a more electron deficient zinc ion so the more effective it can act as a Lewis acid. This means decreasing the  $pK_a$  of the zinc bound water molecule allows

the zinc bound hydroxide to be available at lower pH, but which would reduce its nucleophilicity compared with hydroxide anion. So overall the main roles of zinc ion in metallo-  $\beta$ -lactamase are to form a metal ion bound hydroxide-ion for the nucleophilic attack on the carbonyl carbon atom of the  $\beta$ -lactam and to stabilise the negative charge generated in the tetrahedral intermediate formed (**Scheme 2.12**).

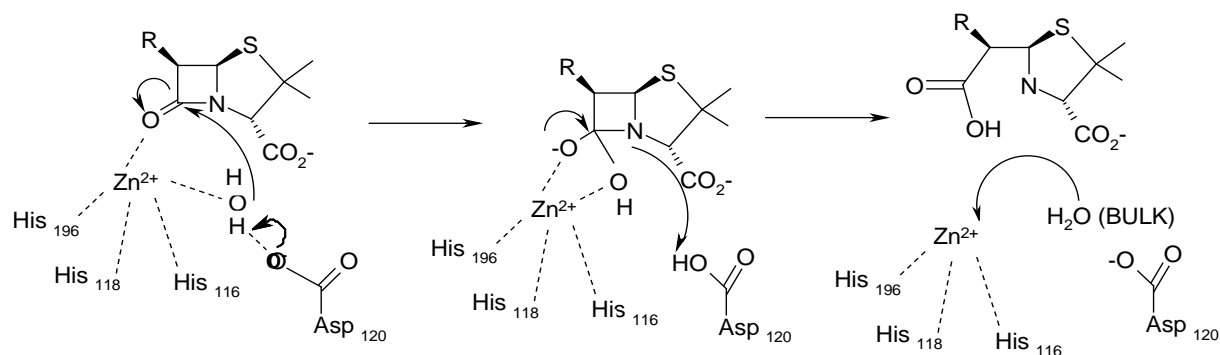


**Scheme 2.12:** Nucleophilic attack on the carbonyl carbon atom of the  $\beta$ -lactam ring and stabilisation of the tetrahedral intermediate.

### 2.1.9 – Mechanisms for Metallo- $\beta$ -lactamases

Presumably, if both mono-zinc and di-zinc enzymes are active they will have different catalytic mechanisms due to the different environments of zinc ion, and the orientations and flexibilities of the active site residues.

Zinc ion one is bound in the histidine site (3H) of the enzyme (**Scheme 2.13**) and the first catalytic mechanism was proposed by Carfi et al.<sup>43</sup> The main features of this mechanism resemble those of zinc peptidases such as carboxypeptidase and thermolysin.<sup>54,60</sup>



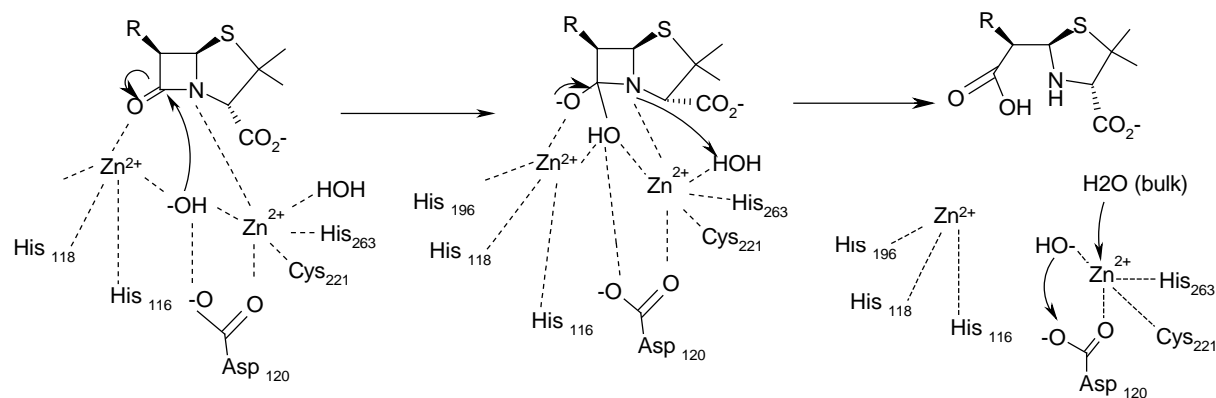
**Scheme 2.13** – Catalytic mechanism for mono-zinc in metallo- $\beta$ -lactamases.

As shown in **Scheme 2.13** the zinc ion binding in the histidine site (mono-zinc), is tetrahedrally coordinated with three histidine ligands and the fourth ligand from a water molecule is unionised. The water molecule interacts with Asp<sub>120</sub> which acts as a general base during the reaction to remove a proton resulting in effective hydroxide attack on the  $\beta$ -lactam carbonyl carbon atom. This produces an oxyanion in the tetrahedral intermediate which is stabilised by the zinc ion and the side chain amide group of Asn<sub>233</sub>, forming an 'oxyanion hole'. The process results in a change in the coordination number of the zinc ion from a four-coordinate tetrahedral structure to a five coordinate trigonal bipyramidal arrangement. Following the formation of the tetrahedral

intermediate, the C-N bond at the  $\beta$ -lactam ring is cleaved as the proton is accepted from Asp<sub>120</sub> and transferred to the nitrogen atom.<sup>23</sup>

Bounaga et al.<sup>17</sup> revisited the mechanism of mono-zinc enzyme with an analysis of the pH rate profile, inhibitor binding studies and solvent kinetic isotope effects and concluded that the zinc-bound water was already ionised at neutral pH, i.e. it existed as metal-bound hydroxide-ion.<sup>55</sup> Furthermore, Bounaga et al. suggested the formation of a dianionic tetrahedral intermediate based on the pH-rate profile.<sup>40</sup> A dianionic tetrahedral intermediate helps the  $\beta$ -lactam ring to open and generate a carboxylate anion rather than the undissociated acid.<sup>1</sup>

The mechanism of the di-zinc enzyme is based on the crystal structure of *Bacteroides fragillis* and  $\beta$ -lactam substrates bound to the enzymes active site<sup>1</sup> undergoing hydrolysis by an analogous mechanism to other hydrolases with a bi-nuclear centre (**Scheme 2.14**).<sup>1</sup>

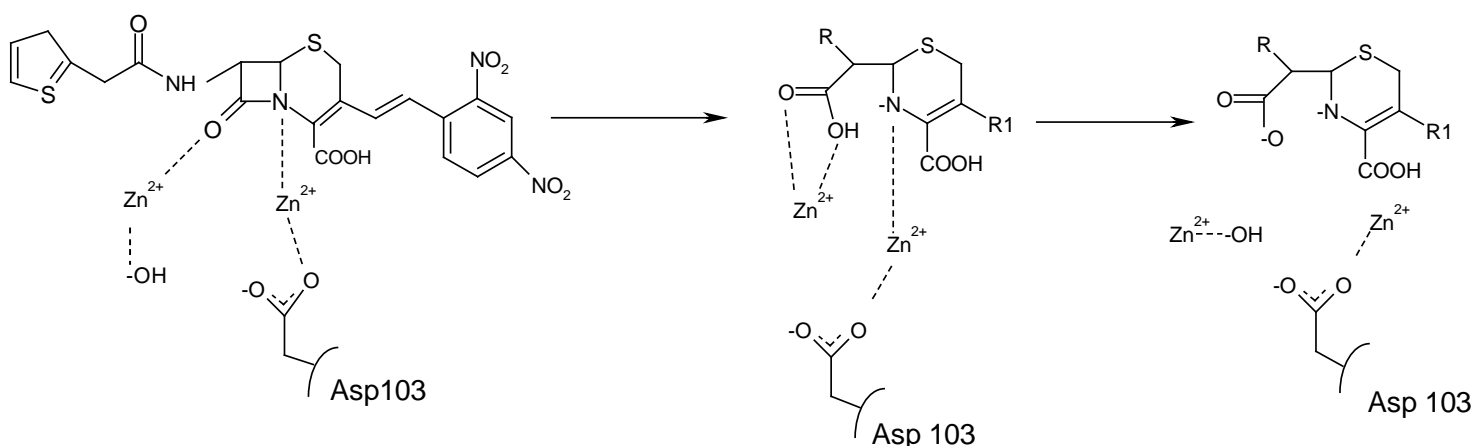


**Scheme 2.14** – Catalytic mechanism for di-zinc of metallo- $\beta$ -lactamase.

The mechanism for the di-zinc metallo- $\beta$ -lactamases proceeds via the hydroxide-ion bridged between two zinc ions. This involves a nucleophilic attack on the carbonyl-carbon atom of the  $\beta$ -lactam, which results in a negatively charged intermediate which is stabilised by the oxyanion hole of the enzyme<sup>1</sup> at zinc one, site 3H. The C-N bond on the  $\beta$ -lactam is cleaved

and a proton is transferred to the amide nitrogen of the  $\beta$ -lactam ring.<sup>23</sup> The water that is coordinated to zinc two, site DCH, is positioned to donate a proton<sup>21</sup> to the leaving nitrogen and the hydroxide-ion formed moves into the vacated water (WAT1) site that then undergoes product dissociation from the enzyme active site.<sup>1</sup>

Another catalytic mechanism was proposed using nitrocefin as the substrate, based on kinetic experiments (**Scheme 2.15**), which showed an accumulation of an intermediate with an intense absorbance at 665nm.<sup>1</sup> The intense absorbance was attributed to a negatively charged nitrogen atom, which coordinates to zinc two by either displacing the water or increasing the metal ion coordination. The negatively charged nitrogen is protonated by a water molecule from the bulk solvent leading to a breakdown of intermediate and product formation.



**Scheme 2.15:** Catalytic mechanism using nitrocefin as a substrate.

### 2.1.10 – Different Metal ions Used to Bind the Active Sites of Metallo- $\beta$ -lactamases

As explained above, zinc ion is a cofactor in metallo-  $\beta$ -lactamases<sup>37,38</sup> and is required for its activity. But other metal ions such as cobalt, cadmium or iron can be exchanged to activate the apo-enzyme (enzyme free from metal ions).<sup>30</sup> The techniques used to structurally identify the binding sites when the metal ion binds to the enzyme are by EXAFS (extended X-ray absorption fine structure) and X-ray crystallography. Studies on other metal ions binding to metallo-  $\beta$ -lactamases (other than zinc ion), to determine the number of metal ions required per enzyme or structurally identify the metal binding sites are performed kinetically or by spectroscopy using NMR, ESR, UV-Vis and PAC spectroscopy.<sup>61,62,63</sup> (PAC spectroscopy is similar to NMR and uses radioactive nuclei which decays via gamma-gamma rays. In PAC the absorption of the electromagnetic energy in a structure or crystal where the transitions between energy levels are formed as a result of the interaction of nuclei that contain an electric quadrupole moment with the crystals electric field).

Reported research suggests that when the zinc ion is substituted with cadmium ion into BcII metallo- $\beta$ -lactamases from *Bacillus cereus* and analysed using NMR and PAC spectroscopy it shows two coordination geometries of different metal ion binding sites.<sup>31</sup> The mono-cadmium enzyme of BcII undergoes exchange of the metal ion between the two active sites. PAC spectroscopy shows one nuclear quadrupole interaction (NQI) to the cysteine site (DCH) and the other NQI to a histidine site (3H). According to the NQI, the cysteine residue is not involved as a ligand when the cadmium binds to the three histidine (3H) site, but UV-Vis spectroscopic analysis shows the metal ion is coordinated to the cysteine residue, because the cadmium ion occupies the cysteine site (DCH) even when the stoichiometry is below one. When the stoichiometry is below one with cadmium ion there is equilibrium between the two metal sites favouring the cysteine site (DCH) in the cadmium ion binding to the enzyme, whereas, when zinc ion has a stoichiometry below one the histidine (3H) site is preferred.<sup>33</sup>

The most recent report by Jacquin et al.<sup>64</sup> suggests cadmium ion binds to BclI in a non-cooperative process. This has been observed by mass spectroscopy showing 100% relative abundance with the presence of one equivalence of cadmium ion titrated. However, when zinc ion was used in the same manner, it was shown that the zinc ion binding to the BclI enzyme shows a positive cooperative binding. Three species were determined in the mass spectrum when different ratios of zinc ion to enzyme were used. As the ratio of zinc ion to enzyme was increased, the three species seen were apo-enzyme at  $M_R$  24961 $\pm$ 2, mono-zinc at  $M_R$  25025 $\pm$ 2 and finally di-zinc enzyme at  $M_R$  25089 $\pm$ 2. The mono-zinc species was observed throughout the whole titration process but with a relative abundance below 20%.<sup>64</sup>

NMR spectroscopy was used to confirm the results from mass spectroscopy, this determined that the addition of one equivalent of cadmium ion shows a maximum signal which was identified as the mono-form using both NMR and PAC spectroscopy. However, as the molar ratio of cadmium ion was increased, the cadmium ion signal decreased and a third signal appeared, this was identified to be the di-cadmium form. This confirms cadmium ion binds as a non-cooperative process as the apo and di-cadmium were never observed simultaneously. When the zinc ion was titrated with increasing molar ratio, the di-zinc form of BclI was observed from the beginning and there was no sign of the mono-zinc species. The only species observed was the apo and di-zinc, which confirms that zinc ion binds to BclI enzyme in a positive cooperative manner and cadmium ion binds in a non-cooperative manner.<sup>64</sup>

Studies have also been conducted where cobalt ions were substituted into metallo- $\beta$ -lactamases (CcrA- *Bacteroidis fragillis* and BclI form *Bacillus cereus*), and analysed using UV-Vis spectroscopy.<sup>30,65</sup> For both the CcrA- *Bacteroides fragillis* and BclI from *Bacillus cereus* cobalt ion substitution shows very similar features with intense bands around 340nm and 348nm, demonstrating ligand to metal charge transfer (LMCT). The spectrum also shows four characteristics of d-d transition bands between 500nm and 650nm.<sup>34</sup> This UV spectrum suggests the cobalt ion occupies the cysteine site whilst the histidine site is occupied with a zinc ion and a heterosubstituted

CoZn-enzyme can be formed.<sup>53</sup> Cadmium ion shows similar results, the cadmium ion binds to the cysteine site (DCH) and the zinc ion binds to the histidine site (3H).<sup>36</sup> When cobalt ion binds to apoBclI in HEPES buffer without any salt (NaCl),<sup>65</sup> it shows an increase in the ratio of cobalt:enzyme to a stoichiometry of above one. The UV-Vis spectrum shows a decrease in the LMCT band to 344nm and an additional band at 383nm is introduced. The results indicate the two cobalt ions bind at different positions having one LMCT as 344nm (representing the mononuclear form) and the other LMCT band at 383nm (representing the dinuclear form). When sodium chloride was added to the buffer, the band at 383nm disappeared and the absorbance at 344nm increased which suggests chloride ion hinders the binding of the second cobalt ion.<sup>36</sup>

Using UV-Vis spectroscopy as an analysis technique, metallo-  $\beta$ -lactamases from *Aeromonas veronii* substituted with cobalt ions have been studied. The spectrum shows a LMCT band with an intense peak at 340nm for the cobalt ion, indicating that the cobalt ion is coordinated by a cysteine active site, and tetrahedrally coordinated.<sup>31</sup> Similarly UV-Vis studies on CphA from *Aeromonas hydrophilia*, which, when substituted with cobalt ions, showed two intense LMCT bands in the region of 289nm and 325nm, additional bands were also observed between 500nm and 650nm.<sup>66</sup> This study also suggests the cobalt ion occupies the cysteine site in CphA, but the appearance of two LMCT bands suggests it is the mono-cobalt CphA species. By contrast BclI from *Bacillus Cereus* and CcrA from *Bacteroides fragilis* shows only one LMCT band.

When L1 from *Strenotrophomanas maltophilia* in subclass B3 is substituted with cobalt ions, a broad band is seen in the visible region of 550nm, but there is no appearance of LMCT bands as seen in B1 and B2 enzymes that are indicative of the cobalt ion binds in the cysteine active site. The band in the visible region indicates the cobalt ion is four or five coordinated<sup>67</sup> and the absence of the LMCT is due to the absence of the cysteine ligand in the active site of L1.<sup>68</sup> This result is therefore consistent with the B1 and B2 enzyme, which both show the LMCT band.<sup>69,70</sup>

In summary, these studies have suggested that zinc and cobalt ions bind cooperatively but cadmium ion binds non-cooperatively. With a stoichiometry of metal ion to enzyme of one or less, cadmium and cobalt ions bind preferentially to the cysteine site (DCH) whereas zinc ion binds to the histidine site (3H).

The purpose of this research will be to further study the binding of metal ions to BcII enzymes using an isothermal titration calorimeter.

### **2.1.11 - Research Aims**

BcII is a metallo- $\beta$ -lactamase which binds metal ions with different affinities, therefore different metal ions such as zinc, cobalt and cadmium will be titrated into apoBcII at different pH's. The purpose of this study is to obtain a detailed thermodynamic understanding of the binding mechanisms of metal ions to BcII 569/H/9 metallo- $\beta$ -lactamases using isothermal titration calorimetry.

The binding data will be correlated with existing kinetic data already available on reactions catalysed by these metalloenzymes. The influence of metal ion binding on  $pK_a$  values of adjacent acid groups will also be assessed by measuring the number of protons lost from the BcII enzyme when the metal ions are coordinated to the apoBcII as the pH is varied.

## 2.2 - Metallo- $\beta$ -lactamase - Experimental

### 2.2.1 - Enzyme Preparation

#### 2.2.1.1 - Materials

All solvents and reagents used were analytical grade or an equivalent grade where possible.

The buffers (acetate  $pK_a$  4.62, cacodylate  $pK_a$  6.14, HEPES  $pK_a$  7.45, MES  $pK_a$  6.07, MOPS  $pK_a$  7.02, PIPES  $pK_a$  6.71), <sup>71</sup> substrate (benzylpenicillin), chelating agent (chelex 100) and the metal salts ( $ZnSO_4$ ,  $CoCl_2$  and  $CdCl_2$ ) used were purchased from Sigma Aldrich.

Buffers and aqueous solutions were prepared just prior to the experiment using deionised ultra pure water (18 M $\Omega$ cm) and NaCl was used to maintain constant ionic strength.

The expression plasmid DNA pET9a-BclI for the production of metallo-  $\beta$ -lactamase (BclI) was provided by Dr Christian Damblon at Leicester University. Pre-prepared ZnBclI solution in 10 mM HEPES was kindly supplied from the University of Liege, Belgium and this and the one made in Huddersfield were further purified as described later. The bacterium JM101 for the isolation of DNA was supplied by Adriana Badarau from the University of Newcastle.

Special care was taken when preparing solutions to ensure there was no contamination with metals. Plastic beakers were used and where glassware, including quartz cuvettes, were used, they were soaked in 20 %  $HNO_3$  overnight and washed thoroughly with 0.1 M NaOH, then ultra pure water.

### 2.2.1.2 - Instrumentation

The absorbance readings from which the kinetic data was calculated were made on a Cary 4000 UV-Vis spectrophotometer equipped with a twelve compartment thermostat. The rate constants were calculated using a Cary Win UV kinetics application

All the pH measurements were made using a Beckman  $\Phi$ 40 pH meter using calibration buffers at pH 7 phosphate “green” and pH 4 phthalates “red”.

The BcII was purified using fast protein liquid chromatography (FPLC) on an AKTA Prime equipment from Amersham Pharmacia Biotech. The parameters used were:

Flow rate 3 ml/min, pressure 0.5 mPa, 5 ml fractions were collected and the enzyme eluted monitoring absorbance at 280 nm.

The centrifuges used during the process of obtaining BcII were:

- Allegra X15 centrifuge (Beckman)
- Optima L-look ultracentrifuge (Beckman)

Proton NMR's were recorded on a 400 MHz instrument (Bruker, Germany) and used to determine the EDTA concentration in apoBcII.

A Perkin Elmer AAnalysers atomic absorption spectrophotometer was used to determine the concentration of zinc ion in buffers and apoBcII solutions.

Thermodynamic titrations were made using an isothermal titration calorimeter (ITC) from Microcal.

### 2.2.2 – Production of Competent Cells

The DNA from Christian Damblon (Leicester University) was isolated using an *E. coli* strain JM101 as competent cells. The JM101 *E. coli* strain was transformed on an LB agar (Lenox L broth base) overnight at 37°C. After 18 h, a single colony was selected and transferred to 5 ml LB medium and incubated overnight under orbital agitation at 37°C.

This LB preculture (500  $\mu$ l) was used to inoculate 50 ml of LB medium and incubated under orbital agitation at 37°C until the absorbance at 595 nm reached 0.375. It was then placed onto ice for 10 minutes and centrifuged for seven minutes at 2,500 rpm (4°C). The pellet was resuspended in 10 ml of CaCl<sub>2</sub> solution (60 mM CaCl<sub>2</sub>, 15% glycerol, 10 mM PIPES, pH 7). The resuspended pellet was centrifuged for a further five minutes at 2,500 rpm (4°C) and the pellet resuspended in 10 ml CaCl<sub>2</sub> solution and left on ice for 30 minutes. It was centrifuged again for a further five minutes at 2500 rpm (4°C), and then resuspended in 500  $\mu$ l (5x100  $\mu$ l additions) CaCl<sub>2</sub> solution.

The expression plasmid DNA (1  $\mu$ l) was added to the competent cells (100  $\mu$ l) and plated onto an LB agar. The bacteria were transformed overnight at 37°C. After 18h the colonies were selected and transferred into two 5 ml LB media with 50  $\mu$ g/ml kanamycin and left overnight under orbital agitation at 37°C for about 7 hours.

The bacterial culture was then used to isolate the DNA using the isolation of DNA kit (Promega).

### 2.2.3 - Production of BclI

BclI enzyme was produced using the expression plasmid DNA pET9a-BclI supplied by Dr Christian Damblon, University of Leicester or DNA isolated using the Promega kit. The expression plasmid was used to transform the *E.coli* competent cells BL21 (DE3). The expression plasmid DNA (1  $\mu$ l) was added to the competent cells (100  $\mu$ l) and plated onto an LB agar (Lenox L broth base). After 18 h the colonies were selected and transferred initially into 5 ml LB media and placed under orbital agitation at 37 °C for about 7 hours. All media contained 50  $\mu$ g/ml of kanamycin.

The LB preculture (50  $\mu$ l) of BL21/pET9a-BclI was used to inoculate 50 ml of fresh G4M9 minimal medium (0.02 g/l CaCl<sub>2</sub>, 4 g/l glucose, 0.25 g/l MgSO<sub>4</sub>, 1 g/l NH<sub>4</sub>Cl, 1 g/l NaCl, 14.6 g/l Na<sub>2</sub>HPO<sub>4</sub>, 5.5 g/l KH<sub>2</sub>PO<sub>4</sub> at pH 7.20) containing kanamycin and left overnight under orbital agitation at 37 °C. The overnight culture (10 ml) was added to fresh G4M9 minimal medium (2 x 500 ml) and placed under orbital agitation at 37°C until the resulting optical density reached 1.25 at 600 nm. The production of BclI was then induced by adding 5 x 10<sup>-4</sup> M isopropyl- $\beta$ -D-thiogalactopyranoside (IPTG) and left for 4 more hours under orbital agitation. The cells were harvested by centrifugation at 10,000 rpm for 15 min. The supernatant was discarded and the pellet resuspended in MES buffer A (30 ml, 0.02 M MES, 2X10<sup>-4</sup> M ZnSO<sub>4</sub>, pH 6.35) and then frozen at -80 °C.

## **2.2.4 - Isolation and Purification of *Bacillus Cereus* 569/H/9 (BcII) Metallo- $\beta$ -lactamase.**

### **2.2.4.1 - Isolation**

To isolate the BcII metallo- $\beta$ -lactamase, the pellets described in the previous section were thawed, and then the cells were disrupted using a cell disrupter, at 12.5 Kpsi to break open the cells and release the BcII. These cells were centrifuged at 30,000 rpm for one hour and the supernatant was filtered using a 0.45  $\mu$ M Millipore filter before further purification.

### **2.2.4.2 - Purification**

The filtered supernatant was purified using fast protein liquid chromatography (FPLC). The supernatant was loaded on a SP-HP (sulphopropyl-hiprep) sepharose strong cation exchange fast flow column that was previously equilibrated using 200-300 ml of MES buffer A (20mM MES,  $2 \times 10^{-4}$  M  $ZnSO_4$ , pH 6.35). Once the supernatant was loaded and the column was washed with MES buffer A (200 ml), the enzyme was eluted using a linear gradient from 0-1 M NaCl salt concentration using the same buffer. The fractions containing the enzyme were identified using an absorbance at 280 nm. The fractions with the enzyme were combined and concentrated to 2 ml by ultracentrifugation to remove excess salt from the mixture by centrifugal concentrator using Vivaspins (Sartorius). The concentrated enzyme was rediluted in buffer A (20 ml) and passed through the column again and those fractions containing the enzyme were collected to obtain a much purer BcII enzyme. The purification chromatograms are shown in **Figures 2.5 and 2.6**.

## Chapter 2.2 - Metallo- $\beta$ -lactamase - Experimental

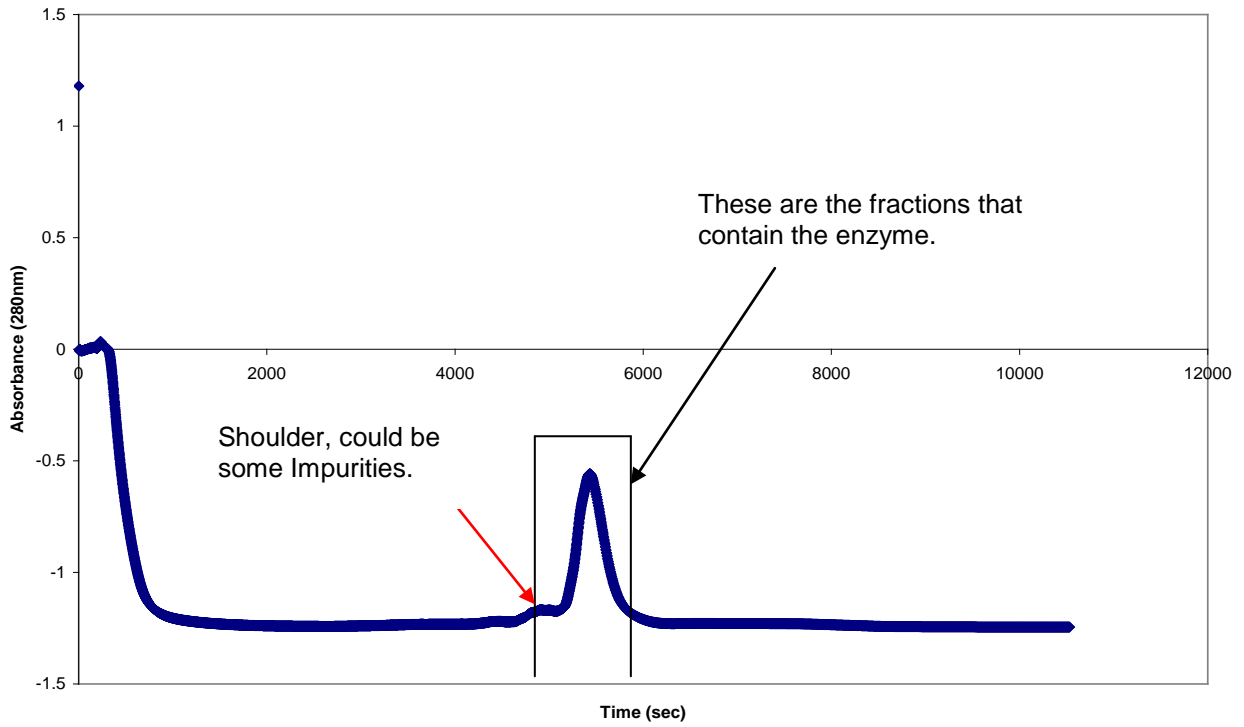


**Figure 2.5:** Chromatogram of first purification of BclI.

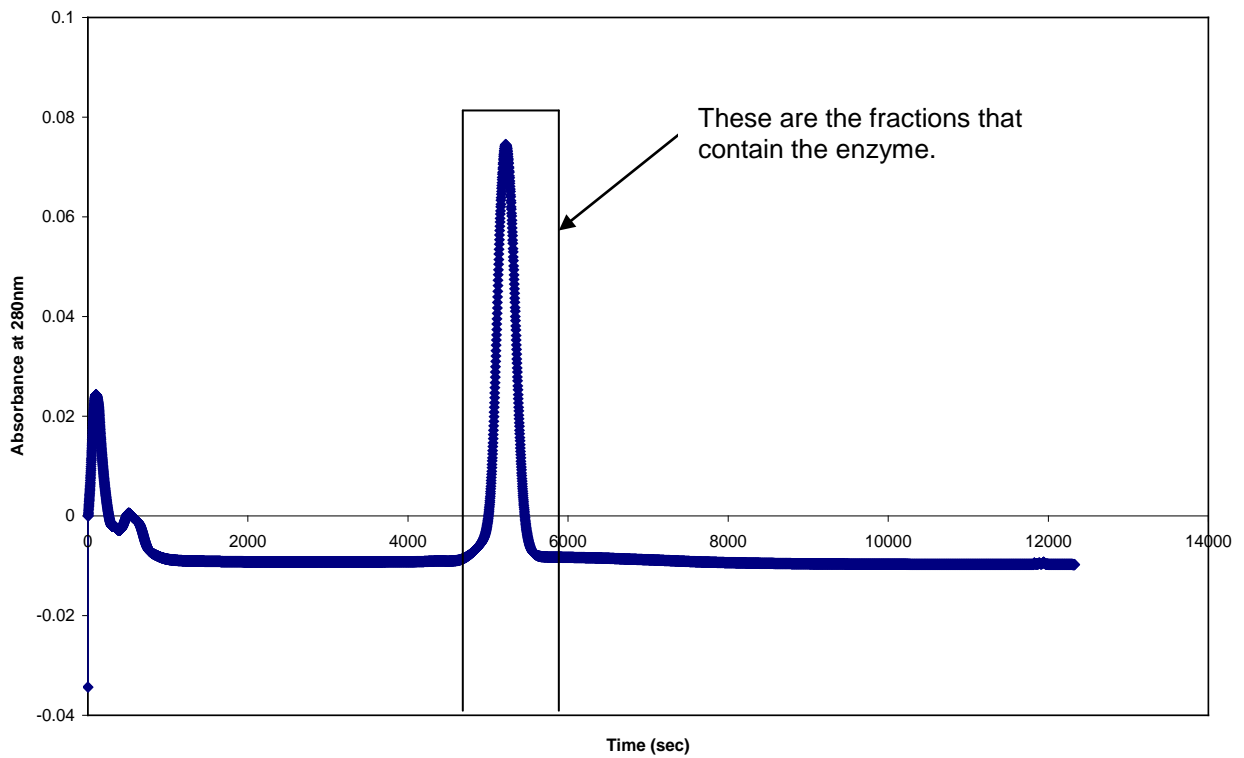


**Figure 2.6:** Chromatogram of second purification of BclI.

These are typical chromatograms for the enzyme being purified. The peaks show where the enzyme was present in the fractions. The fractions collected for this particular enzyme purification as shown in **Figure 2.5** were 28-35 and for **Figure 2.6**, the fractions collected were 26-33. **Figure 2.5** shows the peak due to the enzyme but there is a shoulder which could be due to some impurities still present. Hence the enzyme was passed through the column again and **Figure 2.6** shows a sharp peak with no shoulder.

#### **2.2.4.3 - General Procedure to Determine the Enzyme Concentration**

The concentration of the BcII enzyme was determined from the absorbance at 280 nm. The absorbance at 280 nm was divided by the extinction coefficient of BcII ( $30,500 \text{ M}^{-1}\text{cm}^{-1}$ ) to determine the concentration of the enzyme.

#### **2.2.4.4 - Determination of Enzyme Activity Based on the Rate of Hydrolysis of Benzylpenicillin**

In a typical experiment, the activity of the enzyme was determined by placing 2.0 ml of solution (enzyme (ZnBcII or apoBcII):  $1 \times 10^{-6} \text{ M}$ , buffer:  $2 \times 10^{-2} \text{ M}$ , NaCl:  $0.1 \text{ M}$ ,  $\text{ZnSO}_4$   $2 \times 10^{-4} \text{ M}$  (zinc ion was only added in some cases)) in a quartz cuvette in the thermostat cell block of the UV-spectrophotometer for 5 mins to incubate at  $25^\circ\text{C}$ . The reaction was initiated by adding 200  $\mu\text{l}$  of 10 mM benzylpenicillin solution was added to the solution in the cell giving a concentration of about  $1 \times 10^{-3} \text{ M}$ . The rate of reaction was followed by the decrease in absorbance at 236 nm, with time.

This procedure was used in three different ways throughout the research:

1. For zinc BcII enzyme activity the above procedure was followed with the addition of zinc ion.

Two stages were undertaken after the zinc ion was removed from the BcII solution.

2. Any residual activity of the apoBcII enzyme (prepared by removing zinc ion from the enzyme) was determined as above but without the addition of metal ion salt.
3. Finally, reactivation of the apoBcII enzyme was checked by the re-introduction of zinc ion to the enzyme following the above procedure. 70-80% of enzyme was recovered.

#### **2.2.4.5 - Determination of Rate Constants**

The decrease in the concentration of penicillin due to hydrolysis is exponential and the absorbance versus time curves were fitted to a simple first order rate law to obtain the pseudo first order rate constants,  $k_{obs}$ . To determine the second order rate constant  $k_{cat}/K_m$ , the  $k_{obs}$  was divided by the concentration of enzyme used. The typical values of  $k_{cat}/K_m$  determined were between  $1 \times 10^5 \text{ M}^{-1}\text{s}^{-1}$  –  $7.5 \times 10^5 \text{ M}^{-1}\text{s}^{-1}$ , indicative of an active enzyme.

#### **2.2.4.6 - Removal of Zinc ion from ZnBcII by Dialysis**

Both the ZnBcII produced in Huddersfield and ZnBcII supplied by the University of Liege were converted to apoBcII using the following procedure:

ZnBcII was dialysed with 0.02 M EDTA added to the ZnBcII solution and left stirring overnight. The EDTA from the BcII solution was removed by dialysing the solution in MES buffer over a 12 hour period initially in four steps against MES 0.02 M containing 1 M NaCl at pH 6.35 and then finally another four steps against MES 0.02 M containing 0.1 M NaCl at pH 6.35. Both buffers used were treated with Chelex 100 (2 g/100 ml) overnight before use to remove residual metal ions.

#### **2.2.4.7 - Determination of Zinc ion Concentration in ApoBclI and Buffers**

Residual zinc metal ion concentrations in the BclI solutions and buffer solutions were determined by atomic absorption spectroscopy with the following parameters: lamp wavelength at 213.9 nm, current 7 mA and Slit width 0.7 nm. A range of different concentrations of zinc sulphate were used as standards (0.001 ppm – 0.2 ppm).

The residual zinc ion concentration in buffers was around  $1 \times 10^{-9}$  M and for apoBclI it was about  $1 \times 10^{-7}$  M when the concentration of apoBclI was  $10^{-4}$  M.

#### *2.2.4.8 - Determination of EDTA concentration in apoBclI*

Residual EDTA in the apo solution was determined by proton NMR.

D<sub>2</sub>O was added to the  $1 \times 10^{-4}$  M apoBclI solution, so that D<sub>2</sub>O was present at 10 % by volume. The EDTA concentration was determined by the EDTA NMR signal intensity using a standard EDTA ( $5 \times 10^{-4}$  M) solution added to the enzyme.

In each case, three <sup>1</sup>H NMR spectra were recorded: ZnBclI before dialysis ( $10^{-4}$  M) (**Figure 2.7**), apoBclI after the dialysis (**Figure 2.8**) and apoBclI spiked with  $5 \times 10^{-4}$  M EDTA (**Figure 2.9**) so that the concentration of EDTA present in the apoBclI sample could be calculated.

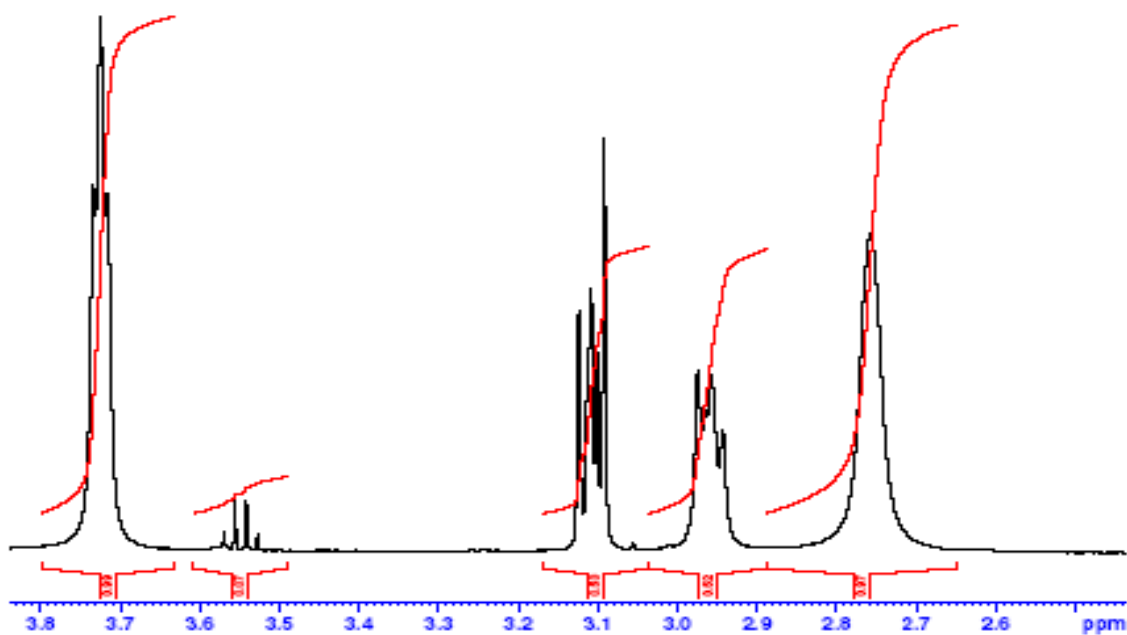


**Figure 2.7:** <sup>1</sup>H NMR spectrum of ZnBclI solution (10<sup>-4</sup> M) before treatment with EDTA.

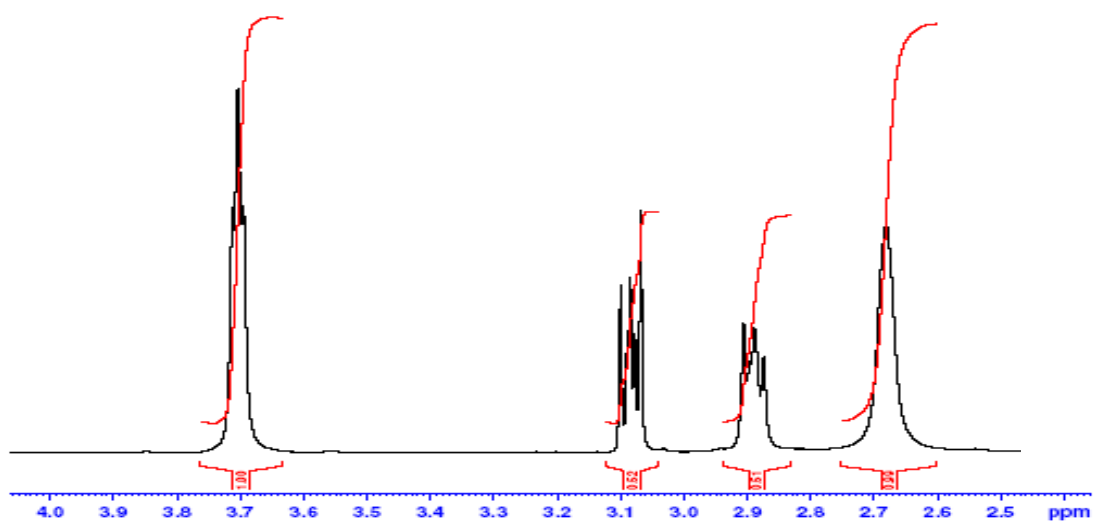


**Figure 2.8:** <sup>1</sup>H NMR spectrum of apoBclI solution (10<sup>-4</sup> M) after dialysis.

The  $^1\text{H}$  NMR spectrum in Figure 2.8 is of apoBclI solution after it was dialysed with EDTA. This can be compared with the spectrum in **Figure 2.9** which is of a BclI solution with EDTA added at  $5 \times 10^{-4}$  M concentration. The signals at 3.15 and 3.55 ppm in **Figure 2.9** are not present in **Figure 2.8** and this can be due to EDTA. The added EDTA is at a concentration in the dialysed BclI solution below the limit of detection by NMR. Based on signal to noise ratios in these spectra we estimate the limit of detection for EDTA in solution to be approximately  $1 \times 10^{-6}$  M. This is 100 times lower than the concentration of apoBclI in solution so we are confident that EDTA is not present in our enzyme solution at a level that would interfere with the titration of zinc ion with the enzyme.

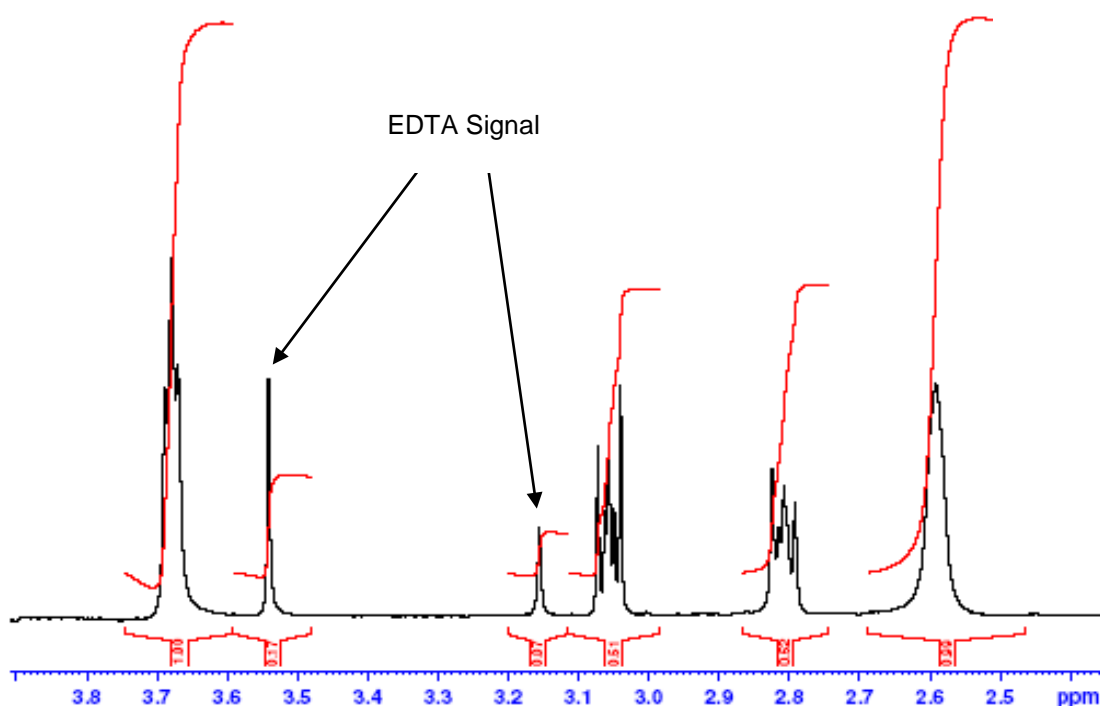


**Figure 2.9:**  $^1\text{H}$  NMR spectrum of ZnBclI solution ( $10^{-4}$  M) after treatment with EDTA.

### 2.2.5 - Settings for Isothermal Titrations

All the experiments were performed at 25°C using 1.8 ml of enzyme solution in the sample cell and 250  $\mu$ l of metal ion solution in the titrating syringe. The reference cell was filled with ultra pure water throughout all the experiments and they were performed in buffers with concentrations of buffer 0.02 M and NaCl 0.1 M at the pH indicated.

The instrument parameters for the ITC experiment on BclI solutions are shown below:

Number of injections: 25 or 64

Reference power: 10 ( $\mu$ cal/sec)

Initial delay: 60 (sec)

Stirring speed: 307 rpm

Injection parameters: Volume: 4  $\mu$ l or 10  $\mu$ l

Duration: 20 (sec)

Spacing: 180 (sec)

Filter period: 2 (sec)

This means each titration involved either 25 or 64 injections of 10  $\mu$ l or 4  $\mu$ l of metal ion solution titrated into the sample cell and the time taken for each injection was 20 secs and between each injection the spacing was 180 sec with a stirring speed of 307 rpm of the syringe.

### 2.2.6 - Estimation of Experimental Error

The experimental errors in the thermodynamic parameters that were determined from the ITC outputs were estimated based on the following:

1. Estimates of the precision of the simulations, determined by trial and error.
2. The fit for the simulation of experimental data in all cases were based on the simulated parameters assigned with the estimation of 95 % of confidence limit and this is expressed as  $\pm$  figures.

The 95% confidence limits associated with the values for the thermodynamic parameters have been assessed in the following ways. They are based on the combined effects of errors in the concentrations of the solutions used, as low concentrations and low volumes are used that can result in inevitable uncertainty, and the measured reproducibility of titration results in replicate experiments. The confidence limits for N (stoichiometric ratio) are given in the table(s). The confidence limits for the binding constants are difficult to assess and an estimate has been made that the values are generally precise to  $\pm$  10-20%. The confidence limits for  $\Delta H^\circ$  values are normally similar. The confidence limits on individual  $\Delta S^\circ$  values have been determined in each case by propagating the confidence limits on the values of  $\Delta H^\circ$  and  $\Delta G^\circ$ , and are often relatively large because  $\Delta S^\circ$  values are calculated from the differences between  $\Delta H^\circ$  and  $\Delta G^\circ$ .

## 2.3 Results

### 2.3.1 - Part One: Zinc ion Titrated into ApoBclI

Part one will present the results of titration experiments where zinc ion solution was titrated into apoBclI solution at different pH's in MES, cacodylate, acetate, MOPS, HEPES and PIPES buffer solutions. It is important to note that the results were collected using several separate batches of apoBclI enzyme.

Before titrations of metal ion solutions into enzyme solutions were performed, blank titrations were performed in which solutions of each of the three metal ions were titrated into solutions of each of the buffers used, to establish whether the metal ions exhibited interactions with the buffers. No measureable heat was detected in any of the cases, other than that due to dilution of the metal ion (measured separately). In addition, no heat was detected due to interactions between the enzyme and each of the buffers in similar blank titrations in which buffer solutions were titrated into enzyme solution.

Zinc ion solution was titrated into ApoBclI solution in six different buffers at six pH's at 25°C as described in the Experimental section.

In the following, titrations are described and simulated at the various pH's in the various buffers. The values for the reaction stoichiometric ratios,  $K_b$  and  $\Delta H_{obs}^{\circ}$ , determined from simulation and  $\Delta S_{obs}^{\circ}$  obtained by calculation from  $K_b$ , and  $\Delta H_{obs}^{\circ}$  are summarised in **Table 2.13** and discussed as a whole later.

It should be pointed out here that the values of  $\Delta S_{obs}^{\circ}$  obtained from the free energy of binding, from  $K_b$ , and  $\Delta H_{obs}^{\circ}$  actually contain a temperature independent term, an enthalpy term due to protons released and neutralised by the buffer. They are included at this stage simply because they will give us a good indication how the  $\Delta S_{obs}^{\circ}$  values are calculated from the ITC. But the

values are a complex mixture of terms as will be elaborated upon later and in the discussion section. Note - “bearing in mind there is relatively large confidence limits on the stoichiometric ratios”

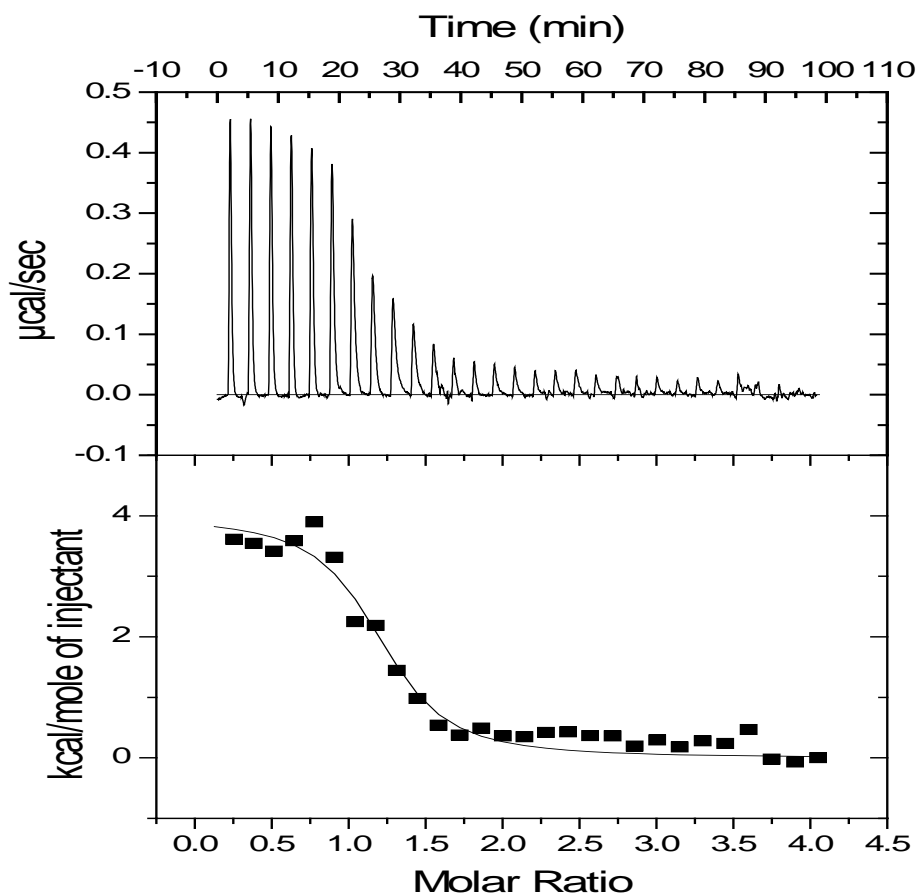


**Figure 2.10:** ITC output for  $\text{ZnSO}_4$  solution ( $3.6 \times 10^{-4}$  M) titrated into apoBclI solution ( $1.8 \times 10^{-5}$  M) in MES buffer at pH 5.20 at 25 °C.

A typical calorimetric output is shown in **Figure 2.10**. This is for a titration at pH 5.20 in MES buffer. In all cases when zinc ion is involved, as here, this output represents an endothermic reaction and is simulated as a single binding event. In this case, the isotherm is simulated with a stoichiometric ratio of  $1.2(\pm 0.2):1$  ( $\text{Zn}^{2+}$ : Enz), the binding constant ( $K_b$ ) is  $1.2(\pm 0.4) \times 10^6 \text{ M}^{-1}$ ,  $\Delta H^{\circ}_{\text{obs}}$  is  $17 (\pm 2) \text{ kJ mol}^{-1}$  and it is compensated by a positive  $\Delta S^{\circ}_{\text{obs}}$  of  $172 (\pm 32) \text{ J mol}^{-1} \text{ K}^{-1}$ .

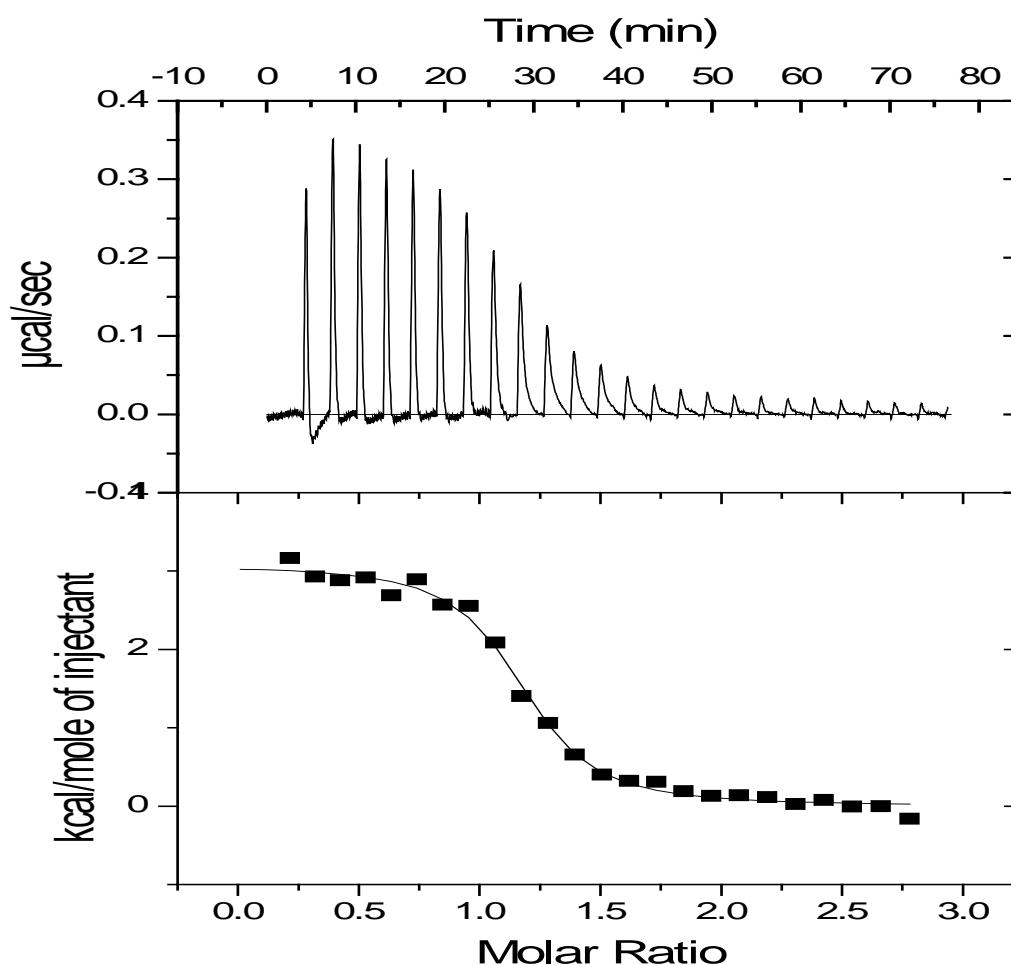


**Figure 2.11:** ITC output for  $\text{ZnSO}_4$  solution ( $3.6 \times 10^{-4}$  M) titrated into apoBclI solution ( $1.8 \times 10^{-5}$  M) in MES buffer at pH 5.60 at 25 °C.

At pH 5.60 in MES buffer, a single binding event also appears (**Figure 2.11**) with a stoichiometric ratio of  $1.3 (\pm 0.2): 1$  ( $\text{Zn}^{2+} : \text{Enz}$ ), a binding constant ( $K_b$ ) of  $2.8 (\pm 0.2) \times 10^6 \text{ M}^{-1}$ ,  $\Delta H_{\text{obs}}^{\circ}$  of  $13 (\pm 4) \text{ kJ mol}^{-1}$  and  $\Delta S_{\text{obs}}^{\circ}$  of  $166 (\pm 38) \text{ J mol}^{-1} \text{ K}^{-1}$ . The values for the  $\text{Zn}^{2+} : \text{Enz}$  ratio,  $K_b$ ,  $\Delta H_{\text{obs}}^{\circ}$  and,  $\Delta S_{\text{obs}}^{\circ}$  at this pH, are similar to those at pH 5.20.

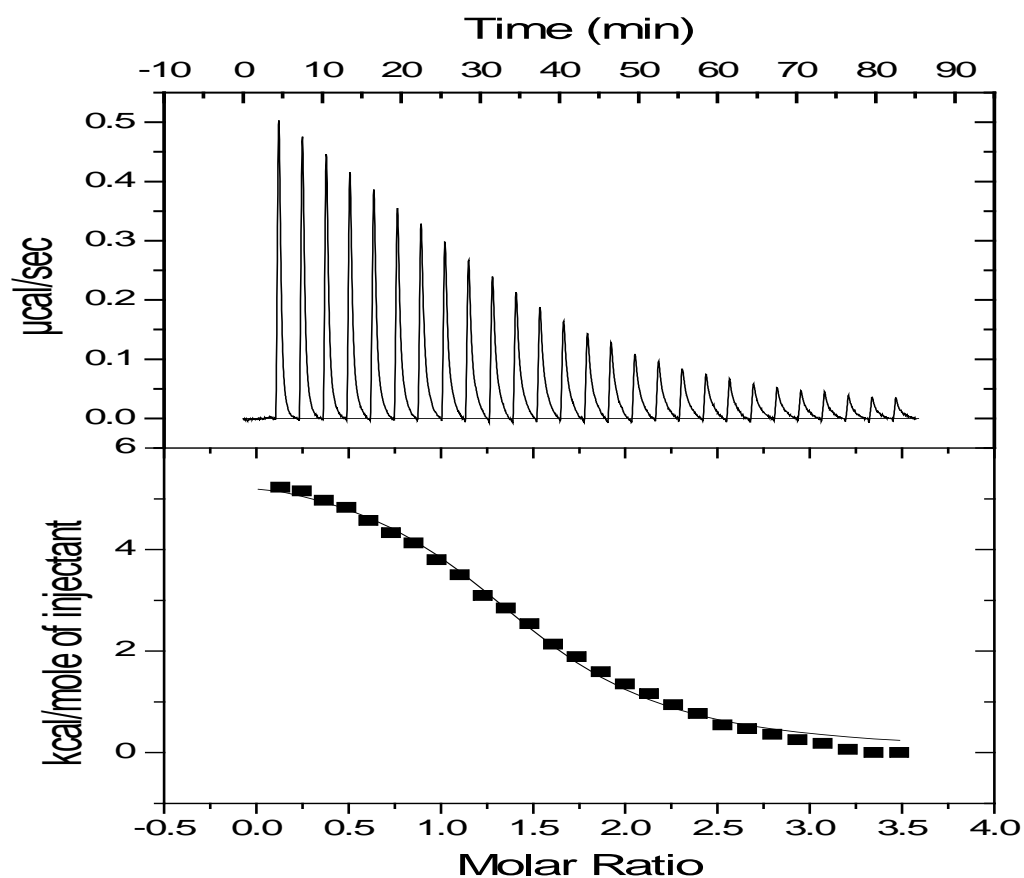


**Figure 2.12:** ITC output for  $\text{ZnSO}_4$  solution ( $3.6 \times 10^{-4}$  M) titrated into apoBclI solution ( $1.8 \times 10^{-5}$  M) in MES buffer at pH 6.0 at 25 °C.

As the pH is increased from 5.60 to 6.0, the titration of zinc ion solution into apoBclI solution (**Figure 2.12**) still shows a single binding event but with a stoichiometric ratio that increases to 1.7 ( $\pm 0.5$ ):1 ( $\text{Zn}^{2+}$ : Enz),  $K_b$  decreases to  $1.1(\pm 0.1) \times 10^5 \text{ M}^{-1}$  due to a reduction in  $\Delta H_{\text{obs}}^{\circ}$  to 7 ( $\pm 2$ )  $\text{kJ mol}^{-1}$  but a less favourable  $\Delta S_{\text{obs}}^{\circ}$  of 130 ( $\pm 20$ )  $\text{J mol}^{-1} \text{ K}^{-1}$ . The  $K_b$  value is significantly lower than at pH 5.60.

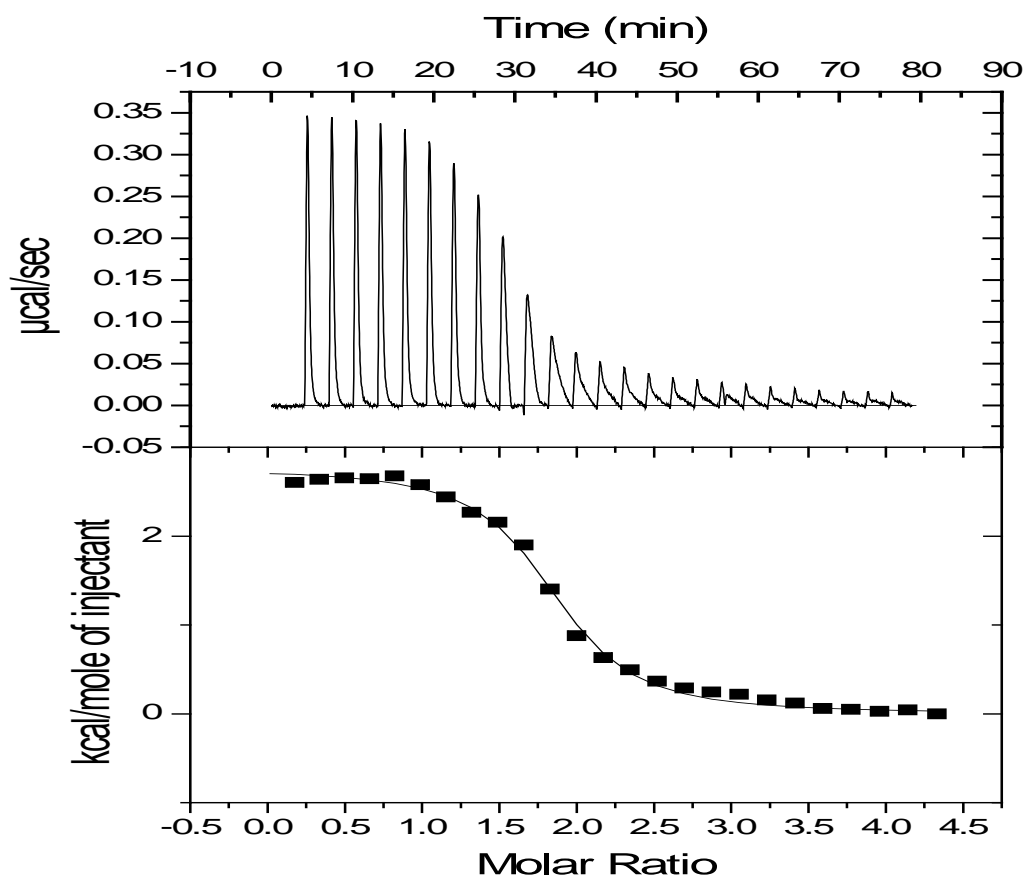


**Figure 2.13:** ITC output for  $\text{ZnSO}_4$  solution ( $3.6 \times 10^{-4}$  M) titrated into apoBclI solution ( $1.8 \times 10^{-5}$  M) in MES buffer at pH 6.35 at 25 °C.

In **Figure 2.13** the experimental data and simulation for zinc ion solution titrated into apoBclI solution at pH 6.35 is still characteristic of a single binding event. The stoichiometric ratio is now 1.80 ( $\pm 0.4$ ):1 ( $\text{Zn}^{2+}$ : Enz). The stoichiometric ratio has increased as the pH has increased from pH 5.20. At pH 6.35  $K_b$  is  $1.6 (\pm 0.2) \times 10^6$  M,  $\Delta H_{\text{obs}}^{\circ}$  is 12 ( $\pm 6$ )  $\text{kJ mol}^{-1}$  and  $\Delta S_{\text{obs}}^{\circ}$  is 157 ( $\pm 40$ )  $\text{J mol}^{-1} \text{K}^{-1}$ .

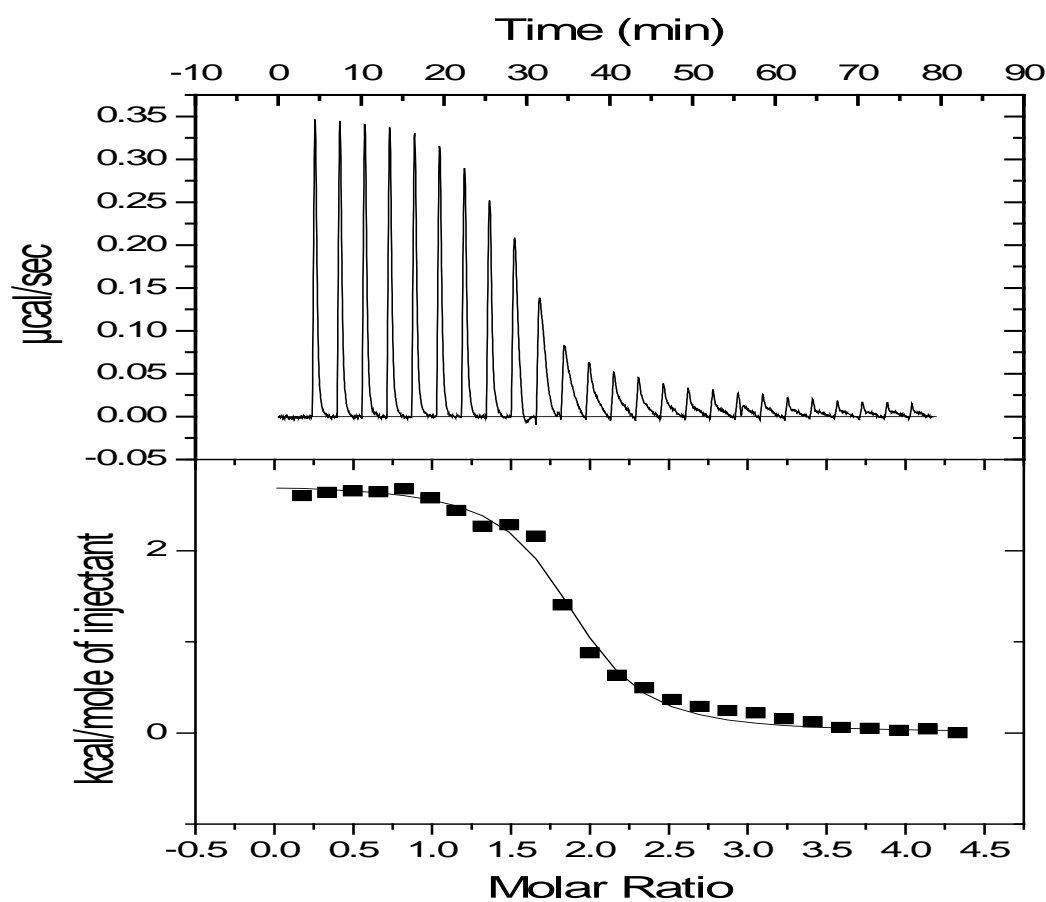


**Figure 2.14:** ITC output of  $\text{ZnSO}_4$  solution ( $3.6 \times 10^{-4}$  M) titrated into apoBclI solution ( $1.8 \times 10^{-5}$  M) in MES buffer at pH 6.80 at 25 °C.

At pH 6.80, a single binding event is again seen in **Figure 2.14**. The stoichiometric ratio is now  $2.0 (\pm 0.3):1$  ( $\text{Zn}^{2+}$ : Enz).  $K_b$  is  $2.0 (\pm 0.4) \times 10^6 \text{ M}^{-1}$ ,  $\Delta H^\circ_{\text{obs}}$  is  $11 (\pm 3) \text{ kJ mol}^{-1}$  and  $\Delta S^\circ_{\text{obs}}$  is  $159 (\pm 35) \text{ J mol}^{-1} \text{ K}^{-1}$ .

The fact that only one binding event is seen (one end point) implies that at pH 6.80, where two zinc ions bind per enzyme, the two binding sites are occupied simultaneously. If the zinc ions did not bind simultaneously then two end points would have been seen in the titration.

A summary of the results for zinc ions binding to apoBclI in MES buffer is given in **Table 2.3**. It can be seen that the molar ratio of zinc ions binding to the apoBclI increases from one to two as the pH is increased. From pH 5.20 to pH 6.80 the binding constants are quite similar of the order  $10^6 \text{ M}^{-1}$ , except the value at pH 6.0 for which we currently have no explanation. The  $\Delta H_{\text{obs}}^{\circ}$  and the apparent  $\Delta S_{\text{obs}}^{\circ}$  vary as the pH is increased as do the number of zinc ions binding.

**Table 2.3:** Simulated data for zinc ion solution titrated into apoBclI in MES buffer.

		pH				
		5.20	5.60	6.0	6.35	6.80
<b>MES Buffer</b>	N ( $\text{Zn}^{2+}:\text{Enz}$ )	1.2 ( $\pm 0.2$ )	1.3 ( $\pm 0.2$ )	1.7 ( $\pm 0.5$ )	1.8 ( $\pm 0.2$ )	2.0 ( $\pm 0.3$ )
	$K_b (\text{M}^{-1})$	$1.2(\pm 0.4) \times 10^6$	$2.8(\pm 0.2) \times 10^6$	$1.1(\pm 0.1) \times 10^5$	$1.6(\pm 0.2) \times 10^6$	$2.0(\pm 0.4) \times 10^6$
	$\Delta H_{\text{obs}}^{\circ} (\text{kJ mol}^{-1})$	17 ( $\pm 2$ )	13 ( $\pm 4$ )	7 ( $\pm 2$ )	12 ( $\pm 6$ )	11 ( $\pm 3$ )
	$\Delta S_{\text{obs}}^{\circ} (\text{J mol}^{-1} \text{K}^{-1})$	172 ( $\pm 38$ )	166 ( $\pm 20$ )	130 ( $\pm 20$ )	157 ( $\pm 40$ )	159 ( $\pm 35$ )

The positive entropies of binding are interesting for a formally bimolecular association reaction which might be expected to show a large negative change. This is probably due to desolvation and liberation of water molecules upon zinc ion binding to enzyme.

Another interesting observation is that the binding stoichiometry varies with pH which indicates that it is associated with proton release. Any production of protons would be neutralised by the excess buffer present and this process would contribute to the observed changes in heat. Therefore similar titrations were performed using cacodylate buffer, to see if the buffer has an effect on the enthalpy measured on binding of zinc ion to apoBclI.

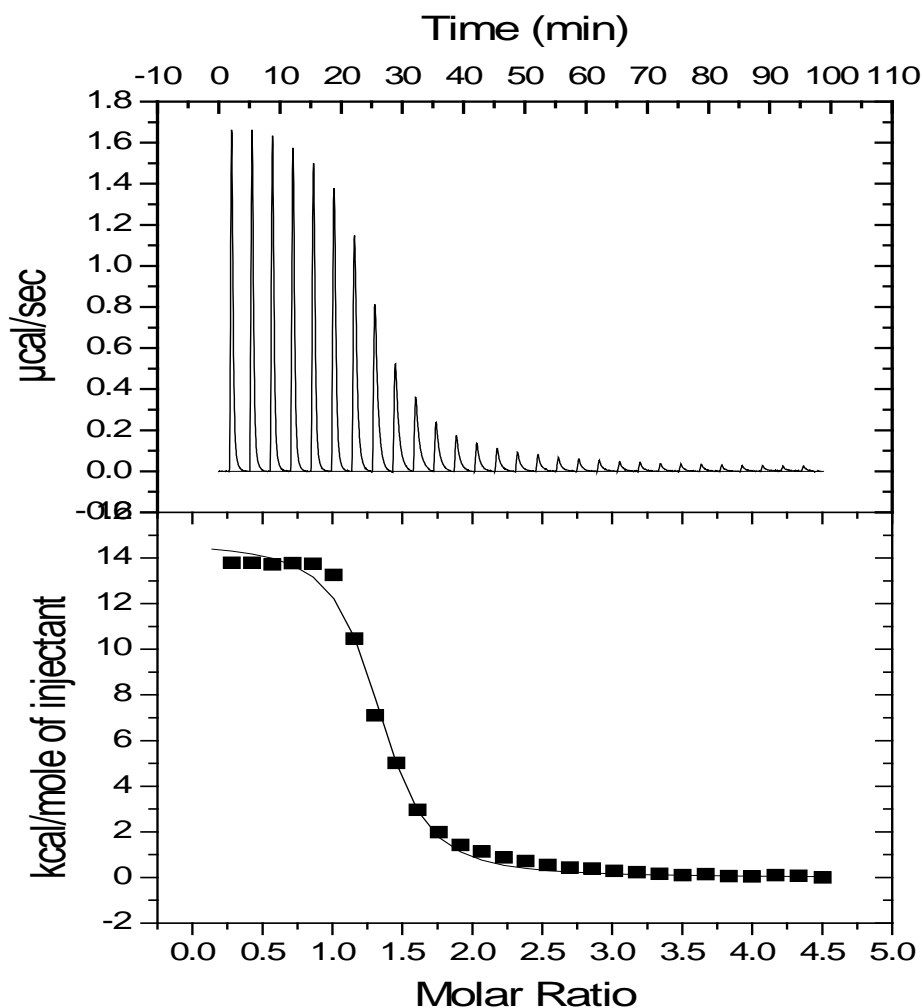


**Figure 2.15:** ITC output for  $\text{ZnSO}_4$  solution ( $3.6 \times 10^{-4}$  M) titrated into apoBclI solution ( $1.8 \times 10^{-5}$  M) in cacodylate buffer at pH 5.20 at 25 °C.

At pH 5.20, the isotherm recorded in cacodylate in **Figure 2.15** is simulated in terms of a stoichiometric ratio of 1.3 ( $\pm 0.2$ ):1 ( $\text{Zn}^{2+}$ : Enz),  $K_b$  of  $1.4 (\pm 0.3) \times 10^6 \text{ M}^{-1}$ ,  $\Delta H_{\text{obs}}^{\circ}$  is  $62 (\pm 8) \text{ kJ mol}^{-1}$  and apparent  $\Delta S_{\text{obs}}^{\circ}$  is  $328 (\pm 30) \text{ J mol}^{-1} \text{ K}^{-1}$ . Comparing to the titration in MES buffer at pH 5.20 the stoichiometry and  $K_b$  are very similar. The large differences seen in  $\Delta H_{\text{obs}}^{\circ}$  and the apparent  $\Delta S_{\text{obs}}^{\circ}$  must be due to the cacodylate buffer which has a different enthalpy of ionisation to that for MES.

Figures 2.16 to 2.19 show the titration isotherms in cacodylate buffer between pH 5.60 to 6.80 and the simulation data is given below each figure in a table.

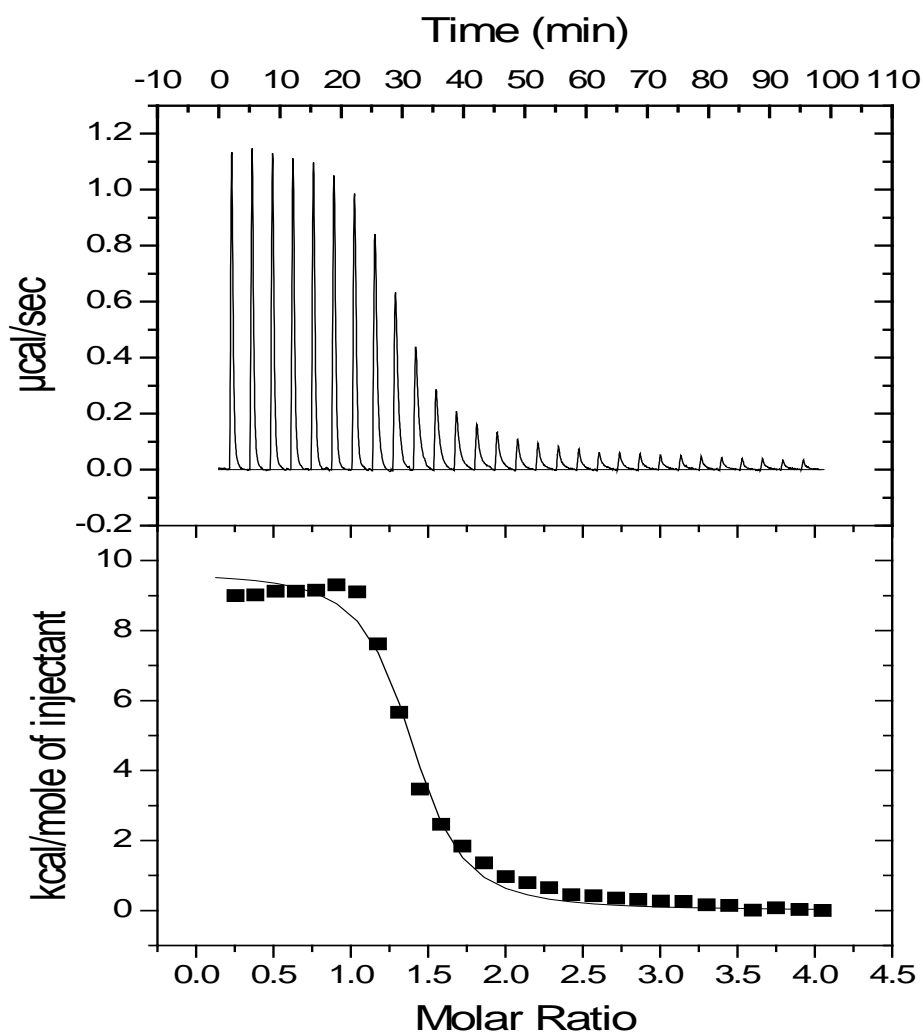


**Figure 2.16:** ITC output for  $\text{ZnSO}_4$  solution ( $3.6 \times 10^{-4}$  M) titrated into apoBclI solution ( $1.8 \times 10^{-5}$  M) in cacodylate buffer at pH 5.60 at 25 °C.

**Table 2.4:** Simulation data for the titration in Figure 2.16.

N ( $\text{Zn}^{2+}:\text{Enz}$ )	1.4 ( $\pm 0.2$ )
$K_b$ ( $\text{M}^{-1}$ )	$2.1 (\pm 0.3) \times 10^6$
$\Delta H_{\text{obs}}^{\circ}$ ( $\text{kJ mol}^{-1}$ )	41 ( $\pm 5$ )
$\Delta S_{\text{obs}}^{\circ}$ ( $\text{J mol}^{-1} \text{K}^{-1}$ )	258 ( $\pm 20$ )

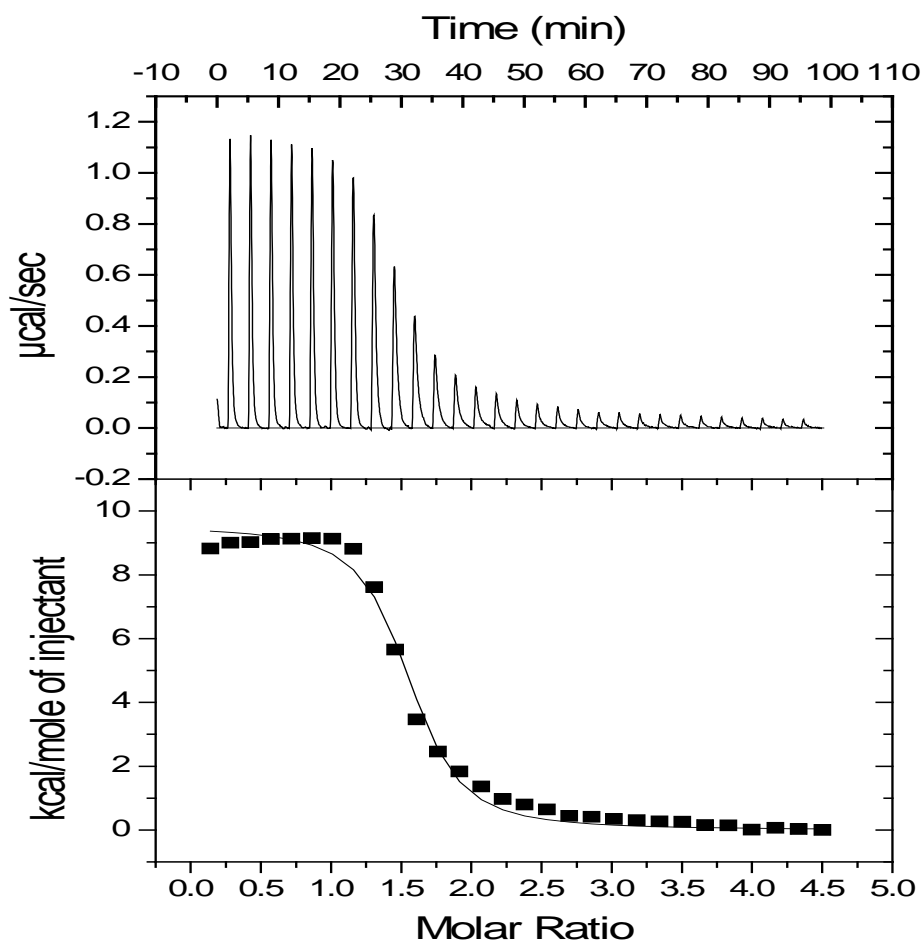


**Figure 2.17:** ITC output for  $\text{ZnSO}_4$  solution ( $3.6 \times 10^{-4}$  M) titrated into apoBclI solution ( $1.8 \times 10^{-5}$  M) in cacodylate buffer at pH 6.0 at 25 °C.

**Table 2.5:** Simulation data for the titration in Figure 2.17.

$N (\text{Zn}^{2+}:\text{Enz})$	$1.5 (\pm 0.4)$
$K_b (\text{M}^{-1})$	$2.5 (\pm 0.4) \times 10^6$
$\Delta H_{\text{obs}}^{\circ} (\text{kJ mol}^{-1})$	$40 (\pm 10)$
$\Delta S_{\text{obs}}^{\circ} (\text{J mol}^{-1} \text{K}^{-1})$	$256 (\pm 60)$

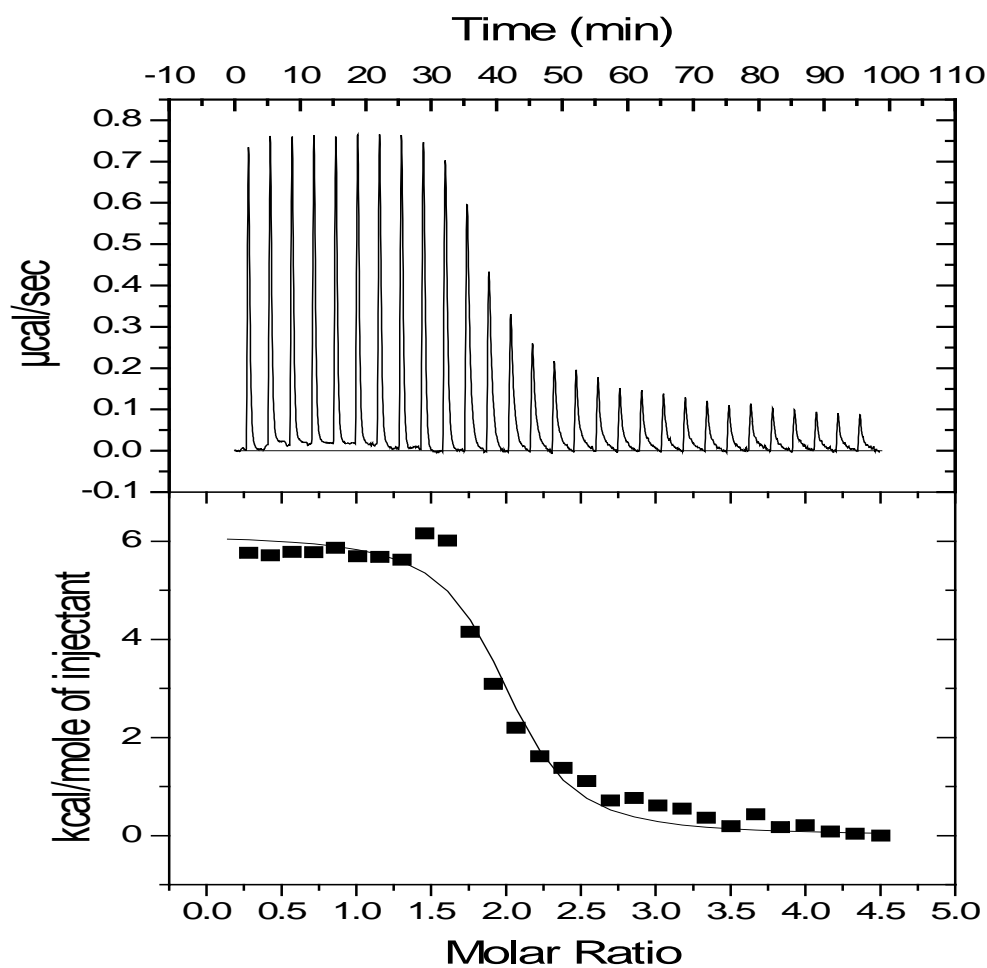


**Figure 2.18:** ITC output for  $\text{ZnSO}_4$  solution ( $3.6 \times 10^{-4}$  M) titrated into apoBclI solution ( $1.8 \times 10^{-5}$  M) in cacodylate buffer at pH 6.35 at 25 °.

**Table 2.6:** Simulation data for the titration in Figure 2.18.

N ( $\text{Zn}^{2+}$ :Enz)	2.0 ( $\pm 0.3$ )
$K_b$ ( $\text{M}^{-1}$ )	$2.3 (\pm 0.3) \times 10^6$
$\Delta H_{\text{obs}}^{\circ}$ ( $\text{kJ mol}^{-1}$ )	26 ( $\pm 8$ )
$\Delta S_{\text{obs}}^{\circ}$ ( $\text{J mol}^{-1} \text{K}^{-1}$ )	207 ( $\pm 23$ )

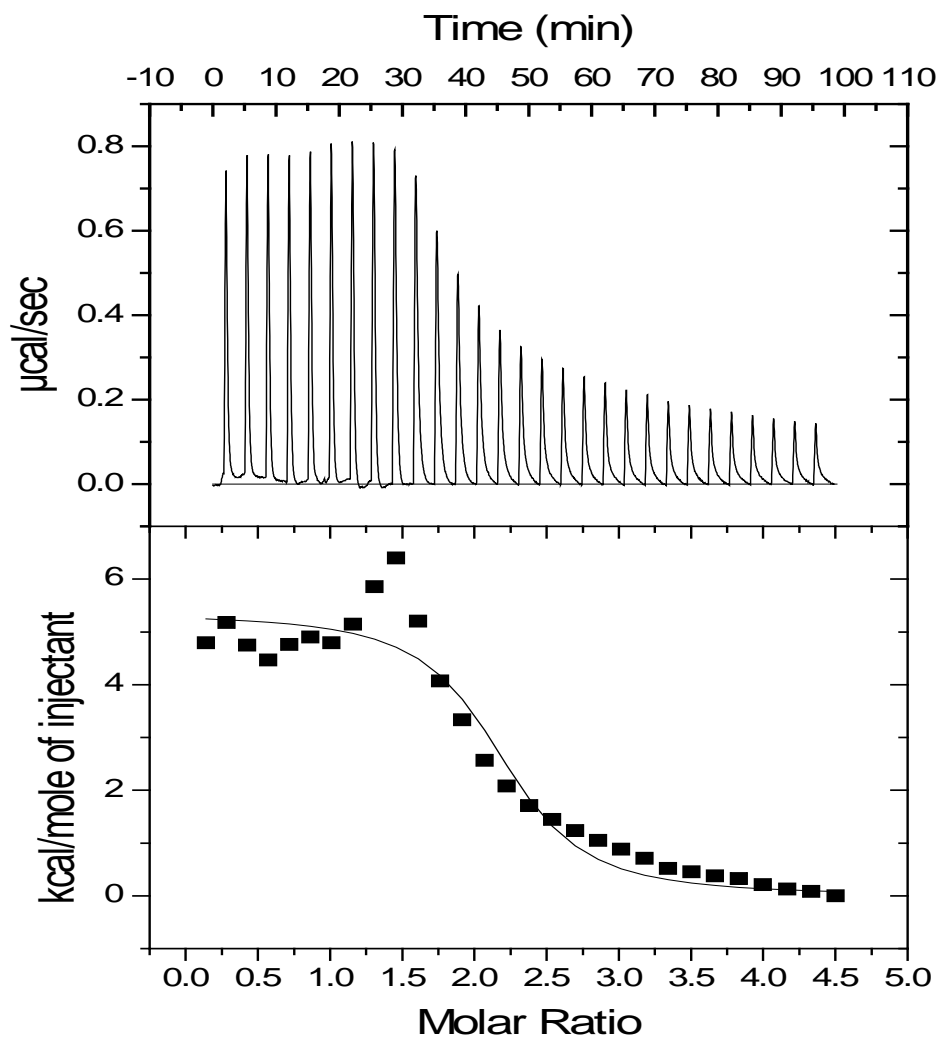


**Figure 2.19:** ITC output for  $\text{ZnSO}_4$  solution ( $3.6 \times 10^{-4}$  M) titrated into apoBclI solution ( $1.8 \times 10^{-5}$  M) in cacodylate buffer at pH 6.80 at 25 °C.

**Table 2.7:** Simulation data for the titration in Figure 2.19.

$N (\text{Zn}^{2+}:\text{Enz})$	$2.2 (\pm 0.6)$
$K_b (\text{M}^{-1})$	$2.4 (\pm 1) \times 10^6$
$\Delta H_{\text{obs}}^{\circ} (\text{kJ mol}^{-1})$	$22 (\pm 4)$
$\Delta S_{\text{obs}}^{\circ} (\text{J mol}^{-1} \text{K}^{-1})$	$193 (\pm 50)$

Here we shall just look at just two of the buffers used to see the trend and the other data will be shown later and discussed as a whole.

**Table 2.8:** Simulation data for zinc ion solution titrated into apoBclI in MES and cacodylate buffer.

		pH				
		5.20	5.60	6.0	6.35	6.80
<b>MES Buffer</b>	N (Zn <sup>2+</sup> :Enz)	<b>1.2 (<math>\pm</math> 0.2)</b>	<b>1.3 (<math>\pm</math> 0.2)</b>	<b>1.7 (<math>\pm</math> 0.5)</b>	<b>1.8 (<math>\pm</math> 0.2)</b>	<b>2.0 (<math>\pm</math> 0.3)</b>
	K <sub>b</sub> (M <sup>-1</sup> )	1.2( $\pm$ 0.4) x10 <sup>6</sup>	2.8( $\pm$ 0.2)x10 <sup>6</sup>	1.1( $\pm$ 0.1)x10 <sup>5</sup>	1.6( $\pm$ 0.2)x10 <sup>6</sup>	2.0( $\pm$ 0.4) x10 <sup>6</sup>
	$\Delta H^{\circ}_{\text{obs}}$ (kJ mol <sup>-1</sup> )	17 ( $\pm$ 2)	13 ( $\pm$ 4)	7 ( $\pm$ 2)	12 ( $\pm$ 6)	11 ( $\pm$ 3)
	$\Delta S^{\circ}_{\text{obs}}$ (J mol <sup>-1</sup> K <sup>-1</sup> )	172 ( $\pm$ 38)	166 ( $\pm$ 20)	130 ( $\pm$ 20)	157 ( $\pm$ 40)	159 ( $\pm$ 35)
<b>Cacodylate Buffer</b>	N (Zn <sup>2+</sup> :Enz)	<b>1.3 (<math>\pm</math> 0.2)</b>	<b>1.4 (<math>\pm</math> 0.2)</b>	<b>1.5 (<math>\pm</math> 0.4)</b>	<b>2.0 (<math>\pm</math> 0.3)</b>	<b>2.2 (<math>\pm</math> 0.6)</b>
	K <sub>b</sub> (M <sup>-1</sup> )	1.4( $\pm$ 0.3) x10 <sup>6</sup>	2.8( $\pm$ 0.4) X10 <sup>6</sup>	2.5( $\pm$ 0.4)x10 <sup>6</sup>	2.3( $\pm$ 0.3)x10 <sup>6</sup>	2.4( $\pm$ 1) x10 <sup>6</sup>
	$\Delta H^{\circ}_{\text{obs}}$ (kJ mol <sup>-1</sup> )	62 ( $\pm$ 8)	41 ( $\pm$ 5)	40 ( $\pm$ 10)	26( $\pm$ 8)	22 ( $\pm$ 4)
	$\Delta S^{\circ}_{\text{obs}}$ (J mol <sup>-1</sup> K <sup>-1</sup> )	328 ( $\pm$ 30)	258 ( $\pm$ 20)	256 ( $\pm$ 60)	207 ( $\pm$ 23)	191 ( $\pm$ 50)

Comparing the data obtained in cacodylate and MES buffers (**Table 2.8**), the following points arise:

1. The stoichiometric ratio of Zn<sup>2+</sup>: Enz increases from one to two as the pH increases from 5.20 to pH 6.80 in both buffers.
2. Only single binding events are seen throughout, implying that when two zinc ions bind it is by cooperative binding. This is in agreement with a recent report by Jacquin et al.<sup>62</sup>
3. Binding constants measured in the buffers are similar and of the order of 10<sup>6</sup> M<sup>-1</sup> at all pH's with an exception at pH 6.0 in MES buffer which, as it is seen not seen in cacodylate buffer, may be an experimental error, in which case we can conclude the K<sub>b</sub> does not vary significantly over the pH range, 5.20 to 6.80.
4. Observed molar enthalpies of binding vary with buffer type. If protons are released upon zinc ion binding, then the heat released by

neutralisation with buffer will vary due to the different dissociation enthalpies of the buffer. In MES buffer there does not seem to be significant variation with pH whereas in cacodylate buffer, the value of  $\Delta H_{\text{obs}}^{\circ}$  falls as the pH is increased.

To elucidate the intrinsic thermodynamic parameters, other titrations were performed the same pH's using HEPES, MOPS, PIPES and acetate buffers. The experimental data simulations of titrations in HEPES and MOPS buffers are shown in the following pages.

The experimental titration data in HEPES and MOPS are shown in **Figures 2.20 to 2.23**. Interestingly, the observed heat changes in these buffers appear exothermic in contrast to the previous endothermic ones, which highlight the important contribution of buffer to the overall process. In HEPES and MOPS buffers there is only a single binding event observed consistent with the results in other buffers. The simulation data is shown summarised in **Table 2.13**.

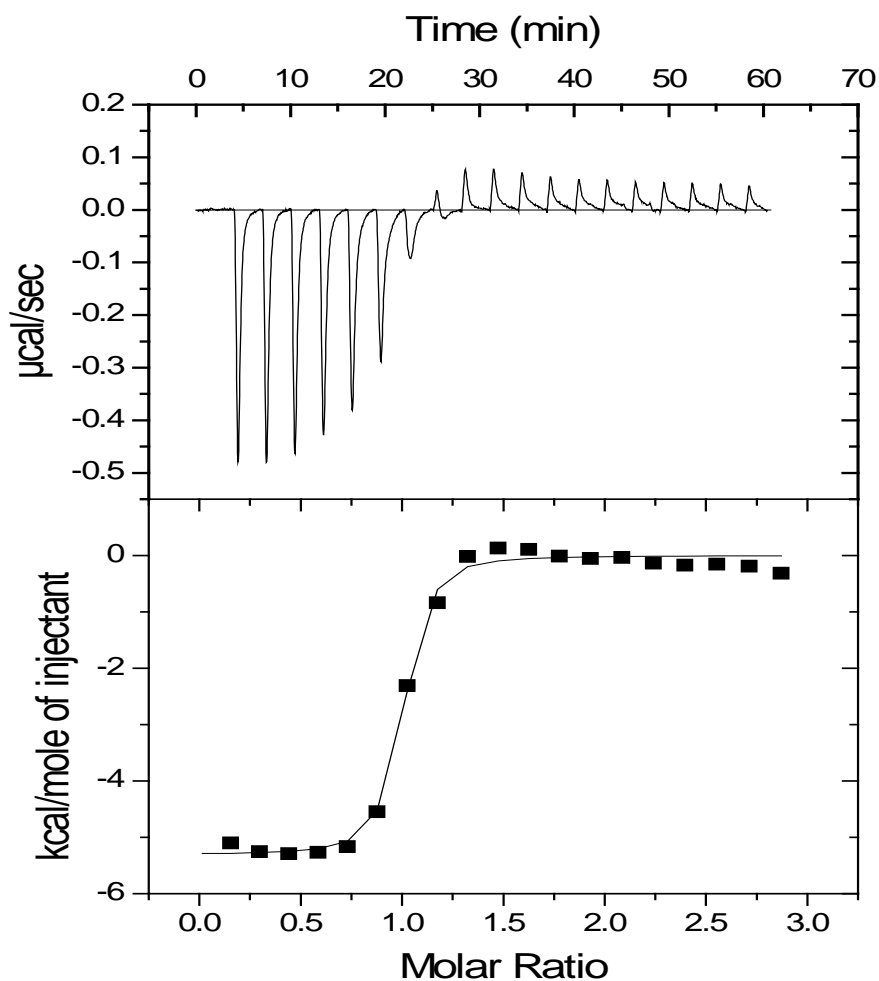


**Figure 2.20:** ITC output for  $\text{ZnSO}_4$  solution ( $3.6 \times 10^{-4}$  M) titrated into apoBclI solution ( $1.8 \times 10^{-5}$  M) in HEPES buffer at pH 6.80 at 25 °C.

**Table 2.9:** Simulation data for the titration in Figure 2.20.

N ( $\text{Zn}^{2+}:\text{Enz}$ )	1.1 ( $\pm 0.2$ )
$K_b$ ( $\text{M}^{-1}$ )	$1.99$ ( $\pm 0.4$ ) $\times 10^7$
$\Delta H_{\text{obs}}^{\circ}$ ( $\text{kJ mol}^{-1}$ )	-16 ( $\pm 2$ )
$\Delta S_{\text{obs}}^{\circ}$ ( $\text{J mol}^{-1} \text{K}^{-1}$ )	90 ( $\pm 15$ )

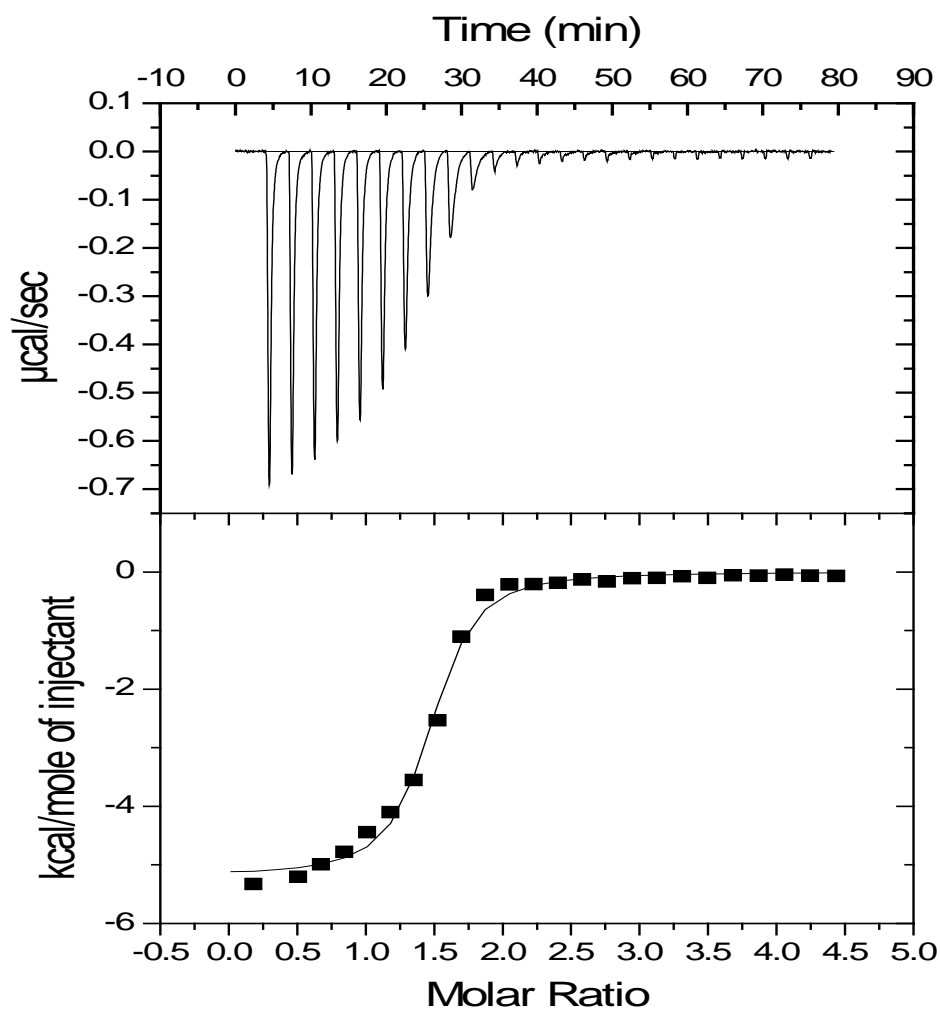


**Figure 2.21:** ITC output for  $\text{ZnSO}_4$  solution ( $3.6 \times 10^{-4}$  M) titrated into apoBclI solution ( $1.8 \times 10^{-5}$  M) in HEPES buffer at pH 7.20 at 25 °C.

**Table 2.10:** Simulation data for the titration in Figure 2.21.

$N (\text{Zn}^{2+}:\text{Enz})$	1.4 ( $\pm 0.2$ )
$K_b (\text{M}^{-1})$	$2.93 (\pm 0.4) \times 10^6$
$\Delta H_{\text{obs}}^{\circ} (\text{kJ mol}^{-1})$	-22 ( $\pm 3$ )
$\Delta S_{\text{obs}}^{\circ} (\text{J mol}^{-1} \text{K}^{-1})$	51 ( $\pm 19$ )

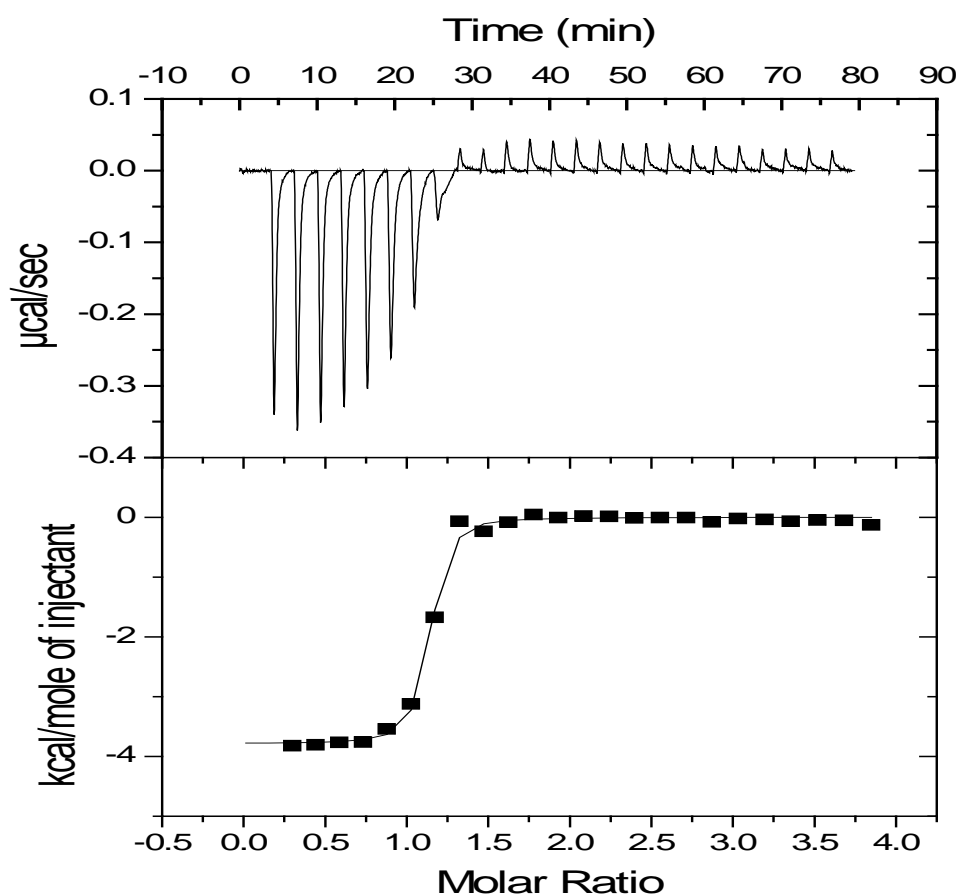


**Figure 2.22:** ITC output for  $\text{ZnSO}_4$  solution ( $3.6 \times 10^{-4}$  M) titrated into apoBclI solution ( $1.8 \times 10^{-5}$  M) in MOPS buffer at pH 6.80 at 25 °C.

**Table 2.11:** Simulation data for the titration in Figure 2.22.

$N (\text{Zn}^{2+}:\text{Enz})$	$0.9 (\pm 0.2)$
$K_b (\text{M}^{-1})$	$1.43 (\pm 0.3) \times 10^7$
$\Delta H_{\text{obs}}^{\circ} (\text{kJ mol}^{-1})$	$-22 (\pm 6)$
$\Delta S_{\text{obs}}^{\circ} (\text{J mol}^{-1} \text{K}^{-1})$	$62 (\pm 20)$

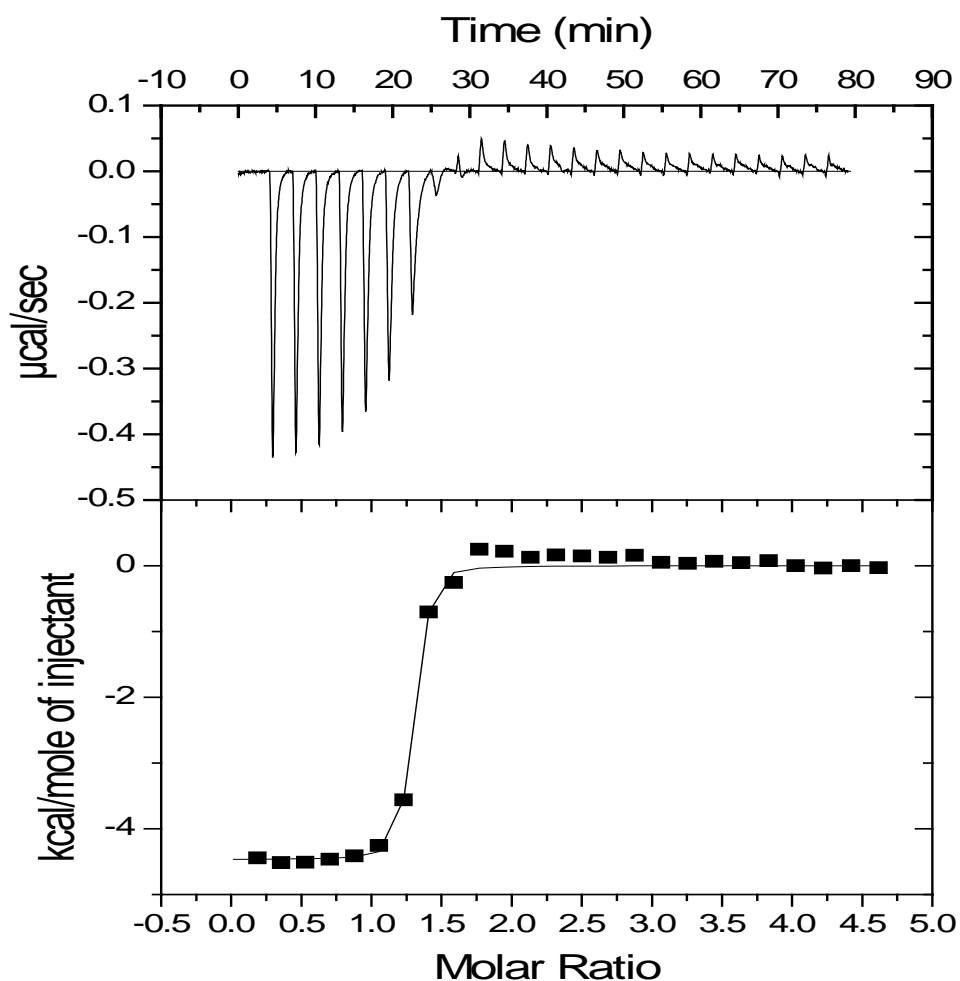


**Figure 2.23:** ITC output for  $\text{ZnSO}_4$  solution ( $3.6 \times 10^{-4}$  M) titrated into apoBclI solution ( $1.8 \times 10^{-5}$  M) in MOPS buffer at pH 7.20 at 25 °C.

**Table 2.12:** Simulation data for the titration in Figure 2.23.

$N (\text{Zn}^{2+}:\text{Enz})$	$1.2 (\pm 0.2)$
$K_b (\text{M}^{-1})$	$5 (\pm 1.1) \times 10^7$
$\Delta H_{\text{obs}}^{\circ} (\text{kJ mol}^{-1})$	$-19 (\pm 9)$
$\Delta S_{\text{obs}}^{\circ} (\text{J mol}^{-1} \text{K}^{-1})$	$85 (\pm 55)$

The overall simulation data for all the titrations of zinc ion binding to apoBclI in six different buffers are shown below in **Table 2.13**.

**Table 2.13:** Summary of simulation data for **zinc** ion solution titrated into apoBclI solution.

		<b>pH</b>					
<b>Buffers</b>		5.20	5.60	6.0	6.35	6.80	7.20
<b>Acetate</b> ( $\Delta H_{\text{ion (buffer)}} = 0.49 \text{ kJ mol}^{-1}$ ) <sup>71</sup>	N (Zn <sup>2+</sup> :Enz) K <sub>b</sub> (M <sup>-1</sup> ) $\Delta H^{\circ}_{\text{obs}}$ (kJ mol <sup>-1</sup> ) $\Delta S^{\circ}_{\text{obs}}$ (J mol <sup>-1</sup> K <sup>-1</sup> )	0.3 ± 0.6 1.13 (±0.2) × 10 <sup>5</sup> 45 (±10) 249 (±40)	0.7 ± 0.6 1.33 (±0.1) × 10 <sup>5</sup> 20 (±3) 132 (±32)				
<b>MES</b> ( $\Delta H_{\text{ion (buffer)}} = 15.53 \text{ kJ mol}^{-1}$ ) <sup>71</sup>	N (Zn <sup>2+</sup> :Enz) K <sub>b</sub> (M <sup>-1</sup> ) $\Delta H^{\circ}_{\text{obs}}$ (kJ mol <sup>-1</sup> ) $\Delta S^{\circ}_{\text{obs}}$ (J mol <sup>-1</sup> K <sup>-1</sup> )	<b>1.2 (± 0.2)</b> 1.2 (±0.4) × 10 <sup>6</sup> 17 (±2) 172 (±38)	<b>1.3 (± 0.2)</b> 2.8 (±0.2) × 10 <sup>6</sup> 13 (±4) 166 (±20)	<b>1.7 (± 0.5)</b> 1.1 (±0.1) × 10 <sup>5</sup> 7 (±2) 130 (±20)	<b>1.8 (± 0.2)</b> 1.6 (±0.2) × 10 <sup>6</sup> 12 (±6) 157 (±40)	<b>2.0 (± 0.3)</b> 2.0 (±0.4) × 10 <sup>6</sup> 11 (±3) 159 (±35)	
<b>Cacodylate</b> ( $\Delta H_{\text{ion (buffer)}} = -1.96 \text{ kJ mol}^{-1}$ ) <sup>71</sup>	N (Zn <sup>2+</sup> :Enz) K <sub>b</sub> (M <sup>-1</sup> ) $\Delta H^{\circ}_{\text{obs}}$ (kJ mol <sup>-1</sup> ) $\Delta S^{\circ}_{\text{obs}}$ (J mol <sup>-1</sup> K <sup>-1</sup> )	<b>1.3 (± 0.2)</b> 1.4 (±0.3) × 10 <sup>6</sup> 62 (±8) 328 (±30)	<b>1.4 (± 0.2)</b> 2.8 (±0.4) × 10 <sup>6</sup> 41 (±5) 258 (±20)	<b>1.5 (± 0.4)</b> 2.5 (±0.4) × 10 <sup>6</sup> 40 (±10) 256 (±60)	<b>2.0 (± 0.3)</b> 2.3 (±0.3) × 10 <sup>6</sup> 26 (±8) 207 (±23)	<b>2.2 (± 0.6)</b> 2.4 (±1) × 10 <sup>6</sup> 22 (±4) 191 (±50)	
<b>PIPES</b> ( $\Delta H_{\text{ion (buffer)}} = 11.45 \text{ kJ mol}^{-1}$ ) <sup>71</sup>	N (Zn <sup>2+</sup> :Enz) K <sub>b</sub> (M <sup>-1</sup> ) $\Delta H^{\circ}_{\text{obs}}$ (kJ mol <sup>-1</sup> ) $\Delta S^{\circ}_{\text{obs}}$ (J mol <sup>-1</sup> K <sup>-1</sup> )			1.3 ± 0.5 1.75 (±0.1) × 10 <sup>5</sup> 17 (±3) 172 (±32)	1.5 ± 0.6 1.25 (±0.4) × 10 <sup>5</sup> 20 (±5) 166 (±36)	1.6 ± 0.5 2.37 (±0.5) × 10 <sup>6</sup> 11 (±2) 159 (±40)	1.7 ± 0.3 5.50 (±0.6) × 10 <sup>5</sup> 6 (±2) 131 (±30)
<b>MOPS</b> ( $\Delta H_{\text{ion (buffer)}} = 21.82 \text{ kJ mol}^{-1}$ ) <sup>71</sup>	N (Zn <sup>2+</sup> :Enz) K <sub>b</sub> (M <sup>-1</sup> ) $\Delta H^{\circ}_{\text{obs}}$ (kJ mol <sup>-1</sup> ) $\Delta S^{\circ}_{\text{obs}}$ (J mol <sup>-1</sup> K <sup>-1</sup> )					0.9 ± 0.2 1.43 (±0.3) × 10 <sup>7</sup> -22 (±6) 62 (±20)	1.2 ± 0.2 5 (±1.0) × 10 <sup>7</sup> -19 (±9) 85 (±55)
<b>HEPES</b> ( $\Delta H_{\text{ion (buffer)}} = 21.01 \text{ kJ mol}^{-1}$ ) <sup>71</sup>	N (Zn <sup>2+</sup> :Enz) K <sub>b</sub> (M <sup>-1</sup> ) $\Delta H^{\circ}_{\text{obs}}$ (kJ mol <sup>-1</sup> ) $\Delta S^{\circ}_{\text{obs}}$ (J mol <sup>-1</sup> K <sup>-1</sup> )					1.1 ± 0.2 1.99 (±0.4) × 10 <sup>7</sup> -16 (±2) 90 (±15)	1.4 ± 0.2 2.93 (±0.4) × 10 <sup>6</sup> -22 (±3) 51 (±19)

From **Table 2.13**, the main conclusions are:

1. The number of zinc ions binding to apoBclI increases from one to two as the pH is increased from 5.2 to 6.80. This is illustrated in **Figure 2.24**, using data from two of the buffers used at every pH studied. The graph roughly follows a sigmoidal trend typical of an ionisation process.
2. When two zinc ions bind, the binding is cooperative (one end point so indicative of one binding event).
3. Binding constants are broadly similar across the pH range.

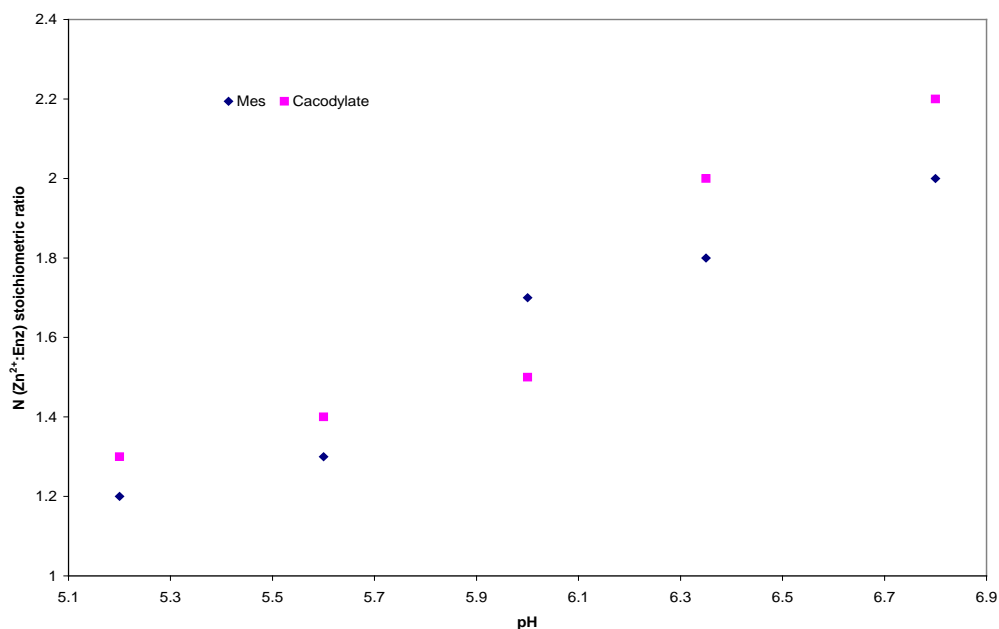


**Figure 2.24:** Plot of  $N (\text{Zn}^{2+}:\text{Enz})$  against pH for zinc ion binding to apoBclI in MES and cacodylate buffer at 25 °C.

Before any further conclusions can be drawn about the detailed nature of the binding process the molar enthalpy of binding data needs to be analysed to allow for released protons which then react with the buffer.

### 2.3.1.1 - Dissociation of Acid Groups on BclI when Zinc ion Binds

The observed molar enthalpy change ( $\Delta H^{\circ}_{\text{obs}}$ ) obtained from the titration includes heats from other events taking place as well as the binding of zinc ion to the enzyme. The other heats included are from the conformational changes that the enzyme might undergo when the metal binds ( $\Delta H_{\text{conf}}$ ) and, if the metal binding is accompanied by dissociation of one or more ( $n$ ) acid groups on the enzyme, these  $n$  released protons react with the buffer in solution, the heats of these processes also have to be included. Consequently  $\Delta H^{\circ}_{\text{obs}}$ , can be expressed as:

$$\Delta H^{\circ}_{\text{obs}} = \Delta H^{\circ}_{\text{bind}} + \Delta H^{\circ}_{\text{conf}} + n (\Delta H^{\circ}_{\text{ion (enz)}} + \Delta H^{\circ}_{\text{ion (buffer)}})$$

The combination of  $\Delta H^{\circ}_{\text{bind}} + \Delta H^{\circ}_{\text{conf}}$  is referred to as the intrinsic enthalpy of binding  $\Delta H^{\circ}_{\text{int.}}$ , so:

$$\Delta H^{\circ}_{\text{obs}} = \Delta H^{\circ}_{\text{int}} + n (\Delta H^{\circ}_{\text{ion (enz)}} + \Delta H^{\circ}_{\text{ion (buffer)}})$$

Where measurements have been made in more than one buffer at a given pH, a plot of  $\Delta H^{\circ}_{\text{obs}}$  against  $\Delta H^{\circ}_{\text{ion (buffer)}}$  gives  $n$  (number of protons) as the gradient and  $\Delta H^{\circ}_{\text{int}} + n \Delta H^{\circ}_{\text{ion (enz)}}$  as the intercept:

$$\Delta H^{\circ}_{\text{obs}} = (\Delta H^{\circ}_{\text{int}} + n \Delta H^{\circ}_{\text{ion (enz)}}) + n \Delta H^{\circ}_{\text{ion (buffer)}}$$

In principle, the two terms contributing to the value of the intercept can be separated by plotting the latter at each pH used in the experiment against  $n$ . (it is worth noting that strictly, since the buffer is reacting with a proton to form the undissociated form of the buffer, the expression should be written as  $-\Delta H^{\circ}_{\text{ion (buffer)}}$ , but conventionally the equation tends to be written as shown).

**Figure 2.25** shows the plot of  $\Delta H^{\circ}_{\text{obs}}$  against  $\Delta H^{\circ}_{\text{ion (buffer)}}$  for the three buffers used at pH 5.20. The value for  $n$  (number of protons released) was found to be 2.3. This is the total number of protons that are released upon binding and includes those that dissociate from groups on the enzyme for each zinc ion that

binds and possibly the water bound to the zinc ion if its  $pK_a$  changes on binding to the enzyme.

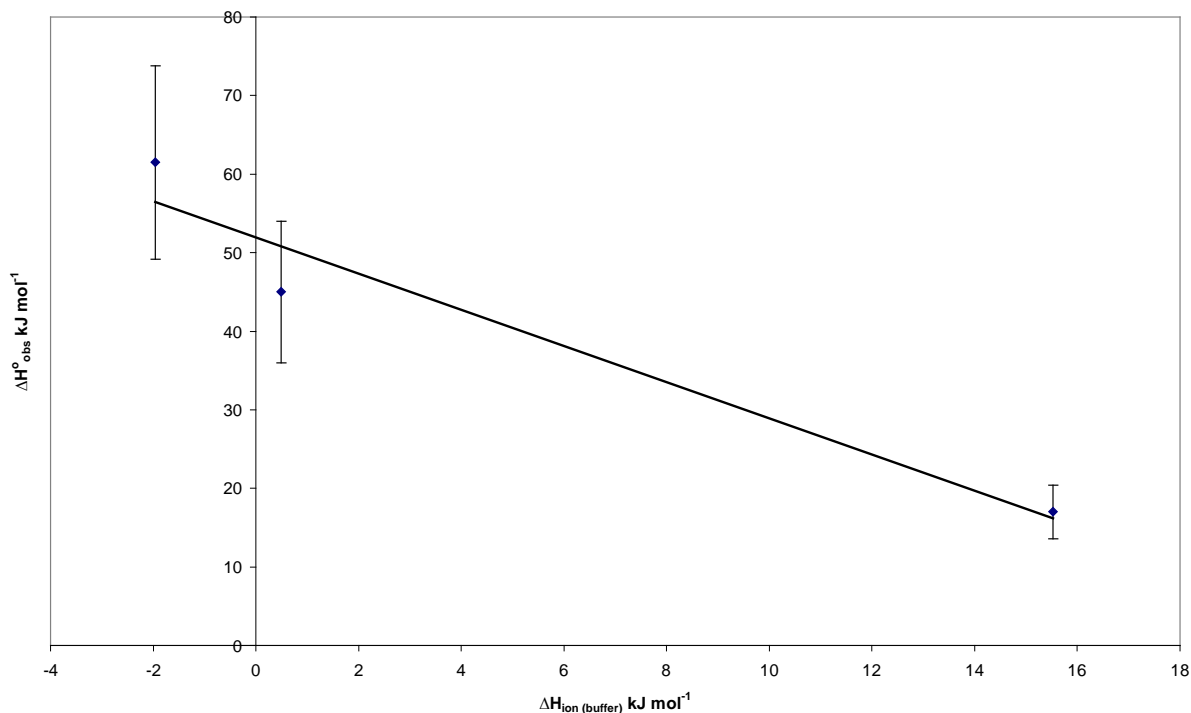


**Figure 2.25:**  $\Delta H^{\circ}_{\text{obs}}$  against  $\Delta H^{\circ}_{\text{ion (buffer)}}$  at pH 5.20 for zinc ions titrated into apoBclI solution

Data recorded at all pH's studied were treated in the same way and the values of  $n$  (number of protons released) and  $\Delta H^{\circ}_{\text{int}} + n\Delta H^{\circ}_{\text{ion (enzyme)}}$  are shown in **Table 2.14**.

**Table 2.14:** Values of  $n$  and  $(\Delta H^{\circ}_{\text{int}} + n\Delta H^{\circ}_{\text{ion (enzyme)})$  as a function of pH for zinc ion binding to apoBclI.

<i>pH</i>	<i>n (number of protons released by the enzyme)</i>	$\Delta H^{\circ}_{\text{int}} + n\Delta H^{\circ}_{\text{ion (enzyme)}}$ ( <i>kJ mol<sup>-1</sup></i> )
5.20	2.3 ( $\pm 0.5$ )	52 ( $\pm 10$ )
5.60	1.2 ( $\pm 0.4$ )	30 ( $\pm 10$ )
6.0	1.9 ( $\pm 0.5$ )	37 ( $\pm 5$ )
6.35	0.7 ( $\pm 0.3$ )	25 ( $\pm 5$ )
6.80	1.7 ( $\pm 0.3$ )	21 ( $\pm 5$ )
7.20	2.6 ( $\pm 0.5$ )	36 ( $\pm 5$ )

Looking at the data in **Table 2.14**, the number of protons released is around two at all except pH's 5.60 and 6.35. These appear to be out of line with the other values and, given the large uncertainties on the values, are assumed to be erroneous. The intercept of **Figure 2.25** equates to  $(\Delta H_{\text{int}}^{\circ} + n\Delta H_{\text{ion (enz)}}^{\circ})$ . Separating these terms to determine  $\Delta H_{\text{int}}^{\circ}$  is not easy. In this work we have made the assumption that  $\Delta H_{\text{ion (enz)}}^{\circ}$  is constant through the pH range studied and plotted  $\Delta H_{\text{int}}^{\circ} + n\Delta H_{\text{ion (enz)}}^{\circ}$  against  $n$  (number of protons released) as shown in Figure 2.26. We thus obtain  $\Delta H_{\text{int}}^{\circ}$  as the intercept and  $\Delta H_{\text{ion (enz)}}^{\circ}$  from the gradient.

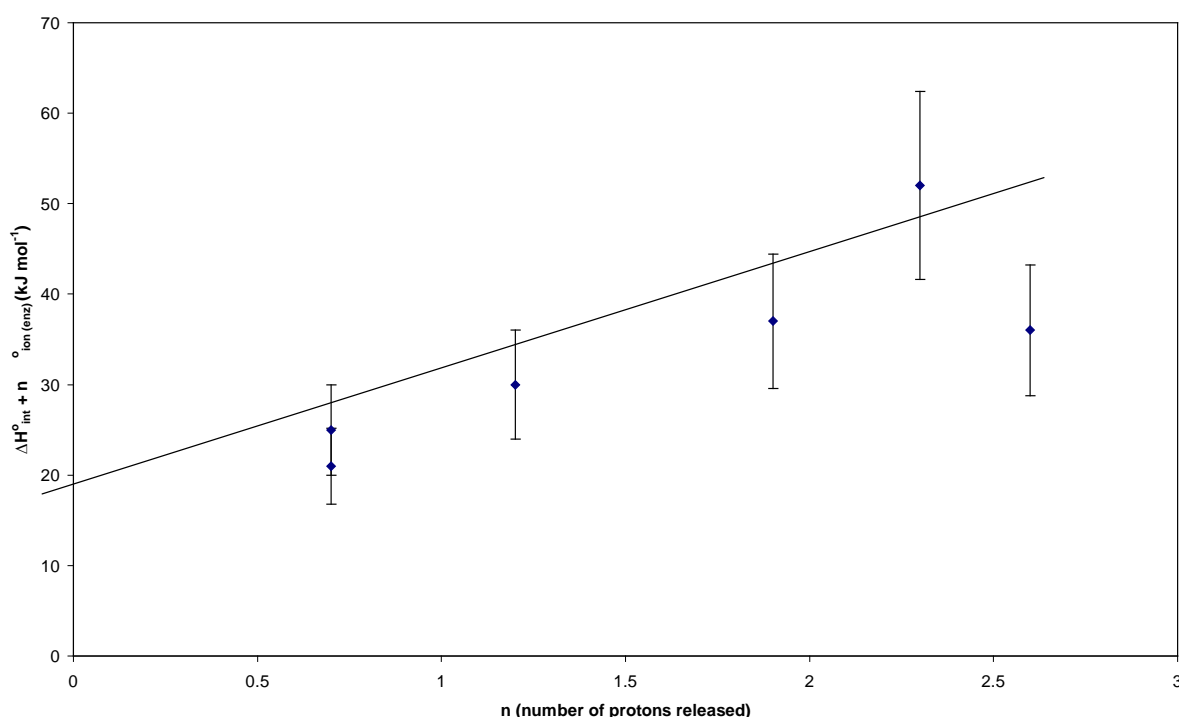


**Figure 2.26:** A plot of  $(\Delta H_{\text{int}}^{\circ} + n\Delta H_{\text{ion (enz)}}^{\circ})$  against  $n$  the number of protons released when zinc ion binds to apoBcll.

Clearly these values of  $\Delta H_{\text{int}}^{\circ}$  and  $\Delta H_{\text{ion (enz)}}^{\circ}$  are subject to large uncertainties, nevertheless, values estimated from **Figure 2.26** are:

$$\Delta H_{\text{int}}^{\circ} = 16 (\pm 10) \text{ kJ mol}^{-1} \text{ and } \Delta H_{\text{ion (enz)}}^{\circ} = 11 (\pm 5) \text{ kJ mol}^{-1}.$$

Entropy Calculations

As indicated earlier the values of  $\Delta S^{\circ}_{\text{obs}}$  are complicated because, as they are simply calculated from the equilibrium constant and  $\Delta H^{\circ}_{\text{obs}}$  they include the enthalpy of ionisation of the buffer.

The ITC titration involves the following equilibrium:



At a constant pH, the equilibrium binding constant  $K_b$  is independent of buffer type and concentration because although the protons released are neutralised by the buffer, the ratio of  $\text{BH}^+$  to B remains effectively constant and because the buffer concentration is in vast excess of the enzyme concentration.

$$K_b = \frac{(\text{EnzM})(\text{BH}^+)}{(\text{EnzH})(\text{M})(\text{B})}$$

However, the observed heat changes  $\Delta H^{\circ}_{\text{obs}}$  are dependent on the buffer as described above. Consequently, if  $\Delta H^{\circ}_{\text{obs}}$  and the free energy calculated from  $K_{\text{obs}}$  is used to calculate a term  $\Delta S^{\circ}_{\text{obs}}$  it actually contains  $\Delta H^{\circ}_{\text{ion (buffer)}}$ . Therefore, the entropy term associated with the binding process should be calculated from:

$$\Delta G^{\circ}_{\text{obs}} - (\Delta H^{\circ}_{\text{obs}} + n\Delta H^{\circ}_{\text{ion (buffer)}}) = -T\Delta S^{\circ}_{\text{calc}}$$

In the above equation, the enthalpy of ionisation of the buffer is added to  $\Delta H^{\circ}_{\text{obs}}$  because of the neutralisation, by the buffer, of the protons released is the reverse process of ionisation of the buffer. Now, the entropy change excludes the contribution from the reaction of the buffer with released protons. It is labelled as,  $\Delta S^{\circ}_{\text{calc}}$ . It is also independent of buffer and comprises:

$$\Delta S^{\circ}_{\text{calc}} = (\Delta S^{\circ}_{\text{bind}} + \Delta S^{\circ}_{\text{conf}}) + n (\Delta S^{\circ}_{\text{ion (enz)}}) = \Delta S^{\circ}_{\text{int}} + n (\Delta S^{\circ}_{\text{ion (enz)}})$$

Calculating the entropy changes from this equation gives a new summary **Table 2.15** of data replacing **Table 2.13**.

**Table 2.15:** Summary of simulation data for **zinc** ion solution titrated into apoBclI solution with  $\Delta S^{\circ}_{\text{calc}}$ .

		<b>pH</b>					
<b>Buffers</b>		5.20	5.60	6.0	6.35	6.80	7.20
<b>Acetate</b> ( $\Delta H_{\text{ion (buffer)}} = 0.49 \text{ kJ mol}^{-1}$ ) <sup>71</sup>	N (Zn <sup>2+</sup> :Enz) K <sub>b</sub> (M <sup>-1</sup> ) $\Delta H^{\circ}_{\text{obs}}$ (kJ mol <sup>-1</sup> ) $\Delta S^{\circ}_{\text{obs}}$ (J mol <sup>-1</sup> K <sup>-1</sup> )	0.3 ± 0.6 1.13 (±0.2) × 10 <sup>5</sup> 45 (±10) 252 (±40)	0.7 ± 0.6 1.33 (±0.1) × 10 <sup>5</sup> 20 (±3) 167 (±32)				
<b>MES</b> ( $\Delta H_{\text{ion (buffer)}} = 15.53 \text{ kJ mol}^{-1}$ ) <sup>71</sup>	N (Zn <sup>2+</sup> :Enz) K <sub>b</sub> (M <sup>-1</sup> ) $\Delta H^{\circ}_{\text{obs}}$ (kJ mol <sup>-1</sup> ) $\Delta S^{\circ}_{\text{obs}}$ (J mol <sup>-1</sup> K <sup>-1</sup> )	<b>1.2 (± 0.2)</b> 1.2(±0.4) × 10 <sup>6</sup> 17 (±2) 293 (±38)	<b>1.3 (± 0.2)</b> 2.8(±0.2) × 10 <sup>6</sup> 13 (±4) 229 (±20)	<b>1.7 (± 0.5)</b> 1.1(±0.1) × 10 <sup>5</sup> 7 (±2) 219 (±20)	<b>1.8 (± 0.2)</b> 1.6(±0.2) × 10 <sup>6</sup> 12 (±6) 195 (±40)	<b>2.0 (± 0.3)</b> 2.0(±0.4) × 10 <sup>6</sup> 11 (±3) 194 (±35)	
<b>Cacodylate</b> ( $\Delta H_{\text{ion (buffer)}} = -1.96 \text{ kJ mol}^{-1}$ ) <sup>71</sup>	N (Zn <sup>2+</sup> :Enz) K <sub>b</sub> (M <sup>-1</sup> ) $\Delta H^{\circ}_{\text{obs}}$ (kJ mol <sup>-1</sup> ) $\Delta S^{\circ}_{\text{obs}}$ (J mol <sup>-1</sup> K <sup>-1</sup> )	<b>1.3 (± 0.2)</b> 1.4(±0.3) × 10 <sup>6</sup> 62 (±8) 311 (±30)	<b>1.4 (± 0.2)</b> 2.8(±0.4) × 10 <sup>6</sup> 41 (±5) 251 (±20)	<b>1.5 (± 0.4)</b> 2.5(±0.4) × 10 <sup>6</sup> 40 (±10) 244 (±60)	<b>2.0 (± 0.3)</b> 2.3(±0.3) × 10 <sup>6</sup> 26(±8) 204 (±23)	<b>2.2 (± 0.6)</b> 2.4(±1) × 10 <sup>6</sup> 22 (±4) 191 (±50)	
<b>PIPES</b> ( $\Delta H_{\text{ion (buffer)}} = 11.45 \text{ kJ mol}^{-1}$ ) <sup>71</sup>	N (Zn <sup>2+</sup> :Enz) K <sub>b</sub> (M <sup>-1</sup> ) $\Delta H^{\circ}_{\text{obs}}$ (kJ mol <sup>-1</sup> ) $\Delta S^{\circ}_{\text{obs}}$ (J mol <sup>-1</sup> K <sup>-1</sup> )			1.3 ± 0.5 1.75 (±0.1) × 10 <sup>5</sup> 17 (±3) 230 (±32)	1.5 ± 0.6 1.25(±0.4) × 10 <sup>5</sup> 20 (±5) 192 (±36)	1.6 ± 0.5 2.37(±0.5) × 10 <sup>6</sup> 11 (±2) 186 (±40)	1.7 ± 0.3 5.50 (±0.6) × 10 <sup>5</sup> 6 (±2) 230 (±30)
<b>MOPS</b> ( $\Delta H_{\text{ion (buffer)}} = 21.82 \text{ kJ mol}^{-1}$ ) <sup>71</sup>	N (Zn <sup>2+</sup> :Enz) K <sub>b</sub> (M <sup>-1</sup> ) $\Delta H^{\circ}_{\text{obs}}$ (kJ mol <sup>-1</sup> ) $\Delta S^{\circ}_{\text{obs}}$ (J mol <sup>-1</sup> K <sup>-1</sup> )					0.9 ± 0.2 1.43 (±0.3) × 10 <sup>7</sup> -22 (±6) 114 (±20)	1.2 ± 0.2 5 (±1.0) × 10 <sup>7</sup> -19 (±9) 272 (±55)
<b>HEPES</b> ( $\Delta H_{\text{ion (buffer)}} = 21.01 \text{ kJ mol}^{-1}$ ) <sup>71</sup>	N (Zn <sup>2+</sup> :Enz) K <sub>b</sub> (M <sup>-1</sup> ) $\Delta H^{\circ}_{\text{obs}}$ (kJ mol <sup>-1</sup> ) $\Delta S^{\circ}_{\text{obs}}$ (J mol <sup>-1</sup> K <sup>-1</sup> )					1.1 ± 0.2 1.99 (±0.4) × 10 <sup>7</sup> -16 (±2) 133 (±15)	1.4 ± 0.2 2.93 (±0.4) × 10 <sup>6</sup> -22 (±3) 233 (±19)

In Table 2.15 the  $\Delta S^{\circ}_{\text{calc}}$  values are shown.  $\Delta S^{\circ}_{\text{calc}}$  equates to  $\Delta S^{\circ}_{\text{int}} + n (\Delta S^{\circ}_{\text{ion (enz)}}$ ) as explained on Page 84. To determine  $\Delta S^{\circ}_{\text{int}}$  and  $\Delta S^{\circ}_{\text{ion (enz)}}$ , the average values of  $\Delta S^{\circ}_{\text{calc}}$  at each pH, calculated from the values in each of the buffer (**Table 2.16**) are plotted against n(number of protons released) across the pH range as shown in **Figure 2.27**. From this graph we obtain the  $\Delta S^{\circ}_{\text{int}}$  as the intercept and the gradient of this graph is the  $\Delta S^{\circ}_{\text{ion (enz)}}$ .

**Table 2.16:** Average  $\Delta S^{\circ}_{\text{calc}}$  and n (number of protons released) at all pH's for zinc ion binding to apoBcll.

	pH					
	5.20	5.60	6.0	6.35	6.80	7.20
Average $\Delta S^{\circ}_{\text{calc}}$ ( $\text{J mol}^{-1} \text{K}^{-1}$ )	285 ( $\pm 32$ )	216 ( $\pm 25$ )	231 ( $\pm 40$ )	197 ( $\pm 35$ )	164 ( $\pm 30$ )	245 ( $\pm 35$ )
n (number of protons released)	2.3 ( $\pm 0.5$ )	1.2 ( $\pm 0.4$ )	1.9 ( $\pm 0.5$ )	0.7 ( $\pm 0.3$ )	1.7 ( $\pm 0.3$ )	2.6 ( $\pm 0.5$ )

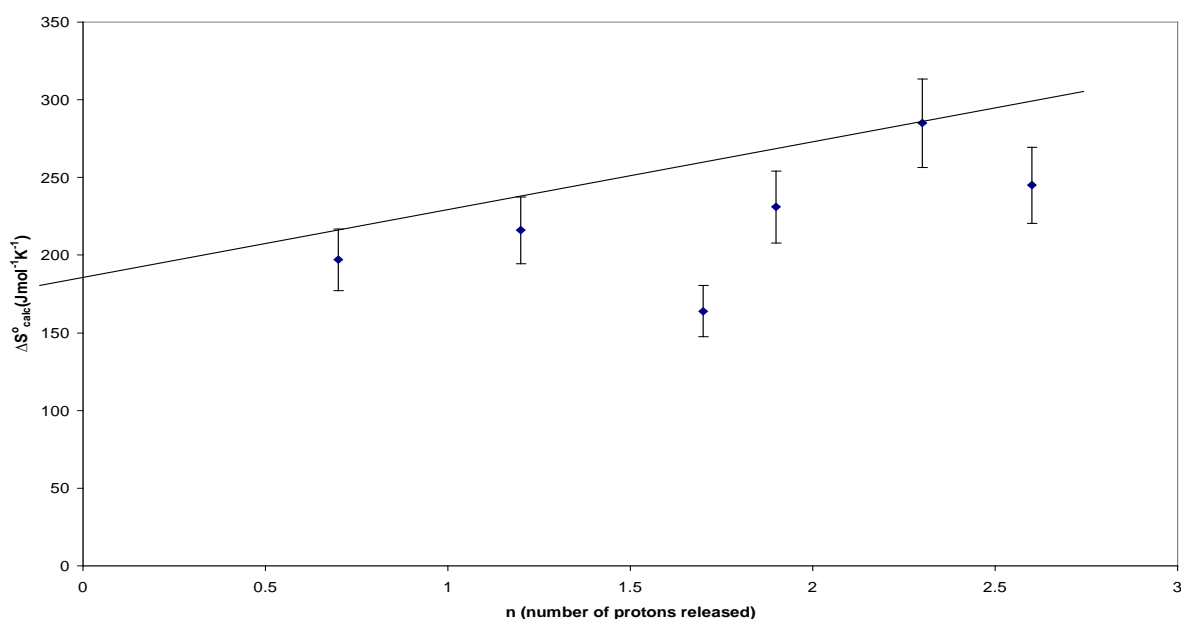


**Figure 2.27:**  $\Delta S^{\circ}_{\text{calc}}$  against n the number of protons released when zinc ion binds to apoBcll.

From the graph in **Figure 2.27** the values of  $\Delta S^{\circ}_{\text{int}}$  and  $\Delta S^{\circ}_{\text{ion (enz)}}$  estimated are:  
 $\Delta S^{\circ}_{\text{int}} = 161 (\pm 11) \text{ Jmol}^{-1} \text{ K}^{-1}$  and  $\Delta S^{\circ}_{\text{ion (enz)}} = 36 (\pm 10) \text{ Jmol}^{-1} \text{ K}^{-1}$ .

### **2.3.2 - Part two: Cobalt ion Titrated into ApoBcII**

Part two presents the results of titration experiments using a solution of cobalt ions to titrate against a solution of apoBcII (apo  $\beta$ -lactamase). The conditions used were the same as those used for the zinc titrations.

All experiments were done in duplicate or triplicate and the results shown in the following tables are averages of two or three measurements. Another point to note is that several separately prepared batches of BcII were used. Although efforts were made to ensure that each batch was purified to the same extent. It is conceivable that batch to batch variation might have caused some slight inconsistencies in the data which are difficult to take into account and to quantify.

All the titration calorimetric enthalpy data has been corrected for the heats of dilution. As for zinc, the heat changes were measured as a function of both pH and buffer type.

As can be seen in **Figure 2.28**, the titration output for cobalt ion binding to apoBclI in MES buffer at pH 5.20 shows a single binding event with an endothermic reaction. The data was simulated using a single binding model that gave the data shown in **Table 2.17**.

Similar experiments and data interpretations are reported for different conditions in the following Figures and Tables.

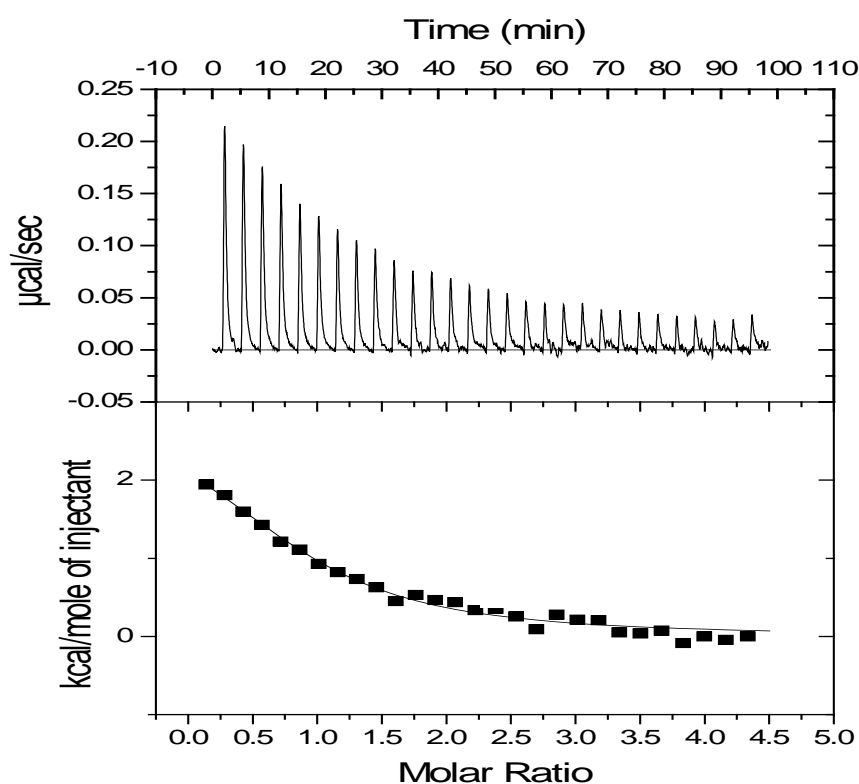


**Figure 2.28:** ITC output for  $\text{CoCl}_2$  solution ( $3.6 \times 10^{-4}$  M) titrated into apoBclI solution ( $1.8 \times 10^{-5}$  M) in MES buffer at pH 5.20 at 25 °C.

**Table 2.17:** Simulation data for the titration of  $\text{CoCl}_2$  solution ( $3.6 \times 10^{-4}$  M) into apoBclI solution ( $1.8 \times 10^{-5}$  M) in MES buffer at pH 5.20 at 25 °C.

N ( $\text{Co}^{2+}$ :Enz)	0.92 ( $\pm 0.3$ )
$K_b$ ( $\text{M}^{-1}$ )	$1.20 (\pm 0.1) \times 10^5$
$\Delta H_{\text{obs}}^{\circ}$ ( $\text{kJ mol}^{-1}$ )	13 ( $\pm 3$ )
$\Delta S_{\text{obs}}^{\circ}$ ( $\text{J mol}^{-1} \text{K}^{-1}$ )	140 ( $\pm 25$ )

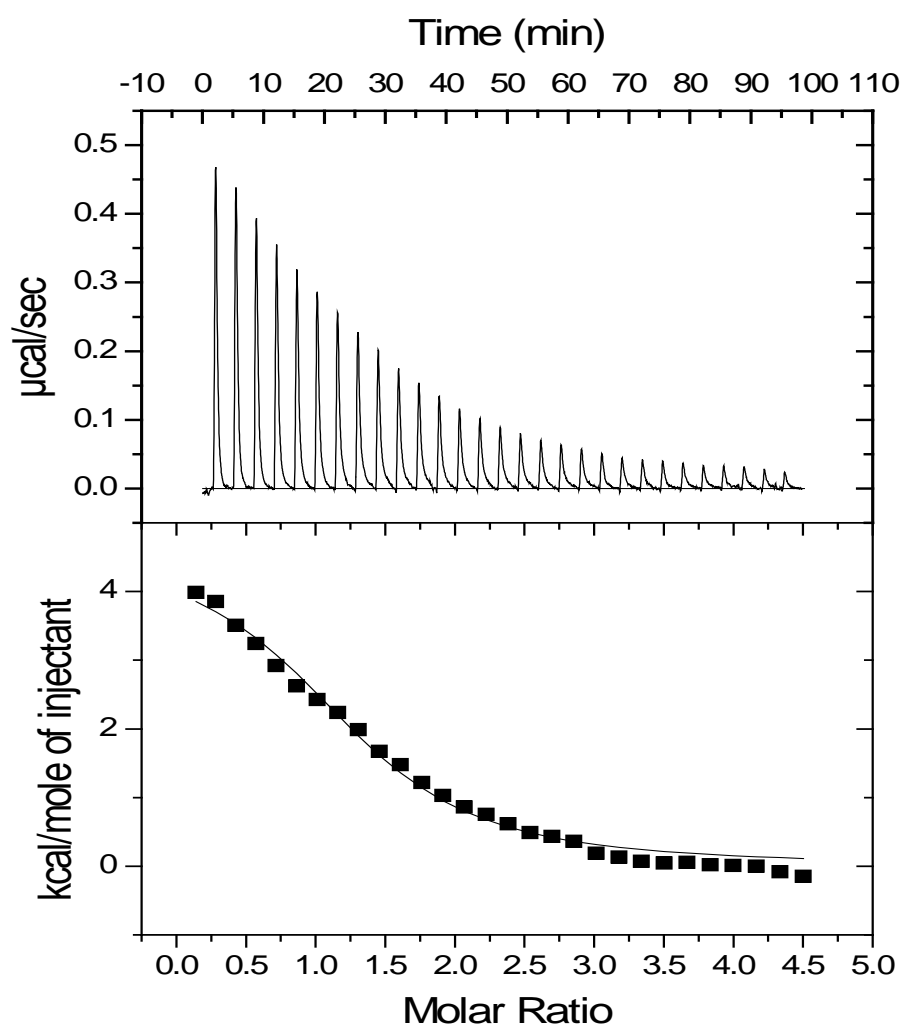


**Figure 2.29:** ITC output for  $\text{CoCl}_2$  solution ( $3.6 \times 10^{-4}$  M) titrated into apoBclI solution ( $1.8 \times 10^{-5}$  M) in MES buffer at pH 5.60 at 25 °C.

**Table 2.18:** Simulation data for the titration of  $\text{CoCl}_2$  solution ( $3.6 \times 10^{-4}$  M) titrated into apoBclI solution ( $1.8 \times 10^{-5}$  M) in MES buffer at pH 5.60 at 25 °C.

N ( $\text{Co}^{2+}:\text{Enz}$ )	1.3 ( $\pm 0.4$ )
$K_b$ ( $\text{M}^{-1}$ )	$2.4 (\pm 0.2) \times 10^5$
$\Delta H_{\text{obs}}^{\circ}$ ( $\text{kJ mol}^{-1}$ )	19 ( $\pm 5$ )
$\Delta S_{\text{obs}}^{\circ}$ ( $\text{J mol}^{-1} \text{K}^{-1}$ )	168 ( $\pm 30$ )

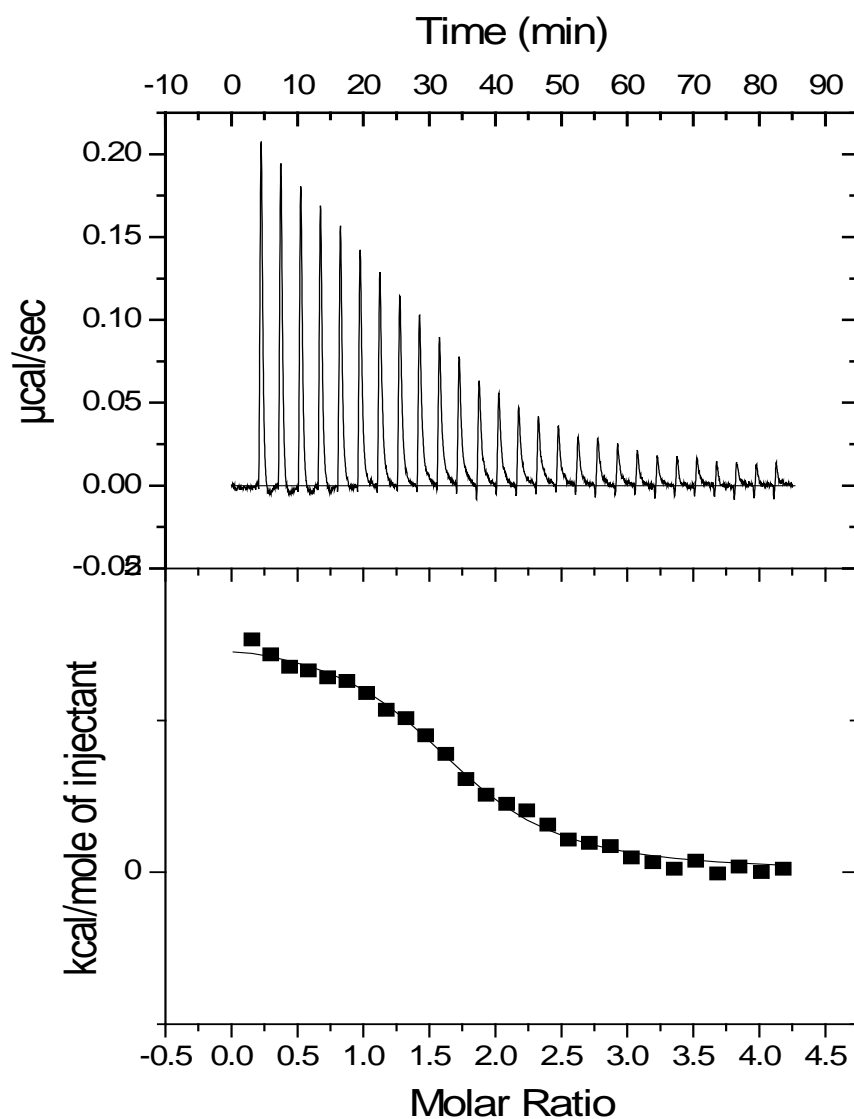


**Figure 2.30:** ITC output and summary data for  $\text{CoCl}_2$  solution ( $3.6 \times 10^{-4}$  M) titrated into apoBclI solution ( $1.8 \times 10^{-5}$  M) in MES buffer at pH 6.0 at  $25^\circ\text{C}$ .

**Table 2.19:** Simulation data for the titration of  $\text{CoCl}_2$  solution ( $3.6 \times 10^{-4}$  M) titrated into apoBclI solution ( $1.8 \times 10^{-5}$  M) in MES buffer at pH 6.0 at  $25^\circ\text{C}$ .

$N (\text{Co}^{2+}:\text{Enz})$	$1.5 (\pm 0.4)$
$K_b (\text{M}^{-1})$	$3.78 (\pm 0.3) \times 10^5$
$\Delta H_{\text{obs}}^\circ (\text{kJ mol}^{-1})$	$24 (\pm 5)$
$\Delta S_{\text{obs}}^\circ (\text{J mol}^{-1} \text{K}^{-1})$	$187 (\pm 40)$

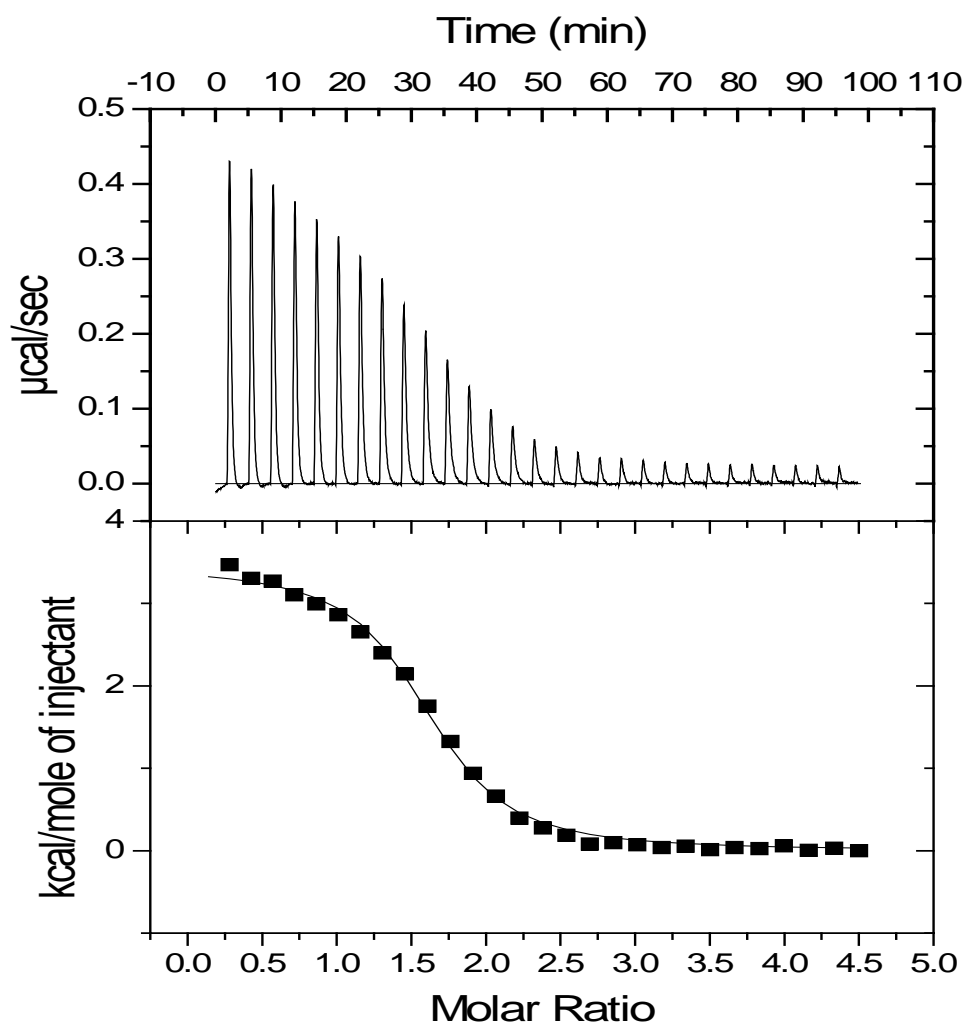


**Figure 2.31:** ITC output for  $\text{CoCl}_2$  solution ( $3.6 \times 10^{-4}$  M) titrated into apoBclI solution ( $1.8 \times 10^{-5}$  M) in MES buffer at pH 6.35 at 25 °C.

**Table 2.20:** Simulation data for the titration of  $\text{CoCl}_2$  solution ( $3.6 \times 10^{-4}$  M) titrated into apoBclI solution ( $1.8 \times 10^{-5}$  M) in MES buffer at pH 6.35 at 25 °C.

$N (\text{Co}^{2+}:\text{Enz})$	$1.6 (\pm 0.3)$
$K_b (\text{M}^{-1})$	$1.1 (\pm 0.2) \times 10^6$
$\Delta H_{\text{obs}}^{\circ} (\text{kJ mol}^{-1})$	$14 (\pm 4)$
$\Delta S_{\text{obs}}^{\circ} (\text{J mol}^{-1} \text{K}^{-1})$	$164 (\pm 40)$

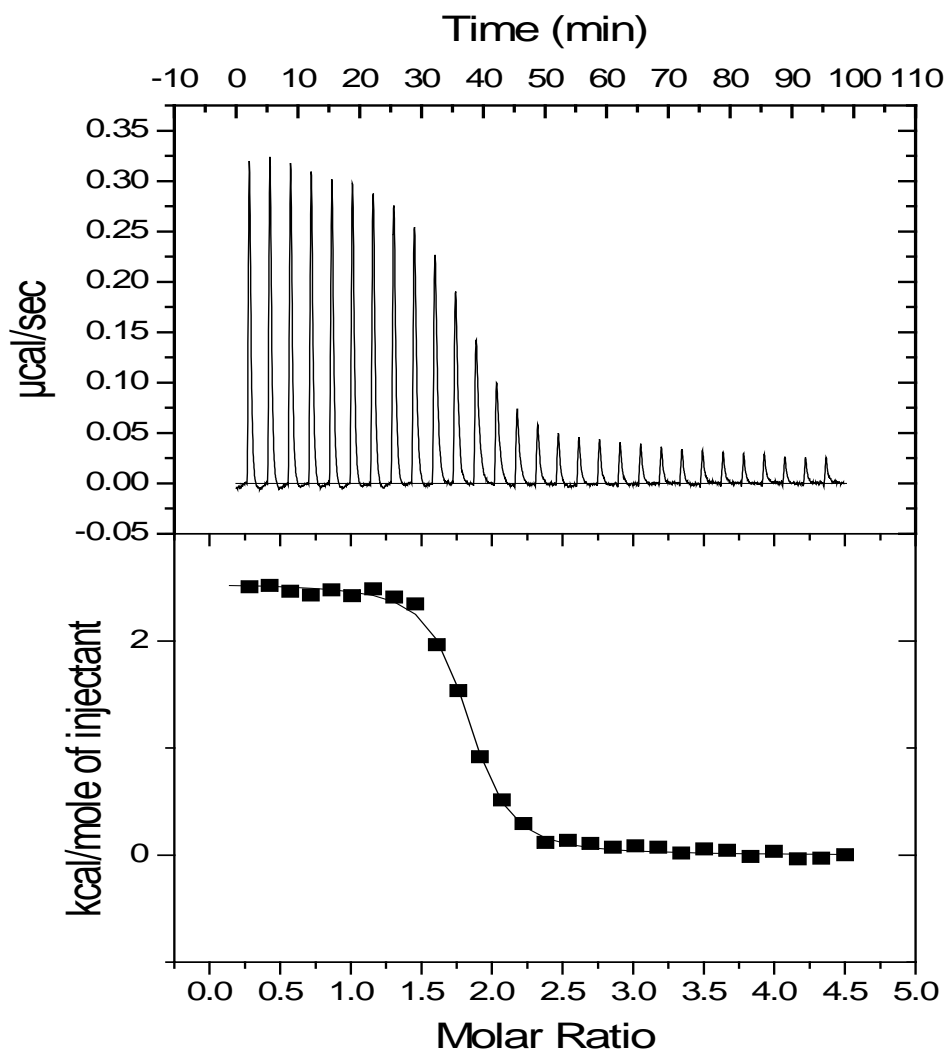


**Figure 2.32:** ITC output for  $\text{CoCl}_2$  solution ( $3.6 \times 10^{-4}$  M) titrated into apoBclI solution ( $1.8 \times 10^{-5}$  M) in MES buffer at pH 6.80 at 25 °C.

**Table 2.21:** Simulation data for the titration of  $\text{CoCl}_2$  solution ( $3.6 \times 10^{-4}$  M) titrated into apoBclI solution ( $1.8 \times 10^{-5}$  M) in MES buffer at pH 6.80 at 25 °C.

$N (\text{Co}^{2+}:\text{Enz})$	$1.8 (\pm 0.2)$
$K_B (\text{M}^{-1})$	$4.74 (\pm 0.4) \times 10^6$
$\Delta H_{\text{obs}}^{\circ} (\text{kJ mol}^{-1})$	$11 (\pm 2)$
$\Delta S_{\text{obs}}^{\circ} (\text{J mol}^{-1} \text{K}^{-1})$	$163 (\pm 35)$

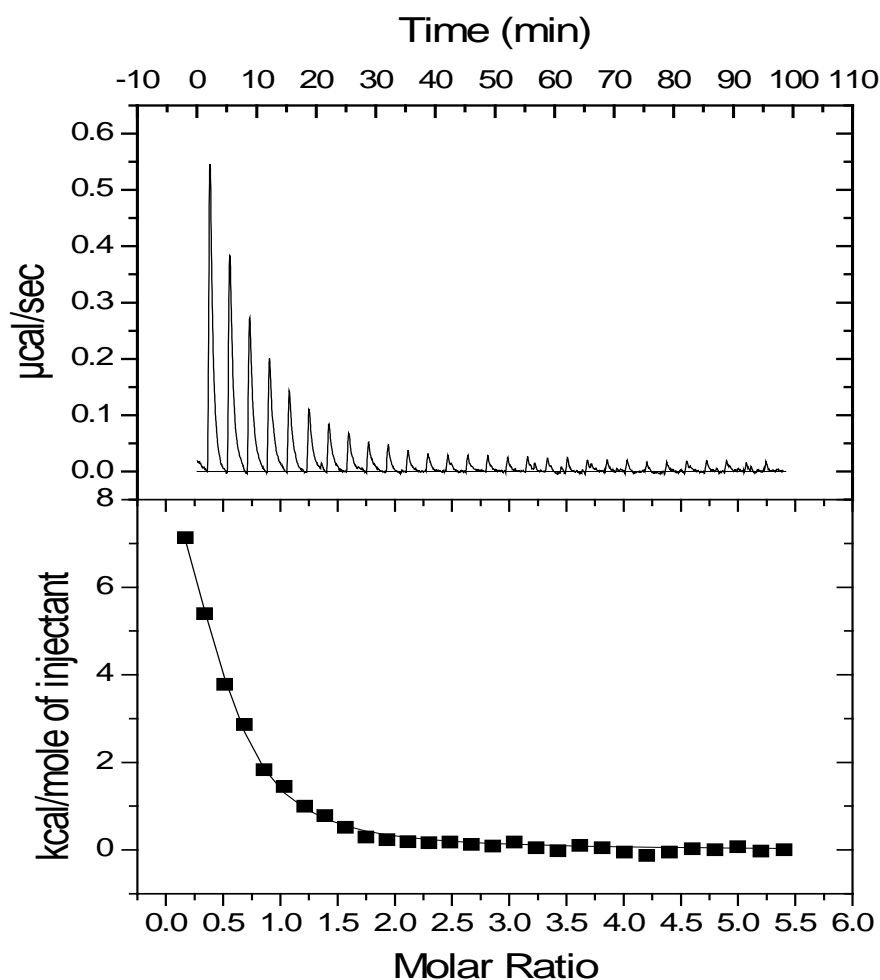


**Figure 2.33:** ITC output for  $\text{CoCl}_2$  solution ( $3.6 \times 10^{-4}$  M) titrated into apoBclI solution ( $1.8 \times 10^{-5}$  M) in cacodylate buffer at pH 5.20 at 25 °C.

**Table 2.22:** Simulation data for the titration of  $\text{CoCl}_2$  solution ( $3.6 \times 10^{-4}$  M) titrated into apoBclI solution ( $1.8 \times 10^{-5}$  M) in cacodylate buffer at pH 5.20 at 25 °C.

$N (\text{Co}^{2+}:\text{Enz})$	$0.44 (\pm 0.3)$
$K_b (\text{M}^{-1})$	$3.3 (\pm 0.7) \times 10^5$
$\Delta H_{\text{obs}}^{\circ} (\text{kJ mol}^{-1})$	$48 (\pm 10)$
$\Delta S_{\text{obs}}^{\circ} (\text{J mol}^{-1} \text{K}^{-1})$	$266 (\pm 30)$

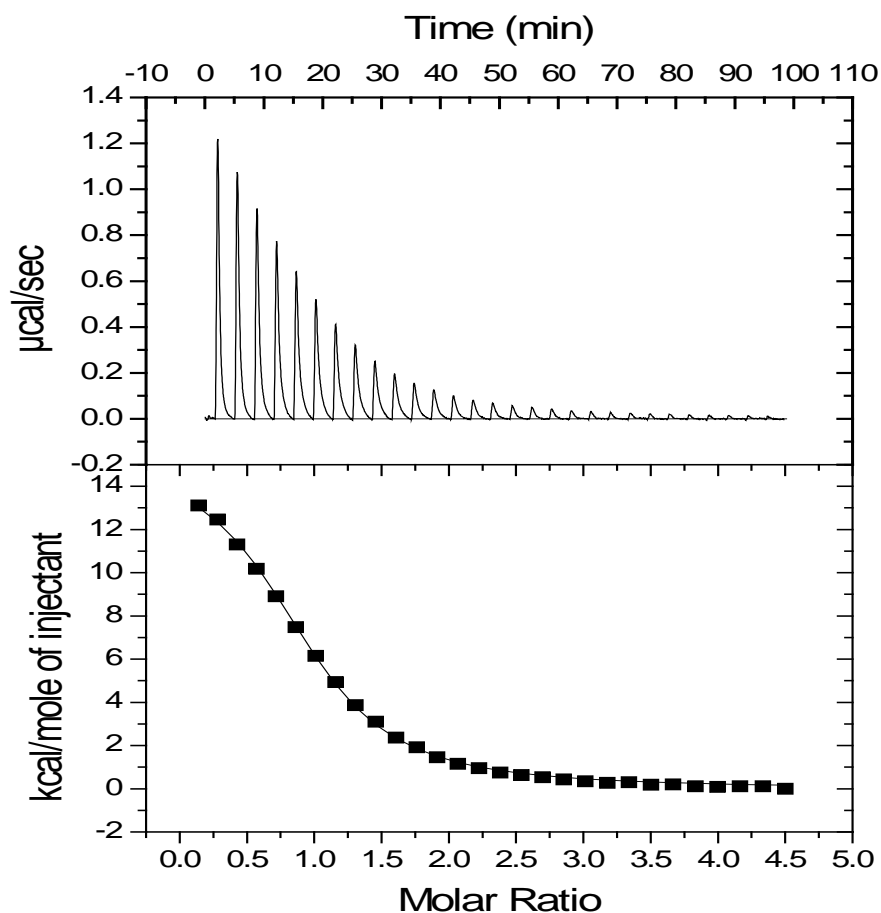


**Figure 2.34:** ITC output for  $\text{CoCl}_2$  solution ( $3.6 \times 10^{-4}$  M) titrated into apoBclI solution ( $1.8 \times 10^{-5}$  M) in cacodylate buffer at pH 5.60 at 25 °C.

**Table 2.23:** Simulation data for  $\text{CoCl}_2$  solution ( $3.6 \times 10^{-4}$  M) titrated into apoBclI solution ( $1.8 \times 10^{-5}$  M) in cacodylate buffer at pH 5.60 at 25 °C.

$N (\text{Co}^{2+}:\text{Enz})$	$0.94 (\pm 0.4)$
$K_b (\text{M}^{-1})$	$3.48 (\pm 0.5) \times 10^5$
$\Delta H_{\text{obs}}^{\circ} (\text{kJ mol}^{-1})$	$65 (\pm 12)$
$\Delta S_{\text{obs}}^{\circ} (\text{J mol}^{-1} \text{K}^{-1})$	$325 (\pm 20)$

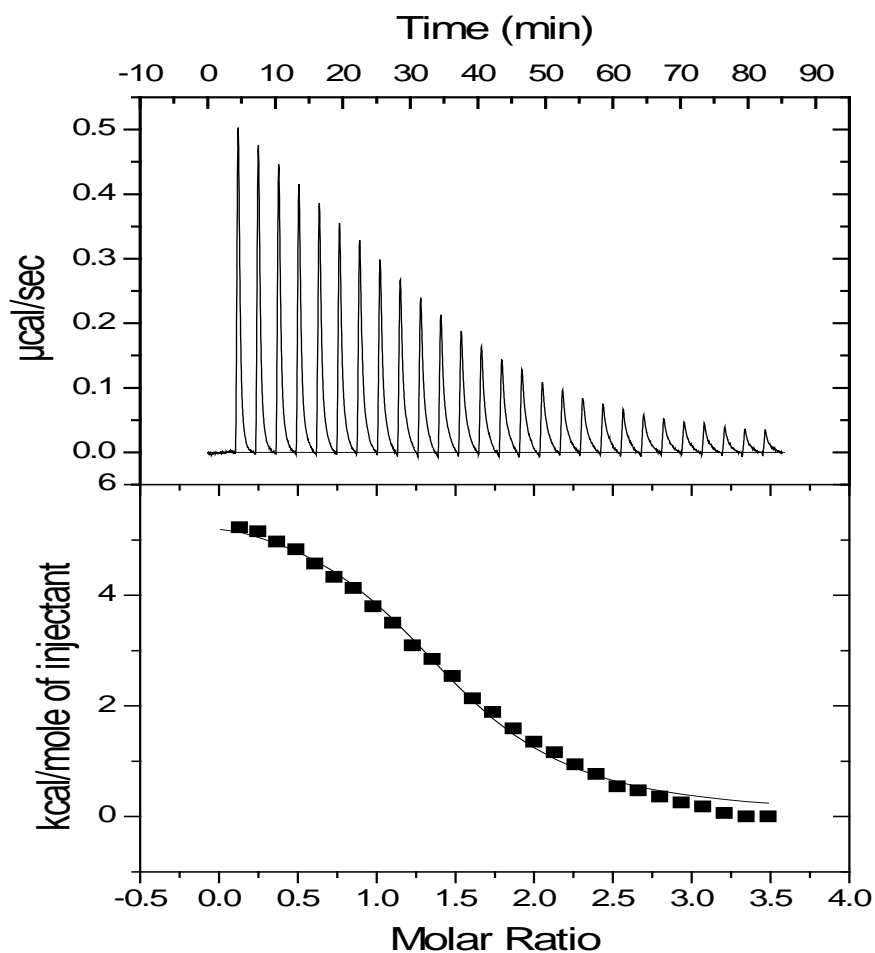


**Figure 2.35:** ITC output for  $\text{CoCl}_2$  solution ( $3.6 \times 10^{-4}$  M) titrated into apoBclI solution ( $1.8 \times 10^{-5}$  M) in cacodylate buffer at pH 6.0 at 25 °C.

**Table 2.24:** Simulation data for  $\text{CoCl}_2$  solution ( $3.6 \times 10^{-4}$  M) titrated into apoBclI solution ( $1.8 \times 10^{-5}$  M) in cacodylate buffer at pH 6.0 at 25 °C.

$N (\text{Co}^{2+}:\text{Enz})$	$1.36 (\pm 0.4)$
$K_b (\text{M}^{-1})$	$2.28 (\pm 0.4) \times 10^5$
$\Delta H_{\text{obs}}^{\circ} (\text{kJ mol}^{-1})$	$60 (\pm 15)$
$\Delta S_{\text{obs}}^{\circ} (\text{J mol}^{-1} \text{K}^{-1})$	$315 (\pm 60)$

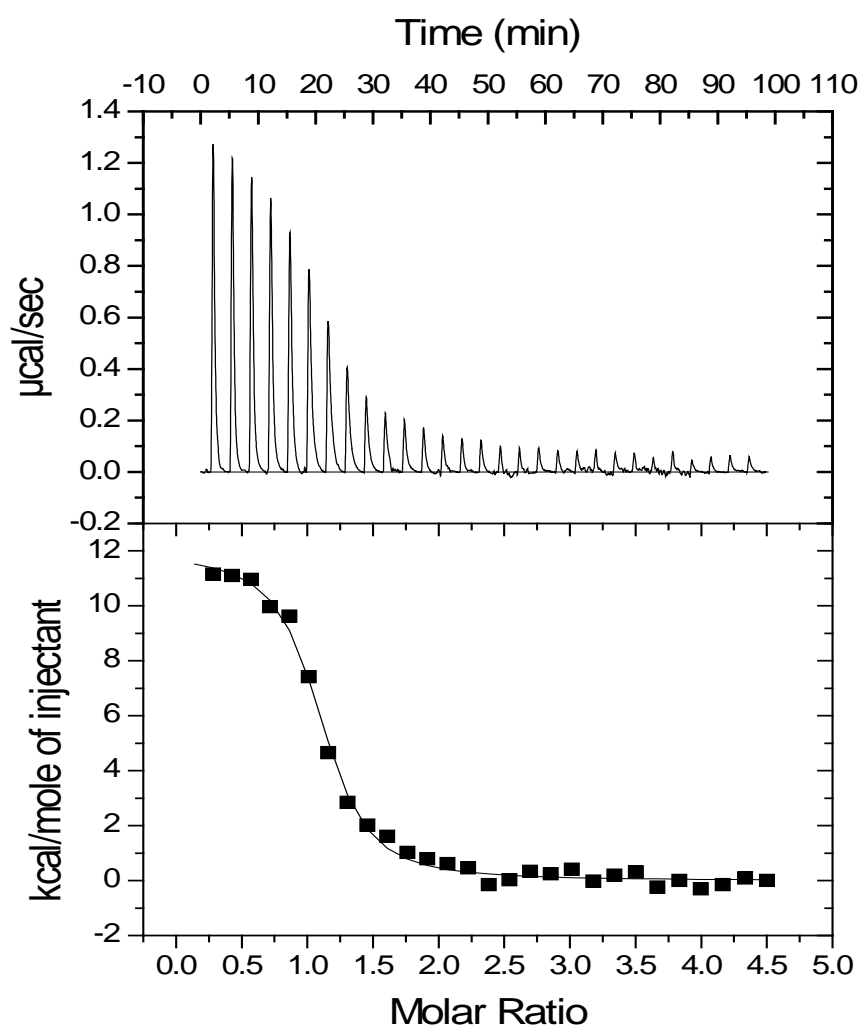


**Figure 2.36:** ITC output for  $\text{CoCl}_2$  solution ( $3.6 \times 10^{-4}$  M) titrated into apoBclI solution ( $1.8 \times 10^{-5}$  M) in cacodylate buffer at pH 6.35 at 25 °C.

**Table 2.25:** Simulation data for  $\text{CoCl}_2$  solution ( $3.6 \times 10^{-4}$  M) titrated into apoBclI solution ( $1.8 \times 10^{-5}$  M) in cacodylate buffer at pH 6.35 at 25 °C.

N ( $\text{Co}^{2+}$ :Enz)	1.9 ( $\pm 0.4$ )
$K_b$ ( $\text{M}^{-1}$ )	$1.17 (\pm 0.1) \times 10^6$
$\Delta H_{\text{obs}}^{\circ}$ ( $\text{kJ mol}^{-1}$ )	69 ( $\pm 16$ )
$\Delta S_{\text{obs}}^{\circ}$ ( $\text{J mol}^{-1} \text{K}^{-1}$ )	346 ( $\pm 40$ )

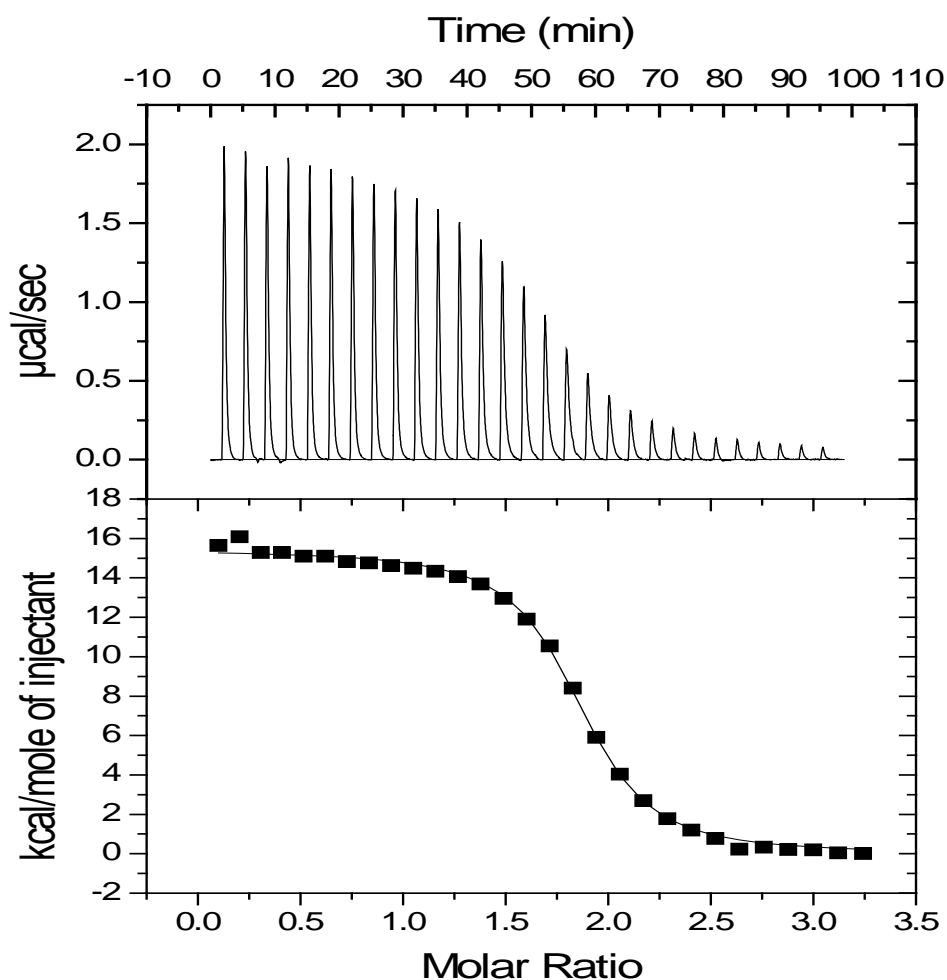


**Figure 2.37:** ITC output for  $\text{CoCl}_2$  solution ( $3.6 \times 10^{-4}$  M) titrated into apoBclI solution ( $1.8 \times 10^{-5}$  M) in cacodylate buffer at pH 6.80 at 25 °C.

**Table 2.26:** Simulation data for  $\text{CoCl}_2$  solution ( $3.6 \times 10^{-4}$  M) titrated into apoBclI solution ( $1.8 \times 10^{-5}$  M) in cacodylate buffer at pH 6.80 at 25 °C.

N ( $\text{Co}^{2+}$ :Enz)	2.3 ( $\pm 0.4$ )
$K_b$ ( $\text{M}^{-1}$ )	$2.49 (\pm 0.4) \times 10^6$
$\Delta H_{\text{obs}}^{\circ}$ ( $\text{kJ mol}^{-1}$ )	65 ( $\pm 12$ )
$\Delta S_{\text{obs}}^{\circ}$ ( $\text{J mol}^{-1} \text{K}^{-1}$ )	338 ( $\pm 55$ )

Below in **Table 2.27**, is summarised all the experimental data for cobalt ion titrations into apoBclI solution at various pH's and buffers.

**Table 2.27:** Summary of simulation data for **cobalt** ion solution titrated into apoBclI solution.

		pH					
Buffers		5.20	5.60	6.0	6.35	6.80	7.20
<b>Acetate</b> ( $\Delta H_{\text{ion (buffer)}} = 0.49 \text{ kJ mol}^{-1}$ ) <sup>71</sup>	N (Co <sup>2+</sup> :Enz) K <sub>b</sub> (M <sup>-1</sup> ) $\Delta H_{\text{obs}}^{\circ}$ (kJ mol <sup>-1</sup> ) $\Delta S_{\text{obs}}^{\circ}$ (J mol <sup>-1</sup> K <sup>-1</sup> )	0.7 ± 0.7 5.42(± 0.7)x10 <sup>4</sup> 9 (± 3) 120 (± 24)	1.0 ± 0.8 1.19(± 0.1)x10 <sup>5</sup> 13 (± 4) 141 (± 25)				
<b>MES</b> ( $\Delta H_{\text{ion (buffer)}} = 15.53 \text{ kJ mol}^{-1}$ ) <sup>71</sup>	N (Co <sup>2+</sup> :Enz) K <sub>b</sub> (M <sup>-1</sup> ) $\Delta H_{\text{obs}}^{\circ}$ (kJ mol <sup>-1</sup> ) $\Delta S_{\text{obs}}^{\circ}$ (J mol <sup>-1</sup> K <sup>-1</sup> )	0.9 ± 0.3 1.2 (± 0.1)x10 <sup>5</sup> 13 (± 3) 140 (± 25)	1.3 ± 0.4 2.37 (± 0.2)x10 <sup>5</sup> 19 (± 5) 168 (± 30)	1.5 ± 0.4 3.78(± 0.3)x10 <sup>5</sup> 24 (± 5) 187 (± 40)	1.6 ± 0.3 1.11(± 0.2)x10 <sup>6</sup> 15 (± 4) 164 (± 40)	1.8 ± 0.2 4.73 (± 0.4)x10 <sup>6</sup> 11 (± 2) 163 (± 35)	
<b>Cacodylate</b> ( $\Delta H_{\text{ion (buffer)}} = -1.96 \text{ kJ mol}^{-1}$ ) <sup>71</sup>	N (Co <sup>2+</sup> :Enz) K <sub>b</sub> (M <sup>-1</sup> ) $\Delta H_{\text{obs}}^{\circ}$ (kJ mol <sup>-1</sup> ) $\Delta S_{\text{obs}}^{\circ}$ (J mol <sup>-1</sup> K <sup>-1</sup> )	0.4 ± 0.3 3.3 (± 0.7)x10 <sup>5</sup> 48 (± 10) 266 (± 30)	0.9 ± 0.4 3.48 (± 0.5)x10 <sup>5</sup> 65 (± 12) 325 (± 20)	1.4 ± 0.4 2.28(± 0.4)x10 <sup>6</sup> 60 (± 15) 315 (± 60)	1.9 ± 0.2 1.17(± 0.1)x10 <sup>6</sup> 69 (± 16) 346 (± 40)	2.3 ± 0.4 2.49 (± 0.4)x10 <sup>6</sup> 65 (± 12) 338 (± 55)	
<b>PIPES</b> ( $\Delta H_{\text{ion (buffer)}} = 11.45 \text{ kJ mol}^{-1}$ ) <sup>71</sup>	N (Co <sup>2+</sup> :Enz) K <sub>b</sub> (M <sup>-1</sup> ) $\Delta H_{\text{obs}}^{\circ}$ (kJ mol <sup>-1</sup> ) $\Delta S_{\text{obs}}^{\circ}$ (J mol <sup>-1</sup> K <sup>-1</sup> )			1.1 ± 0.2 1.76 (± 0.2)x10 <sup>6</sup> 50 (± 10) 287 (± 70)	1.7 ± 0.4 9.44 (± 0.7)x10 <sup>6</sup> 14 (± 3) 161 (± 60)	2.0 ± 0.7 7.12 (± 0.9)x10 <sup>5</sup> 8 (± 2) 140 (± 52)	2.3 ± 0.7 5.93 (± 0.9)x10 <sup>5</sup> 7 (± 1) 134 (± 30)
<b>MOPS</b> ( $\Delta H_{\text{ion (buffer)}} = 21.82 \text{ kJ mol}^{-1}$ ) <sup>71</sup>	N (Co <sup>2+</sup> :Enz) K <sub>b</sub> (M <sup>-1</sup> ) $\Delta H_{\text{obs}}^{\circ}$ (kJ mol <sup>-1</sup> ) $\Delta S_{\text{obs}}^{\circ}$ (J mol <sup>-1</sup> K <sup>-1</sup> )					1.3 ± 0.3 6.15 (± 1)x10 <sup>5</sup> -15 (± 3) 59 (± 40)	1.6 ± 0.2 1.30 (± 0.4)x10 <sup>6</sup> -16 (± 4) 84 (± 50)
<b>HEPES</b> ( $\Delta H_{\text{ion (buffer)}} = 21.01 \text{ kJ mol}^{-1}$ ) <sup>71</sup>	N (Co <sup>2+</sup> :Enz) K <sub>b</sub> (M <sup>-1</sup> ) $\Delta H_{\text{obs}}^{\circ}$ (kJ mol <sup>-1</sup> ) $\Delta S_{\text{obs}}^{\circ}$ (J mol <sup>-1</sup> K <sup>-1</sup> )					2.2 ± 0.2 1.98 (± 0.4)x10 <sup>7</sup> -10 (± 0.6) 105 (± 40)	1.5 ± 0.2 3.85 (± 0.3)x10 <sup>6</sup> -24 (± 5) 44 (± 22)

From the previous figures it can be seen that single binding events are observed throughout the pH and buffer range studied. From **Table 2.27** it can be seen that the ( $\text{Co}^{2+}$ : Enz) molar ratio increases from one at low pH to two as the pH is increased. The anomalous result of 0.44 at pH 5.20 in cacodylate buffer may be due to an error or the purity of the particular batch of enzyme used. All the other titrations at pH 5.20 appear to give a molar ratio of approximately 1.0.

The stoichiometric ratio of cobalt ion to enzyme binding changes in a similar manner to that observed for zinc ion as the pH is increased, and, in both cases, when two metal ions bind, it is by a cooperative process. The same trend is also followed by the titrations being endothermic in MES, cacodylate and Pipes buffers but exothermic in HEPES and MOPS buffers. The binding constant increases from  $10^5 \text{ M}^{-1}$  to  $10^6 \text{ M}^{-1}$  as the pH is increased from pH 5.20 to 6.80.

As mentioned before, the observed molar enthalpies of binding differ with buffer type depending on the number of protons being released upon binding of cobalt ions, and the heat released by neutralisation with the buffer due to different dissociation enthalpies. For example, in MES buffer the observed enthalpy increases from pH 5.20 to pH 6.0 and then falls as the pH is increased further, whereas in cacodylate buffer the value of observed enthalpy increases as the pH is increased from pH 5.20 to 6.80.

The trend in stoichiometric ratio with pH for buffers MES and cacodylate (**Figure 2.38**) is similar to that for zinc ion (**Figure 2.24**), with N (the number of metal ions per enzyme molecule) increasing from 1.0 to about 2.0 over the pH range.

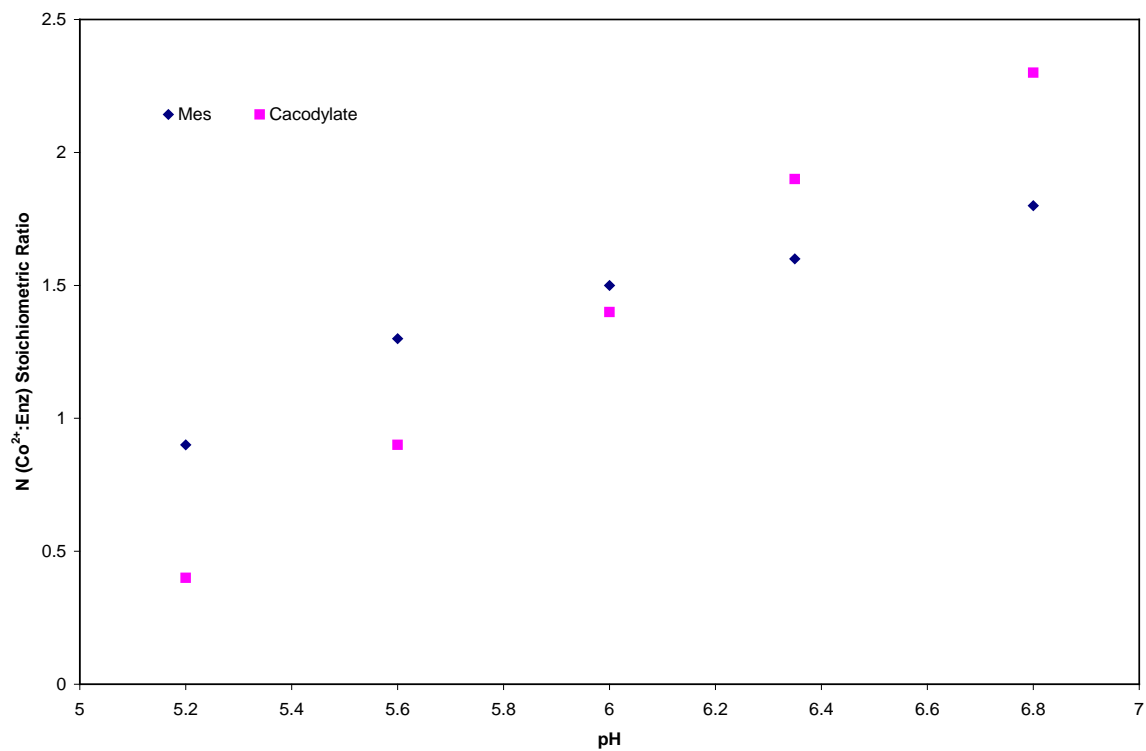


**Figure 2.39:** Stoichiometric ratio ( $\text{Co}^{2+}:\text{Enz}$ ) against pH for cobalt ion binding to apoBclI in MES and cacodylate buffer at 25°C.

### 2.3.2.1 - Dissociation of Acid Groups when Cobalt ion Binds to BcII

The  $\Delta H^{\circ}_{\text{obs}}$  data from the experimental simulations can be treated to allow for the contribution from the neutralisation of the protons released by metal ion binding to the enzyme by the buffer. For each pH, a plot of  $\Delta H^{\circ}_{\text{obs}}$  against  $\Delta H^{\circ}_{\text{ion}}(\text{buffer})$  has a gradient equal to  $n$  (number of protons released by the enzyme) and an intercept equal to  $(\Delta H^{\circ}_{\text{int}} + n\Delta H^{\circ}_{\text{ion}}(\text{enz}))$ . For example, the plot at pH 6.35 is shown in **Figure 2.39**, using the data for MES, cacodylate and PIPES buffer. Values for  $n$  and  $(\Delta H^{\circ}_{\text{int}} + n\Delta H^{\circ}_{\text{ion}}(\text{enz}))$  at each pH are given in **Table 2.28**.

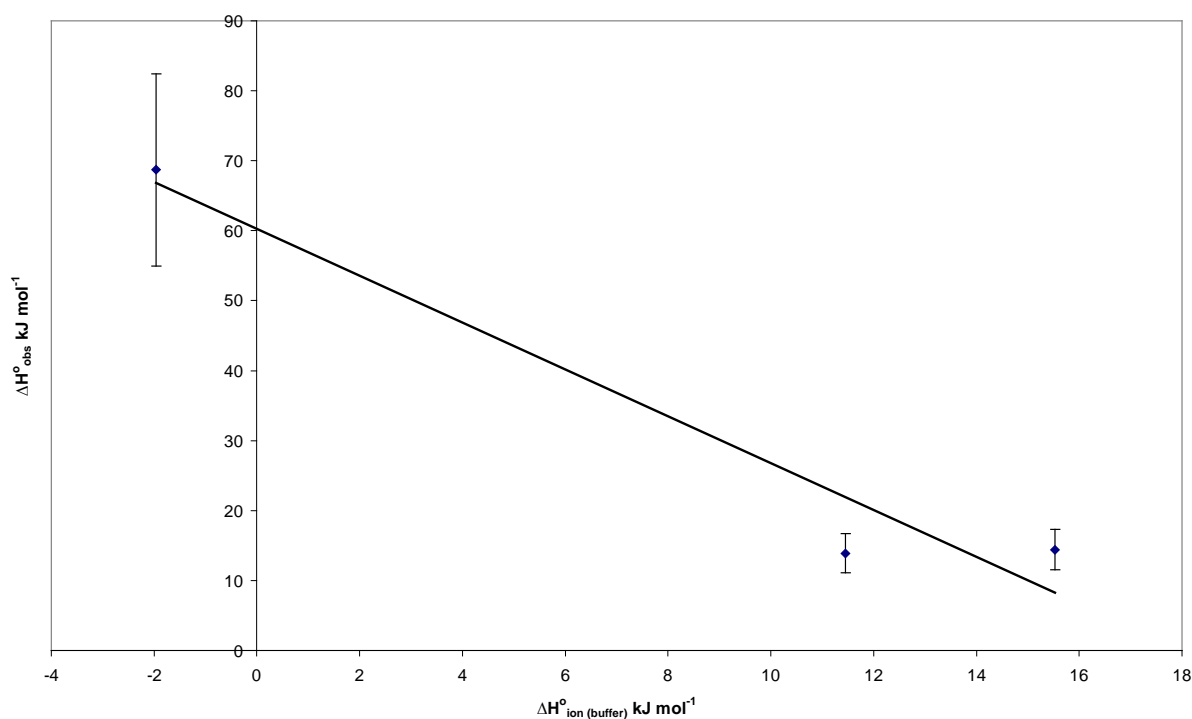


**Figure 2.40:**  $\Delta H^{\circ}_{\text{obs}}$  against  $\Delta H^{\circ}_{\text{ion}}(\text{buffer})$  at pH 6.35 for cobalt ions titrated into apoBcII solution.

**Table 2.28:** Values of  $n$  (number of protons released by the enzyme when cobalt ion binds to the enzyme) and  $\Delta H^{\circ}_{int} + n\Delta H^{\circ}_{ion (enzyme)}$  as a function of pH for cobalt ion binding to apoBcII using the  $\Delta H^{\circ}_{obs}$  values.

<i>pH</i>	<i>n (number of protons released by enzyme)</i>	$\Delta H^{\circ}_{int} + n\Delta H^{\circ}_{ion (enzyme)}$ (kJ mol <sup>-1</sup> )
5.20	1.2 ( $\pm$ 1.0)	29 ( $\pm$ 15)
5.60	1.5 ( $\pm$ 1.0)	40 ( $\pm$ 20)
6.0	1.7 ( $\pm$ 1.0)	59 ( $\pm$ 10)
6.35	3.3 ( $\pm$ 0.8)	63 ( $\pm$ 10)
6.80	3.4 ( $\pm$ 0.8)	56 ( $\pm$ 10)
7.20	2.6 ( $\pm$ 2.0)	37 ( $\pm$ 20)

**Table 2.28** shows how  $n$  (the number of protons released by the enzyme when cobalt ion binds) and the enthalpy change associated with cobalt ion binding and associated ionisation processes vary with pH. The experimental uncertainties of these data are relatively large, because the graph from which these are determined have few points and those few points themselves have significant uncertainties. Nevertheless, the trend is clear, and the number of protons released increases as pH is increased (**Figure 2.40**), perhaps not surprisingly since the number of cobalt ions binding increases with pH.

It is interesting that the number of protons released on cobalt binding to apoBcII increases with pH (**Figure 2.40**) whereas with zinc ion binding the number of protons released remains approximately constant over the pH range. This suggests that cobalt and zinc ions may bind in different ways, perhaps to different coordination sites on the enzyme.

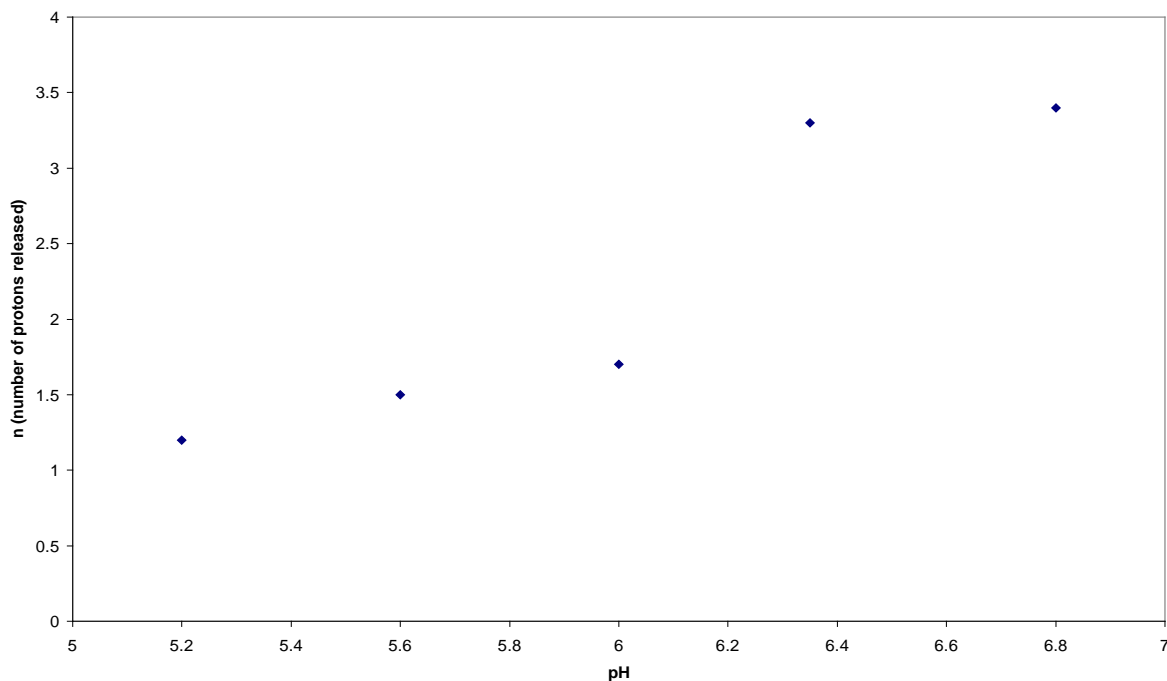


**Figure 2.41:** The trend of  $n$  (number of protons released) with pH for cobalt binding to apoBclI.

The intercepts in **Figure 2.39** equate to  $(\Delta H_{\text{int}}^{\circ} + n\Delta H_{\text{ion (enz)}}^{\circ})$  and a plot of these values against  $n$  (**Figure 2.41**) gives  $\Delta H_{\text{int}}^{\circ}$  as the intercept and  $\Delta H_{\text{ion (enz)}}^{\circ}$  as the gradient.

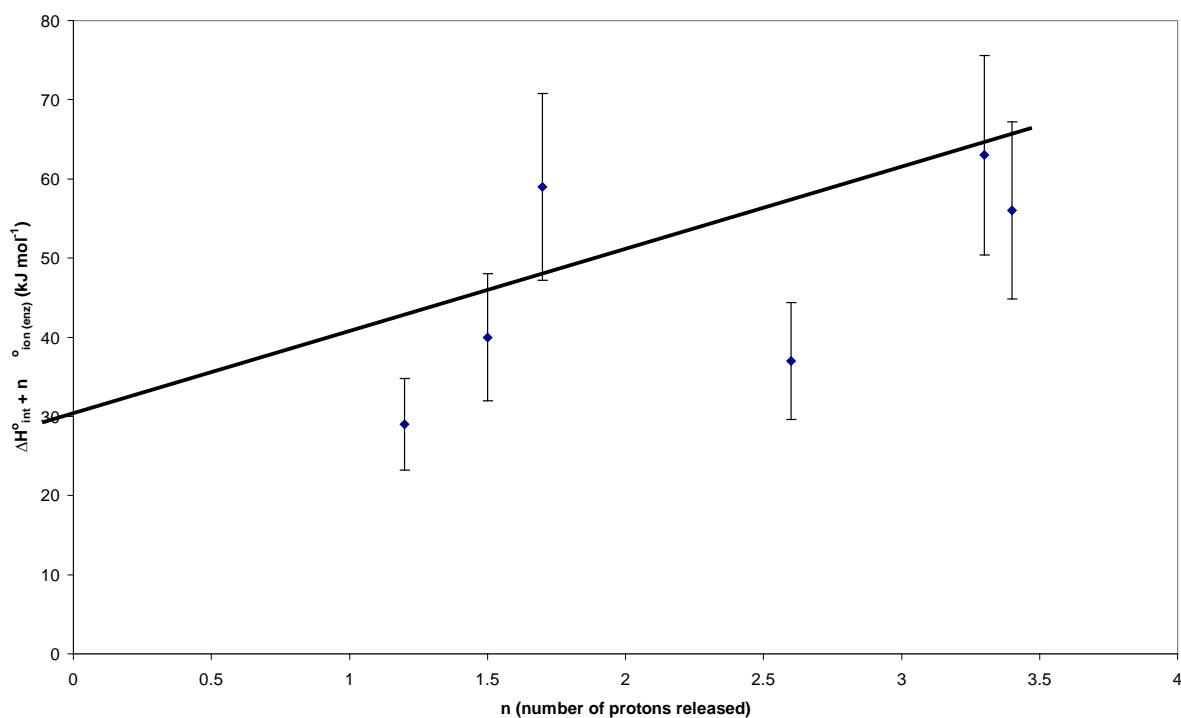


**Figure 2.41:**  $\Delta H^{\circ}_{\text{int}} + n\Delta H^{\circ}_{\text{ion (enz)}}$  against  $n$  the number of protons released when cobalt ion binds to apoBclI.

From **Figure 2.41**, it can be seen that the values for  $\Delta H^{\circ}_{\text{int}}$  and  $\Delta H^{\circ}_{\text{ion (enz)}}$  for cobalt ion binding to apoBclI is subject to large uncertainties. Nevertheless, values estimated are:  $\Delta H^{\circ}_{\text{int}} = 27(\pm 16)$  kJ mol<sup>-1</sup> and  $\Delta H^{\circ}_{\text{ion (enz)}} = 9(\pm 4)$  kJ mol<sup>-1</sup>.

### Entropy Calculations

As mentioned before the  $\Delta S^{\circ}_{\text{obs}}$  values are complicated and the actual meaningful values need to be calculated as already described (page 84) and a new summary (Table 2.29) of data replaces that in Table 2.27.

**Table 2.29:** Summary of simulation data for **cobalt** ion solution titrated into apoBclI solution with  $\Delta S^{\circ}_{\text{calc}}$ .

		pH					
Buffers		5.20	5.60	6.0	6.35	6.80	7.20
<b>Acetate</b> ( $\Delta H_{\text{ion (buffer)}} = 0.49 \text{ kJ mol}^{-1}$ ) <sup>71</sup>	N (Co <sup>2+</sup> :Enz) K <sub>b</sub> (M <sup>-1</sup> ) $\Delta H^{\circ}_{\text{obs}}$ (kJ mol <sup>-1</sup> ) $\Delta S^{\circ}_{\text{obs}}$ (J mol <sup>-1</sup> K <sup>-1</sup> )	0.7 ± 0.7 5.42(± 0.7)x10 <sup>4</sup> 9 (± 3) 123 (± 24)	1.0 ± 0.8 1.19(± 0.1)x10 <sup>5</sup> 13 (± 4) 143 (± 25)				
<b>MES</b> ( $\Delta H_{\text{ion (buffer)}} = 15.53 \text{ kJ mol}^{-1}$ ) <sup>71</sup>	N (Co <sup>2+</sup> :Enz) K <sub>b</sub> (M <sup>-1</sup> ) $\Delta H^{\circ}_{\text{obs}}$ (kJ mol <sup>-1</sup> ) $\Delta S^{\circ}_{\text{obs}}$ (J mol <sup>-1</sup> K <sup>-1</sup> )	0.9 ± 0.3 1.2 (± 0.1)x10 <sup>5</sup> 13 (± 3) 205 (± 25)	1.3 ± 0.4 2.37 (± 0.2)x10 <sup>5</sup> 19 (± 5) 246 (± 30)	1.5 ± 0.4 3.78(± 0.3)x10 <sup>5</sup> 24 (± 5) 396 (± 40)	1.6 ± 0.3 1.11(± 0.2)x10 <sup>6</sup> 15 (± 4) 336 (± 40)	1.8 ± 0.2 4.73 (± 0.4)x10 <sup>6</sup> 11 (± 2) 341 (± 35)	
<b>Cacodylate</b> ( $\Delta H_{\text{ion (buffer)}} = -1.96 \text{ kJ mol}^{-1}$ ) <sup>71</sup>	N (Co <sup>2+</sup> :Enz) K <sub>b</sub> (M <sup>-1</sup> ) $\Delta H^{\circ}_{\text{obs}}$ (kJ mol <sup>-1</sup> ) $\Delta S^{\circ}_{\text{obs}}$ (J mol <sup>-1</sup> K <sup>-1</sup> )	0.4 ± 0.3 3.3 (± 0.7)x10 <sup>5</sup> 48 (± 10) 259 (± 30)	0.9 ± 0.4 3.48 (± 0.5)x10 <sup>5</sup> 65 (± 12) 314 (± 20)	1.4 ± 0.4 2.28(± 0.4)x10 <sup>6</sup> 60 (± 15) 312 (± 60)	1.9 ± 0.2 1.17(± 0.1)x10 <sup>6</sup> 69 (± 16) 326 (± 40)	2.3 ± 0.4 2.49 (± 0.4)x10 <sup>6</sup> 65 (± 12) 318 (± 55)	
<b>PIPES</b> ( $\Delta H_{\text{ion (buffer)}} = 11.45 \text{ kJ mol}^{-1}$ ) <sup>71</sup>	N (Co <sup>2+</sup> :Enz) K <sub>b</sub> (M <sup>-1</sup> ) $\Delta H^{\circ}_{\text{obs}}$ (kJ mol <sup>-1</sup> ) $\Delta S^{\circ}_{\text{obs}}$ (J mol <sup>-1</sup> K <sup>-1</sup> )			1.1 ± 0.2 1.76 (± 0.2)x10 <sup>6</sup> 50 (± 10) 353 (± 70)	1.7 ± 0.4 9.44 (± 0.7)x10 <sup>6</sup> 14 (± 3) 307 (± 60)	2.0 ± 0.7 7.12 (± 0.9)x10 <sup>5</sup> 8 (± 2) 271 (± 52)	2.3 ± 0.7 5.93 (± 0.9)x10 <sup>5</sup> 7 (± 1) 218 (± 30)
<b>MOPS</b> ( $\Delta H_{\text{ion (buffer)}} = 21.82 \text{ kJ mol}^{-1}$ ) <sup>71</sup>	N (Co <sup>2+</sup> :Enz) K <sub>b</sub> (M <sup>-1</sup> ) $\Delta H^{\circ}_{\text{obs}}$ (kJ mol <sup>-1</sup> ) $\Delta S^{\circ}_{\text{obs}}$ (J mol <sup>-1</sup> K <sup>-1</sup> )					1.3 ± 0.3 6.15 (± 1)x10 <sup>5</sup> -15 (± 3) 309 (± 40)	1.6 ± 0.2 1.30 (± 0.4)x10 <sup>6</sup> -16 (± 4) 254 (± 50)
<b>HEPES</b> ( $\Delta H_{\text{ion (buffer)}} = 21.01 \text{ kJ mol}^{-1}$ ) <sup>71</sup>	N (Co <sup>2+</sup> :Enz) K <sub>b</sub> (M <sup>-1</sup> ) $\Delta H^{\circ}_{\text{obs}}$ (kJ mol <sup>-1</sup> ) $\Delta S^{\circ}_{\text{obs}}$ (J mol <sup>-1</sup> K <sup>-1</sup> )					2.2 ± 0.2 1.98 (± 0.4)x10 <sup>7</sup> -10 (± 0.6) 346 (± 40)	1.5 ± 0.2 3.85 (± 0.3)x10 <sup>6</sup> -24 (± 5) 229 (± 22)

As explained in part one (Page 84) with zinc ion,  $\Delta S^{\circ}_{\text{calc}}$  consists of several components. To determine  $\Delta S^{\circ}_{\text{int}}$  and  $\Delta S^{\circ}_{\text{ion (enz)}}$ , the average values of  $\Delta S^{\circ}_{\text{calc}}$  (**Table 2.30**) at each pH is plotted against n (number of protons released) as shown in **Figure 2.42** because  $\Delta S^{\circ}_{\text{calc}}$  equates to  $\Delta S^{\circ}_{\text{int}} + n (\Delta S^{\circ}_{\text{ion (enz)}}$ ). From this graph we obtain the  $\Delta S^{\circ}_{\text{int}}$  as the intercept and the gradient of this graph is the  $\Delta S^{\circ}_{\text{ion (enz)}}$ .

**Table 2.30:** Average  $\Delta S^{\circ}_{\text{calc}}$  and n (number of protons released) at all pH's for cobalt ion binding to apoBclI.

	pH					
	5.20	5.60	6.0	6.35	6.80	7.20
Average $\Delta S^{\circ}_{\text{calc}}$ ( $\text{J mol}^{-1} \text{K}^{-1}$ )	196 ( $\pm 35$ )	234 ( $\pm 30$ )	354 ( $\pm 50$ )	323 ( $\pm 45$ )	317 ( $\pm 40$ )	234 ( $\pm 35$ )
n (number of protons released)	1.2 ( $\pm 1$ )	1.5 ( $\pm 1$ )	1.7 ( $\pm 1$ )	3.3 ( $\pm 0.8$ )	3.4 ( $\pm 0.8$ )	2.6 ( $\pm 2.0$ )

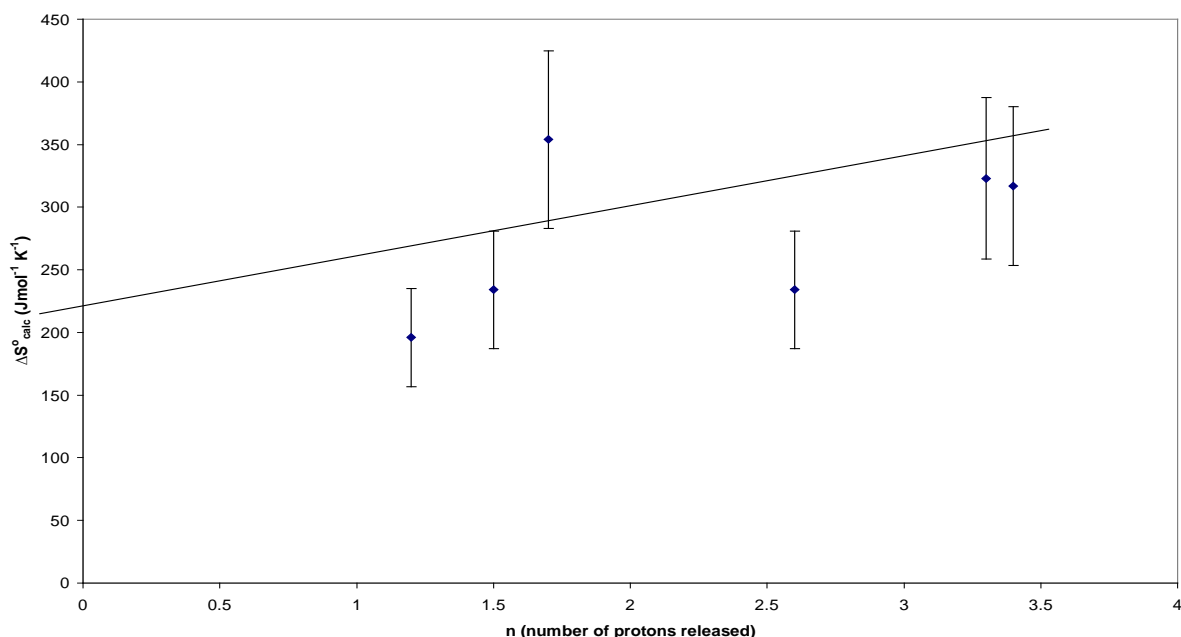


**Figure 2.42:**  $\Delta S^{\circ}_{\text{calc}}$  against n the number of protons released when cobalt ion binds to apoBclI.

From the graph in **Figure 2.42** the values of  $\Delta S^{\circ}_{\text{int}}$  and  $\Delta S^{\circ}_{\text{ion (enz)}}$  estimated are:  
 $\Delta S^{\circ}_{\text{int}} = 198 \text{ J mol}^{-1} \text{K}^{-1}$  and  $\Delta S^{\circ}_{\text{ion (enz)}} = 34 \text{ J mol}^{-1} \text{K}^{-1}$ .

### 2.3.3 - Part Three: Cadmium ion Titrated into ApoBclI

Part three presents the results of titration experiments of cadmium ion solutions against apoBclI solutions. The same buffers and pH's have been used as for zinc ion and cobalt ion titrations, with the exception of acetate buffer.

The calorimetric output for a cadmium ion titration into apoBclI at pH 5.20 in MES buffer (**Figure 2.43**) shows a single binding endothermic isotherm with a stoichiometric ratio of 0.9 ( $\pm 0.3$ ):1 ( $\text{Cd}^{2+}$ :Enz),  $K_b$  of  $4.68 (\pm 0.6) \times 10^5 \text{ M}^{-1}$ ,  $\Delta H^\circ_{\text{obs}}$  of  $66 (\pm 14) \text{ kJ mol}^{-1}$  and  $\Delta S^\circ_{\text{obs}}$  of  $275 (\pm 50) \text{ J mol}^{-1} \text{ K}^{-1}$ . Therefore at low pH, all the metal ions ( $\text{Zn}^{2+}$ ,  $\text{Co}^{2+}$  and  $\text{Cd}^{2+}$ ) bind to apoBclI in the ratio of 1:1 with a single binding event.

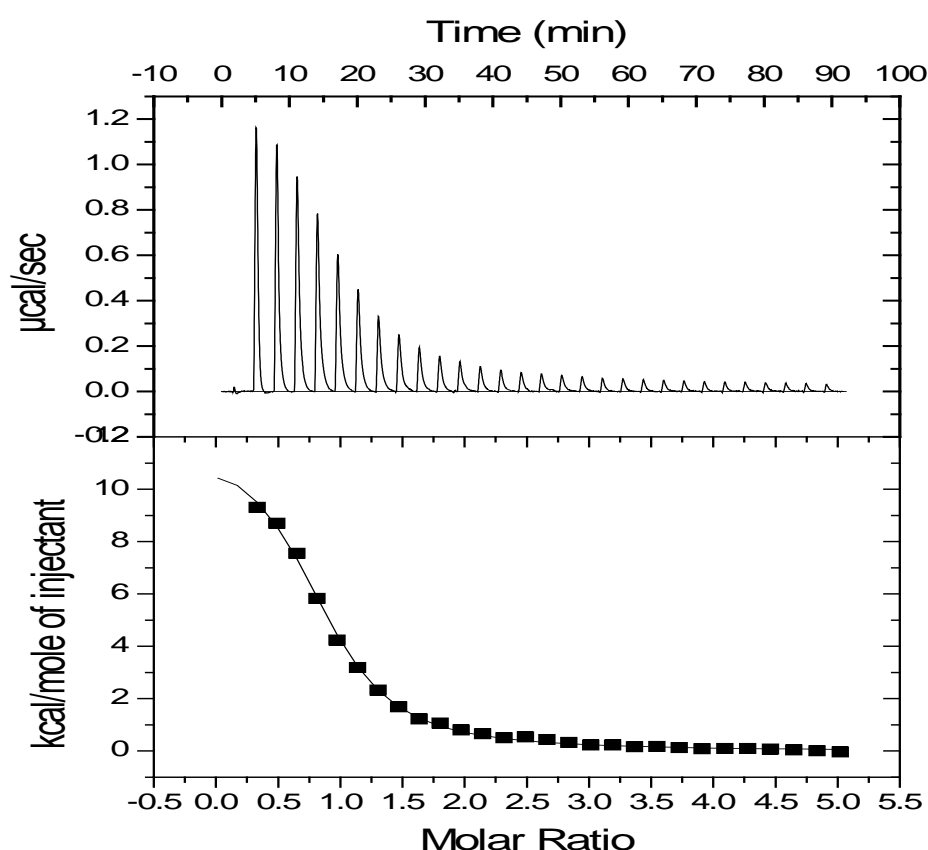


**Figure 2.43:** ITC output for  $\text{CdCl}_2$  solution ( $3.6 \times 10^{-4} \text{ M}$ ) titrated into apoBclI solution ( $1.8 \times 10^{-5} \text{ M}$ ) in MES buffer at pH 5.20 at  $25^\circ \text{C}$

Similarly, the typical calorimetric output of cadmium ion into apoBclI at pH 5.60 (**Figure 2.44**) in cacodylate buffer also shows a single binding event that represents an endothermic reaction. The experimental data simulation gives a stoichiometric ratio of 0.9 ( $\pm 0.3$ ):1 ( $\text{Cd}^{2+}$ : Enz),  $K_b$  of  $6.24 (\pm 1) \times 10^5 \text{ M}^{-1}$ ,  $\Delta H^\circ_{\text{obs}}$  of  $50 (\pm 10) \text{ kJ mol}^{-1}$  and  $\Delta S^\circ_{\text{obs}}$  of  $277 (\pm 30) \text{ J mol}^{-1} \text{ K}^{-1}$ .

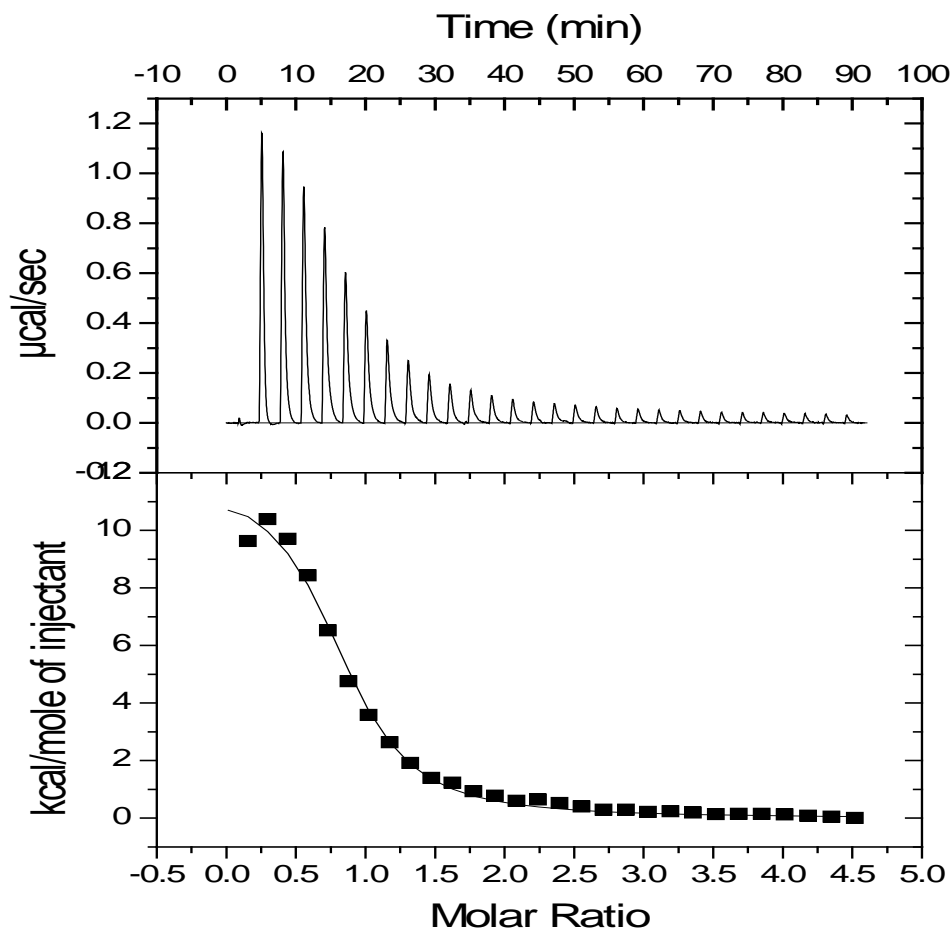


**Figure 2.44:** ITC output for  $\text{CdCl}_2$  solution ( $3.6 \times 10^{-4} \text{ M}$ ) into apoBclI solution ( $1.8 \times 10^{-5} \text{ M}$ ) in cacodylate buffer at pH 5.20 at  $25^\circ \text{C}$

However, the titration isotherms at pH 6.80 and 7.20 differ significantly from those with zinc ion and cobalt ion titrations. Data simulated for pH 7.20 in HEPES buffer is shown in **Figure 2.45**. The striking observation is that two distinct binding events are now seen, the second binding event occurs only when the first is complete. This means two cadmium ions bind to apoBclI in a

non-cooperative way, with two distinct steps, each of which corresponds to one cadmium ion per mole of enzyme.

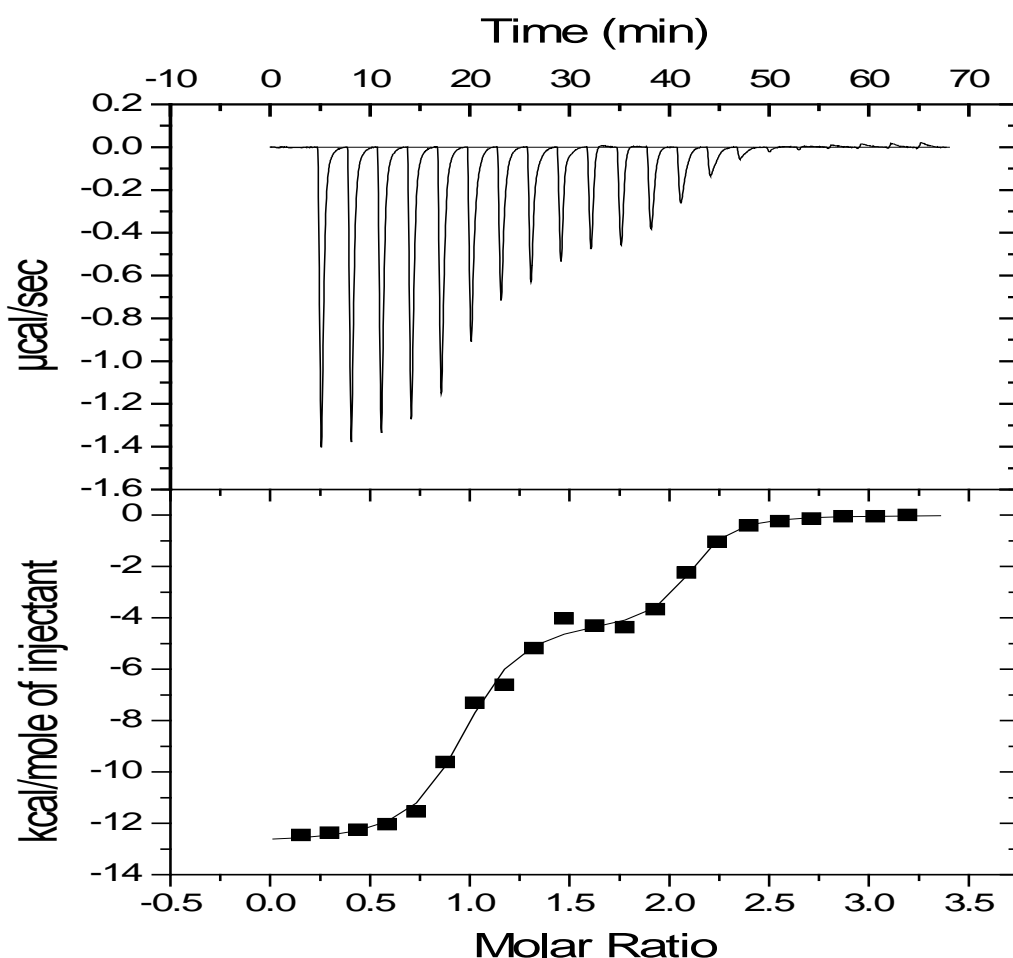


**Figure 2.45:** ITC output for  $\text{CdCl}_2$  solution ( $3.6 \times 10^{-4}$  M) titrated into apoBclI solution ( $1.8 \times 10^{-5}$  M) in HEPES buffer at pH 7.20 at 25 °C

From the experimental data simulation the stoichiometric ratio for the first binding site is 1.02 ( $\pm 0.3$ ):1 ( $\text{Cd}^{2+}$ : Enz) with a  $K_b$  of  $3.65 (\pm 0.5) \times 10^8 \text{ M}^{-1}$ , an  $\Delta H_{\text{obs}}^{\circ}$  of  $-52 (\pm 10) \text{ kJ mol}^{-1}$  and  $\Delta S_{\text{obs}}^{\circ}$  of  $60 (\pm 12) \text{ Jmol}^{-1} \text{ K}^{-1}$ . The second binding site parameters obtained are 0.9 ( $\pm 0.3$ ):1 ( $\text{Cd}^{2+}$ : Enz) with a  $K_b$  of  $5.29 (\pm 0.8) \times 10^6 \text{ M}^{-1}$ , a  $\Delta H_{\text{obs}}^{\circ}$  of  $-20 (\pm 5) \text{ kJ mol}^{-1}$  and  $\Delta S_{\text{obs}}^{\circ}$  of  $-10 (\pm 3) \text{ Jmol}^{-1} \text{ K}^{-1}$ .

The overall data for all the titrations for cadmium ion binding to apoBclI in different buffers and pH is shown in **Table 2.32**.

**Table 2.31** : Summary of simulation data for **cadmium** ion solution titrated into apoBclI solution.

		pH								
Buffers		5.20	5.60	6.0	6.35		6.80		7.20	
<b>MES</b> ( $\Delta H_{\text{ion}}^{\text{(buffer)}} = 15.53 \text{ kJ mol}^{-1}$ ) <sup>71</sup>	N (Cd <sup>2+</sup> :Enz) K <sub>b</sub> (M <sup>-1</sup> ) $\Delta H_{\text{obs}}^{\circ}$ (kJ mol <sup>-1</sup> ) $\Delta S_{\text{obs}}^{\circ}$ (J mol <sup>-1</sup> K <sup>-1</sup> )	0.9 ± 0.3 4.68(±0.6)×10 <sup>5</sup> 66 (±14) 275 (±50)	1.2 ± 0.2 1.62(±0.2)×10 <sup>6</sup> 46 (±9) 273 (±60)	1.0 ± 0.2 6.14(±0.5)×10 <sup>6</sup> -13 (±4) 86 (±35)	0.7 ± 0.3 1.55(±0.2)×10 <sup>8</sup> -19 (±4) 95 (±36)	1.4 ± 0.5 2.01(±0.3)×10 <sup>6</sup> -15 (±6) 71 (±16)	1.0 ± 0.3 8.10(±0.7)×10 <sup>7</sup> -19 (±3) 89 (±20)	1.5 ± 0.7 1.06(±0.1)×10 <sup>6</sup> -9 (±2) 82 (±10)		
<b>Cacodylate</b> ( $\Delta H_{\text{ion}}^{\text{(buffer)}} = -1.96 \text{ kJ mol}^{-1}$ ) <sup>71</sup>	N (Cd <sup>2+</sup> :Enz) K <sub>b</sub> (M <sup>-1</sup> ) $\Delta H_{\text{obs}}^{\circ}$ (kJ mol <sup>-1</sup> ) $\Delta S_{\text{obs}}^{\circ}$ (J mol <sup>-1</sup> K <sup>-1</sup> )	0.9 ± 0.3 6.24(±1)×10 <sup>5</sup> 50 (±10) 277 (±30)	1.1 ± 0.3 2.1(±0.5)×10 <sup>6</sup> 39 (±7) 269 (±48)	0.8 ± 0.3 5.30(±0.4)×10 <sup>5</sup> -62 (±12) 98 (±4)	0.9 ± 0.3 4.28(±0.3)×10 <sup>8</sup> -52 (±10) -10 (±5)	1.0 ± 0.3 6.9(±0.3)×10 <sup>6</sup> -18 (±5) 72 (±70)	0.9 ± 0.3 5.13(±0.3)×10 <sup>8</sup> -54 (±10) -12 (±20)	0.9 ± 0.3 7.26(±0.4)×10 <sup>6</sup> -19 (±4) 69 (±75)		
<b>PIPES</b> ( $\Delta H_{\text{ion}}^{\text{(buffer)}} = 11.45 \text{ kJ mol}^{-1}$ ) <sup>71</sup>	N (Cd <sup>2+</sup> :Enz) K <sub>b</sub> (M <sup>-1</sup> ) $\Delta H_{\text{obs}}^{\circ}$ (kJ mol <sup>-1</sup> ) $\Delta S_{\text{obs}}^{\circ}$ (J mol <sup>-1</sup> K <sup>-1</sup> )				0.7 ± 0.3 2.35(±0.2)×10 <sup>8</sup> -43 (±10) 17 (±16)	1.0 ± 0.5 5.2(±0.3)×10 <sup>6</sup> -13 (±7) 86 (±18)	1.0 ± 0.3 4.66(±0.6)×10 <sup>8</sup> -49 (±35) 17 (±7)	1.2 ± 0.3 3.93(±1)×10 <sup>6</sup> -19 (±5) 61(±20)	1.1 ± 0.2 3.6(±0.6)×10 <sup>8</sup> -42 (±8) 14 (±15)	1.1 (±0.9)± 0.2 5.85(±0.9)×10 <sup>6</sup> -15 (±5) 78 (±19)
<b>HEPES</b> ( $\Delta H_{\text{ion}}^{\text{(buffer)}} = 21.01 \text{ kJ mol}^{-1}$ ) <sup>71</sup>	N (Cd <sup>2+</sup> :Enz) K <sub>b</sub> (M <sup>-1</sup> ) $\Delta H_{\text{obs}}^{\circ}$ (kJ mol <sup>-1</sup> ) $\Delta S_{\text{obs}}^{\circ}$ (J mol <sup>-1</sup> K <sup>-1</sup> )							1.0 ± 0.3 3.65(±0.5)×10 <sup>8</sup> -52 (±10) -10 (±12)	0.9 ± 0.3 5.29(±0.8)×10 <sup>6</sup> -20 (±5) 63 (±16)	
<b>MOPS</b> ( $\Delta H_{\text{ion}}^{\text{(buffer)}} = 21.82 \text{ kJ mol}^{-1}$ ) <sup>71</sup>	N (Cd <sup>2+</sup> :Enz) K <sub>b</sub> (M <sup>-1</sup> ) $\Delta H_{\text{obs}}^{\circ}$ (kJ mol <sup>-1</sup> ) $\Delta S_{\text{obs}}^{\circ}$ (J mol <sup>-1</sup> K <sup>-1</sup> )							0.9 ± 0.3 3.8(±0.5)×10 <sup>8</sup> -54 (±10) -15 (±10)	1.1 ± 0.3 7.4(±0.9)×10 <sup>6</sup> -17 (±5) 73 (±18)	

The main conclusions gathered from **Table 2.31** are:

- The number of cadmium ions binding per enzyme increases from one to two as the pH is increased from pH 5.20 to 7.20 (with the exception of anomalous data in MES buffer, where at pH 6.80 the data appears to show that three cadmium ions bind). In general, however, two cadmium ions bind to each enzyme molecule at high pH's and, crucially, they bind independently, showing very distinct and different binding parameters. The two cadmium ions bind independently, in a non cooperative way (bind one metal ion at a time).
- When one cadmium ion binds at low pH, it shows relatively weak binding to the enzyme whereas when two cadmium ions bind cooperatively, the first cadmium ion binds very strongly to the enzyme and when the second cadmium ion binds, it binds to the enzyme quite weakly.
- Observed molar enthalpies of binding change from endothermic to exothermic as the pH is increased from pH 5.20 to 7.20 (based on the cacodylate buffer). The change in observed enthalpy from positive to negative is dependent on the binding of the cadmium ion and the dissociated protons released upon cadmium binding and the subsequent heat released by neutralisation with the buffer. The latter can change due to the dissociation of enthalpy of the various buffers.
- The entropy change with cadmium ion binding to the enzyme follows a similar trend throughout from pH 6.0 to 7.20, with low negative entropy for the first binding and small positive entropy for the second binding of cadmium ion. But when only one cadmium ion binds at low pH it has a high and positive entropy change.

The number of cadmium ions binding per enzyme molecule at each pH is plotted against pH in **Figure 2.46**.

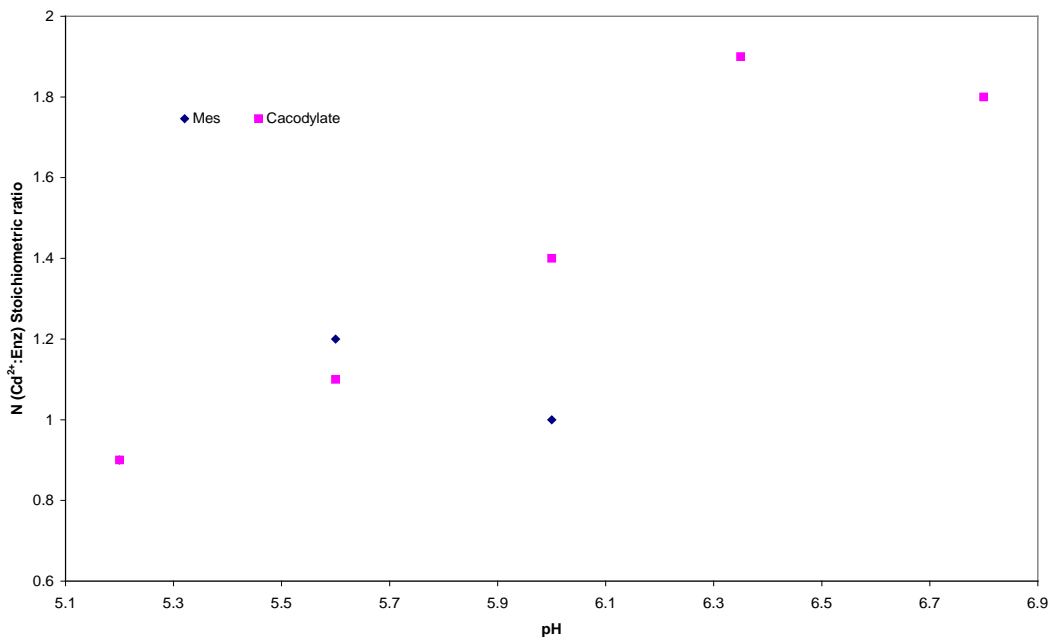


**Figure 2.46:** Plot of N (Cd<sup>2+</sup>: Enz) against pH for cadmium ion binding to apoBclI in MES and cacodylate buffer at 25°C.

As seen in **Figure 2.46** the trend in stoichiometric ratio with pH for cadmium ion binding to apoBclI shows an increase in the number of cadmium ions binding from about 1.0 to about 2.0 as the pH is increased. The trend seen here with the increase in stoichiometric ratio with pH is similar to that observed for both zinc ion and cobalt ion binding (**Figures 2.24 and 2.37**).

### 2.3.3.1 - Dissociation of Acid Groups on BcII when Cadmium ion Binds

As discussed for zinc and cobalt ions, the experimental  $\Delta H_{\text{obs}}^{\circ}$  data can be segregated to allow for the contribution from the change in enthalpy due to the neutralisation of the protons released by metal ion binding to the enzyme by the buffer. For each pH, a plot of  $\Delta H_{\text{obs}}^{\circ}$  against  $\Delta H_{\text{ion (buffer)}}^{\circ}$  has a gradient equal to  $n$  (number of protons released by the enzyme) and an intercept equal to  $\Delta H_{\text{int}}^{\circ} + n\Delta H_{\text{ion (enz)}}^{\circ}$ . For cadmium ion at higher pH there are two individual binding sites and the data for each site is treated individually. For example, the plot at pH 6.80 is shown in **Figure 2.47** for the first binding site and in **Figure 2.48** for the second binding site, using the data for MES, cacodylate and PIPES buffers. Values for  $n$  and  $(\Delta H_{\text{int}}^{\circ} + n\Delta H_{\text{ion (enz)}}^{\circ})$  at each pH are given in **Table 2.33**.

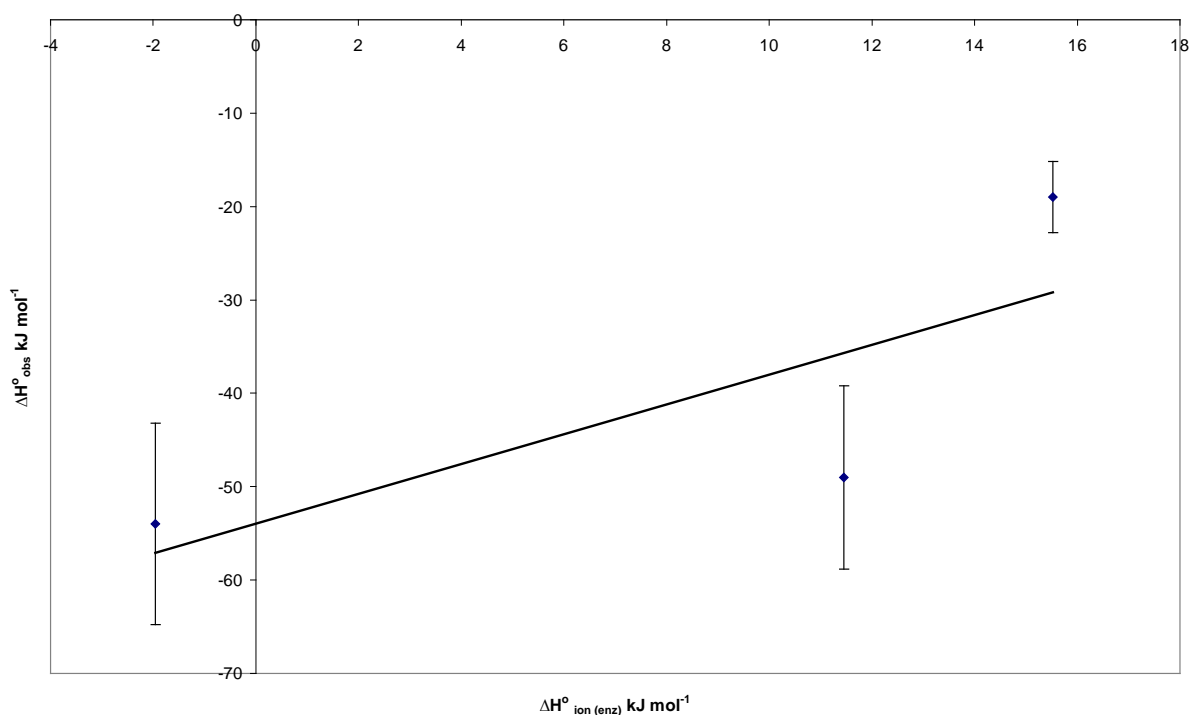


**Figure 2.47:**  $\Delta H_{\text{obs}}^{\circ}$  against  $\Delta H_{\text{ion (buffer)}}^{\circ}$  at pH 6.80 for the first cadmium ion titrated into apoBcII solution.

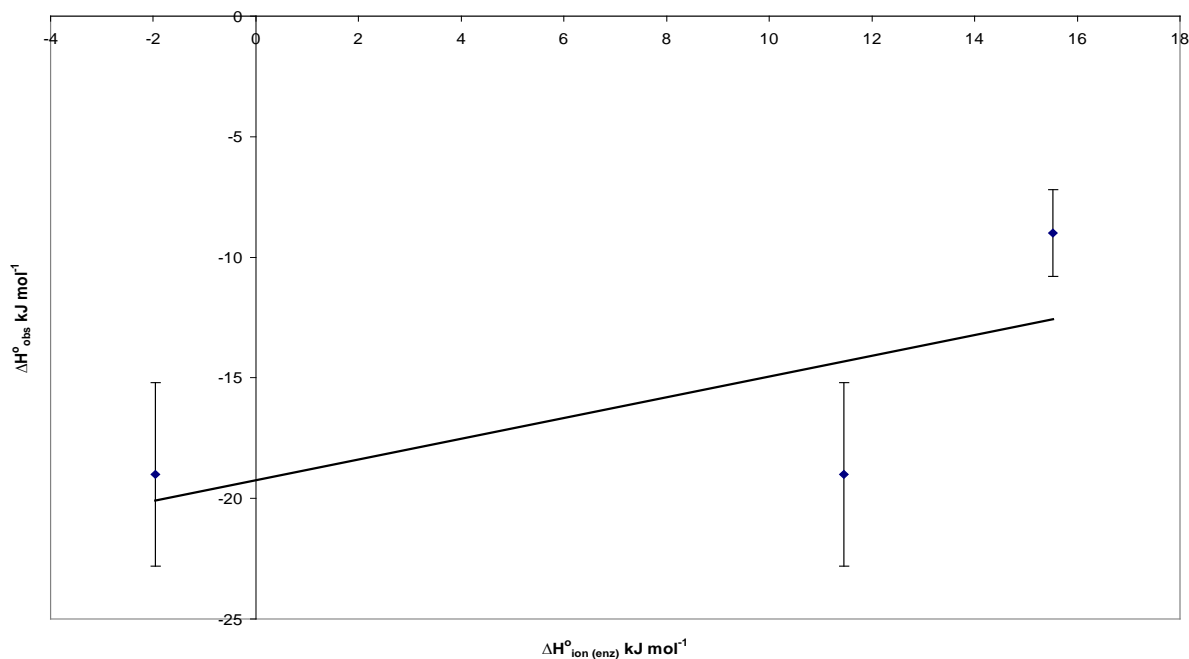


**Figure 2.48:**  $\Delta H^{\circ}_{\text{obs}}$  against  $\Delta H^{\circ}_{\text{ion (buffer)}}$  at pH 6.80 for the second cadmium ion titrated into apoBcII solution.

**Table 2.32:** Values of  $n$  (number of protons released by the enzyme when cadmium ion binds to the enzyme) and  $\Delta H^{\circ}_{\text{int}} + n\Delta H^{\circ}_{\text{ion (enzyme)}}$  as a function of pH for cadmium ion binding to apoBcII.

<i>pH</i>	<i>n (number of protons released by enzyme)</i>		$\Delta H^{\circ}_{\text{int}} + n\Delta H^{\circ}_{\text{ion (enzyme)}}$ ( $\text{kJ mol}^{-1}$ )	
	<i>Site 1</i>	<i>Site 2</i>	<i>Site 1</i>	<i>Site 2</i>
5.20	$1 \pm 0.5$	-	$52 \pm 10$	-
5.60	$1 \pm 0.4$	-	$40 \pm 20$	-
6.0	$2 \pm 0.7$	-	$-57 \pm 10$	-
6.35	$1.7 \pm 0.8$	$0.2 \pm 0.8$	$-51 \pm 10$	$-17 \pm 10$
6.80	$1.7 \pm 1.0$	$0.4 \pm 1.0$	$-54 \pm 10$	$-19 \pm 10$
7.20	$1.0 \pm 0.5$	$0.3 \pm 0.5$	$-29 \pm 20$	$-11 \pm 10$

**Table 2.32** shows how  $n$  (the number of protons released by the enzyme when cadmium ion binds to both the sites) and the enthalpy change associated with

both cadmium ions binding and proton loss by the enzyme varies with pH. The experimental uncertainties of these data are relatively large, because the graph from which these are determined have few points and those few points themselves have significant uncertainties. Nevertheless, the trend is clear and the number of protons released with the first cadmium ion binding increases as the pH is increased as shown in **Table 2.32**, this trend is similar to that seen with the binding of cobalt ion. The second binding site shows the protons released is possibly zero as the values are very low.

The individual enthalpy components can be separated as previously described and  $(\Delta H_{\text{int}}^{\circ} + n\Delta H_{\text{ion (enzyme)}}^{\circ})$  is plotted against  $n$  (number of protons released) to determine  $\Delta H_{\text{int}}^{\circ}$  and  $\Delta H_{\text{ion (enzyme)}}^{\circ}$  as shown in **Figure 2.49**.

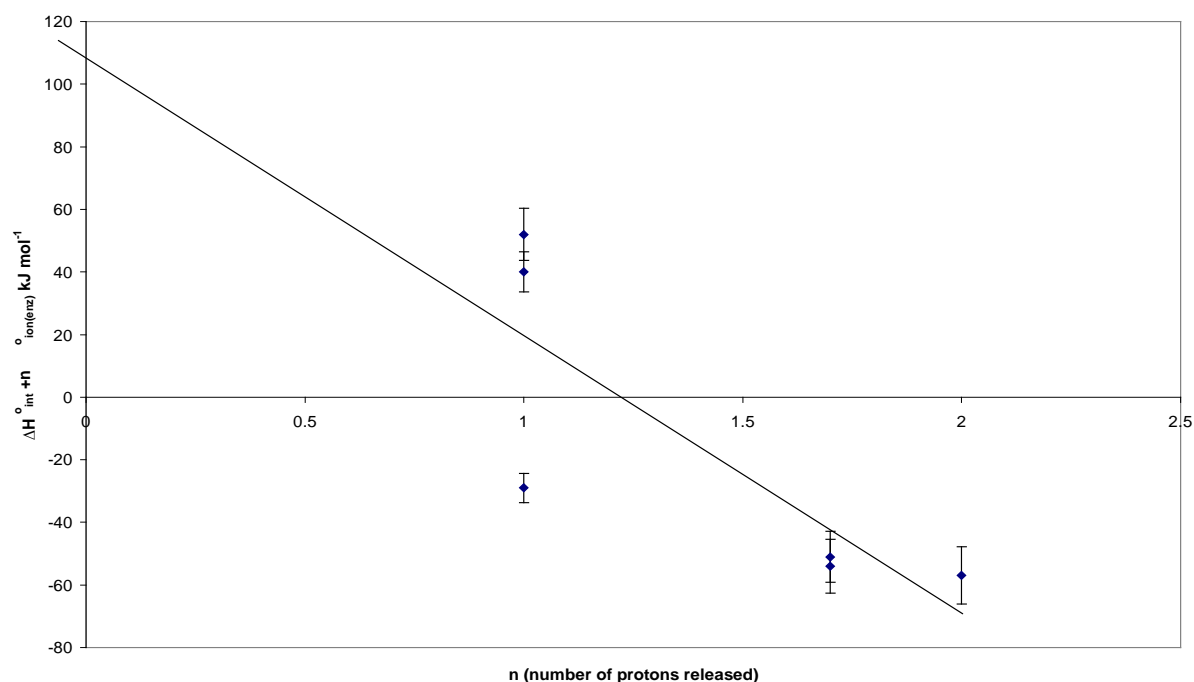


**Figure 2.49:**  $\Delta H_{\text{int}}^{\circ} + n\Delta H_{\text{ion (enzyme)}}^{\circ}$  against  $n$  the number of protons released when the first cadmium ion binds to apoBcll.

From the graph in Figure **2.49** the values determined for  $\Delta H_{\text{int}}^{\circ}$  and  $\Delta H_{\text{ion (enzyme)}}^{\circ}$  are:  $\Delta H_{\text{int}}^{\circ} = 108 (\pm 35) \text{ kJ mol}^{-1}$  and  $\Delta H_{\text{ion (enzyme)}}^{\circ} = -89 (\pm 15) \text{ kJ mol}^{-1}$ .

It is not possible to determine the individual components for the second cadmium ion as the data is limited and  $n$  is small and unvaried.

Entropy Calculations

As indicated before, the  $\Delta S^{\circ}_{\text{obs}}$  values are complex, as they were calculated without correction for the ionisation of buffer.

Therefore **Table 2.33** replaces **Table 2.31** with the  $\Delta S^{\circ}_{\text{calc}}$  calculated as previously described.

**Table 2.33:** Summary of simulation data for **cadmium** ion solution titrated into apoBclI solution with  $\Delta S^{\circ}_{\text{calc}}$ .

		pH								
Buffers		5.20	5.60	6.0	6.35		6.80		7.20	
<b>MES</b> ( $\Delta H_{\text{ion (buffer)}} = 15.53 \text{ kJ mol}^{-1}$ ) <sup>71</sup>	N (Cd <sup>2+</sup> :Enz) K <sub>b</sub> (M <sup>-1</sup> ) $\Delta H^{\circ}_{\text{obs}}$ (kJ mol <sup>-1</sup> ) $\Delta S^{\circ}_{\text{obs}}$ (J mol <sup>-1</sup> K <sup>-1</sup> )	0.9 ± 0.3 4.68(±0.6)×10 <sup>5</sup> 66 (±14) 382 (±50)	1.2 ± 0.2 1.62(±0.2)×10 <sup>6</sup> 46 (±9) 322 (±60)	1.0 ± 0.2 6.14(±0.5)×10 <sup>6</sup> -13 (±4) 191 (±35)	0.7 ± 0.3 1.55(±0.2)×10 <sup>8</sup> -19 (±4) 182 (±36)	1.4 ± 0.5 2.01(±0.3)×10 <sup>6</sup> -15 (±6) 81 (±16)	1.0 ± 0.3 8.1(±0.7)×10 <sup>7</sup> -19 (±3) 176 (±20)	1.5 ± 0.7 1.06(±0.1)×10 <sup>6</sup> -9 (±2) 106 (±10)		
<b>Cacodylate</b> ( $\Delta H_{\text{ion (buffer)}} = -1.96 \text{ kJ mol}^{-1}$ ) <sup>71</sup>	N (Cd <sup>2+</sup> :Enz) K <sub>b</sub> (M <sup>-1</sup> ) $\Delta H^{\circ}_{\text{obs}}$ (kJ mol <sup>-1</sup> ) $\Delta S^{\circ}_{\text{obs}}$ (J mol <sup>-1</sup> K <sup>-1</sup> )	0.9 ± 0.3 6.24(±1)×10 <sup>5</sup> 50 (±10) 272 (±30)	1.1 ± 0.3 2.1(±0.5)×10 <sup>6</sup> 39 (±7) 245 (±48)	0.8 ± 0.3 5.30(±0.4)×10 <sup>5</sup> -62 (±12) 6 (±4)	0.9 ± 0.3 4.28(±0.3)×10 <sup>8</sup> -52 (±10) 120 (±5)	1.0 ± 0.3 6.9(±0.3)×10 <sup>6</sup> -18 (±5) 371 (±70)	0.9 ± 0.3 5.1(±0.3)×10 <sup>8</sup> -54 (±10) 115 (±20)	0.9 ± 0.3 7.26(±0.4)×10 <sup>6</sup> -19 (±4) 360 (±75)		
<b>PIPES</b> ( $\Delta H_{\text{ion (buffer)}} = 11.45 \text{ kJ mol}^{-1}$ ) <sup>71</sup>	N (Cd <sup>2+</sup> :Enz) K <sub>b</sub> (M <sup>-1</sup> ) $\Delta H^{\circ}_{\text{obs}}$ (kJ mol <sup>-1</sup> ) $\Delta S^{\circ}_{\text{obs}}$ (J mol <sup>-1</sup> K <sup>-1</sup> )				0.7 ± 0.3 2.35(±0.2)×10 <sup>8</sup> -43 (±10) 81 (±16)	1.0 ± 0.5 5.2(±0.3)×10 <sup>6</sup> -13 (±7) 93 (±18)	1.0 ± 0.3 4.7(±0.6)×10 <sup>8</sup> -49 (±35) 27 (±7)	1.2 ± 0.3 3.93(±1)×10 <sup>6</sup> -19 (±5) 118(±20)	1.1 ± 0.2 3.6(±0.6)×10 <sup>8</sup> -42 (±8) 61 (±15)	1.1 ± 0.2 5.8(±0.9)×10 <sup>8</sup> -15 (10) 91 (±19)
<b>HEPES</b> ( $\Delta H_{\text{ion (buffer)}} = 21.01 \text{ kJ mol}^{-1}$ ) <sup>71</sup>	N (Cd <sup>2+</sup> :Enz) K <sub>b</sub> (M <sup>-1</sup> ) $\Delta H^{\circ}_{\text{obs}}$ (kJ mol <sup>-1</sup> ) $\Delta S^{\circ}_{\text{obs}}$ (J mol <sup>-1</sup> K <sup>-1</sup> )								1.0 ± 0.3 3.7(±0.5)×10 <sup>8</sup> -52 (±10) 60 (±12)	0.9 ± 0.3 5.29(±0.8)×10 <sup>6</sup> -20 (±5) 83(±16)
<b>MOPS</b> ( $\Delta H_{\text{ion (buffer)}} = 21.82 \text{ kJ mol}^{-1}$ ) <sup>71</sup>	N (Cd <sup>2+</sup> :Enz) K <sub>b</sub> (M <sup>-1</sup> ) $\Delta H^{\circ}_{\text{obs}}$ (kJ mol <sup>-1</sup> ) $\Delta S^{\circ}_{\text{obs}}$ (J mol <sup>-1</sup> K <sup>-1</sup> )								0.9 ± 0.3 3.8(±0.5)×10 <sup>8</sup> -54 (±10) 56 (±10)	1.1 ± 0.3 7.4(±0.9)×10 <sup>6</sup> -17 (±5) 96 (±18)

As  $\Delta S_{\text{calc}}^{\circ}$  equates to  $\Delta S_{\text{int}}^{\circ} + n\Delta S_{\text{ion (enz)}}^{\circ}$ . To determine the individual components  $\Delta S_{\text{calc}}^{\circ}$  consists, the plot in **Figure 2.50** shows  $\Delta S_{\text{calc}}^{\circ}$  against  $n$  (number of protons released) and **Table 2.34** shows the values used for **Figure 2.50** to determine  $\Delta S_{\text{int}}^{\circ}$  and  $\Delta S_{\text{ion(enz)}}^{\circ}$ . Only the first binding site is used to determine these values as it is difficult and not accurate values with the second binding site as the number of protons released is close to zero.

**Table 2.34:** Average  $\Delta S_{\text{calc}}^{\circ}$  and  $n$  (number of protons released) at all pH's for cadmium ion binding to apoBclI for site one.

	pH					
	5.20	5.60	6.0	6.35	6.80	7.20
Average $\Delta S_{\text{calc}}^{\circ}(\text{J mol}^{-1} \text{K}^{-1})$	327 ( $\pm 40$ )	284 ( $\pm 50$ )	99 ( $\pm 20$ )	128 ( $\pm 25$ )	106 ( $\pm 15$ )	59 ( $\pm 12$ )
$n$ (number of protons released)	1.0 ( $\pm 0.5$ )	1.0 ( $\pm 0.4$ )	2.0 ( $\pm 0.7$ )	1.7 ( $\pm 0.8$ )	1.7 ( $\pm 1.0$ )	1.0 ( $\pm 0.5$ )

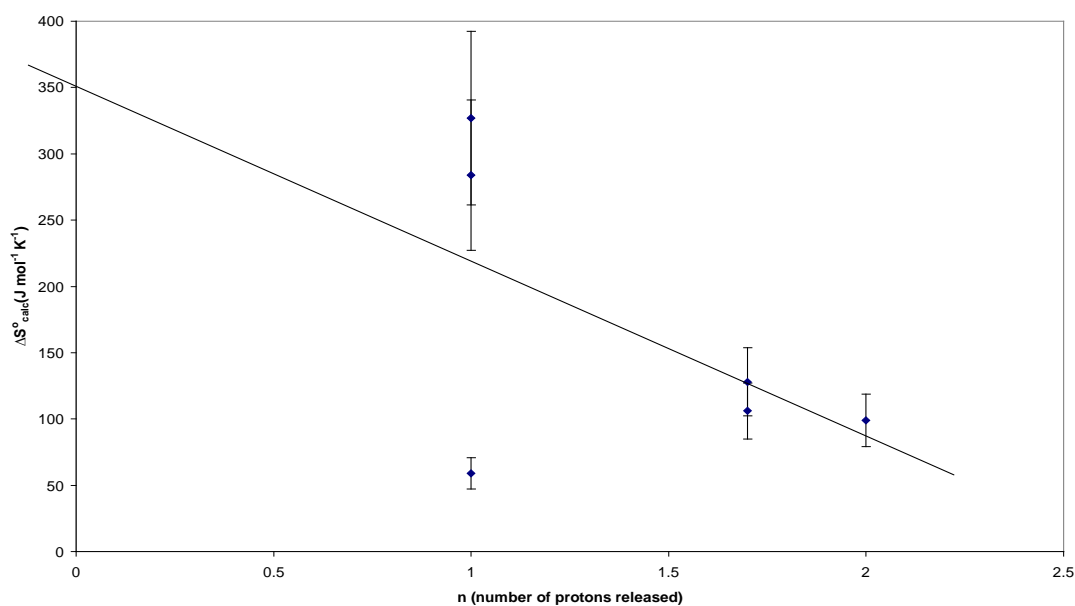


**Figure 2.50:**  $\Delta S_{\text{calc}}^{\circ}$  against the number of protons released when the first cadmium ion binds to apoBclI.

From the graph in **Figure 2.50** the values of  $\Delta S_{\text{int}}^{\circ}$  and  $\Delta S_{\text{ion (enz)}}^{\circ}$  estimated are:

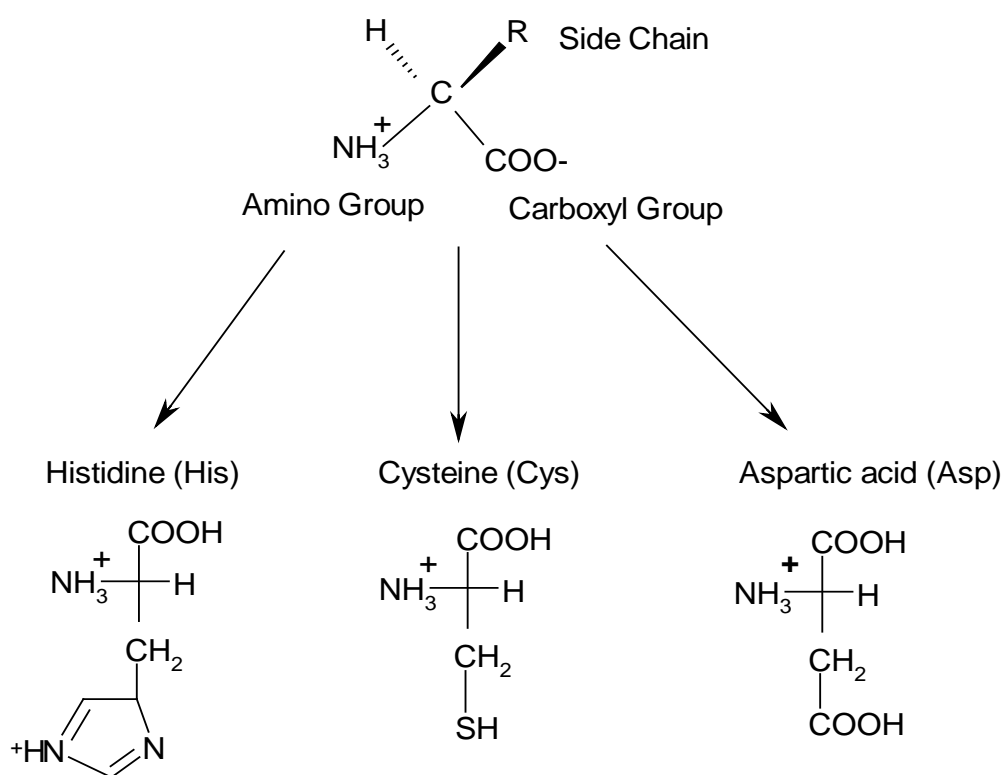
$$\Delta S_{\text{int}}^{\circ} = 357 (\pm 70) \text{ J mol}^{-1} \text{ K}^{-1} \text{ and } \Delta S_{\text{ion (enz)}}^{\circ} = -136 (\pm 10) \text{ J mol}^{-1} \text{ K}^{-1}.$$

## 2.4 - Discussion

### 2.4.1 - Amino Acids

Proteins, such as enzymes are polymeric chains of amino acids linked by amide/peptide groups. Studies based on X-ray diffraction and on NMR studies have shown that in apoBclI the important amino acids involved in metal ion binding to apoBclI are histidine, cysteine and aspartic acid (**Scheme 2.16**).

The structures of these amino acids are as shown below:



**Scheme 2.16:** Amino acid structures

The side chains of these three amino acids all have acid functional groups that can dissociate. For example, the side chain imidazole of histidine can be cationic or neutral whereas the side chain carboxylic acid of aspartic acid can be anionic or neutral. Each amino acid side chain has a specific  $pK_a$  dictating

the pH range under which  $H^+$  dissociation occurs, but within different proteins they may vary because of the microenvironment.

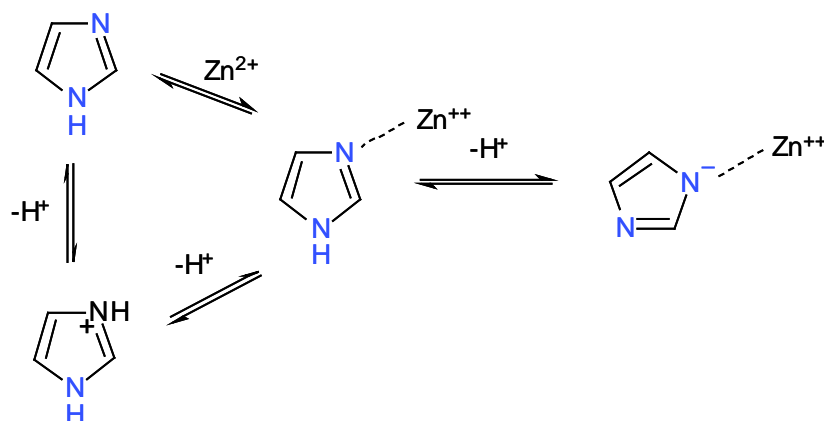
### 2.4.2 - Ionisation and Binding of Metal ions to Ligands

Metal ion binding to apoBclI occurs through coordination to the side chains of the amino acid residues. It is possible and probable that metal ion coordination may result in changes to the  $pK_a$  of ionisable hydrogens on those side chains that are unionised before coordination, and even the  $pK_a$  of water coordinated to the metal ion may change when the metal ion binds to the enzyme. Such changes can result in the dissociation of hydrogen ions simultaneously with coordination of the metal ions. The possible ligands and their ionisation states associated with apoBclI are shown below:

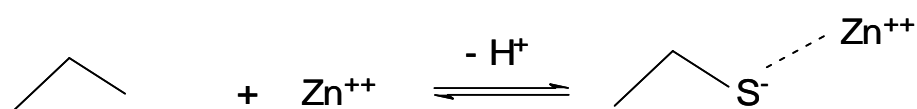


The extent to which the amino acid side chain is dissociated depends on the pH and its  $pK_a$ . If metal ion binding causes the  $pK_a$  of the amino acid side chain ligand to fall from a value above to one below the solution pH, then dissociation of a hydrogen ion will occur. This is illustrated in **Scheme 2.17**.

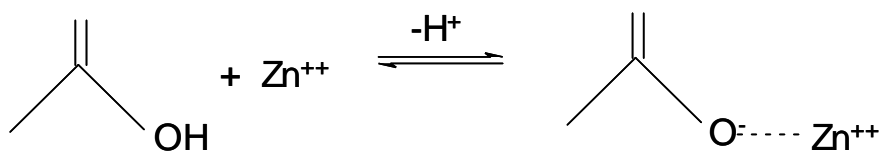
Imidazole



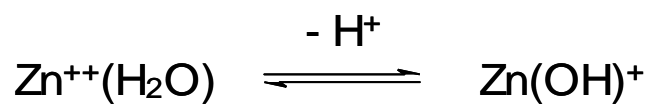
Thiol



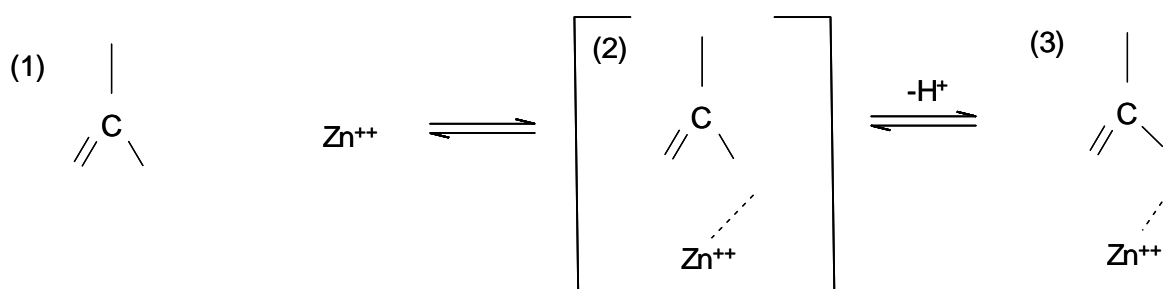
Carboxylate



Water

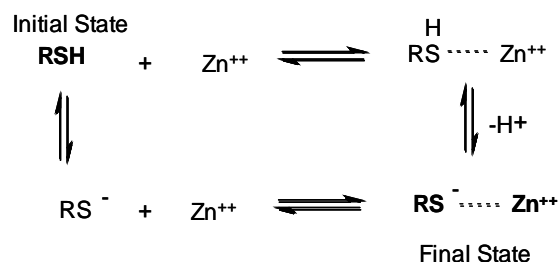
**Scheme 2.17:** Ionisations of ligands when zinc ion binds.

For example, undissociated carboxylic acid residues of aspartic acid cannot bind metal ions whereas neutral imidazole residues of histidine can. The carboxylic acid group of an aspartate residue is more likely to be dissociated before metal ion binding, unless it has an unusually high  $pK_a$ . Whether or not a proton is lost upon binding depends on the initial ionisation state. So if a carboxylate anion is the dominant form of an aspartate residue at a particular pH then no proton is lost upon binding. As shown in **Scheme 2.18** it is very unlikely for the carboxylate to be in the form shown by (2) due to its low  $pK_a$ , therefore metal ion bound carboxylate will only be in its dominant form shown by (3).



Scheme 2.18

Conversely a thiol group of a cysteine at neutral pH probably exists predominantly in its undissociated form and metal ion binding would significantly reduce its  $pK_a$  so that a proton might be lost i.e. cysteine only binds in its anionic form (**Scheme 2.19**). The thiol residue may be ionised if it is part of an ion-pair e.g.  $\text{ImiH}^+ \cdots \text{SCys}^-$  as found for example in papain.



Scheme 2.19

Finally, the water bound to a metal ion may ionise when the metal ion binds to the enzyme depending on its  $pK_a$  and the pH. In addition to this direct effect on the ligands metal ion binding to enzymes may also perturb the  $pK_a$  of neighbouring amino acid side chains near the active site. This could be important when a second metal ion binds as a metal ion already present must perturb the micro-environment. The  $pK_a$  of water bound to a metal ion may differ from that in the simple hydrated ion because of charge transfer from the ligands changing the positive charge density on the metal ion and due to changes in coordination number e.g. hydrated zinc ion has 6 water molecules attached whereas in many enzymes it is 4 or 5 coordinated.

### 2.4.3 - Number of Metal ions Bound

BcII from *B-cereus* strain 569/H/9 has two metal ion binding sites.<sup>26-38</sup> According to x-ray crystallography, site one (3H) is four coordinated with three histidine ligands and one solvent ligand. Site two (DCH) is five coordinated with histidine, cysteine, aspartic acid, a solvent ligand and a bridging water or hydroxide-ion. As mentioned previously in the introduction, the two metal ions bound to sites one and two are found to be relatively close to each other at a distance of 3.7-4.4 Å.<sup>23-24</sup> The two binding sites seem to have different metal ion affinities, where the first metal ion is generally bound with high affinity, and the second metal ion binds more weakly to the enzyme.<sup>21</sup>

How metal ions ( $Zn^{2+}$ ,  $Co^{2+}$ , and  $Cd^{2+}$ ) bind to apoBcII when the pH is varied was investigated by ITC, titrating the apo-enzyme against the metal ion at a fixed pH. The results from the work reported in this thesis show that the number of metal ions bound varies with pH (**Table 2.35**). The binding of metal ions to the apo-enzyme is partially a competition between the metal ion and protons for some of the protein ligands and at a given pH may not result in a simple stoichiometry because they may be a mixture of species present. Nonetheless, for convenient discussion, we shall use simple ratios of metal

ions to enzyme (**Table 2.35**). The number of zinc, cobalt or cadmium ions binding to apoBcII in solution increases from one to two as the pH is increased from 5.20 to 6.80 (**Table 2.35**). At low pH (5.20 and 5.60) only one metal ion binds to the apoBcII, whereas at high pH two metal ions bind to apoBcII. The stoichiometry of 1:1 for metal ion to enzyme ratio cannot be the result of half the enzyme being in the binuclear state and the other half still apo state because the ITC is a titration experiment in which metal ion is added until the end-point is reached. Previous work from this laboratory showed that enzyme activity decreased with decreasing pH due to an apparent two enzyme ionisations of  $pK_a$  of both about 5.7. However, this decrease in activity could be overcome by increasing the concentration of zinc ions.<sup>17,72</sup> This data is now interpreted as due to the loss of zinc ion from the active binuclear enzyme to form the inactive mononuclear one.

When two zinc or cobalt ions bind to apoBcII at high pH, only a single binding event is observed in the titration by ITC. This implies zinc and cobalt ions probably bind to the enzyme in a positive cooperative way. Jacquin et al<sup>64</sup> have investigated how zinc ion binds to apoBcII, but only at pH 7.5, using ESI-MS, MS and NMR spectroscopy and their results are also consistent with positive cooperative binding. They found evidence for the di-zinc species from the beginning of zinc addition even at relatively low zinc ion concentrations, Selevsek et al<sup>73</sup> have also investigated this by ESI-MS spectroscopy at pH 7.0, and they also suggest that the di-zinc species is present even at low zinc ion concentrations.<sup>73</sup> This suggests that at about pH 7 when zinc ion binds, both sites on the enzyme are occupied at the same time and that there is little or no mononuclear enzyme present. This is positive cooperativity. Earlier work from this laboratory<sup>74</sup> also used ITC to titrate zinc ion into apoBcII and also reported that only a single binding event was observed when two zinc ions bind at pH 7.1 in MOPS buffer.<sup>74</sup> The work reported in this thesis shows that a single binding event to form the binuclear enzyme is observed even at lower pH's.

A single binding event was also observed when two cobalt ions binds at neutral pH and this is also consistent with a previous study that showed the

presence of di-cobalt form when the ratio of cobalt ion to enzyme is below one,<sup>75</sup> at pH 7.5 in Hepes buffer using UV-visible titration that showed features in the spectra corresponding to both the mono and the di-zinc species.<sup>75</sup> DeSeny et al also looked at the binding of cobalt ion to apoBcII and showed equal scrambling of the metal ions between the two binding sites.<sup>76</sup> This implies both the sites are occupied at the same time. Therefore the single binding event observed in the work reported here with cobalt ion at neutral pH also suggests it binds in a positive cooperative way.

A summary of the number of metal ions bound as a function of pH is given in **Table 2.35**.

**Table 2.35:** The number of metal ions binding to apoBcII as a function of pH.

pH	Zinc ion	Cadmium ion		Cobalt ion
5.20	1.0 ( $\pm 0.5$ )	1.0 ( $\pm 0.3$ )	-	1.0 ( $\pm 0.5$ )
5.60	1.0 ( $\pm 0.5$ )	1.0 ( $\pm 0.3$ )	-	1.0 ( $\pm 0.5$ )
6.00	1.6 ( $\pm 0.5$ )	1.0 ( $\pm 0.3$ )	-	1.3 ( $\pm 0.3$ )
6.35	1.9 ( $\pm 0.3$ )	1.0 ( $\pm 0.3$ )	1.0 ( $\pm 0.5$ )	1.8 ( $\pm 0.3$ )
6.80	2.0 ( $\pm 0.3$ )	1.0 ( $\pm 0.3$ )	1.0 ( $\pm 0.5$ )	2.0 ( $\pm 0.3$ )

With cadmium ion binding to apoBcII a similar trend is observed, with the number of metal ions binding increasing from one to two as the pH is increased. However, this metal ion shows two distinct binding events at higher pH's showing that cadmium ions bind sequentially to the enzyme. Jacquin et al have also studied cadmium ion binding to apoBcII using MS and NMR spectroscopy<sup>64</sup> and the experimental data showed that at pH 7.5 with low concentrations of cadmium ion, only the mono-form was detected. The binuclear form was only detected with high concentrations of cadmium ion. Therefore the work reported here is consistent with previous findings and implies the binding sites are occupied sequentially in a non-cooperative way.

As discussed, the number of metal ions binding to apoBclI increases from one to two as the pH is increased. The plot in **Figure 2.51** shows how the number of zinc ions increases as the pH is increased. If the binding of the second metal ion requires one of the new ligands to lose a proton in order for it to bind, then a pH dependence of the concentration of di-zinc species should be similar to an ionisation curve. The plot in **Figure 2.51** shows how the stoichiometric ratio of zinc ions to enzyme varies with pH in MES buffer. The buffer used is always in excess of the concentration of the enzyme so therefore the pH is constant for each titration, and this remains constant throughout the reaction even though a relatively small amount of protons are liberated upon metal ion binding. The ratio varies from 1.2 at pH 5.20 to 2.0 at pH 6.80. A curve has been drawn through the points assuming that the ratio is stable at 1.0 at low pH and stable at 2.0 at high pH. Despite the assumptions the figure does show an apparent sigmoidal curve with apparent  $pK_a$  of 5.8. If the curve is taken as representing the ionisation of a hydrogen ion from one of the ligands upon second metal ion binding, then it would exhibit the  $pK_a$  of 5.8.

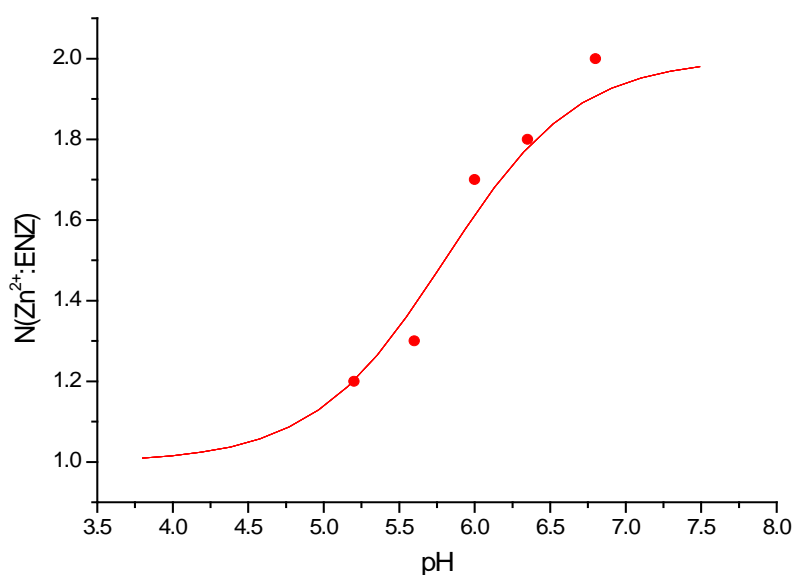
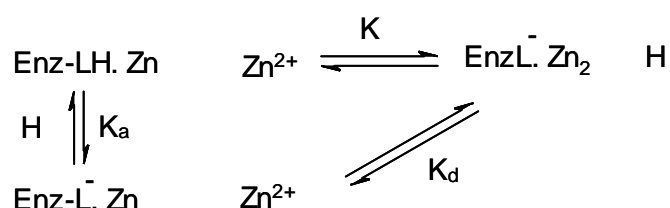


**Figure 2.51:** The ratio  $N(\text{Zn}^{2+}:\text{Enz})$  against pH for zinc ion binding to apoBclI in MES buffer. The solid line represents the fit for the experimental data points to a simple ionisation model.

This treatment, using how the zinc ion to enzyme ratio varies with pH, to identify hydrogen ion dissociation events on the enzyme, obviously can only be applied to the binding of the second zinc ion over the pH range studied here. If the binding of a second zinc ion requires two or more ligands to be ionised then the slope of the plot of fraction metal-bound against pH would have a slope greater than one, which it does not in **Figure 2.51** (in Figure 2.51 the slope of one is calculated from the sigmoidal portion of the graph not from a linear graph). So even if the plot is not ideally sigmoidal to give an accurate  $pK_a$ , it is good enough to demonstrate that only one ligand loses a proton upon binding the second metal ion

The binding of the second zinc ion to the mono-nuclear enzyme can be described by the following set of equilibria (**Scheme 2.20**):



**Scheme 2.20:** Conversion of zinc one (EnzLHZn) to zinc two (EnzLHZn<sub>2</sub>) with ionisation of one ligand.

With a  $pK_a$  of 5.8, the second zinc ion is fully bound at pH above 6.5. Around pH 6.0 the enzyme exists in both the mono and the di-form roughly in a 50:50 ratio. The fraction of the di-form is given by:

$$\text{Fraction (Di-Zinc form)} = \frac{\text{L}^- \cdot \text{Zn}_2}{E_{\text{TOT}}} = \frac{K_a}{\text{H}^+ + K_a} \cdot \frac{\text{Zn}}{K_d}$$

The fraction in the di-form is derived using a simple approach assuming only the mono-zinc enzyme with the ligand ionised binds to the second zinc ion and this is derived using the following method:

$$\text{Fraction} = \frac{L^{\cdot-} \cdot Zn_2}{(L^{\cdot-} \cdot Zn_2) + (L^{\cdot-} \cdot Zn) + (LH \cdot Zn)} \quad \text{i.e.} \quad \frac{L^{\cdot-} \cdot Zn_2}{E_{TOT}}$$

The two equilibria are:

$$K_a = \frac{(L^{\cdot-} \cdot Zn) (H^+)}{(LH \cdot Zn)} = \frac{(L^{\cdot-} \cdot Zn) (H^+)}{E_{TOT} - (L^{\cdot-} \cdot Zn) - (L^{\cdot-} \cdot Zn_2)}$$

$$K_d = \frac{(L^{\cdot-} \cdot Zn) (Zn)}{(L^{\cdot-} \cdot Zn_2)}$$

Rearrangement gives:

$$(L^{\cdot-} \cdot Zn) = \frac{K_a}{H^+ + K_a} \cdot E_{TOT} \quad (L^{\cdot-} \cdot Zn) = \frac{K_d (L^{\cdot-} \cdot Zn_2)}{Zn}$$

so:

$$\frac{K_d (L^{\cdot-} \cdot Zn_2)}{Zn} = \frac{K_a}{H^+ + K_a} \cdot E_{TOT}$$

From this, the fraction (di-form) is derived as shown above.

At high pH when the  $H^+$  concentration is less than the  $K_a$ , all of the enzyme exists in the binuclear form whereas at low pH when  $H^+$  concentration is

greater than  $K_a$ , the fraction of zinc two is inversely proportional to the hydrogen ion concentration.

As explained earlier the plot in **Figure 2.51** shows a slope of approximately one, indicating that there is one ligand in the enzyme to be ionised on binding the second zinc ion, which implies that the other ligands in the second site are already in a state suitable for metal ion binding. The identification of the ligand that is ionised is helped by reviewing the structure and mechanism of action of metallo- $\beta$ -lactamases. The apparent  $pK_a$  determined from our ITC experiments most likely correspond to either the cysteine 221 ligand or the zinc bound water molecule. The  $pK_a$  of cysteine 221 in the apo-enzyme is 7.85<sup>2</sup> and this could decrease in the mono-zinc enzyme due to the positively charged environment. It is possible that the  $pK_a$  of 7.85 in the apo-enzyme actually corresponds to the ionisation of a cysteine-imidazolium ion pair rather than the thiol itself. Either way if this is the ionisation observed in **Figure 2.51** it implies that proton loss is required for binding the second metal ion.

The alternative ligand that could be ionised is the zinc-bound water, that has  $pK_a$ 's reported from 4.60- 5.60<sup>2,40, 45</sup>, in very good agreement with our value of 5.8. From previous kinetic studies<sup>40</sup> it was suggested that the  $pK_a$  of zinc bound water to be 5.6, but catalytic activity at low pH depended on the ionisation of two groups and the decrease in activity was dependent on zinc ion concentration indicative of zinc dissociation at lower pH. Other reports have suggested an even lower  $pK_a$  for the zinc-bound water.<sup>2</sup> From this, the ligand ionised here with a  $pK_a$  of 5.8 is likely to be the cysteine ligand as the zinc bound water molecule is likely to be ionised in the mono-zinc form of the enzyme.

#### 2.4.4 - Buffer Effect

It is important to emphasise the role of the buffer in the observed heat changes upon metal ion titration of the apo-enzyme. The nature of the buffer sometimes has a dominant effect on the energetics of binding metal ions to apoBclI. As can be seen from **Tables 2.13 and 2.27** for zinc and cobalt ion endothermic reactions are detected for the binding process in acetate, MES, cacodylate and PIPES buffers. However, in HEPES and MOPS, the binding event is exothermic. This different behaviour is due to the differing heats associated with the buffer reacting with the released hydrogen ions (in other words the value of  $-\Delta H_{\text{ion (buffer)}}$ ). Some buffers have small heats of neutralisation and therefore the observed values largely reflect the interaction of the metal ion with the enzyme. However, others have such large heat changes that the observed values are dominated by the buffer. This makes particularly the accurate determination of the number of protons released upon binding difficult as will be discussed later.

### 2.4.5 - Binding Constants

Metal ion binding to the apo-enzyme may involve the liberation of protons which are neutralised by the buffer. However, the buffer used is always in excess of the concentration of the enzyme and therefore the pH is constant for each titration and remains constant throughout the reaction. So even though a relatively small amount of protons are liberated upon metal ion binding and these are involved with an equilibrium with buffer this does not affect the observed equilibrium constant for metal ion binding to the enzyme because the concentration of the conjugate buffer base is effectively constant.

The *association* binding constants at each pH determined in different buffers show some variation as can be seen in **Table 2.36**. For example, at pH 6.0 for zinc ion the binding constant observed in MES buffer is  $1.10 \times 10^5 \text{ M}^{-1}$  and in cacodylate buffer is  $2.45 \times 10^6 \text{ M}^{-1}$ . It is likely that this variation is associated with interaction between the enzyme and the buffer components. This is not unlikely as this sort of interaction has been observed before for example, MES buffer has been shown to be a good inhibitor when bound to *Bacteroides fragilis* enzyme.<sup>42</sup>

**Table 2.36:** Binding constants determined by ITC for zinc, cobalt and cadmium ion binding to apoBclI.

Binding Constants $K_b$ ( $M^{-1}$ )		pH					
		5.20	5.60	6.00	6.35	6.80	7.20
Acetate	Zn <sup>2+</sup>	1.13( $\pm$ 0.18) $\times 10^5$	1.33( $\pm$ 0.08) $\times 10^5$				
	Co <sup>2+</sup>	5.42 ( $\pm$ 0.65) $\times 10^4$	1.19 ( $\pm$ 0.10) $\times 10^5$				
MES	Zn <sup>2+</sup>	1.18 ( $\pm$ 0.35) $\times 10^5$	2.75 ( $\pm$ 0.21) $\times 10^6$	1.10 ( $\pm$ 0.12) $\times 10^5$	1.56 ( $\pm$ 0.23) $\times 10^6$	2.01 ( $\pm$ 0.36) $\times 10^6$	
	Co <sup>2+</sup>	1.20 ( $\pm$ 0.06) $\times 10^5$	2.37 ( $\pm$ 0.17) $\times 10^5$	3.78 ( $\pm$ 0.30) $\times 10^5$	1.11 ( $\pm$ 0.20) $\times 10^6$	4.73 ( $\pm$ 0.36) $\times 10^6$	
	Cd <sup>2+</sup>	4.68 ( $\pm$ 0.56) $\times 10^5$	1.62 ( $\pm$ 0.24) $\times 10^6$	6.14 ( $\pm$ 0.54) $\times 10^6$	1.55 ( $\pm$ 0.23) $\times 10^8$ 2.0 ( $\pm$ 0.30) $\times 10^6$	8.10 ( $\pm$ 0.72) $\times 10^7$ 1.06 ( $\pm$ 0.10) $\times 10^6$	
Cacodylate	Zn <sup>2+</sup>	1.40 ( $\pm$ 0.27) $\times 10^5$	2.10 ( $\pm$ 0.34) $\times 10^6$	2.45 ( $\pm$ 0.44) $\times 10^6$	2.30 ( $\pm$ 0.28) $\times 10^6$	2.40 ( $\pm$ 0.96) $\times 10^6$	
	Co <sup>2+</sup>	3.30 ( $\pm$ 0.73) $\times 10^5$	3.48 ( $\pm$ 0.52) $\times 10^5$	2.28 ( $\pm$ 0.36) $\times 10^6$	1.17 ( $\pm$ 0.13) $\times 10^6$	2.49 ( $\pm$ 0.40) $\times 10^6$	
	Cd <sup>2+</sup>	6.24 ( $\pm$ 1.25) $\times 10^5$	2.10 ( $\pm$ 0.53) $\times 10^6$	5.30 ( $\pm$ 0.42) $\times 10^5$	4.28 ( $\pm$ 0.26) $\times 10^8$ 6.97 ( $\pm$ 0.33) $\times 10^6$	5.13 ( $\pm$ 0.25) $\times 10^8$ 7.26 ( $\pm$ 0.38) $\times 10^6$	
PIPES	Zn <sup>2+</sup>			1.75 ( $\pm$ 0.10) $\times 10^5$	1.25 ( $\pm$ 0.38) $\times 10^5$	2.37 ( $\pm$ 0.52) $\times 10^6$	5.50 ( $\pm$ 0.63) $\times 10^5$
	Co <sup>2+</sup>			1.76 ( $\pm$ 0.24) $\times 10^6$	9.44 ( $\pm$ 0.66) $\times 10^6$	7.12 ( $\pm$ 0.92) $\times 10^5$	5.93 ( $\pm$ 0.86) $\times 10^5$
	Cd <sup>2+</sup>					2.35 ( $\pm$ 0.16) $\times 10^8$ 5.22 ( $\pm$ 0.26) $\times 10^6$	4.66 ( $\pm$ 0.60) $\times 10^8$ 3.93 ( $\pm$ 0.12) $\times 10^6$
MOPS	Zn <sup>2+</sup>					1.43 ( $\pm$ 0.27) $\times 10^7$	5.00 ( $\pm$ 1.12) $\times 10^7$
	Co <sup>2+</sup>					6.15 ( $\pm$ 0.123) $\times 10^5$	1.30 ( $\pm$ 0.38) $\times 10^6$
	Cd <sup>2+</sup>						
HEPES	Zn <sup>2+</sup>					1.99 ( $\pm$ 0.38) $\times 10^7$	2.93 ( $\pm$ 0.41) $\times 10^6$
	Co <sup>2+</sup>					1.98 ( $\pm$ 0.41) $\times 10^7$	3.85 ( $\pm$ 0.30) $\times 10^6$
	Cd <sup>2+</sup>						
						3.81 ( $\pm$ 0.49) $\times 10^8$ 7.41 ( $\pm$ 0.87) $\times 10^6$	

Until now the strength of the metal ion binding to apoBclI has been stated as the binding constant ( $K_b$ ). The binding of the metal ion will now be discussed as the dissociation constant which is the form commonly used in the literature and the relationship between  $K_b$  and  $K_d$  is as follows:

$$K_d = 1/ K_b.$$

The following dissociation constants in **Table 2.37** for zinc, cobalt and cadmium ions coordinated to apoBclI have been reported previously.<sup>36</sup> These values were determined using competition experiments with the chromophoric chelator Mag-fura-2<sup>36</sup> for zinc and cadmium ion and cobalt ion dissociation constant was determined using spectral changes of the enzyme upon cobalt ion binding<sup>36</sup> to the enzyme in HEPES buffer at pH 7.0. For both binding sites zinc and cadmium ion have higher binding affinity than cobalt ion. The affinities decrease from zinc to cadmium to cobalt ion ( $Zn^{2+} > Cd^{2+} > Co^{2+}$ ).<sup>36</sup> The dissociation constants reported in **Table 2.37** can be compared with the association constants determined from our research as shown in **Table 2.36**.

**Table 2.37:** Dissociation constants for zinc, cobalt and cadmium ions for BclI in HEPES buffer at pH 7.0.<sup>36</sup>

	Zinc ion	Cadmium ion	Cobalt ion
Site one - $K_d$ (M)	$6.2 \times 10^{-10} (\pm 0.08)$	$8.3 \times 10^{-9} (\pm 0.5)$	$9.3 \times 10^{-8} (\pm 1.5)$
Site two ( $K_d$ ) (M)	$1.5 \times 10^{-7} (\pm 0.7)$	$5.9 \times 10^{-6} (\pm 1)$	$6.6 \times 10^{-5} (\pm 1)$

One very significant difference between our observation and those that gave rise to the data in **Table 2.37** is that we were unable to resolve the two binding events for zinc and for cobalt ion. We conclude that this is because the binding of these two metal ions around neutral pH at the two sites is cooperative in both cases, i.e. binding to these two sites occurs effectively simultaneously. This is not in agreement with the results of DeSeny<sup>36</sup> for which separate binding constant are observed for metal ions 1 and 2.

The dissociation constant determined from our work for zinc ion binding to apoBclI at pH 6.80 in HEPES buffer is  $5 \times 10^{-8}$  M determined by isothermal titration calorimetry (ITC). Preliminary work by A.Badarau at pH 7.1 also observed a single binding event for two zinc ions binding to apoBclI using ITC reported a dissociation constant of  $3 \times 10^{-8} (\pm 0.5)$  M.<sup>74</sup> The study by DeSeny et al<sup>36</sup> also for two zinc ion binding reported the dissociation constant to be  $8 \times 10^{-8}$  M at pH 7.0 and Jaquin et al determined the dissociation constant to be lower than  $8 \times 10^{-8}$  M at pH 7.5.<sup>64</sup> Therefore our dissociation constant is in reasonable agreement with previous results.

Cobalt ion binding is similar to zinc ion binding in that a single binding event was observed in ITC due to positive cooperative binding. The dissociation constant determined in our work for cobalt ion binding at pH 6.80 in HEPES buffer is  $7.69 \times 10^{-8}$  M. This dissociation constant cannot be compared directly, but it is broadly similar to the dissociation constant of  $9.3 \times 10^{-8}$  M for site one of cobalt ion binding reported in **Table 2.37**.

When cadmium ion binds to apoBclI, two distinct binding events were observed by ITC. The dissociation constant determined here at pH 7.20 in HEPES buffer is  $2.79 \times 10^{-9}$  M for the first cadmium ion binding and  $1.8 \times 10^{-7}$  M for the second cadmium ion binding. These dissociation constants are very much similar to those reported by DeSeny<sup>36</sup> (**Table 2.37**) as  $8.3 \times 10^{-9} (\pm 0.5)$  for the first cadmium ion and  $5.9 \times 10^{-6} (\pm 1)$  for the second cadmium ion.

### 2.4.6 - Enthalpies and Entropies of Binding

The observed molar enthalpy is the energy determined when the metal ion binds to the enzyme but it includes several factors as already discussed. As the pH increases from 5.20 to 7.20, the observed molar enthalpy decreases in all buffers when zinc ion binds to apoBcII. Whereas when cobalt ion binds to apoBcII, the observed molar enthalpy increases as the pH is increased. But when cadmium ion binds to apoBcII, the observed molar enthalpy also decreases as the pH is increased and the binding changes from endothermic to exothermic.

The magnitudes of the observed molar enthalpies also vary between the metal ions in the same buffer. For instance at pH 5.20 for zinc ion binding to apoBcII in cacodylate buffer the observed molar enthalpy is  $62 \text{ kJ mol}^{-1}$ , for cobalt ion it is  $48 \text{ kJ mol}^{-1}$  and for cadmium ion it is  $50 \text{ kJ mol}^{-1}$ . This variation may suggest that although the metal ions bind in the same way to the enzyme, the strength of binding between the metal ion and ligand is different. Conversely, the differences may indicate different binding sites e.g. for the mononuclear enzyme zinc binds to the 3H site whereas cobalt binds to the DCH site.

As described earlier, the observed molar enthalpy include a number of different components of heats ( $\Delta H_{\text{obs}}^{\circ} = \Delta H_{\text{int}}^{\circ} + n (\Delta H_{\text{ion (enz)}}^{\circ} + \Delta H_{\text{ion (buffer)}}^{\circ})$ ). Therefore an attempt has been made to separate these thermodynamic parameters for the binding of the metal ion to the enzyme from those associated with the dissociation of hydrogen ions from the enzyme and their neutralisation by the buffer. The values for  $\Delta H_{\text{int}}^{\circ}$  were determined in the usual way and then an attempt was made to separate the  $\Delta H_{\text{ion (enz)}}^{\circ}$  from  $\Delta H_{\text{int}}^{\circ}$ . As discussed earlier, assumptions made in order to do this are that the enthalpy of binding is constant at all pH's and that the enthalpies of ionisation of hydrogen ions on the enzyme are also constant, which are probably poor assumptions, so the  $\Delta H_{\text{int}}^{\circ}$  values are not regarded as very reliable although indicative of the magnitude. Nevertheless, the values of the separated terms are shown in **Table 2.38**. The main observation is that cadmium ion binding is

fundamentally different to that of cobalt and zinc ion. The data for cadmium ion refer to the formation of the mono-nuclear enzyme whereas that for zinc and cobalt ion is for the binuclear enzyme.

**Table 2.38:** Enthalpy of intrinsic and ionisation of enzyme for zinc, cobalt and cadmium ions when binding to apoBclI.

	$\Delta H^{\circ}_{\text{int}}$ kJ mol <sup>-1</sup>	$\Delta S^{\circ}_{\text{int}}$ J mol <sup>-1</sup> K <sup>-1</sup>	$\Delta H^{\circ}_{\text{ion(enz)}}$ kJ mol <sup>-1</sup>	$\Delta S^{\circ}_{\text{ion(enz)}}$ J mol <sup>-1</sup> K <sup>-1</sup>
Zinc ion	16 ( $\pm$ 10)	161 ( $\pm$ 11)	11 ( $\pm$ 5)	36 ( $\pm$ 10)
Cobalt ion	27 ( $\pm$ 16)	198 ( $\pm$ 9)	9 ( $\pm$ 4)	34 ( $\pm$ 5)
Cadmium ion	108 ( $\pm$ 35)	357 ( $\pm$ 70)	-89 ( $\pm$ 15)	-136 ( $\pm$ 10)

The corrected calculated entropy shows similar trends to those seen for the corresponding enthalpy changes. In particular, cadmium ion binding displays significantly different values to those for zinc and cobalt ion. The binding of cadmium ion to apo BclI is accompanied by hugely positive entropy change ( $\Delta S^{\circ}_{\text{int}}$ ) whereas the associated entropy change for ionisation of the ligands is negative in contrast to the positive values seen for zinc and cobalt ion. Even allowing for the inaccuracies in the data, it is clear that there are significant differences as the mono-nuclear cadmium enzyme is formed compared with the bi-nuclear zinc and cobalt ion species.

It is fair to say that desolvation of the cadmium ion plays a significant role in determining the binding and the positive entropy change is also consistent with the metal ion oscillating between two sites. Finally, one could speculate that cadmium ion binding is accompanied by a restriction of movement of the ligands upon ionisation, giving rise to a negative  $\Delta S^{\circ}_{\text{ion(enz)}}$ .

Both the  $\Delta H^{\circ}_{\text{int}}$  and  $\Delta H^{\circ}_{\text{ion(enz)}}$  and  $\Delta S^{\circ}_{\text{int}}$  and  $\Delta S^{\circ}_{\text{ion(enz)}}$  for Enz-Cd<sub>2</sub> formation is not quoted because it was very difficult to determine both values for the second cadmium ion due to the very small number of protons released, attempts were made to obtain this but it was very unsuccessful and also this would equate to very large errors.

### 2.4.7 - Number of Protons Released

As stated above some of the heat changes are dominated by the buffer and so the accurate determination of the number of protons released upon metal ion binding to the apo-enzyme is not always possible from the data available. Although each individual metal ion can give rise to a satisfactory model, it is more difficult to obtain a self-consistent model for all three metal ions.

The number of protons released is obtained from plotting the observed enthalpy changes against the enthalpy of ionisation of the buffer (page 81). The number of metal ions binding and the number of protons released when zinc, cobalt and cadmium ions bind to apoBcII at different pH's are shown in **Tables 2.39, 2.40 and 2.41**, which actually show a reasonable degree of consistency.

**Table 2.39:** *n* (number of protons released) at different pH's for zinc ion binding to apoBcII determined from  $\Delta H^{\circ}_{\text{obs}}$  values.

<i>pH</i>	<i>n (number of protons released by the enzyme) from <math>\Delta H^{\circ}_{\text{obs}}</math></i>
5.20	2.3 ( $\pm$ 0.5)
5.60	1.2 ( $\pm$ 0.4)
6.0	1.9 ( $\pm$ 0.5)
6.35	0.7 ( $\pm$ 0.3)
6.80	1.7 ( $\pm$ 0.3)
7.20	2.6 ( $\pm$ 0.5)

**Table 2.40:**  $n$  (number of protons released) at different pH's for cobalt ion binding to apoBcII determined using  $\Delta H^{\circ}_{\text{obs}}$  and  $\Delta S^{\circ}_{\text{obs}}$  values.

<i>pH</i>	<i>n (number of protons released by the enzyme) from <math>\Delta H^{\circ}_{\text{obs}}</math></i>
5.20	1.2 ( $\pm$ 1.0)
5.60	1.5 ( $\pm$ 1.0)
6.0	1.7 ( $\pm$ 1.0)
6.35	3.3 ( $\pm$ 0.8)
6.80	3.4 ( $\pm$ 0.8)
7.20	2.6 ( $\pm$ 2.0)

**Table 2.41:**  $n$  (number of protons released) at different pH's for cadmium ion binding to apoBcII determined using  $\Delta H^{\circ}_{\text{obs}}$  values.

<i>pH</i>	<i>n (number of protons released by the enzyme) from <math>\Delta H^{\circ}_{\text{obs}}</math></i>	
	<i>Site 1</i>	<i>Site 2</i>
5.20	1.0 ( $\pm$ 0.5)	-
5.60	1.0 ( $\pm$ 0.4)	-
6.0	2.0 ( $\pm$ 0.7)	-
6.35	1.7 ( $\pm$ 0.8)	0.2 ( $\pm$ 0.8)
6.80	1.7 ( $\pm$ 1.0)	0.4 ( $\pm$ 1.0)
7.20	1.0 ( $\pm$ 0.5)	0.3 ( $\pm$ 0.5)

A summary of the number of metal ions binding and the number of protons released when zinc, cobalt and cadmium ions bind to apoBclI at different pH's is shown below in **Table 2.42**.

**Table 2.42:** Metal ions binding and number of protons released with change in pH when zinc, cobalt and cadmium ion binds to apoBclI.

pH	Zinc ion		Cobalt ion		Cadmium ion			
	N (Zn <sup>2+</sup> :Enz)	n (no of protons released)	N (Co <sup>2+</sup> :Enz)	n (no of protons released)	N (Cd <sup>2+</sup> :Enz)		n (no of protons released)	
5.20	1.0 ( $\pm 0.5$ )	2.3 ( $\pm 0.5$ )	1.0 ( $\pm 0.5$ )	1.2 ( $\pm 1.0$ )	1.0 ( $\pm 0.3$ )	-	1.0 $\pm$ 0.5	-
5.60	1.0 ( $\pm 0.5$ )	1.2 ( $\pm 0.4$ )	1.0 ( $\pm 0.5$ )	1.5 ( $\pm 1.0$ )	1.0 ( $\pm 0.3$ )	-	1.0 $\pm$ 0.4	-
6.0	1.6 ( $\pm 0.5$ )	1.9 ( $\pm 0.5$ )	1.3 ( $\pm 0.3$ )	1.7 ( $\pm 1.0$ )	1.0 ( $\pm 0.3$ )	-	2.0 $\pm$ 0.7	-
6.35	1.9 ( $\pm 0.3$ )	0.7 ( $\pm 0.3$ )	1.8 ( $\pm 0.3$ )	3.3 ( $\pm 0.8$ )	1.0 ( $\pm 0.3$ )	1.0 ( $\pm 0.5$ )	1.7 $\pm$ 0.8	0.2 $\pm$ 0.8
6.80	2.0 ( $\pm 0.3$ )	1.7 ( $\pm 0.3$ )	2.0 ( $\pm 0.3$ )	3.4 ( $\pm 0.8$ )	1.0 ( $\pm 0.3$ )	1.0 ( $\pm 0.5$ )	1.7 $\pm$ 1.0	0.4 $\pm$ 1.0
7.20	1.6 ( $\pm 0.5$ )	2.6 ( $\pm 0.5$ )	1.8 ( $\pm 0.3$ )	2.6 ( $\pm 2.0$ )	1.0 ( $\pm 0.3$ )	1.0 ( $\pm 0.5$ )	1.0 $\pm$ 0.5	0.3 $\pm$ 0.5

Before discussing these individual values, it is worth making some general comments. Firstly, it is clear that metal ion binding is associated with the release of protons at all pH's studied. This implies that some of the enzyme ligands required for metal ion binding exists in their protonated state in the apo-enzyme and so metal ion binding to the apo-enzyme represents a competition between the metal ion and the proton for the ligand which explains the variation of the number of metal ions bound with pH.

Consequently there may not be a simple stoichiometry because there may be a mixture of species present (**Table 2.42**). Nonetheless, for convenience we shall discuss the results using whole numbers of protons released. Secondly it appears that the maximum number of protons released on forming the binuclear enzyme is three. Assuming that the bridged water between the two metal ions is in the form of a hydroxide-ion, then one of these protons must be from the metal-bound water leaving a maximum of only two ligands in the protein which require ionisation for metal ion binding to occur. Previous work from this laboratory has shown that the  $pK_a$  of the active site cysteine is 7.85, obtained from alkylation of the apo-enzyme with iodoacetamide. Presumably therefore one of the protons released would come from this cysteine leaving the third to come from a protonated histidine.

One would assume that it is possible for the number of protons released to decrease with increasing pH as a ligand in the apo-enzyme may become ionised as its  $pK_a$  falls below the pH. It also seems reasonable that the number of protons released may increase as the number of bound metal ions increases from one to two.

When zinc ion binds to apoBcll, protons are formed by dissociation of one or more of the coordinating amino acid side chains and/or from the metal-bound water. The number of protons released appears to be two when the mono zinc enzyme is formed at low pH. On average it also seems to be two protons released at most pH's and whether or not one or two metal ions are binding and so the value of around one at pH 6.35 looks suspect (**Table 2.42**).

When cobalt ion binds to apoBcII, the number of protons released increases from one to three as the pH is increased. At low pH when one cobalt ion is binding only one proton is released and at high pH when two cobalt ions are binding three protons are released. At pH 7.2 there is an apparent decrease in the number of protons released to two.

Cadmium ion binding to apoBcII shows distinct mono- and bi-nuclear species. When the first cadmium ion binds, the number of protons released increases from one to two as the pH is increased and then, similar to cobalt ion binding, decreases at pH 7.2. At high pH when the second cadmium ion binds to apoBcII it is not clear whether none or one additional proton is released.

It is interesting that the number of protons released with pH is different for zinc ion binding to apoBcII compared with that for cobalt and cadmium ions. The most notable difference is that cobalt ion binding appears to result in more hydrogen ions dissociated (at high pH) than the other two metal ions, although it is possible that cadmium releases a total of three protons on forming the binuclear enzyme, given the uncertainty in the number of protons released on going from one to two cadmium ions (**Table 2.42**).

### 2.4.8 - Possible Models to Explain Metal ion Binding Results

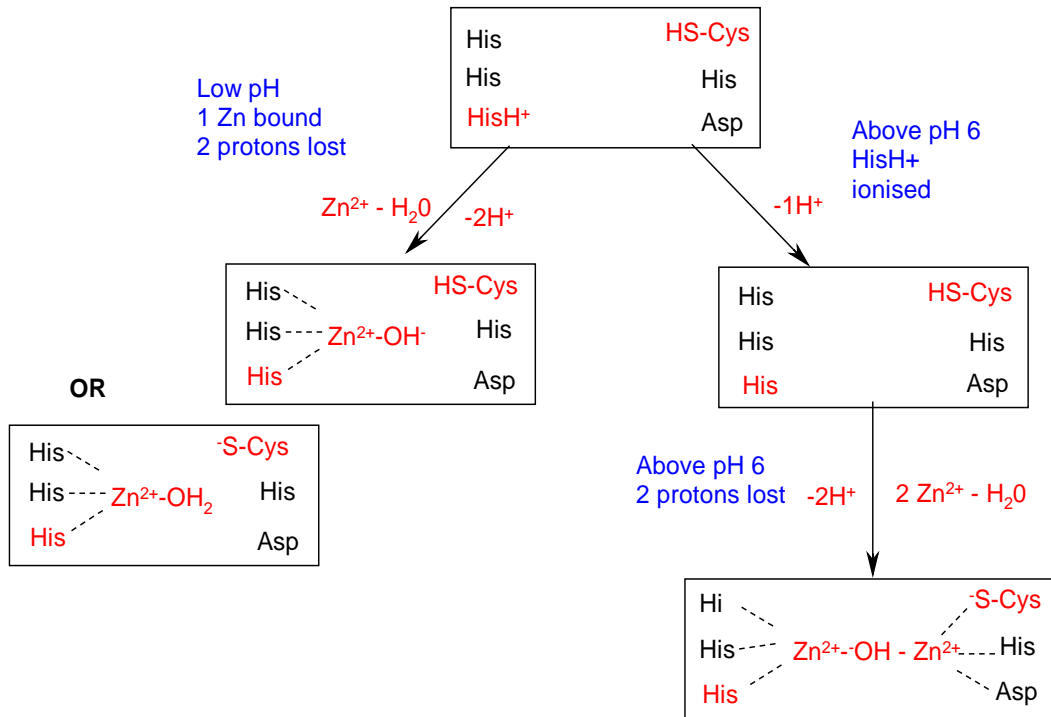
#### Zinc ion

At low pH (below pH 6) we have shown that one zinc ion binds to the apoBcII and this process releases two protons. A possible explanation for the two protons released is that one proton is released from the imidazolium ion (in its protonated form at low pH) on a histidine ligand when the zinc ion binds to the 3H site one. As the zinc ion binds it causes the  $pK_a$  of uncoordinated histidine of around 7 to fall from above the solution pH to below it or, more simply, only the neutral imidazole form can coordinate to zinc. A possible source of the second proton is that it is released from a water molecule bound to the highly electropositive enzyme-bound zinc ion. This is not unreasonable as the  $pK_a$  of water bound ZnBcII has been reported to be between 4.8-5.6<sup>2, 40,45</sup> depending on the zinc ion concentration and this compares with the  $pK_a$  of water bound to zinc ion in bulk solution which is known to be 9.0.<sup>77</sup> So when the pH is below the  $pK_a$  of hydrated zinc ion in aqueous solution but above the  $pK_a$  of water bound ZnBcII, a zinc ion coordinated water molecule will ionise when the zinc ion binds to the enzyme. This model implies that in site one (3H) of the apo-enzyme two histidines are neutral and one protonated, so when one zinc ion binds to apoBcII at site one and is coordinated by three histidines and a solvent molecule, one of the histidine residues loses a proton on coordination and the water molecule bound to the zinc ion also loses a proton.

An alternative process that could release a proton is from the cysteine thiol in site two (DCH). The  $pK_a$  reported by A.Badarau et al.<sup>2</sup> for the active site cysteine is 7.85, but which, upon zinc ion binding to the 3H site one, could decrease due to the creation of a more positively charged environment. Therefore there is a possibility for a proton to be released from the cysteine thiol upon forming the mono-zinc enzyme, even though it is not involved in metal ion binding. The second proton could be released from the imidazolium ion while the water bound ZnBcII remains protonated. So this alternative route of releasing protons from the thiol and imidazolium ion can only happen assuming both of their  $pK_a$ 's are <6 when the metal ion binds to the enzyme.

A third, but unlikely, possibility is that both protons released are from two 3H imidazolium ions. This is unlikely because it would require the cysteine thiol in site two to be already ionised at pH 5 – 6, so that no further protons are released when the second zinc binds to site two.

Above pH 6.0 two zinc ions bind to apoBcII, but under these conditions it appears that still only two protons are released upon metal ion binding to the enzyme. A possible model to explain why no further protons are released on forming the binuclear enzyme is as follows: for the zinc ion binding at site one (3H) it is possible that the imidazolium ion from the histidine residue, which was the source of a proton at lower pH, is now dissociated and in its neutral form in the apo-enzyme at these higher pH's. So the coordination of zinc ion does not require the simultaneous loss of a proton. The aqueous Zn bound water molecule described above may still be a source of proton release on binding to the enzyme. This water molecule almost certainly bridges between the two bound zinc ions as hydroxide-ion so there must always be a proton released on forming the di-zinc enzyme from the apo-enzyme and hydrated zinc ion. At the binding site of the second zinc ion (site 2 or the DCH site) it is probable that the thiol group on the cysteine residue remains undissociated at neutral pH and so proton loss is still required to yield the thiolate anion for metal ion binding to occur. The carboxylic acid group of the aspartic acid and the imidazole of the histidine of the DCH site are already in their ionised states suitable for metal ion coordination. It seems unlikely that the histidine imidazole would dissociate further to form its anion on metal ion binding. The model outlined in **Scheme 2.21**, while speculative, seems a reasonable basis on which to explain why only two protons are generated when one or two zinc ions bind to apoBcII at all pH's. .



**Scheme 2.21:** Zinc ion binding and the protons released when binding to apoBclI.

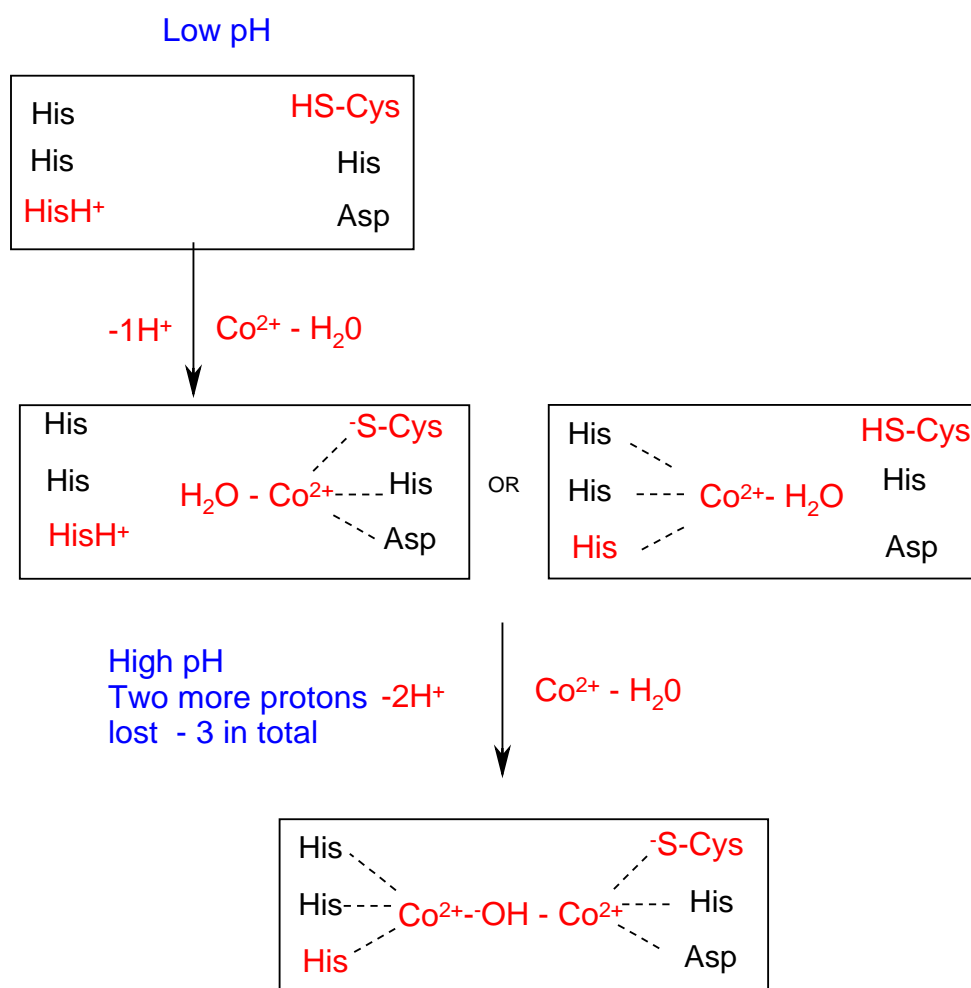
### Cobalt ion

Similar to zinc ion binding, one cobalt ion binds to apoBcII at low pH, rising, in an apparent one step process, to two, as the pH is increased to above 6.0. The number of protons released when cobalt ion binds to apoBcII as the pH increases from 5.20 to 7.20 increases from one to three as the number of metal ions bound also increases from one to two. When one cobalt ion binds at low pH one proton is released and when two cobalt ions bind three protons are released.

For the mono-cobalt species, the possible explanation for the one proton released at low pH is that it comes from either the 3H site one imidazolium ion or from the DCH site two cysteine thiol. If the first cobalt ion binds to the DCH site the single proton released is probably from the cysteine thiol. It has been suggested that cobalt ion in mono CoBcII form binds to site two during the hydrolysis of penicillin G<sup>80</sup> and that the enzyme is catalytically active with both one or two cobalt ions and site two is the primary catalytic site.<sup>80,81</sup> If this is the case it is likely that the proton released upon forming the mono-nuclear enzyme from apoBcII is from the site two cysteine thiol group. The pK<sub>a</sub> for water bound CoBcII has been reported to be 6.3<sup>2</sup> so it is not inconceivable that the second proton comes from this. However, if 6.3 is an accurate value then the one proton released upon metal ion binding is likely to be from the imidazolium ion or the thiol group as the water bound CoBcII will remain in its protonated form at low pH. Even though metal ion binding to either site one or two releases only one proton directly, it is possible that there is a secondary effect by lowering the pK<sub>a</sub> of an adjacent group due to the positively charged environment.

Above pH 6.0, the number of protons released increases to three and the number of cobalt ions binding increases to two. A possible explanation for the three protons released is: one proton from the imidazolium ion, one proton from the cysteine thiol and the third proton is from a metal-coordinated water molecule. The overall picture for cobalt ion binding to apoBcII is shown in **Scheme 2.22**.

Finally, there appears to be a decrease in the number of protons released at pH 7.2 from three to two (**Table 2.42**). This is probably due to the partial ionisation of the cysteine thiol in the apo-enzyme, which as previously stated, has a  $pK_a$  of 7.8 and so proton release is not necessary upon metal ion binding.



**Scheme 2.22:** Cobalt ion binding and the protons released when binding to apoBclI

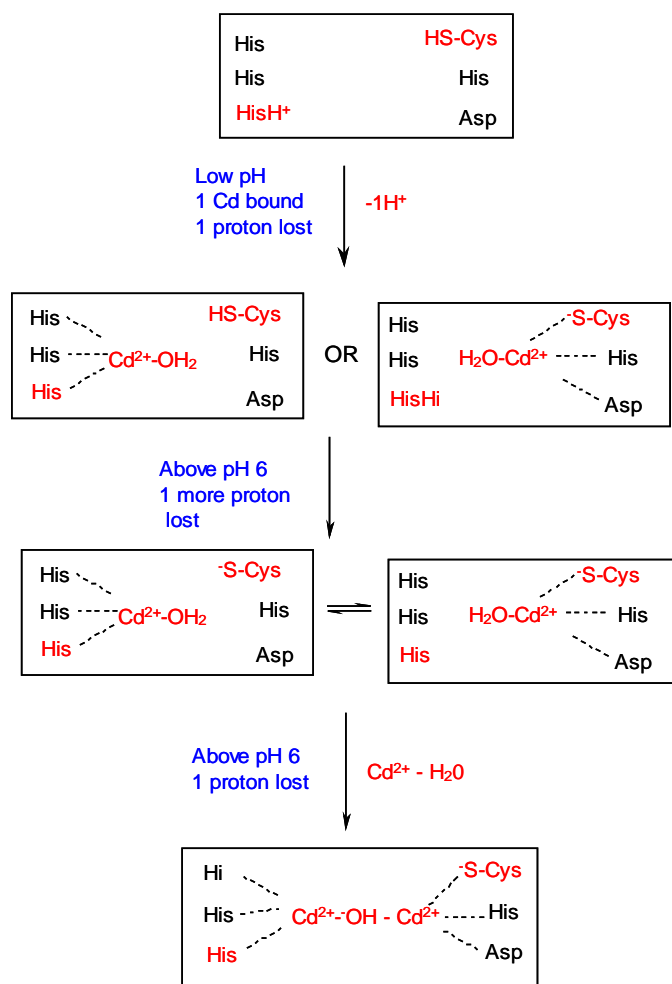
### Cadmium ion

Unlike zinc and cobalt ion binding to apoBclI, cadmium ion shows two distinct binding steps as the number of metal ions bound increases from one to two. Between pH 5.2 -6.0 only one cadmium ion binds to apoBclI and this releases only one proton. The two binding sites available for the cadmium ion are the same as those for zinc ion binding - site one (3H) and site two (DCH). But cadmium has been reported to oscillate between the two sites on a time scale between 100 ns and 0.01 ms at pH 6.0 when cadmium ion is substituted for the native form of BclI.<sup>78</sup> Due to this oscillation it is not obvious where the proton is released from, as it could be from the imidazolium ion if binding occurs to site one or the thiol group if binding is to site two. It seems unlikely that the single proton lost is that from the water bound CdBclI as the  $pK_a$  of water bound CdBclI is higher than water bound ZnBclI due to the reduced positive charge on the Cd.<sup>2</sup> Cadmium ion has been shown by EXAFS<sup>79</sup> to be pentacoordinated to three histidine ligands with two additional oxygen atoms that are probably two water molecules. In contrast, the zinc ion is tetraordinated to the three histidine ligands with only one oxygen atom which is either a water molecule or a hydroxide-ion.<sup>27</sup>

Similar to cobalt ion, there appears to be a decrease in the number of protons released at pH 7.2 (**Table 2.42**). This is probably due to the partial ionisation of the cysteine thiol in the apo-enzyme, which is as previously stated has a  $pK_a$  of 7.8<sup>2</sup> and so proton release from this source is not necessary upon metal ion binding.

As the pH is increased two cadmium ions bind but the ITC titration shows separate steps for forming the mono- and bi- nuclear species. When the first cadmium ion binds above pH 6 it now releases two protons which could be from site one imidazolium ion and the water molecule bound to cadmium ion. Alternatively, assuming it oscillates more at high pH than at low pH, then the two protons released could be explained by one proton coming from the imidazolium ion from site one and the second proton from the thiol group in site two.

When the second cadmium ion binds at high pH ( $> 6$ ), the enzyme possibly loses one more proton. We speculate that this proton is from the bridging water molecule. From previous studies the  $pK_a$  of water bound CdBCII is 8.6,<sup>2</sup> and so it is likely that the  $pK_a$  for the water molecule that bridges two metal ions is less than this. So it is reasonable to assume when two cadmium ions bind the  $pK_a$  of bridging water molecule in Cd<sub>2</sub>BCII falls below the pH of solution, therefore releasing a proton from the water molecule. This model is explained and summarised in **Scheme 2.23**.



**Scheme 2.23:** Cadmium ion binding and the protons released when binding to apoBCII.

## 2.5 - Conclusion

The results of the ITC experiments have shown very clearly how  $Zn^{2+}$ ,  $Co^{2+}$ , and  $Cd^{2+}$  bind to the apoBcll enzyme over a pH range of 5.20 to 7.20. They add significantly to what is already known about the nature of metal ion binding to apoBcll. In the case of zinc ion, only one zinc ion binds at pH's 5.20 to 5.60 with two metal ions bind above pH 6.0. When two metal ions bind, they do so cooperatively, in that only a single binding event is observed for the two metal ions. The metal ion binding events are accompanied by proton dissociation. Precise values for the number of protons released were difficult to obtain but we estimate that two protons are released by the enzyme when either one or two zinc ions bind.

A model to explain these results involves zinc ion binding at the 3H site (site one), releasing protons from the imidazolium ion and a zinc-bound water molecule. Alternatively the protons could be released from the imidazolium ion and the thiol group. When the second zinc ion binds at higher pH it binds to the DCH site (site two) and the two protons released could be from the thiol group and a zinc-bound water molecule that bridges between the two metal ions.

When cobalt ions are introduced to apoBcll the behaviour is very similar, in that only one metal ion bind at pH's 5.20 and 5.60. Above pH 6.0, two metal ions bind cooperatively showing only a single binding event in the titration. Cobalt ion binding to apoBcll is accompanied by protons dissociating. One proton is released at low pH, but when two cobalt ions bind at higher pH the number of protons released increases to three. The model used to explain the cobalt metal ion binding involves the first cobalt ion binding to the DCH site. When one cobalt ion binds at low pH, only one proton is released which, if the cobalt ion is binding to the DCH site, originates from the thiol group. If the cobalt ion binds to the 3H site in the mono-nuclear enzyme, the proton could be from the imidazolium ion.

The binding association constants for zinc ion, whether one or two zinc ions are bound, are of order  $10^6 \text{ M}^{-1}$  and for cobalt ion are  $10^5 \text{ M}^{-1}$ . This stronger binding for zinc ion than for cobalt ion is consistent with previous measurements made using competition experiments with chelator Mag-fura-2 and spectral changes.<sup>36</sup> The molar enthalpies of binding for both zinc and cobalt ion are endothermic but are strongly entropy driven.

The behaviour of cadmium ion binding to apoBclI is different. Only one cadmium ion binds at low pH and two at higher pH. But the two metal ions bind quite separately, with two distinct binding events shown by the ITC titrations. The two cadmium ions bind to the enzyme non-cooperatively. With cadmium ion the molar enthalpies of binding change from endothermic at low pH when one cadmium binds to exothermic at high pH when two cadmium ion bind.

The binding association constant for one cadmium ion binding at low pH is of the order  $10^6 \text{ M}^{-1}$ . When two cadmium ions bind, the first cadmium ion binds to the enzyme with a higher binding constant of the order  $10^8 \text{ M}^{-1}$ , whereas the second cadmium ion has about a 100 fold lower affinity for binding than the first cadmium ion.

The following model for cadmium ion binding to apoBclI was proposed. At low pH when one cadmium ion binds only one proton is released. Previous workers have suggested that when one cadmium ion binds to apoBclI, it oscillates between the two binding sites. If this is the case then it seems reasonable that the single proton released comes from the imidazolium ion or from the thiol group depending on to which site cadmium ion binds. When both cadmium ions bind at high pH, a total of 3 protons are released. When the first of these two cadmium ions binds at high pH two protons are released and we propose that these are possibly from the imidazolium ion and the thiol group. When the second cadmium ion binds an additional proton is released, and this is possibly from the cadmium-bound water molecule that bridges between the two metal ions.

## 2.6 - References

1. Page, M.I., Badarau, A., The mechanisms of catalysis by metallo- $\beta$ -lactamases, *Bioorg. Chem. Appl*, **2008**, 1-14.
2. Page, M.I., Badarau, A., The variation of catalytic efficiency of *Bacillus Cereus* metallo- $\beta$ -lactamases with different active sites metal ions, *Biochemistry*, **2006**, 45, 10654-10666.
3. Garrity, J.D., Bennett, B., Crowder, M.W., Direct evidence that the reaction intermediate of metallo- $\beta$ -lactamases L1 is metal-bound, *Biochemistry*, **2005**, 44, 1078-1087.
4. Page, M.I., The chemistry of  $\beta$ -lactam, ed M.I, pg 129.
5. Baldwin, G.S., Edwards, G.F.S., Kiener, P.A., Tully, M.J., Waley, S.G., and Abraham, E.P., Production of a variant of beta-lactamase II with selectivity decreased cephalosporinase activity by a mutant of *Bacillus cereus* 569/H/9, *Biochem, J.*, **1980**, 191, 11-116.
6. Livermore, D.M., All are  $\beta$ -lactams created equal? , *Scand. J. Infect. Dis. Suppl.*, **1996**, 101, 33-43.
7. Concha, N.O., Rasmussen, B.A., Bush, K and Herzberg, O., Crystal structure of the wide spectrum binuclear zinc- $\beta$ -lactamases from *Bacteroides Fragilis*, *Structure*, **1996**, 7 (4), 823-836.
8. Horn, J.R., Ramaswamy and Murphy, K.P., Structure and energetics of protein-protein interactions: The role of conformational heterogeneity in OMTKY3 binding to serine proteases. *J.Mol.Biology*, **2003**, 331, 497-508.
9. Badarau, A., Reactivity and inhibition of metallo- $\beta$ -lactamases, PhD Thesis, **2006**, University of Huddersfield.
10. Frere, J.M., Beta-lactamase and bacterial resistance to antibiotics, *Mol. Microbiol*, **1995**, 16(3), 385-395.
11. Murphy, B.P., Pratt, R.F., *Biochemistry*, **1991**, 30, 3640-3649.
12. Murphy, B.P., Pratt, R.F., *Biochemistry*, **1998**, 256, 669-672.
13. Huang, W., Petrosino, J., Hirsch, M., Shenkin, P.S., Palzkill, T., *J.Mol. Biol*, **1996**, 258, 688-703.

14. Lamotter-Brasseur, J., Knox, J., Kelly, J.A., Charlier, P., Franze, E., Dideberg, O., Frere, J.M., *Biotech. Genet. Eng. Rev*, **1994**, 12, 189-230.
15. Page, M. I., Vilkinova, B., Layland, N.J., *J. Am. Chem. Soc*, **1995**, 117, 12092-120-5.
16. Ledent, P., Les  $\beta$ -lactamases de class D: proprietes catalytiques et mechanism d'activation partielle induit par les substrates, PhD thesis , **1995**, University of Leige, Belgium.
17. Bounaga, S., Laws, A.P., Galleni, M., Page, M.I., Mechanisms of catalysis and the inhibition of B-Cereus zinc dependent  $\beta$ -lactams, *Biochemistry*, **1998**, 331, 703-711.
18. Payne, D.J., Metallo- $\beta$ -lactamases- a new therapeutic challenge, *J. Med. Microb*, **1993**, 39, 2, 93-99.
19. Seny, D., Prosperi-meys, C., Bebrane, C., Rossilini, G.M., Page, M.I., Noel, P., Frere, J.M., Galleni, M., mutational analysis of the two binding zinc binding sites of the Bacillus cereus 569/H/9 metallo- $\beta$ -lactamases, *Biochem. J*, **2002**, 263, 687-696.
20. Soto, R.P., Zeppezauer, M., Adolph, H., Galleni, M., Frere, J.M., Carfi, A., Dideberg, O., Wouters, J., Hemmingsen, L., Bauer, R., Preferences of  $\text{Co}^{2+}$  and  $\text{Zn}^{2+}$  for two metal sites in Bacillus cereus  $\beta$ -lactamases II: a pertubal angular correlation of  $\gamma$ -rays spectroscopic study, *Biochemistry*, **1999**, 38, 16500-16506.
21. Orellano, E.G., Girardini, J.E., Cricco, J.A., Ceccarelli, E.A., and Vila, A.J., Spectroscopic charecterization of a binuclear metal site in *Bacillus cereus*  $\beta$ -lactamase II, *Biochemistry*, **1998**, 37, 10173-10180.
22. Crowder, M.W., Wang, Z., Franklin, S.L., Zovinka, E.P., Benkovic, S.J., Characterization of the metal-binding sites of the  $\beta$ -lactamase from *Bacteroides fragilis*, *Biochemistry*, **1996**, 35, 12126-12132.
23. Paul-Soto, R., Bauer, R., Frere, J.M., Galleni, M., Meyer-Klauke, W., Nolting, H., Rossolini, G.M., de Seny, D., Hernandez-Valladares, M., Zeppezauer, M. and Adolph, H.W., Mono and binuclear  $\text{Zn}^{2+}$   $\beta$ -lactamase. Role of the conserved cysteine in the catalytic mechanism, *J. Biol. Chem*, **1999**, 274, 13242-13249.

24. Fabiane, S.M., Sohi, M.K., Wan, T., Payne, D.J., Bateson, J.H., Mitchell, T., and Sutton, B.J., Crystal structure of the zinc-dependant  $\beta$ -lactamase from *Bacillus Cereus* at 1.9 Å resolution binuclear active site with features of a mononuclear enzyme, *Biochemistry*, **1998**, 37, 12404-12411.
25. Simm, A.M., Higgins, C.S., Carenbauer, A.L., Crowder, M.W., Bateson, J.H., Bennett, P.M., Clarke, A.R., Halford, D.E., and Walsh, T.R., Characterisation of monomeric L1 metallo-  $\beta$ -lactmase and the role of the N-terminal extension in negative cooperativity and antibiotic hydrolysis, *J. Biol. Chem*, **2002**, 277, 24744-24752.
26. Carfi, A., Duee, E., Galleni, M., Frere, J.M. and Didegberg, O., 1.85 Å resolution structure of the zinc (II)  $\beta$ -lactamase from *Bacillus cereus*, *Acta crystallography. Biol. Crystallogr*, **1998**, D54, 313-323.
27. Carfi, A., Duee, E., Paul-Soto, R., Galleni, M., Frere, J.M. and Didegberg, O., X-ray structure of Zn (II)  $\beta$ -lactamase from *Bacteroides fragilis* in an orthorhombic crystal form, *Acta Crystallogr*, **1998**, D54, 45-57.
28. Felicin, A., Amicosante, A., Oratane et al., An overview of the kinetic parameters of class B  $\beta$ -lactamases, *Biochem, J*, **1993**, 291, 151-155.
29. Felici, A., Amicosante, G., Oratore, A., Strom, R., Ledent, P., Joris, B., Fanuel, L., and Frere, J.M., An overview of the kinetic parameters of class B  $\beta$ -lactamases, *Biochem J*, **1993**, 291, 151-155.
30. Felici, A., Amicosante, G., Kinetic analysis of extension of substrate specificity with *Xanthomonas maltophilia*, *Aeromonas hydrophilia*, and *Bacillus cereus* metallo-  $\beta$ -lactamases, *Antimicrob. Agents and chemotherapy*, **1995**, 39, 192-199.
31. Crawford, P.A., Yang, K.W., Sharma, N., Bennett, B., and Crowder, M.W., Spectroscopic studies on cobalt (II)- substituted metallo-  $\beta$ -lactamase ImiS from *Aeromonas veronii* bv. *Sobria*, *Biochemistry*, **2005**, 44, 5168-5176.
32. Herzberg, O., Fitzgerald, M.P., *Handbook of metalloproteins*, metallo- $\beta$ -lactamases, 3, 217-234.
33. Felicia, A., Amicosante, G., kinetic analysis of extension of substrate specificity with *xanthomonas maltophilia*, *aeromonas hydrophilia* and

- bacillus cereus metallo- $\beta$ -lactamases. *Antimicrob. Agents Chemother*, **2001**, 45, 1254- 1262.
34. George, A., Ombura., Kuo, J.M., Leisa, S., Mullins and Rausel, F.M., Charecterization of the zinc binding sites of bacterial phosphotriesterase, *J. Biol. Chem*, **1992**, 267 (19), 13278-13283.
  35. Sabath, L.D., Abraham, E.P., zinc is a cofactor for cephalosporinase from *Bacillus cereus* 569. *Biochemistry*, **1966**, 98, 11C-13C.
  36. Deseny, D., Heinz, J., Wommer, S., Keifer, M., Meyer-Klauke.W, Galleni, M., Frere, J.M., Bauer, R., Adolph, H.W., Metal ion binding and coordination geometry for wild type and mutants of metallo- $\beta$ -lactamases from bacillus cereus 569/H/9 a combined thermodynamic kinetic and spectroscopic approach, *J.Biol.Chem*, **2001**, 276 (48), 45065-45078.
  37. Concha, N.O., Janson, C.A., Rowling, P., Pearson, S., Cheever, C.A., Clarke, B.P., Lewis, C., Galleni, M., Frere, J.M., Payne, D.J., Bateson, J.H and Abdel-Mequid, S.S., Crystal structure of IMP-1 metallo-  $\beta$ -lactamase from *Pseudomonas aeruginosa* and its complex with a mercaptocarboxylate inhibitor: binding determinants of a potent, broad-spectrum inhibitor, *Biochemistry*, **2000**, 39, 4288-4298.
  38. Concha, N.O., Rasmussen, B.A., Bush, K., and Herzberg, O., Crystal structure of cadmium and mercury-substituted metallo-  $\beta$ -lactamase from *Bacteroides fragilis*, *Protein Sci*, **1997**, 6, 2671-2676.
  39. Crowder, M.W., Wang, Z., Franklin, S.C., Zovinka, E.P., and Benkovic, S.J., *Biochemistry*, **1996**, 35, 12126.
  40. Bounga, S., Laws, A.P., Galleni, M., Page, M.I., The mechanism of catalysis and the inhibition of the *Bacillus Cereus* zinc-dependant  $\beta$ -lactamase , *Biochemistry*, **1998**, 331, 703-711.
  41. Concha, N.O., Rasmussen, B.A., Bush, K., and Herzberg, O., Crystal structure of cadmium and mercury-substituted metallo-  $\beta$ -lactamase from *Bacteroides fragilis*, *Protein Sci*, **1997**, 6, 2671-2676.
  42. Fitzgerald, P.M., Wu, J.K., and Toney, J.H., Unanticipated inhibition of the metallo-  $\beta$ -lactamase from *Bacteroides fragilis* by 4-morpholineethanesulfonic acid (MES):a crystallography study at 1.85Å resolution, *Biochemistry*, **1998**, 37, 6791-6800.

43. Carfi, A., Pares, S., Duee, E., Galleni, M., Duez, C., Frere, J.M., and Dideberg, O., The 3D structure of a zinc metallo-  $\beta$ -lactamase from *Bacillus cereus* reveals a new type of protein fold, *EMBO J*, **1995**, 14, 4914-4921.
44. Wilcox, D.E., Binuclear hydrolases, *Chem. Rev*, **1996**, 96, 2435.
45. Rasia, R.M., and Vila, A.J., Exploring the role and the binding affinity of a second zinc equivalent in *B-cereus* metallo- $\beta$ -lactamase, *Biochemistry*, **2002**, 41, 1853-1860.
46. Wang, Z., Fast, W., Valentine, A.M., and Benkovic, S.J., Metallo- $\beta$ -lactamase: structure and function, *Curr. Opin. Chem.*, **1999**, 3, 614-622.
47. Wommer, S., Rival, S., Heinz, U., Galleni, M., Frère, J.M., Franceschini, N., Amicosante, G., Rasmussen, B., Bauer, R. and Adolph, H.W, Substrate-activated zinc binding of metallo- $\beta$ -lactamases: physiological importance of mononuclear enzymes, *J. Biol. Chem*, **2002**, 277, 24142-24147.
48. Baldwin, G.S., Galdes, A., Hill, H.A., Smith, B.E., Waley, S.G. and Abraham, E.P, Histidine residues as zinc ligands in  $\beta$ -lactamase II, *Biochem. J*, **1978**, 175, 441-7.
49. Vila, A.J., and Fernandez, C.O., Alkaline transition of *Rhus vernicifera* stellacyanin, an unusual blue copper protein, *Biochemistry*, **1997**, 36, 10566-10570.
50. Garau, G., Bebrone, C., Anne, C., Galleni, M., Frere, J.M., and Dideberg, O., A metallo- $\beta$ -lactamase in action: crystal structure of the monozinc carbapenemase CphA and its complex with biapenem, *J.Mol. Biol*, **2005**, 345, 785-795.
51. Guo, J.Q., Wang, S.K., Dong, J., Qiu, H., Scott, R.A., and Giedroc, D.P., X-ray and visible absorption spectroscopy of wild type and mutant T4 gene 32 proteins: His61 not His81 is the non-thiolate zinc ligands, *J.Am. Chem. Soc*, **1995**, 117, 9437-9440.
52. Toney, J.H., Fitzgerald, P.M.D., Grover-sharma, N., Olsan, S.H., May, W.J., Sundelof, J.G., Vanderwall, D.E., Cleary, K.A., Grant, S.K., Wu, J.K., Antibiotic sensitization using biphenyl tetrazoles as potent

- inhibitors of bacteroides fragilis metallo- $\beta$ -lactamases, *Chem. Biol*, **1998**, 5, 185-196.
53. Melino, S., Capo, C., Dragini, B., Aceto, A., Petruzzelli, R., A zinc binding motif conserved in glyoxalase II,  $\beta$ -lactamases and arylsulfatases, *Trends in Biochem. Sci*, **1998**, 23, 381-382.
54. Wang, Z., Fast, W., Valentine, A.M., Benkovic, S.J., Metallo- $\beta$ -lactamases: Structure and mechanism, *Curr. Opin. Chem. Biol*, **1999**, 3, 614-622.
55. Vallee, B.L, Zinc enzymes, 5 (Ed, Sprino, T.G.), **1983**, 1-25.
56. Kimura, E., Shiota, T., Koike, T., Shiro, M., Kadama, M., *J. Am. Chem. Soc*, **1990**, 112, 5805-5811.
57. Bertini, I., Luchinat, C., Rosi, M., Sgamellotti, A., Tarantelli, F., *Inorg. Chem*. **1990**, 29, 1460-1463.
58. Christianson, D.W., Fierke, C.A., *Acc. Chem. Res*, **1996**, 29, 331-339.
59. Vallee, B.L., Aulds, D.S., *Acc. Chem. Res*, **1993**, 26, 543-551.
60. Matthews, B.W., *Acc chem Res*, **1988**, 21, 331-340.
61. Lipscomb, W.N., Annu Review, *Biochemistry*, **1983**, 52, 17-34.
62. Oz, G., Pountney, D.L., Armitage, I.M., NMR spectroscopic studies of  $I=1/2$  metal ions in biological systems, *Biochem. Cell Biol*, **1998**, 76, 223-234.
63. Bauer, R., Adolph, H.W., Andersson, I., Danielsen, E., Formicka, G., Zeppezauer, M., Coordination geometry for cadmium in the catalytic zinc site of horse liver alcohol dehydrogenase: studies by PAC spectroscopy, *Eur. Biophys. J*, **1991**, 20(4), 215-221.
64. Jacquin, O., Balbeur, D., Damblon, C., Marchot, P., Pauw, E.D., Roberts, G., Frere, J.M., Matagne, A, Positively cooperative binding of zinc ions to *Bacillus Cereus* 569/H/9  $\beta$ -lactamases II suggests that the binuclear enzyme is the only relevant form for catalysis, *J.Mol. Biol*, **2009**, 392, 1278-1291.
65. Rasmussen, B.A., and Bush, K., Carbapenem hydrolysing  $\beta$ -lactamases, *Antimicrob. Agents. Chemor*, **1997**, 41, 223-232.
66. de Seny, D., Heinz, U., Wommer, S., Kiefer, M., Meyer-Kluake, W. Galleni, M., Frere, J.M., Bauer, R., and Adolph, H.W., Metal ion binding and coordination geometry for wild type and mutants of

- metallo-  $\beta$ -lactamase from *Bacillus cereus* 569/H/9 (BcII); a combined thermodynamic, kinetic and spectroscopic approach, *J. Biol. Chem*, **2001**, 276 (48), 45065-45078.
67. valladares, M.H., Keifer, M., Heinz, U., Paul-Soto, R., Meyer-Klaucke, W., Nolting, H.F., Zeppezauer, M., Galleni, M., Frere, J.M., Rossolini, G.M., Amicosante, G., Adolph, H.W., Kinetic and spectroscopic characterization of native and metal-substituted  $\beta$ -lactamase from *Aeromonas hydrophilia* AE036 *FEBS, Lett*, **2000**, 467, 221-225.
68. Crawford, P.A., Sharma, N., Chandrasekar, S., Sigdel, T., Walsh, T.R., Spencer, J., and Crowder, M.W., Over-expression, purification and characterization of metallo-  $\beta$ -lactamase ImiS from *Aeromonas veronii* bv. *Sobria*, *Protein expression purify*, **2004**, 36, 272-279.
69. Fast, W., Wang, Z., and Benkovic, S.J., Familial mutations and zinc stoichiometry determine the rate limiting step of Nitrocefin hydrolysis by metallo-  $\beta$ -lactamase from *Bacteroides fragilis*, *Biochemistry*, **2001**, 40, 1640-1650.
70. Crowder, M.W., Yang, K.W., Carenbauer, A.L., Periyannan, G., Seifert, M.E., Rude, N.E., Walsh, T.R., The problem of a solvent exposable disulfide when preparing Co(II)- substituted metallo-  $\beta$ -lactamase L1 from *Stenotrophomonas maltophilia*, *J.Biol, Inorg. Chem*, **2001**, 6, 91-99.
71. Fukada, H., Takahashi., Enthalpy and heat capacity changes for the proton dissociation of various buffer components on 0.1 M potassium chloride, *Sturct. Funct. Genet*, **1998**, 33, 159-166.
72. Bounga, S., Mechanism of Catalysis and Inhibition of *Bacillus Cereus* Class B  $\beta$ -lactamase, PhD Thesis, **1999**, University of Huddersfield.
73. Selevsek, N., Rival, S., Tholey, A., Heinzle, E., Heinz, U., Hemmingsen, L and Adolph, H.W., Zinc ion-induced domain organisation in Metallo-  $\beta$ -lactamase, *J.Biol.Chem*, **2009**, 284, 16419-16431.
74. Badarau, A., Page, M.I., Loss of enzyme activity during turnover of the bacillus cereus  $\beta$ -lactamase catalysed hydrolysis of  $\beta$ -lactams due to loss of zinc ion, *J.Biol.Inorg. Chem*, **2008**, 13, 919-928.

75. Llarrull, L.I., Tioni, M.F., Kowalski, J., Bennett, B., Vila, A.J., Evidence for a dinuclear active site in the metallo- $\beta$ -lactamase BclI with substoichiometric Co(II)., *J.Biol.Chem*, **2007**, 282, 30586-30595.
76. Periyannan, G.R., Costello, A.L., Tierney, D.L., Yang, K.W., Bennett, B., and Crowder, M.W., Sequential Binding of Cobalt (II) to metallo-  $\beta$ -lactamase CcrA, *Biochemistry*, **2006**, 45, 1313-1320.
77. Perrin, D.D., Ionisation constants of inorganic acids and bases in aqueous solution, **1983**, 2<sup>nd</sup> edition., Pergamon, Oxford.
78. Hemmingsen, L., Damblon, C., Antony, J., Jensen, M., Adolph, H.W., Wommer, S., Roberts, G.C.K., and Bauer, R., Dynamics of mononuclear Cadmium  $\beta$ -lactamase revealed by the combination of NMR and PAC spectroscopy, *J.Am.Chem. Soc*, **2001**, 123, 10329-10335.
79. Heinz, U., Bauer, R., Wommer, S., Meyer-Klaucke., Papamichaels, C., Bateson, J., and Adolph, H., Coordination geometries of metal ions in D-or L-captopril-inhibited metallo-  $\beta$ -lactamases, *J.Biol. Chem*, **2003**, 278, 20658-20666.
80. Llarrull, L.I., Tioni, M.F., Vila, A.J., Metal content and localisation during turnover in *B cereus* metallo-  $\beta$ -lactamase., *J.Am.Chem.Soc*, **2008**, 130, 15842-15851.
81. Tioni, M.F., Llarrull, L.I., Andres, A., Poeylout-Palena, Marti, M.A., Saggiu, M., Periyannan, G.R., Mata, E.G., Bennett, B., Murgida, D.H., and Vila, A.J., Trapping and characterisation of a reaction intermediate in Carbapenem hydrolysis by *B.cereus* metallo-  $\beta$ -lactamase., *J.Am.Chem.Soc*, **2008**, 130, 15852-15863.

# **Chapter 3 - Supramolecular Complexes**

## 3.1 - Introduction

### 3.1.1 - Supramolecular Chemistry

Supramolecular chemistry is defined as the 'chemistry of molecular assemblies and of the intermolecular bond' <sup>1</sup>. Supramolecular chemistry can also be defined as 'the chemistry of non-covalent intermolecular binding interactions'. <sup>1</sup> Supramolecular chemistry is involved with many different types of non-covalent intermolecular interactions. The non-covalent interactions include ion-dipole bonding, dipole-dipole bonding, hydrogen bonding, van der Waals forces, coordinate bonding, hydrophobic interactions and electrostatic forces.

Supramolecular chemistry really began in the late 1960's, when Charles Pederson <sup>2</sup> synthesised the first crown ether molecule. This was followed by Jean Marie Lehn <sup>3</sup> who defined supramolecular chemistry after the synthesis of the first cryptand in 1978. <sup>4</sup> In 1987 Jean Marie Lehn won the Nobel Prize for his contribution to supramolecular chemistry. <sup>2,5-8</sup>

The main ideas behind the design of supramolecular complexes are for molecular recognition, self-assembly and self-organisation. One aspect of supramolecular chemistry involves complexes which are designed to have a cavity. The cavity acts as a binding site where another species can bind. Supramolecular complexes are somewhat like enzymes in that a species can bind to the cavity of the ligand in a lock and key mechanism. <sup>9,10</sup> The cavity (active site) of the supramolecular ligand acts as a host and the binding is usually based on non-covalent interactions.

### 3.1.2 - Host and Guest Chemistry

Host and guest chemistry occurs when two species combine together by non-covalent interactions. This can only happen if the guest molecule recognises the cavity of the host molecule which must complement the guest molecule in terms of its size and shape. The host molecule possesses as convergent binding sites (the outer shell of the molecule that consists of lewis basic donors and hydrogen bond acceptors. The guest molecule possesses as divergent binding sites, where the molecule binds inside the host cavity and these are lewis acidic metal cations or hydrogen bond acceptor halide anion.<sup>9</sup>

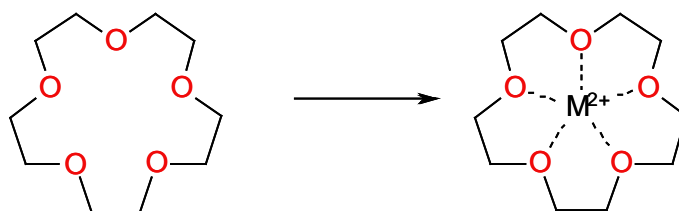
### 3.1.3 - Binding: Chelate and Macrocyclic Effects

Complexes in supramolecular chemistry are usually between chelating ligands and metal ions. The supramolecular complex is sometimes formed by relatively weak binding forces to give a stable structure, but the overall stability of the structure is more than what would be expected from simply the sum of the binding interactions. This is explained by the chelate and macrocyclic effects.

The chelate effect explains why complexes formed between a ligand and a metal ion where the ligand binds to the metal through more than one binding site are very much more stable than would be predicted from the individual binding energies. One way to look at it is that dissociation of the complex requires all the metal-ligand bonds to break at the same time and this is statistically unlikely. Another is through the entropy change associated with the complex formation. In the case of metal binding to crown ether for instance, all the solvent molecules solvating the metal ion are displaced by the ligand and, based on the number of independent species in solution, this means the complex formation is an entropically favourable reaction.



Another influence on binding is the macrocyclic effect. This is an additional stabilising effect with crown ethers, and results in these ligands forming particular stable complexes because the binding sites in the ligand are already orientated correctly for multidentate coordination to the metal ion,<sup>4</sup> as shown in **Scheme 3.1**.



**Scheme 3.1:** Crown ether binding to metal ion showing the macrocyclic effect

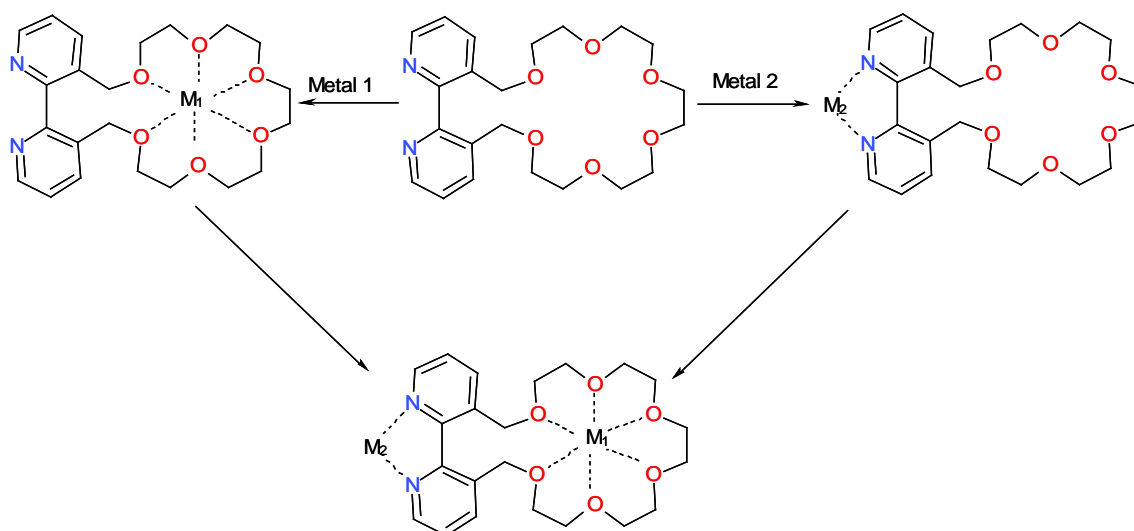
### **3.1.4 - Selectivity of Metal ions Binding to Ligands**

When metal ions form complexes with ligands, the strength of the bonds formed and the stability of the complexes depend on a number of factors. One is obviously steric, and metal ions will only bind strongly if they 'fit' the coordination site. Another is the compatibility between metal ions and the coordinating centre. The hardness and softness of the metal ion and the ligand can be used to describe these compatibilities. Hard metal ions (those with relatively unpolarisable electron shells – e.g. small metal ions, high charge metal ions, alkali metal ions) tend to bind more strongly with hard ligands (those based on oxygen for example). Soft metal ions (often transition metal ions and others with low charge to radius ratios) tend to bind more strongly to soft ligands (e.g. those based on nitrogen).

### 3.1.5 - Allosteric Effects

If a single ligand molecule has two sites on it that can separately bind metal ions then in some cases the presence of a metal ion in one site can influence the way metal ions bind at the second site. This interaction between binding sites is known as the allosteric effect. The two sites that exhibit an allosteric effect are usually very distinct from each other. The allosteric effect is well known in nature, where it is used in a number of different ways as the feedback loop mechanism in metabolic pathways.

The first allosteric effect in supramolecular chemistry was described by Rebek,<sup>11-14</sup> who recognised that for an allosteric effect to occur, it is necessary to have two binding sites - the active site and an allosteric site - and a structure that connects the two and allows them to interact. In the complexes he was studying the first binding site was a crown ether, which is a hard Lewis base and only coordinates to hard Lewis acids (alkali metal ions) and the second binding site was the 2,2-bipyridine site,<sup>15</sup> that coordinates other metal ions. This is shown in **Scheme 3.2**.<sup>13</sup>



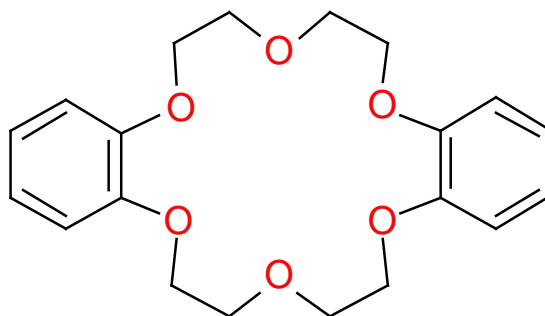
**Scheme 3.2:** The complexes for which Rebek observed an allosteric effect.

The two binding sites must affect each other if an allosteric effect is to be observed. In this case, the coordination of a soft metal ion at the bipyridine site causes the two aromatic groups to become co-planar, so forcing the stereochemistry of the crown ether ring and significantly reducing the facility with which the crown ether can coordinate the harder of the two metal ions.<sup>12-</sup>

14

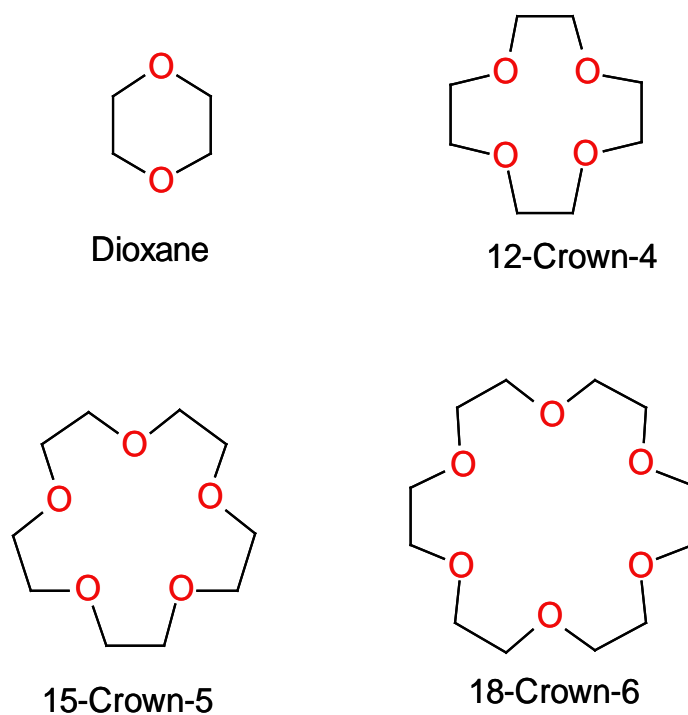
### 3.1.6 - Crown Ethers

Crown ethers were discovered in the late 1960's by Charles Pederson,<sup>2</sup> and the first to be synthesised was dibenzo-18-crown-6 (**Scheme 3.3**).<sup>15</sup>



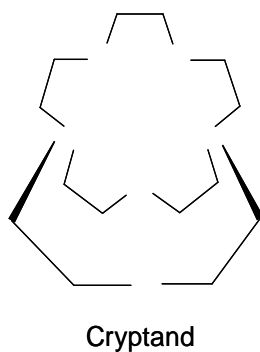
**Scheme 3.3:** Dibenzo-18-crown-6

Crown ether molecules have different numbers of oxygen atoms to create a cyclic structure in different sizes and shapes (**Scheme 3.4**). The cyclic structure of crown ethers consists of ethylene glycol units of –O–CH<sub>2</sub>CH<sub>2</sub>–O– and the best known crown ether is 18-crown-6. In this nomenclature the first number refers to the total number of atoms in the ring and the second number refers to the number of oxygen atoms. The simplest crown ether is dioxane that consists of two oxygen atoms, but the cavity of dioxane is very small. The smallest crown ether metal ions can bind to is 12-crown-4.<sup>16</sup>



**Scheme 3.4:** Different types of crown ethers.

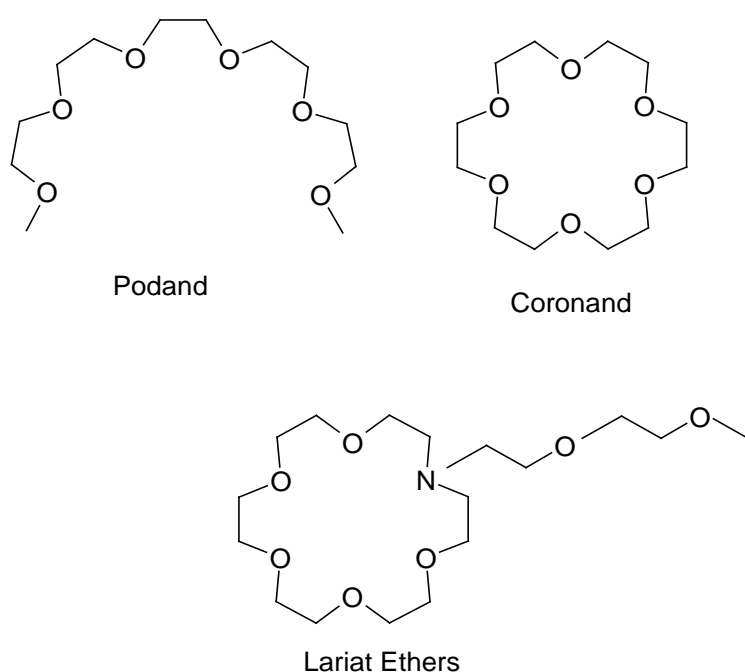
After Pederson discovered crown ethers it became of great interest and Jean Marie Lehn synthesised the first cryptand (**Scheme 3.5**). Cryptands are three dimensional analogues of the original crown ethers in which some of the oxygen atoms are replaced with nitrogen atoms, the resultant bridges giving metal ion coordination sites above the 'two dimensional' ring.



**Scheme 3.5:** Cryptand synthesised by Jean Marie Lehn.

Crown ethers show selectivity towards metal ion binding based on molecular recognition, depending on the size match between the cavity and the metal ion.<sup>17-22</sup> The size of cavity in crown ethers can be changed by varying the number of oxygen atoms in the structure.

There are many related ligands such as coronands, podands and lariat ethers as shown in **Scheme 3.6**. These classes are well developed with different sizes and shapes of structure, but still consist of oxygen atoms linked via dimethylene groups.

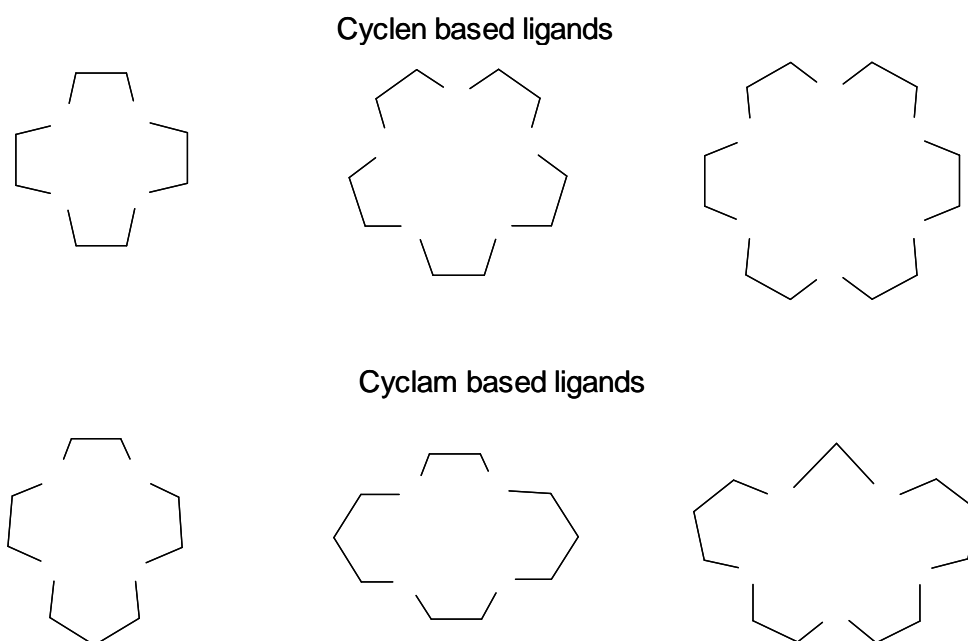


**Scheme 3.6:** Ligand types related to crown ethers

### 3.1.7 - Aza-Crown Ethers

Aza-crown ethers are cyclic ligands similar in structure to the crown ethers, but aza-crown ethers have nitrogen atoms in place of oxygen atoms. The aza-crown ethers come in different sizes and shapes, depending on the number of nitrogen atoms present. The aza-crown ethers have repeating units of  $\text{N}-(\text{CH}_2)_n$ .

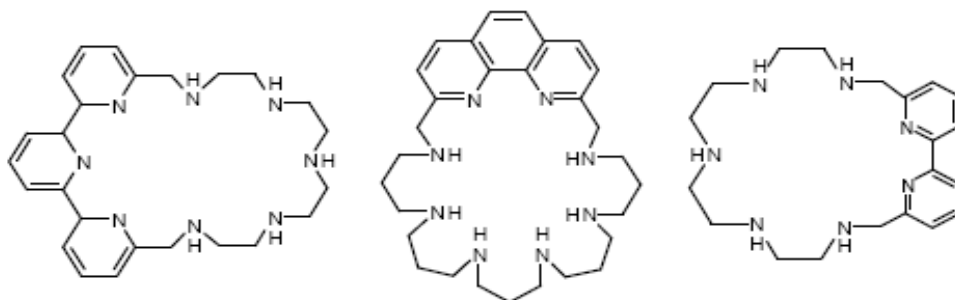
The aza-crown ether ligands are divided into cyclens and cyclams. A cyclen has two methylene groups between each nitrogen atom and cyclam has one or more chains where there are three methylene groups between each nitrogen atom (**Scheme 3.7**).



**Scheme 3.7:** Aza-crown ethers.

The change from oxygen to nitrogen affects the coordination of metal ions to the cavity. Oxygen ligands generally have a high affinity for s-block metal ions, whereas the nitrogen ligands tend to have high affinities towards transition metal ions. This affects the coordination and is a factor in designing ligands with selectivity for specific metal ions.<sup>23</sup>

Aza-crown ethers have not just been reported in supramolecular chemistry. They have also been used for other purposes in the biological field. They were synthesised by Benicini et al (**Scheme 3.8**) for use as receptors for the binding and hydrolysis of ATP,<sup>24</sup> recognising and sensing ATP,<sup>25</sup> and for recognising and selectively binding metal ions and some anions in water.<sup>26-29</sup>



**Scheme 3.8:** Ligands synthesised by Bencini et al. adapted from references 25-27.

### 3.1.8 - Single Crystal X-ray Diffraction Results

The objective of our work was to study the way the ligand fused 2,2'-bipyridine aza-crown-4 (bipy-aza-crown-4) (**Figure 3.1**), which was synthesised by C.Rice, binds to copper(II) ions in solution, particularly in terms of how the two binding sites show selectivity towards copper(II) ions.

The idea was to compare the results obtained using ITC, where the metal ion salt ( $\text{CuCl}_2$ ) in acetonitrile is progressively added to a solution of the ligand, with the results of crystallographic measurements on copper ion complexes of the ligand isolated from methanol solution, and to rationalise the observations in terms of stabilities of the metal ion complexes formed.

According to single crystal x-ray diffraction studies the structure of the pure ligand (bipy-aza-crown-4) isolated as a crystalline solid is as shown in **Figure 3.1**.(C.Rice, unpublished work)

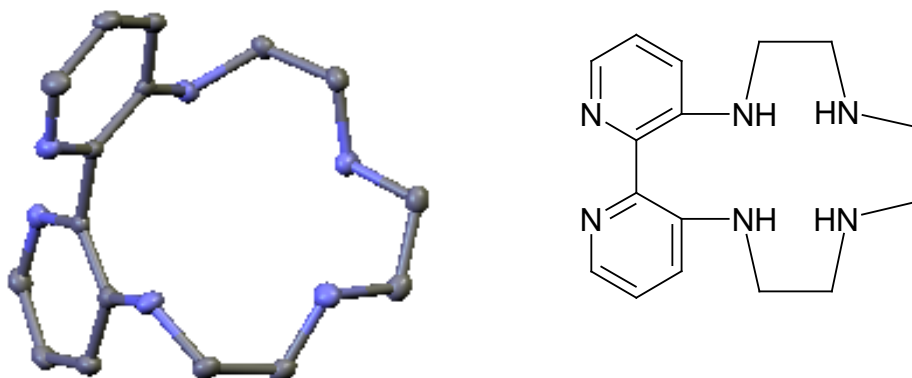


**Figure 3.1:** Structure of bipy-aza-crown-4 ligand (light blue=N, dark blue=C).

Note that the bipyridine rings are twisted in relation to each other, with a torsion angle of  $110^\circ$  (one is coming out of the page the other is going in). This is required for the crown ether to adopt its most stable configuration.

A number of crystal structure determinations were performed in Huddersfield on the ligand and on the copper complex ion salts formed with the ligand

crystallised from methanol following the progressive addition of copper ion to the ligand in solution.<sup>30</sup>

The first crystalline salt identified with a well defined structure was formed after the addition of one equivalent of copper ion (as  $\text{CuCl}_2$ ) to the ligand solution in methanol, and subsequent precipitation. The structure of this species is shown in **Figure 3.2**.

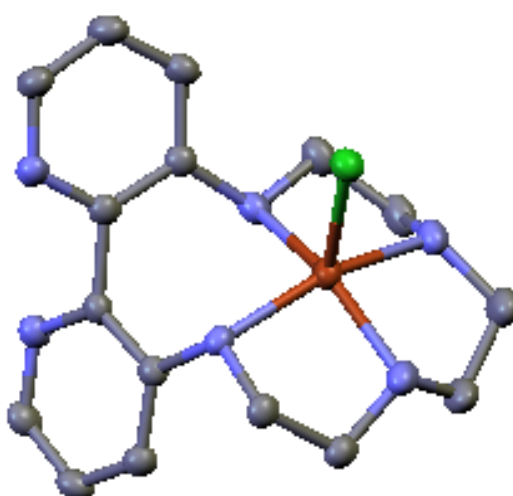


**Figure 3.2:** Crystal structure of bipy-aza-crown-4 with one equivalent of copper ion added (Green= Cl, light blue= N, red= Cu, dark blue= C).

The copper ion appears to bind to the aza-crown-4 unit by coordinating to the four nitrogen atoms in the aza-crown-4 ring. A chloride ion occupies a fifth coordination site on the copper ion.

Following the addition of a second equivalent of copper ion and crystallisation of the resultant salt, a new structure was detected. In this structure (**Figure 3.3**) the additional copper ion is coordinated to the nitrogens on the bipyridine and to three chloride ions. The coordination of this second copper ion appears to distort the ligand structure so that the first copper ion, sitting in the aza-crown-4 ring, loses its bond to one of the aza-crown nitrogens but becomes coordinated to an additional chloride ion so that it now has two directly

coordinated chloride ions compared with the single chloride ion coordinated in the complex with just one bound copper ion.

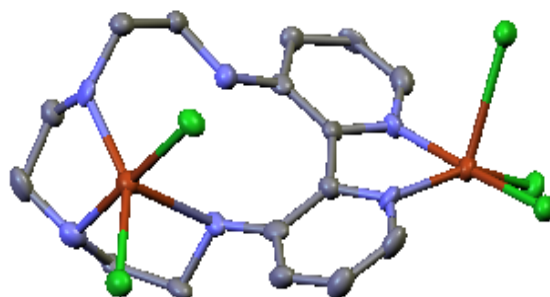


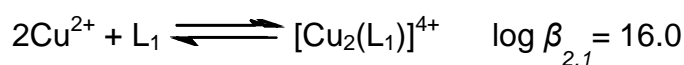
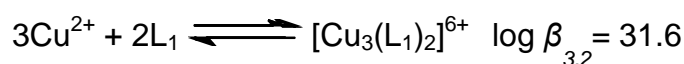
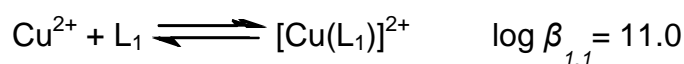
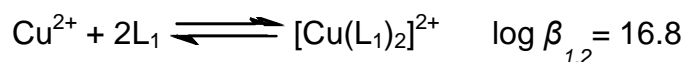
**Figure 3.3:** Bipy-aza-crown-4 when two equivalents of copper ion per ligand are coordinated.

It has been suggested that aspects of this structure may be intuitively unsatisfactory. For example, in the binuclear complex the copper ion in the crown ether coordination site is only three-fold coordinated to the ligand. It is very unusual for such an unsymmetrical species to form. However, there are some very clear conclusions that arise from this x-ray diffraction work concerning the way copper ions bind to the ligand. They are as follows.

1. Copper ion can bind in two distinct sites on the bipy-aza-crown-4 ligand, involving coordination to the bipyridine nitrogen atoms and to the aza-crown ring.
2. Copper ions occupy the crown ether site first, and then bind at the bipyridine site when the crown ether site is saturated.
3. There is no evidence of copper ions bridging between two ligand molecules, as might be expected when coordinating bipyridine nitrogen atoms. It appears that the copper ion binds at the bipyridine site in a 1:1 ratio with the ligand. Two coordination sites on the copper ion are bound to the nitrogens on the ligand.

4. When the bipyridine site is occupied there is distortion at the aza-crown site that changes the bonding to the copper ion. This influence on the aza-crown binding site by a metal ion at the other, bipyridine site, is a prime example of an allosteric effect.
5. In summary, based on the structures of the crystalline precipitate from methanol solution, it appears that copper ions first form a 1:1 complex through coordination at the crown ether site and then a 2:1 complex through coordination of an extra copper ion at the bipyridine site.

The observations above are based on crystallised salts, precipitated from methanol solution. Electronic spectral studies on the formation of complexes between the ligand and added copper ion have also been reported in methanol solution.<sup>30</sup> In these studies, in which a ligand concentration of  $10^{-4}$  M was used, absorption maxima were identified for four soluble ligand-copper ion complexes. The spectra recorded through titrations of metal ion into ligand solution have been interpreted in terms of the following equilibria and formation constants.<sup>30</sup>



The diagram in **Figure 3.4** shows the relative concentrations of the various complexes as copper ion is added. The first absorption maximum corresponds to a stoichiometry equivalent to  $\text{CuL}_2^{2+}$ . The only structure that this could correspond to is one in which a copper ion bridges between bipyridine unit on two ligands. Importantly, this complex ion was NOT identified in crystallographic studies of the isolated complex ion salts. The conclusion must be that the order in which the copper ion occupies coordination sites on the

ligand in solution is not the same as the order in which the complexes crystallise as solids. This observation is significant when interpreting our ITC data later. The second maximum peak observed is when one equivalent of copper ion is added to the ligand and corresponds to the formation of a complex of one copper ion bound to one ligand. This complex could be one in which the copper ion is bound at the crown or at the bipyridine site. Most logically the latter would be expected, given the likely structure of its precursor complex  $\text{CuL}_2^{2+}$ . However, the fact that the next complex to form is of a stoichiometry  $\text{Cu}_3\text{L}_2^{3+}$  casts doubt on this since the stoichiometry can only be explained through a structure in which copper ion bridges two ligands via the bipyridine site and two more occupy the crown ether sites in the two ligands.

The final form is two copper ions binding to one ligand, this agrees with the x-ray studies of the complex ions in the solid state, with one copper ion in the aza-crown unit and the other bound to the bipyridine unit (on one ligand only).

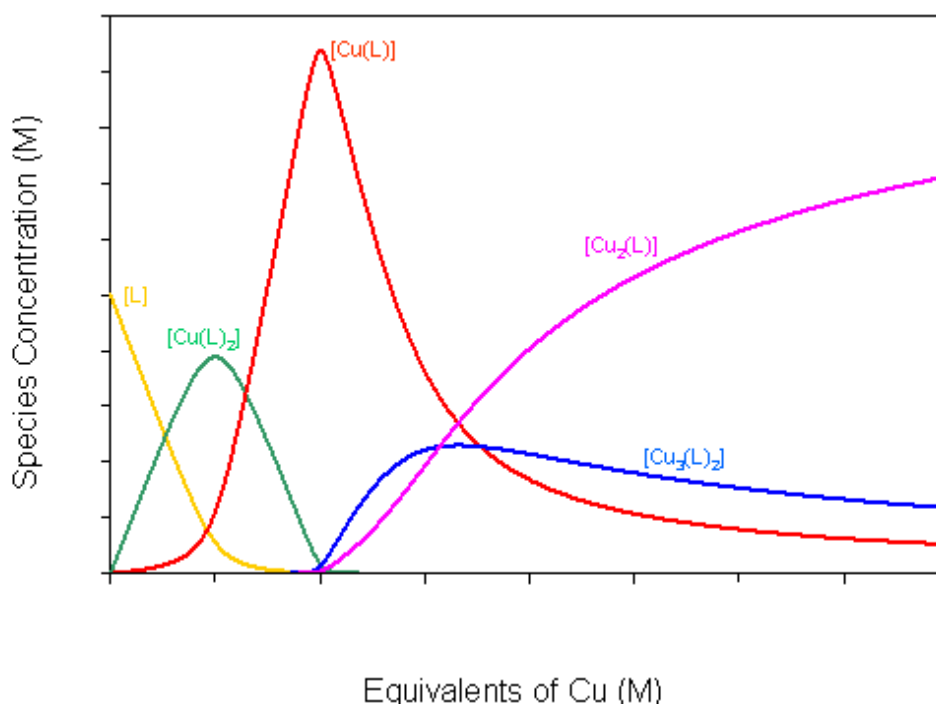


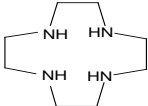
**Figure 3.4:** Complexes formed when copper ion is bound to the bipy-aza-crown-4 ligand, from spectral titration in methanol.<sup>30</sup>

### 3.1.9 - Objective of this Work

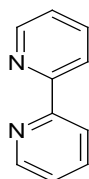
The objective of the work reported in this thesis was to form and study copper ion complexes with the ligand bipy-aza-crown-4 in acetonitrile solution and to compare the mechanisms of complex formation in acetonitrile solution with those obtained from titrations in methanol and crystallisation from this solvent.

The approach has been to investigate the binding of copper ion to the bipy-aza-crown-4 ligand as the metal ion is progressively added, using isothermal titration calorimetry and, using the thermodynamic parameters that emerge from the experiments, to explain the relative stabilities of the structures formed.

Crucially, other ligands which are models of the two binding sites in the bipy-aza-crown-4 ligand have been used in similar experiments for comparison.

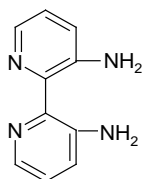
These are 1, 4, 8, 11-tetraazacyclodecane (aza-crown-4)  , 2, 2-

bipyridine (bipy)



and 3,3'-diamino-2,2'-bipyridine

(diaminobipy)



## 3.2 - Experimental

### 3.2.1 – Instrumentation

The following instruments were used during the research:

1. VP-ITC, the Isothermal titration calorimeter (ITC) from Microcal was used to determine the thermodynamic titrations.
2. Cary 4000 UV-VIS spectrophotometer for the UV-Vis studies.
3. Jeol JES FA100 spectrometer to record the ESR spectras.

### 3.2.2 - Solutions for ITC

The following ligands were used: aza-crown-4, 2,2-bipyridine, bipy-aza-crown-4. The bipy-aza-crown-4 and 3,3'-diamino-2,2'-bipyridine (diaminobipy) were synthesised by C.Rice et al, 2,2-bipyridine and aza-crown-4 were purchased from Sigma Aldrich. Other reagents and solvents were from various suppliers and were Analar grade.

Solutions of each of the ligands were prepared in acetonitrile (MeCN) at a concentration of  $5 \times 10^{-4}$  M. Anhydrous copper chloride solution in acetonitrile ( $5 \times 10^{-3}$  M) was used as titrant in all cases. All solutions contained TEAP (tetraethyl-ammonium perchlorate) at 0.10 M. Both the metal ion and ligand solutions were degassed for 2 min before loading into the ITC.

### 3.2.3 - ITC Setting

The sample cell (1.4 ml) was filled with ligand solution and the titrating syringe (250  $\mu$ l) was filled with the metal salt solution. The reference cell was filled with MeCN. The instrumental parameters for the ITC used in this work are shown in **Table 3.1**.

**Table 3.1:** ITC Instrumental settings.

Cell Temp ( $^{\circ}$ C)	25
Reference power ( $\mu$ cal/sec)	34
Initial delay (sec)	200
Syringe concentration (mM)	5
Cell concentration (mM)	0.5
Stirring speed (rpm)	307
Spacing between injections (sec)	300
Volume of injection ( $\mu$ l)	5 or 2

In each experiment there were 50 injections of 5  $\mu$ l metal ion solution and the time taken for each injection was 10 s. For 2  $\mu$ l injection there were 125 injections per titration and the time for each injection was 2 s. Spacing between each injection was 300 s.

### 3.2.4 - UV-Vis Analysis

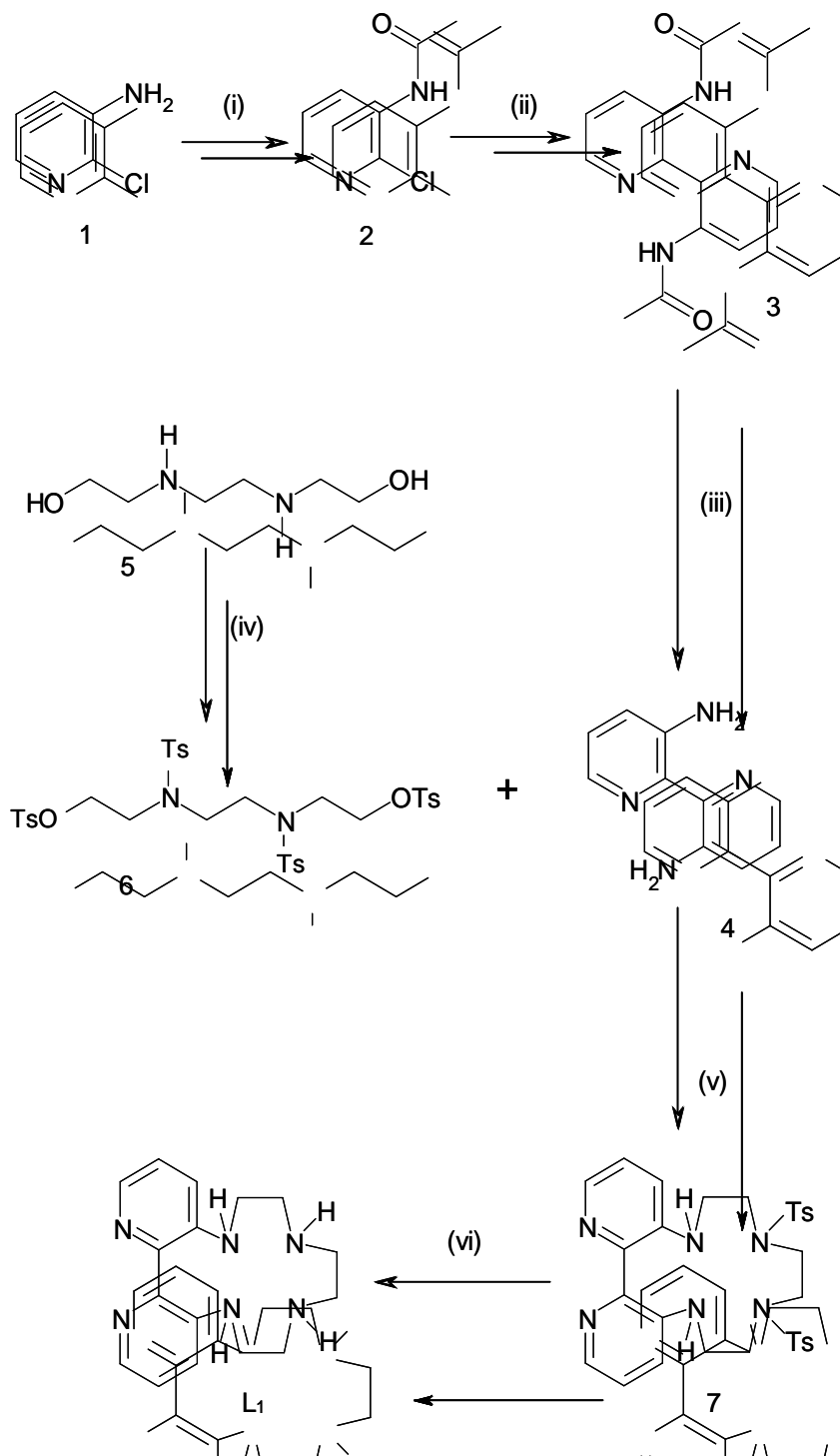
Equivalent titrations of metal ion into ligand solution in acetonitrile were performed on a larger scale outside the cell so that the UV-Vis spectra of the reaction mixtures could be monitored throughout the reaction at 25 °C. 2 ml  $5.0 \times 10^{-4}$  M of ligand solution in acetonitrile with TEAP (0.1 M) was placed in a 1 cm quartz cell. The absorption spectrum was run from 200-800 nm. Aliquots of 10  $\mu$ l  $\text{CuCl}_2$  solution ( $1 \times 10^{-2}$  M) were added. After mixing, the spectra were recorded. The process was continued until a total volume of 220  $\mu$ l of  $\text{CuCl}_2$  solution was added. Reference is made later on about why the solution used here was more concentrated than those used for the ITC experiments.

### 3.2.5 – Electron Spin Resonance (ESR)

Electron spin resonance spectra were recorded for solutions of the four ligands ( $5.0 \times 10^{-4}$  M), and for the same solutions following progressive additions of  $\text{CuCl}_2$  solution ( $1 \times 10^{-2}$  M). Spectra were recorded on a Jeol JES FA100 spectrometer and all spectra shown were recorded at -150 °C.

### 3.2.6 - Synthesis of Ligand: Bipy-aza-crown-4

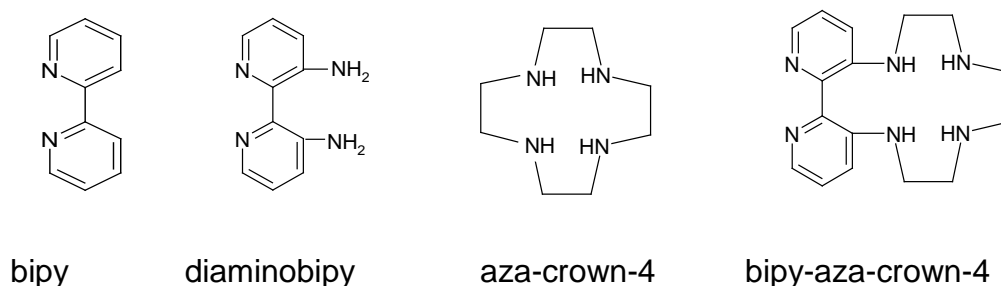
The ligand was synthesised by Cara Felton. The description of the synthesis appears in the Appendix and has been taken verbatim from her PhD thesis.<sup>30</sup>



### 3.3 - Results and Discussion

#### 3.3.1 - Copper ion Binding to Fused 2,2'-bipyridine Azacrown-4 (bipy-aza-crown-4)

Preliminary experiments were carried out with bipy, aza-crown-4 and diaminobipy (**Scheme 3.9**). These ligands represent component parts of the major ligand (bipy-aza-crown-4) used in this work and were used as models for individual binding sites.



**Scheme 3.9**

The results are shown for the titration experiments where anhydrous copper chloride dissolved in acetonitrile was titrated into ligand solutions in acetonitrile (MeCN) with 0.10 M tetraethyl-ammonium perchlorate (TEAP) in all solutions. For each ligand a titration graph of the differential enthalpy of reaction against the molar ratio of titrant to analyte is shown.

In all cases titrations were performed at least twice and usually three times. Uncertainties quoted for all thermodynamic data are based on the variations seen between replicated runs. Where uncertainties are shown as  $\pm$  figures, they refer to estimated 95 % confidence limits.

When interpreting the ITC data it is important to remember that the thermodynamic parameters reflect the *total change* between the 'reactants' and 'products' and may be strongly influenced by the contributions from

changes in solvation and other effects not directly linked to the metal ion/ligand interaction.

### 3.3.2 - Experimental Errors for the Data

The 95% confidence limits associated with the values for the thermodynamic parameters have been assessed as follows. They are based on the combined effects of errors in the concentrations of the solutions used (small volumes and low concentrations result in inevitable uncertainty), and the measured reproducibility of titration results in replicate experiments. The confidence limits for N (stoichiometric ratio) are given in the table(s). The confidence limits for the binding constants are difficult to assess and an estimate has been made that the values of  $\Delta G^\circ$  calculated from  $K_b$  values are generally precise to  $\pm 10\text{-}20\%$ . The confidence limits for  $\Delta H^\circ$  values are normally similar. The confidence limits on individual  $\Delta S^\circ$  values have been determined in each case by propagating the confidence limits on the values  $\Delta H^\circ$  and  $\Delta G^\circ$ , and are often relatively large because  $\Delta S^\circ$  values are calculated from the differences between  $\Delta H^\circ$  and  $\Delta G^\circ$ .

### 3.3.3 - Titrations: Copper ion into Ligands

#### 3.3.3.1 - Copper ion Binding to 2,2-bipyridine (bipy)

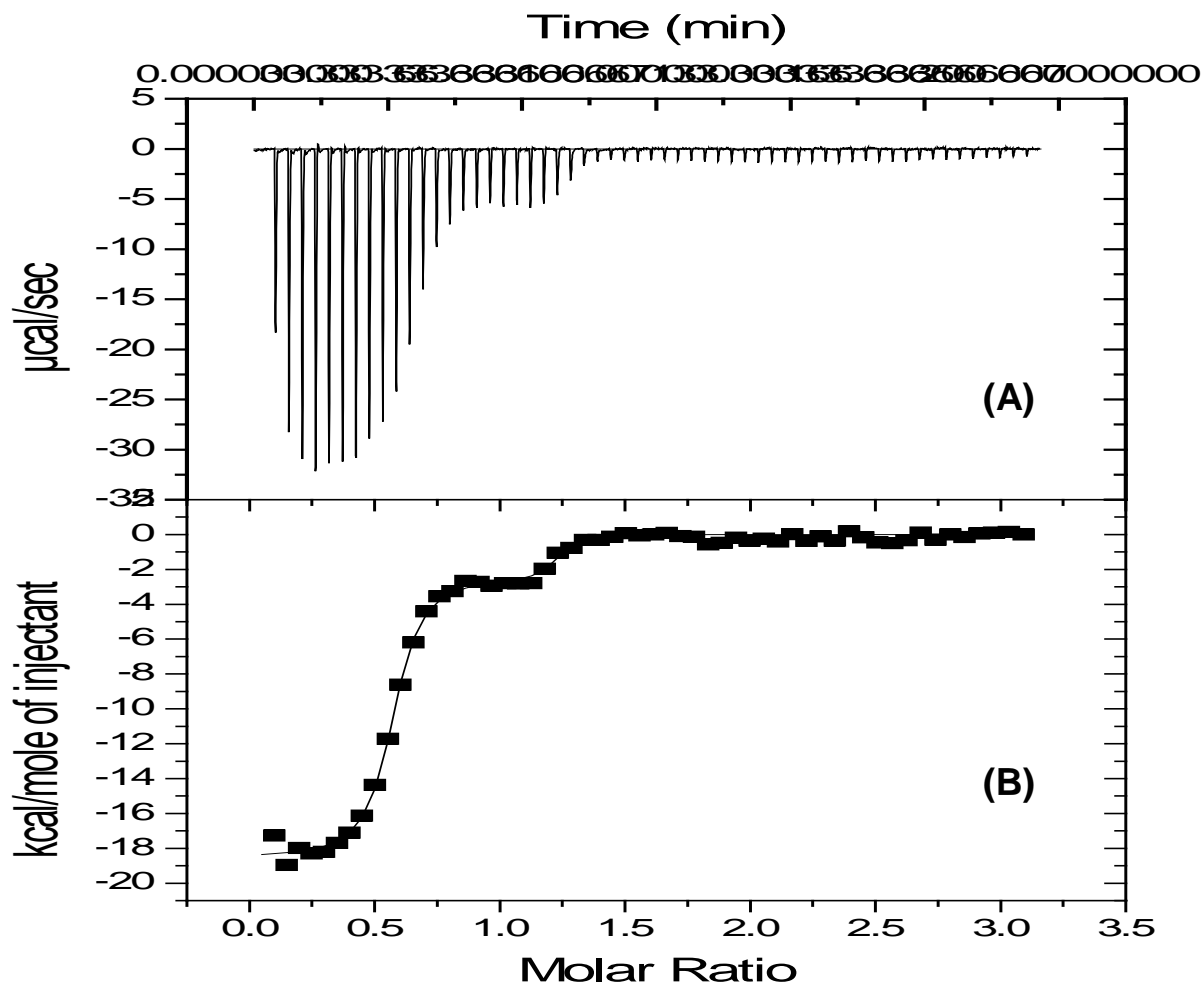


**Figure 3.5** - (A) ITC output for the titration of  $5 \times 10^{-3}$  M  $\text{CuCl}_2$  solution into  $5 \times 10^{-4}$  M bipy in MeCN-TEAP solution and (B) the simulated binding isotherm at  $25^\circ\text{C}$ .

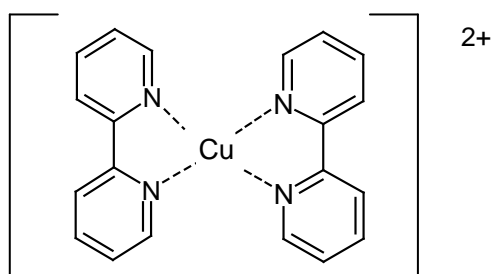
**Figure 3.5** shows the calorimetric output for the titration of  $5 \times 10^{-3}$  M  $\text{CuCl}_2$  into  $5 \times 10^{-4}$  M bipy in MeCN in the presence of 0.1 M TEAP at  $25^\circ\text{C}$ . Note that the first injection of titrant shown in **Figure 3.5 A** gives rise to an abnormally small heat output. This is commonly seen as the syringe needle is frequently not full prior to the first injection because of the long equilibration time. This point has been removed in **Figure 3.5 B** to facilitate simulation. **Table 3.2** displays the

results from the simulation of the experimental data for copper ion titrated into bipy solution. This shows two distinct steps in the titration, with molar ratios at the two equivalence points of 0.55 and an additional 0.66.

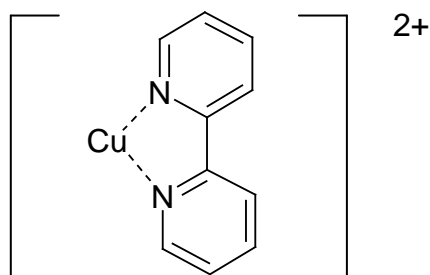
**Table 3.2:** Data for the binding of copper ion to bipy at 25 °C in MeCN, from simulation.

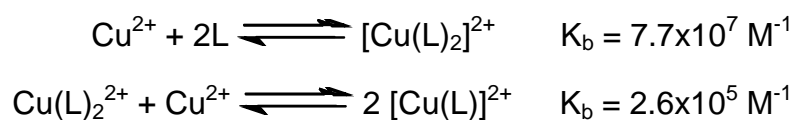
N (Cu <sup>2+</sup> :L)	0.55 (± 0.1)	0.66 (± 0.1)
K <sub>b</sub> ( M <sup>-1</sup> )	7.7(±0.40)X 10 <sup>7</sup>	2.6 (± 0.82) X 10 <sup>5</sup>
ΔH <sup>o</sup> ( kJ mol <sup>-1</sup> )	-78 (±12)	-11 (± 2)
ΔS <sup>o</sup> ( J mol <sup>-1</sup> K <sup>-1</sup> )	-109 (± 60)	77 (± 20)

Uncertainties in N are estimated to be ± 20 %, so N<sub>1</sub> is 0.55 (±0.1) and N<sub>2</sub> is 0.66 (± 0.1) and the the total metal ion to ligand ratio after the second reaction is 1.21 (± 0.2). It seems likely that the first end point corresponds to CuL<sub>2</sub><sup>2+</sup> formation, and the second corresponds to CuL<sup>2+</sup>. The first complex to form could be:



and the second complex :





The much higher value of  $K_b$  for the formation of the first complex is consistent with this model. To form the second complex from the first, copper/nitrogen bonds would have to be broken, consistent with the very much lower overall exothermic enthalpy of reaction and the positive entropy change as  $\text{CuL}_2^{2+}$  reacts with a copper ion to form  $\text{CuL}^{2+}$ . Note that, in both complexes, chloride ligands are also likely to be coordinated to the copper ion and changes in the way these counter ions interact with  $\text{Cu}^{2+}$ , as well as changes in solvation, will contribute to the thermodynamic parameters.

It has been shown in previous research that the bipy ligand can form 1:1 or 2:1 complexes with copper ions,<sup>31</sup> consistent with the structures suggested here.

### 3.3.3.2 - Copper ion Binding to 3,3'-diamino-2,2'-bipyridine (diaminobipy)

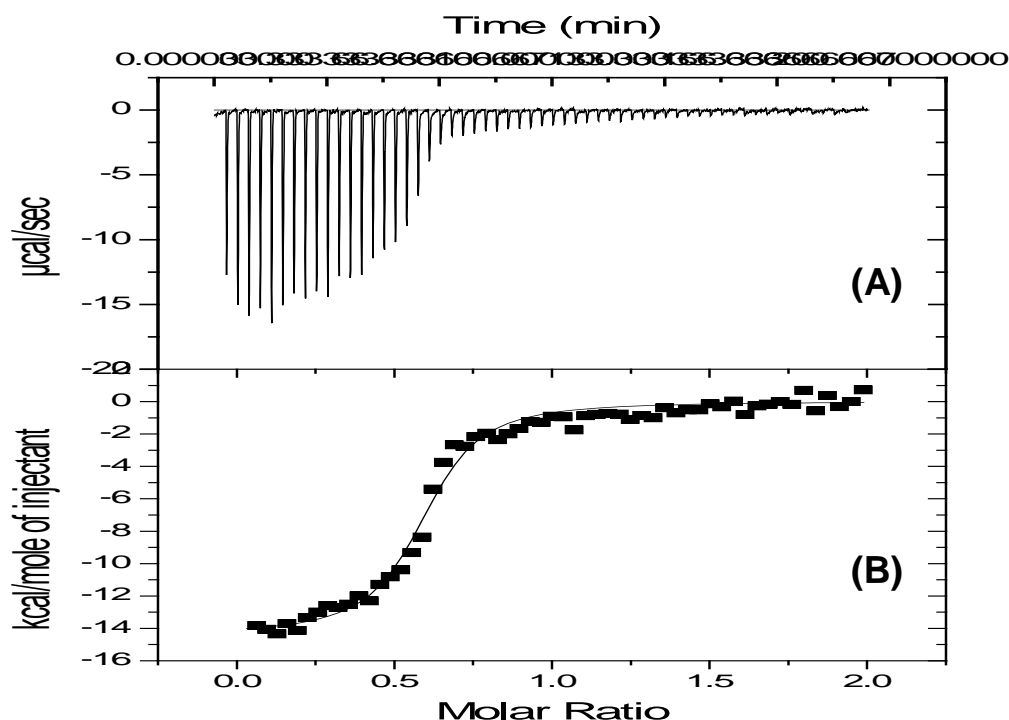


**Figure 3.6:** (A) ITC output for the titration of  $5 \times 10^{-3}$  M  $\text{CuCl}_2$  solution into  $5 \times 10^{-4}$  M diaminobipy in MeCN-TEAP solution and (B) the simulated binding isotherm at  $25^\circ\text{C}$ .

The experimental data in **Figure 3.6** shows a single binding event, in an exothermic reaction. The thermodynamic data from the simulation is shown in **Table 3.3**. The simulation shown is in terms of a single binding event to form  $\text{CuL}_2^{2+}$ . Despite this fairly clear interpretation of the data, it is not inconceivable that a second binding event occurs as there is a very slight inflection in the output at a molar ratio of just over 1.0.

Based on the behaviour of copper(II) with 2,2'-bipyridine, the formation of a  $[\text{CuL}_2]^{2+}$  complex with 3,3'-diamino-2,2'-bipyridine might reasonably have been expected. However attempts to simulate the curve with two binding events were not successful.

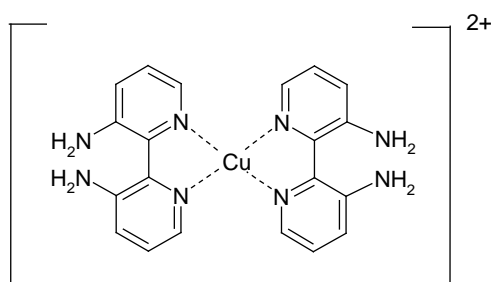
**Table 3.3:** Thermodynamic data for the binding of copper ion to diaminobipy at 25 °C in MeCN, from simulation.

$N (Cu^{2+}:L)$	0.59 ( $\pm 0.1$ )
$K_b ( M^{-1} )$	$1.33 (\pm 0.1) \times 10^5$
$\Delta H^\circ ( kJ mol^{-1} )$	-60 ( $\pm 9$ )
$\Delta S^\circ ( J mol^{-1} K^{-1} )$	-104 ( $\pm 30$ )

A much lower  $K_b$  is determined for the  $CuL_2^{2+}$  diaminobipy complex than for the equivalent complex with bipyridine, possibly reflecting weaker binding between this ligand and copper ion than between bipyridine and copper ions. The entropy of reaction is very similar suggesting that a structurally similar complex might be formed with both ligands.

As stated above, and despite the ITC results, it does seem likely that a second complex  $CuL^{2+}$  forms as the metal-nitrogen bonds in the first,  $CuL_2^{2+}$ , complex are relatively weak, and it is expected that replacing them with chlorides or solvent ligands to form  $CuL^{2+}$  would be relatively facile.

The stoichiometry of the first complex to form corresponds to  $CuL_2^{2+}$ . Whether this involves copper ion coordination through the bipyridine nitrogens or the amine nitrogens is not clear. However, X-ray crystallographic studies of  $Cu^{2+}$  complexes with 3,3'-diamino-2,2'-bipyridine show that the nitrogens on the pyridine rings are more favoured for binding transition metal ions.<sup>31</sup> Bidentate coordination through the two amino groups would involve the formation of less favourable 7-membered ring. It therefore seems more likely that the copper ion is coordinating to the nitrogens on the pyridine rings, with one copper ion coordinating two ligands in a four coordinate complex:



### 3.3.3.3 - Copper ion Binding to 1, 4, 8, 11-tetraazacyclodecane (aza-crown-4)

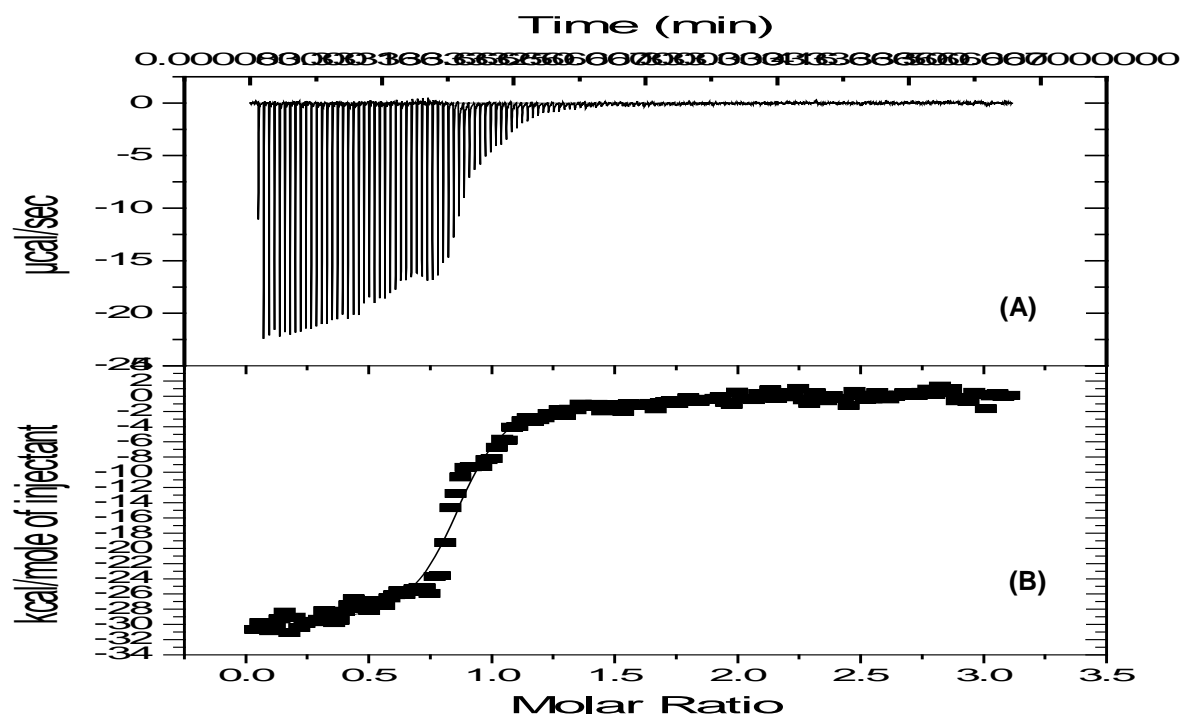


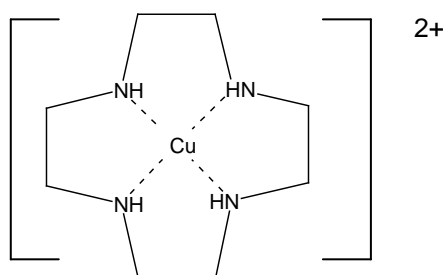
**Figure 3.7:** (A) ITC output for the titration of  $5 \times 10^{-3}$  M copper ion solution into  $5 \times 10^{-4}$  M aza-crown-4 ether solution in MeCN-TEAP solution and (B) the simulated binding isotherm at  $25^\circ\text{C}$ .

The experimental data in **Figure 3.7** is for  $5 \times 10^{-3}$  M  $\text{CuCl}_2$  titrated into  $5 \times 10^{-4}$  M aza-crown-4 and the calorimetric output clearly shows a single binding event. The simulation data is shown in **Table 3.4**.

**Table 3.4:** Thermodynamic data for the binding of copper ion to aza-crown-4 at 25 °C in MeCN, from simulation.

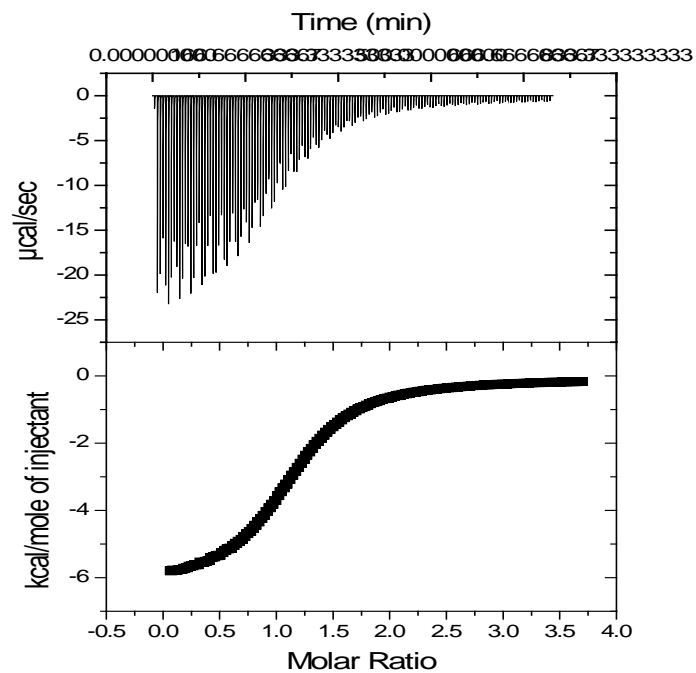
N (Cu <sup>2+</sup> :L)	0.99 (± 0.1)
K <sub>b</sub> ( M <sup>-1</sup> )	1.46 (± 0.08) x 10 <sup>5</sup>
ΔH° ( kJ mol <sup>-1</sup> )	-111 (± 17)
ΔS° ( J mol <sup>-1</sup> K <sup>-1</sup> )	-274 (± 81)

The simulation data in **Table 3.4** shows a single binding event with a molar ratio of 0.99. This molar ratio can only relate to the copper ion binding in the cavity of the aza-crown unit forming a complex:



Despite the fact that this structure is the only feasible product of this titration, the value of K<sub>b</sub> is lower than expected. The high enthalpy of reaction suggests strong bond formation but the large negative entropy of reaction may seem opposite to that expected with a four coordinate chelating ligand. The reason entropy might be expected to increase on chelation is that solvent molecules coordinated to the metal ion and perhaps the ligand are released when the complex forms. The entropy actually decreases may be because Cu<sup>2+</sup> is not strongly solvated in CH<sub>3</sub>CN, reducing the positive contribution to the entropy change associated with loss of the solvation when the complex forms. It is also possible that there is increased solvation due to the generation of partial positive charges on the N ligands. It is worth noting that the similar reaction of 18-crown-6 with Ba<sup>2+</sup> (used for calibration as shown in **Figure 3.8**) in water, for which the loss of solvation of Ba<sup>2+</sup> in water is more significant, shows a much smaller negative, but still entropy of reaction of -21 J mol<sup>-1</sup> K<sup>-1</sup>.

A)



B)

$N (\text{Cu}^{2+}:\text{L})$	$1.19 (\pm 0.1)$
$K_b (\text{M}^{-1})$	$3.64 (\pm 0.18) \times 10^3$
$\Delta H^\circ (\text{kJ mol}^{-1})$	$-26.6 (\pm 2)$
$\Delta S^\circ (\text{J mol}^{-1} \text{K}^{-1})$	$-21 (\pm 4)$

**Figure 3.8:** a) calorimetric output for the titration of  $\text{BaCl}_2$  into 18-crown-6 in water b) simulation data for a).

### 3.3.3.4 - Copper ion Binding to 2,2'-bipyridine Azacrown-4 (bipy-aza-crown-4)

Moving onto the ligand at the centre of this research, **Figure 3.9** shows the calorimetric output for copper ion titrated into solution of the bipy-aza-crown-4 ligand. The titration clearly shows two binding events.

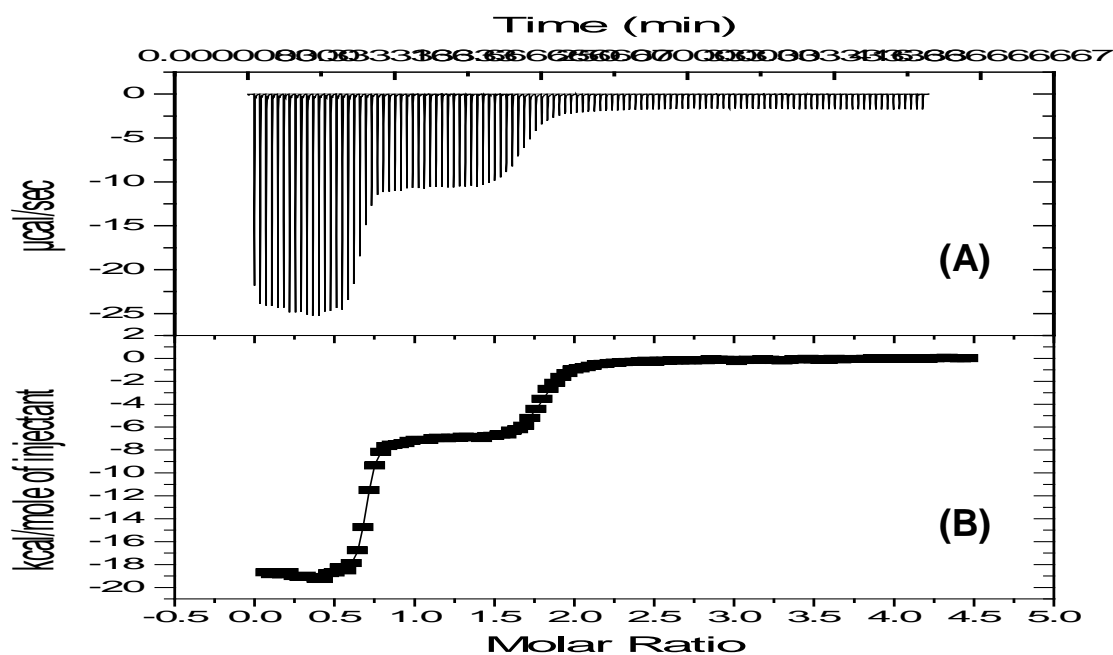


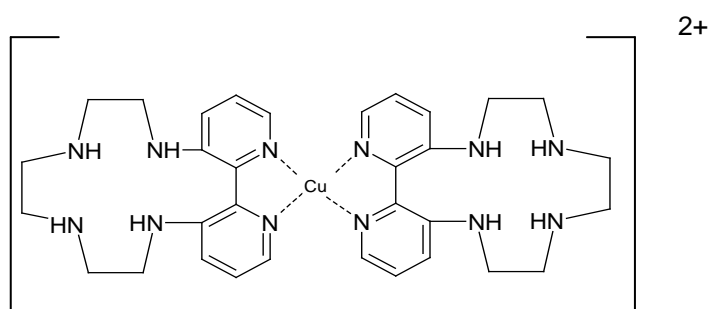
**Figure 3.9:** (A) ITC output for the titration of  $5 \times 10^{-3}$  M  $\text{CuCl}_2$  solution into  $5 \times 10^{-4}$  M bipy-aza-crown-4 solution in MeCN-TEAP solution and (B) the simulated binding isotherm at  $25^\circ\text{C}$ .

**Table 3.5** shows the simulation data. The first end point corresponds to two ligands per copper ion corresponding to  $\text{CuL}_2^{2+}$  formation and the second binding ( $0.55 + 0.91 = 1.46$ ) represents the formation of  $\text{Cu}_3\text{L}_2^{6+}$ .

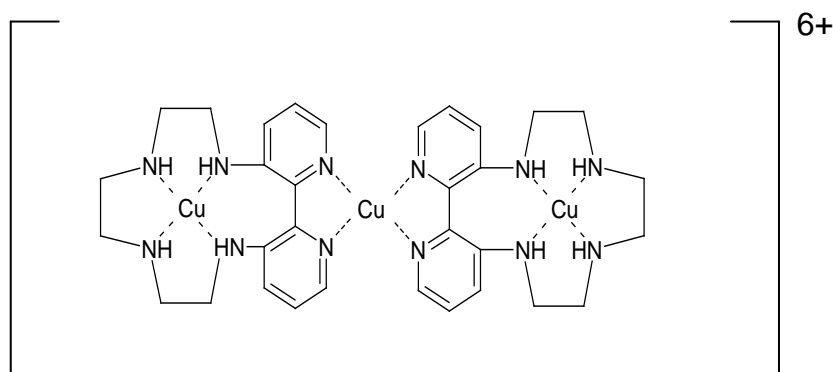
**Table 3.5:** Thermodynamic data for the binding of copper ion to bipy-aza-crown-4 at  $25^\circ\text{C}$  in MeCN.

$N(\text{Cu}^{2+}:\text{L})$	$0.55 (\pm 0.1)$	$0.91 (\pm 0.1)$
$K_b (\text{M}^{-1})$	$4.60 (\pm 0.09) \times 10^8$	$5.81 (\pm 0.17) \times 10^5$
$\Delta H^\circ (\text{kJ mol}^{-1})$	$-88 (\pm 9)$	$-34 (\pm 3)$
$\Delta S^\circ (\text{J mol}^{-1} \text{K}^{-1})$	$-129 (\pm 39)$	$-3 (\pm 2)$

It seems likely that the first complex is:



whereas the second complex forming involves three ligands to two copper ions and could correspond to:



Presumably, chloride ligands could also be coordinated to the copper ion.

The first binding event is characterised by a very large binding constant, a relatively large enthalpy and large negative entropy. The values are not dissimilar to those associated with the formation of the  $\text{CuL}_2^{2+}$  with pure bipy, so the proposed formation of a complex with two bipy-aza-crown-4 ligands, binding at the bipyridine nitrogens, seems reasonable. The second binding event is less exothermic and exhibits a lower binding constant and almost zero entropy change. The binding constant is similar to that measured for copper ion in the pure aza-crown-4 ligand. The smaller enthalpy probably reflects the fact that the crown ether unit is distorted somewhat (two of the coordinating nitrogen atoms on the ligand are part of the seven membered ring formed with  $\text{Cu}^{2+}$ ) and would not be able to bind as strongly when it has the bipyridine group attached as when it is unrestricted. The almost zero

entropy change is not easy to rationalise but we have already seen unexpected entropy changes with the simple aza-crown-4 ligand binding to the copper ion, so we have seen already how entropy changes measured when copper ion binds in an aza-crown cavity are not always easy to predict. However, in this case the zero changes may be related to the fact that the copper/crown complex here is less ordered than the copper complex with the free aza-crown.

The results indicate the formation of a  $\text{CuL}_2^{2+}$  species followed by a  $\text{Cu}_3\text{L}_2^{6+}$  species as more copper ions are added to the ligand solution. This indicates that some copper/ligand complexes that might have been expected are not formed in acetonitrile. For instance, there is no evidence for a  $\text{CuL}^{2+}$  species forming. This might have been expected by analogy with the  $\text{CuL}^{2+}$  complex that forms with bipyridine. There is also no evidence for a  $\text{Cu}_2\text{L}^{4+}$  species which might have formed between a single ligand and one copper ion bound at the bipyridine site and one at the aza-crown cavity.

The overall results of the titrations for each ligand are summarised in **Table 3.6**. We can compare the behaviour of ligands: bipy, diaminobipy and aza-crown-4 titrations and the synthesised ligand bipy-aza-crown-4. The following summarises how copper ion coordinates with these ligands.

- When copper ion is titrated into the bipyridine ligand, two binding events are seen, the first to form  $\text{CuL}_2^{2+}$ , and the second binding with a further 0.66:1 ( $\text{CuL}_2^{2+}$ ).
- With diaminobipy ligand, a single binding event is observed, to form  $\text{CuL}_2^{2+}$ . A weak second binding event may also have been observed.
- When aza-crown-4 ligand is titrated with copper ion, a single binding event is observed to form  $\text{CuL}^{2+}$ .
- The results for bipy-aza-crown-4 ligand show that copper ion binds at the bipy site first forming  $\text{CuL}_2^{2+}$  and then at the aza-crown-4 unit forming  $\text{Cu}_3\text{L}_2^{6+}$ .

(Chloride ions may also coordinate to the copper ions, reducing the nominal charge given in the simplified formulae).

**Table 3.6:** Overall simulation data for copper ion solution titrated into the ligand solutions.

Ligands	In acetonitrile with 0.1 M TEAP					
	2,2-bipyridine		Diaminobipy	Aza-crown-4	Bipy-aza-crown-4	
N (Cu <sup>2+</sup> : L)	0.55 (±0.1)	0.66 (±0.1)	0.59 (±0.1)	0.99 (±0.1)	0.55 (±0.05)	0.91(±0.05)
K (M <sup>-1</sup> )	7.7 (± 0.40) X 10 <sup>7</sup>	2.6 (± 0.82) X 10 <sup>5</sup>	1.3 (± 0.1) X 10 <sup>5</sup>	1.5 (± 0.08) x 10 <sup>5</sup>	4.6 (± 0.09) x 10 <sup>8</sup>	5.8 (± 0.17) x 10 <sup>5</sup>
ΔH° (kJ mol <sup>-1</sup> )	-78 (± 12)	-11 (± 2)	-60 (± 9)	-111 (± 17)	-88 (± 9)	-34 (± 3)
ΔS° (J mol <sup>-1</sup> K <sup>-1</sup> )	-109 (± 60)	77 (± 20)	-104 (±30)	-274 (± 81)	-129 (± 39)	-3 (± 2)
ΔG° (kJ mol <sup>-1</sup> )	-45.2	-30.9	-29.2	-29.6	-49.5	-31.8

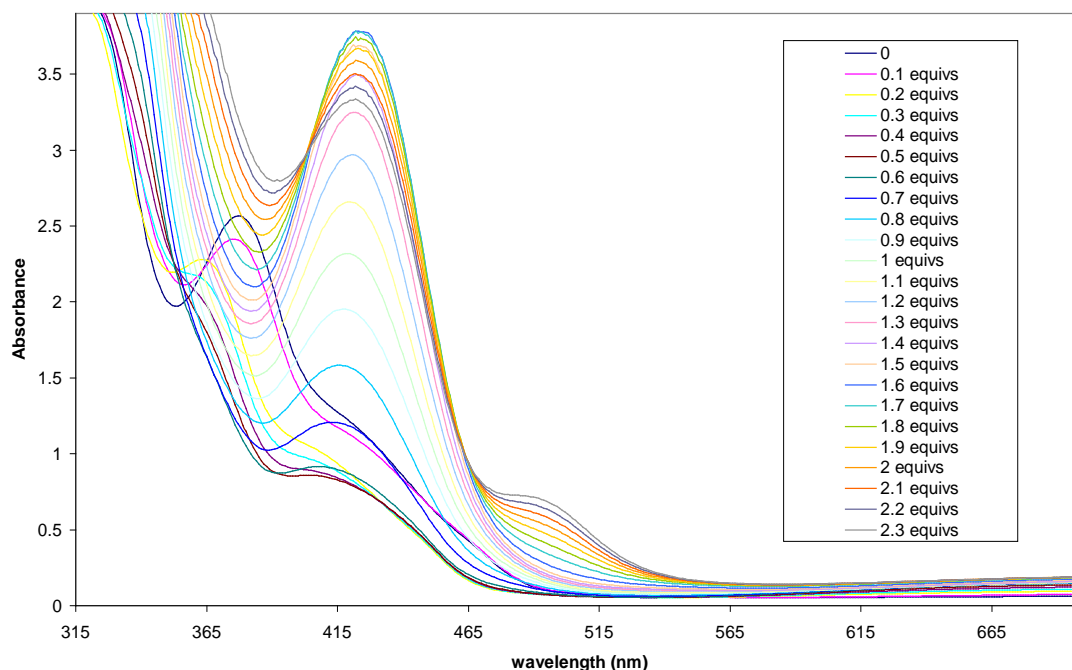
### 3.3.4 – UV-Vis Spectral Analysis

#### 3.3.4.1 - Spectral Titration of Copper ion into Bipy-aza-crown-4.

The objective of these titrations was to reinforce the conclusions of the titration calorimetry work by identifying absorption maxima corresponding to the complexes formed between Cu(II) and the ligands studied in acetonitrile solution and, by monitoring these through titration, to confirm the stoichiometries of the complexes formed.

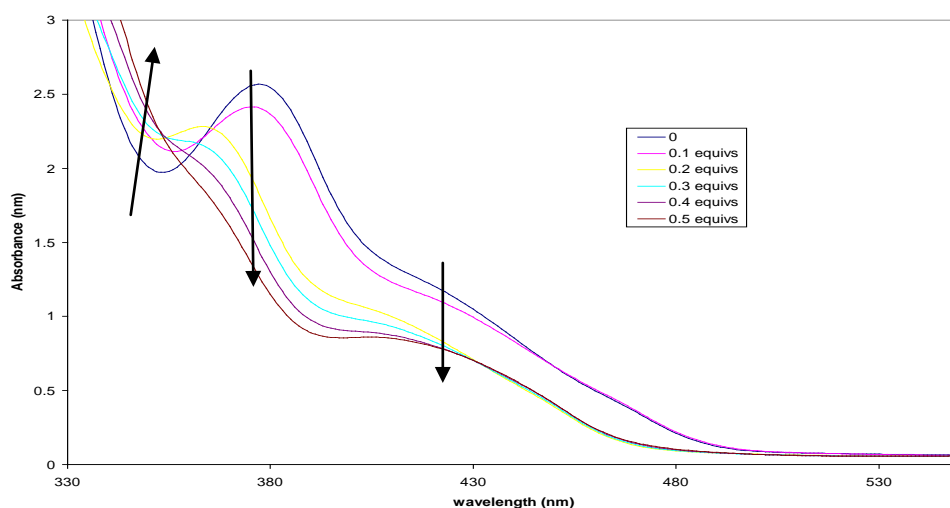
Scans were performed in MeCN solution to monitor complex formation as copper ion solution was added to the ligand solution. Scans were recorded at Cu<sup>2+</sup>: Ligand molar ratios from zero to 2.3 (**Figure 3.10**).

Note, in the following, “equivalents” refers to molar ratios so for example, 2.3 equivalents of copper ion per ligand means a molar ratio Cu<sup>2+</sup>:L of 2.3.



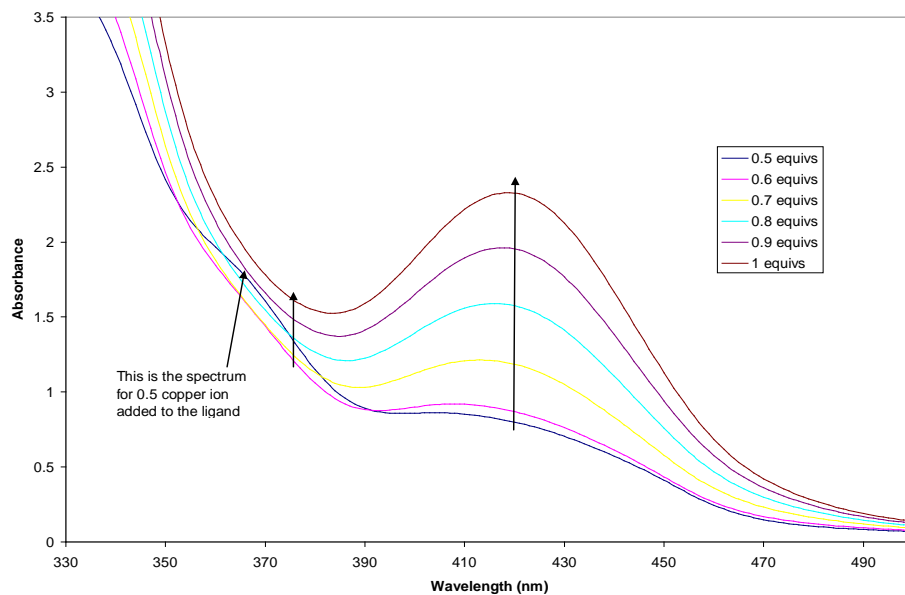
**Figure 3.10:** Absorbance against wavelength for copper ion solution added to bipy-aza-crown-4 in MeCN solution until 2.3 equivalents of copper ion per ligand were added.

**Figures 3.11-3.15** show spectra of solutions in which  $\text{Cu}^{2+}$ : Ligand molar ratios go from zero to 0.5, 0.5 to 1.0, zero to 1.0, 1.0 to 1.5 and finally 1.0 to 2.3 respectively.



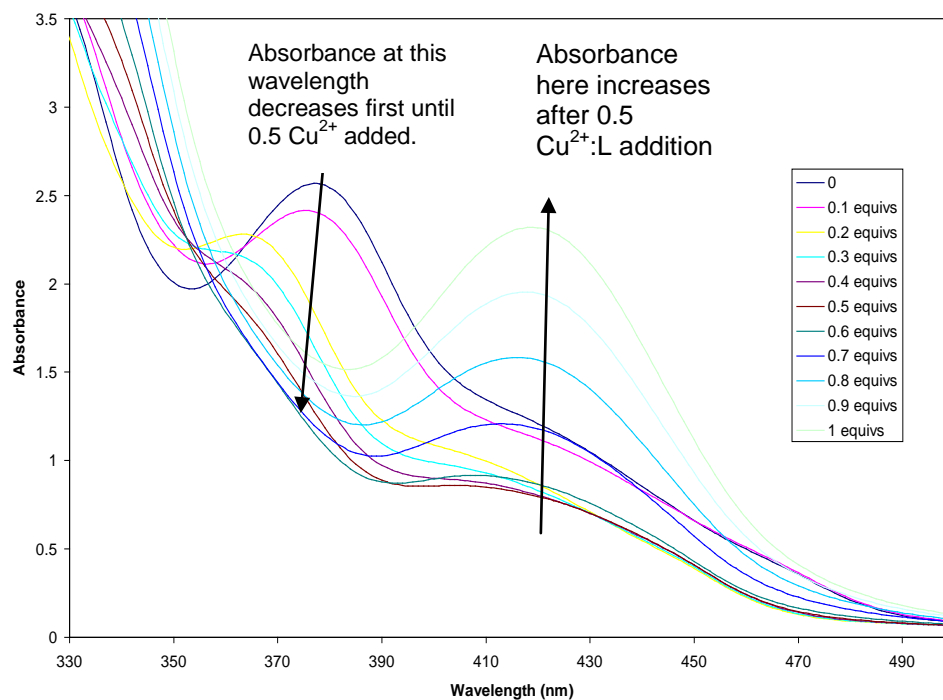
**Figure 3.11:** Absorbance against wavelength for copper ion added to bipy-aza-crown-4 until 0.5 equivalents of copper ion added

The spectra in **Figure 3.11** are for  $\text{Cu}^{2+}$ : L ratios from zero to 0.5. They show the absorbance at 375 nm decreases dramatically as copper ion is added and the absorbance at 350 nm increases. Further changes in the spectra after 0.5 molar equivalents of copper ion addition are shown in **Figure 3.12**.



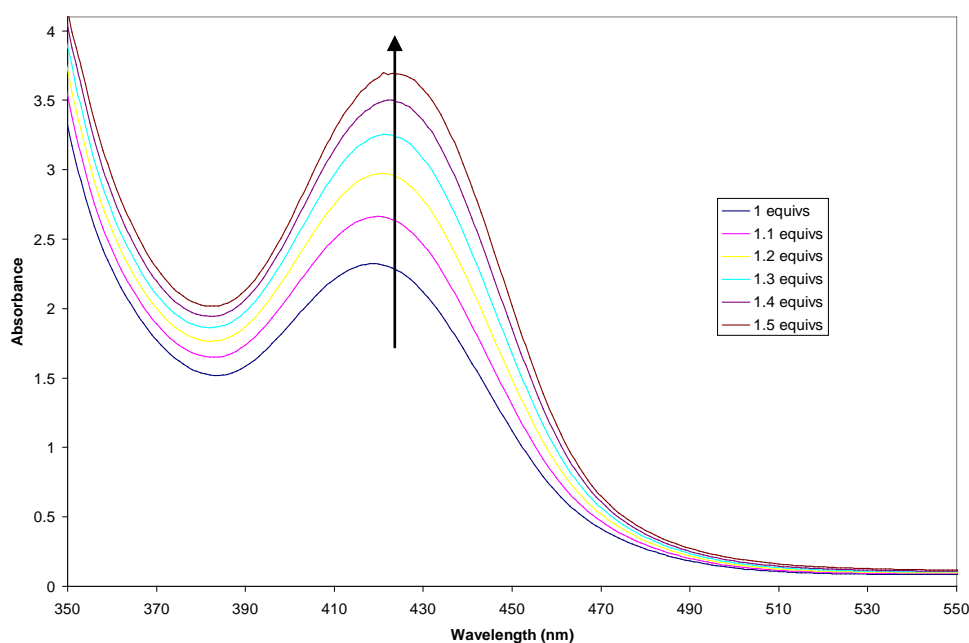
**Figure 3.12:** Absorbance against wavelength for copper ion added to bipyaza-crown-4 from 0.5-1.0 equivalents of copper ion added.

Above the  $\text{Cu}^{2+}:\text{L}$  molar ratio of 0.5, the absorbance at 375 nm stops decreasing and starts to increase slightly. A new absorbance maximum appears at 420 nm and this increases over the  $\text{Cu}^{2+}:\text{L}$  range 0.5 to 1.0.



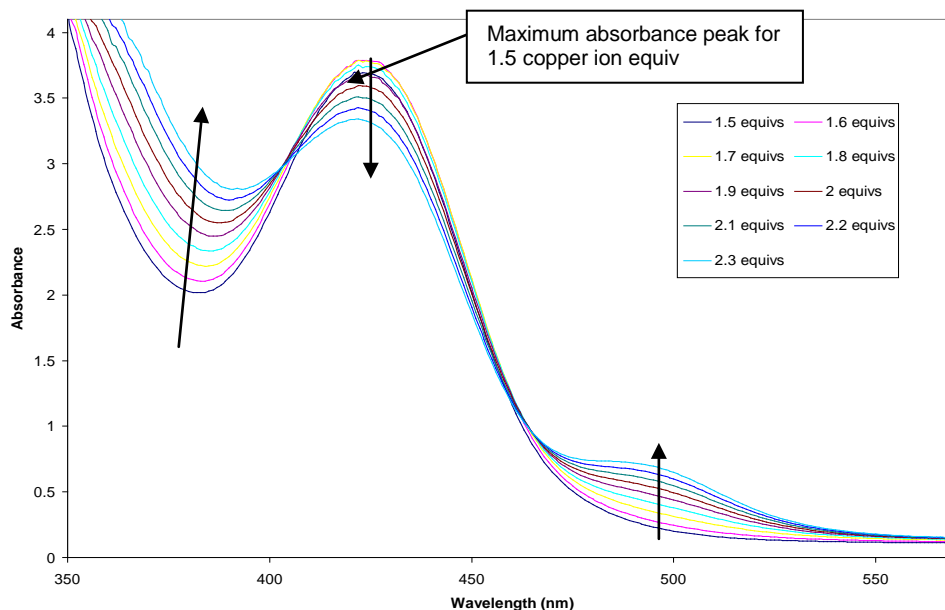
**Figure 3.13:** Absorbance against wavelength for copper ion added to bipyaza-crown-4 until 1.0 equivalent of copper ion added.

**Figure 3.13** shows the spectra from zero to 1.0 of copper ion equivalent added, this figure shows the data in Figures 3.11 and 3.12 combined. From this we can see clearly the changes in absorbance and how there is an apparent dramatic switch in the behaviour after 0.5 molar equivalents of copper ions are added.



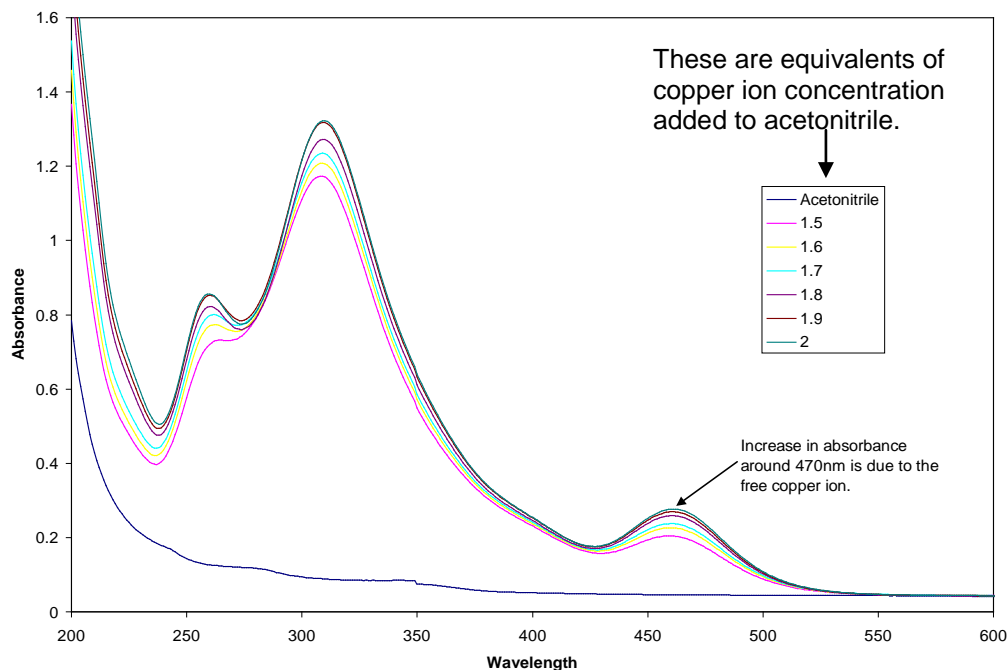
**Figure 3.14:** Absorbance against wavelength for copper ion addition to bipyaza-crown-4 from 1.0 to 1.5 equivalents of copper ion added.

In **Figure 3.14** the spectra are shown for  $\text{Cu}^{2+}$ :L ratios from 1.0 to 1.5. They show the absorbance at 420 nm continues to increase from **Figure 3.12**. Further changes in spectra after 1.5 copper ion equivalents added are shown in **Figure 3.15**.



**Figure 3.15:** Absorbance against wavelength for copper ion addition to bipyaza-crown-4 from 1.5 to 2.3 equivalents added.

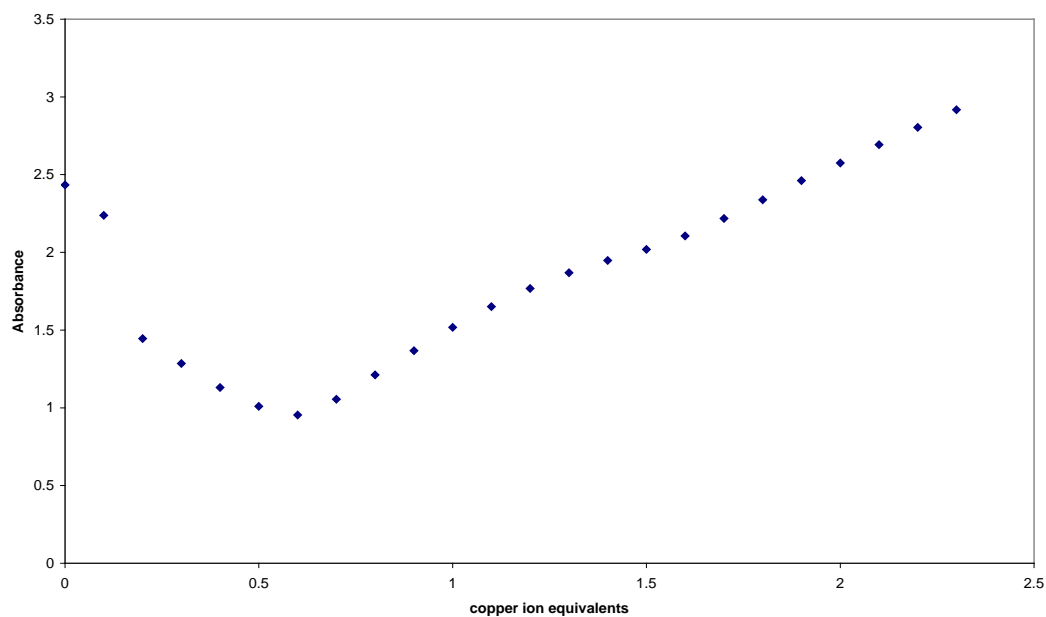
In **Figure 3.15** the spectra are shown for  $\text{Cu}^{2+}$ :L ratios from 1.5 to 2.3. They show the absorbance at 420 nm now decreases as copper ion is added and at 380 nm and 500 nm the absorbances start to increase. The absorbance at 500 nm increases indefinitely as copper ion is added beyond 2.3 equivalents. This maximum is due to excess copper ion in solution. This can be seen in the spectra of anhydrous copper chloride in acetonitrile in **Figure 3.16**, where the absorbance at around 470 nm, spreading to include absorbance at 500 nm and beyond, is increasing.



**Figure 3.16:** Absorbance against wavelength for copper ion addition to acetonitrile.

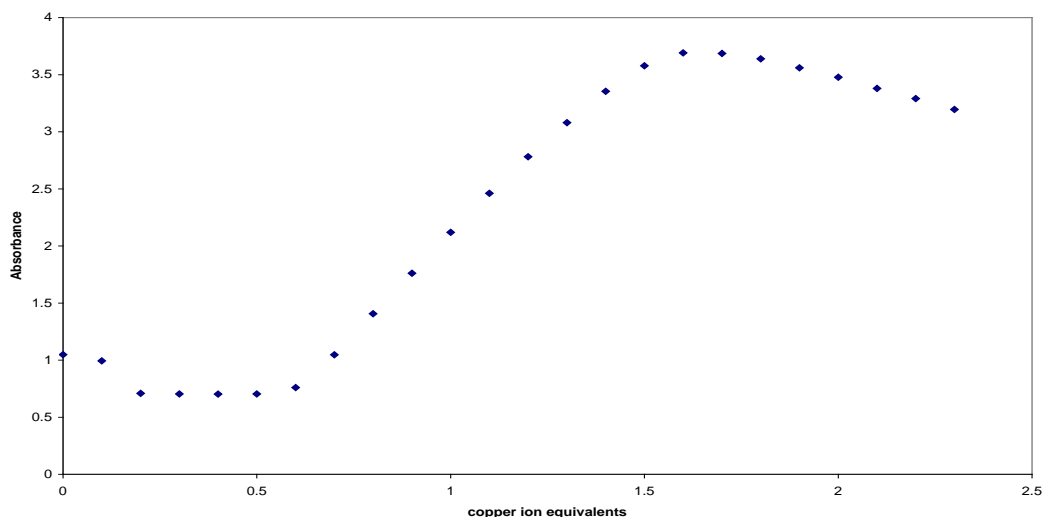
These titrations were performed to identify the absorption maxima that might be associated with the complex ions formed and to plot the absorbance at these wavelengths against molar ratios ( $\text{Cu}^{2+}:\text{L}$ ) so that spectral equivalence points might be identified. The following wavelengths were identified as likely maxima for discrete species in solution: 375 and 420 nm. Absorbance versus amount of copper(II) added plots at these two wavelengths appear in **Figures 3.17** and **3.18**.

It is worth noting that, in the data presented, very high absorbances of 4.0 or more were observed in some spectra, especially at some wavelengths. Attempts were made to use more dilute solutions to avoid this but, in general, only small spectral changes were observed in more dilute solutions and it turned out to be easier to use the spectra shown here. It may be that using dilute solutions, different species may form compare to using high concentration solutions. For example with high concentrations the two species identified to form are  $\text{CuL}_2^{2+}$  and  $\text{Cu}_3\text{L}_2^{6+}$  whereas at low concentrations it may be that the  $\text{CuL}^{2+}$  and  $\text{Cu}_2\text{L}^{4+}$  may form.



**Figure 3.17:** Absorbance versus  $\text{Cu}^{2+}$ :L molar ratio for solution in MeCN solution (ligand concentration =  $5 \times 10^{-4}$  M) at 375nm.

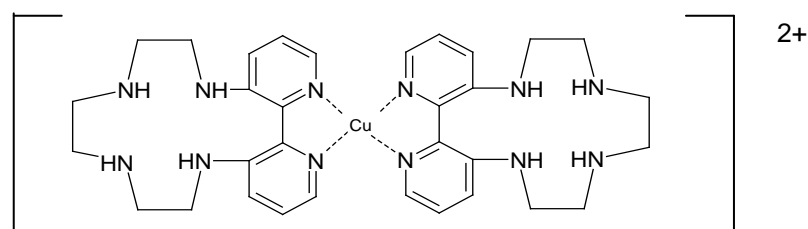
In **Figures 3.17**, the absorbance at 375 nm decreases until just over 0.5  $\text{Cu}^{2+}$ :L molar ratio and then increases. This strongly suggests that whichever species is responsible for absorbance at 375 nm is completely consumed when copper ions are added at 0.5 molar ratio. It seems likely that the species responsible is the unreacted ligand and this result supports our view that the first complex to form is  $\text{CuL}_2^{2+}$ .

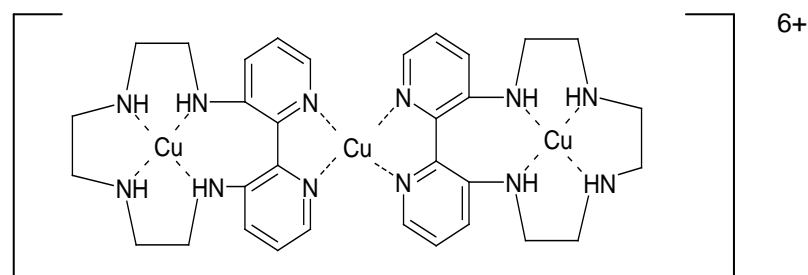


**Figure 3.18:** Absorbance versus  $\text{Cu}^{2+}:\text{L}$  molar ratio for solution in MeCN solution (ligand concentration =  $5 \times 10^{-4}$  M) at 420 nm.

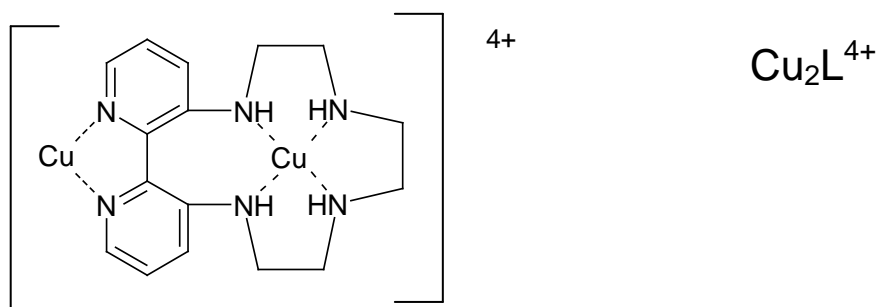
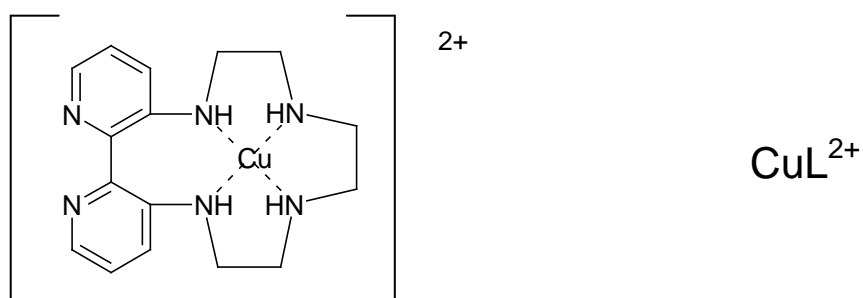
**Figure 3.18** shows how the absorbance at 420 nm varies with concentration of metal ion. The absorbance remains constant until just over 0.5  $\text{Cu}^{2+}:\text{L}$  molar ratio, and increases to 1.5  $\text{Cu}^{2+}:\text{L}$ , falling slightly after this. We suggest that this absorbance maximum is associated with the  $\text{Cu}_3\text{L}_2^{6+}$  species. This species is not formed initially but when  $\text{Cu}^{2+}$  is added to the  $\text{CuL}^{2+}$  complex, conversion to  $\text{Cu}_3\text{L}_2^{6+}$  occurs. The fall in absorbance at higher copper ion concentration is not easy to explain. There will be a dilution effect as excess copper ion solution is added but this would be expected to be smaller than the decrease observed.

The graphs in **Figures 3.17** and **3.18** clearly support the formation of a  $\text{CuL}_2^{2+}$  complex followed by a  $\text{Cu}_3\text{L}_2^{6+}$  complex. The structures of these are shown below. This is entirely consistent with the conclusions from the ITC experiments.





It is worth repeating that this behaviour in acetonitrile contrasts with that in methanol. When the equivalent titrations were performed in methanol, the data (**Figure 3.19**) was interpreted in terms of the initial formation of  $\text{CuL}_2^{2+}$  followed by  $\text{CuL}^{2+}$ , and then by  $\text{Cu}_2\text{L}^{4+}$  and then  $\text{Cu}_3\text{L}_2^{6+}$ . The two species,  $\text{CuL}^{2+}$  and  $\text{Cu}_2\text{L}^{4+}$ , have not been detected in acetonitrile in the work reported in this thesis. It is not obvious why methanol should stabilise these complexes when acetonitrile does not, although of course solvation of charged species by methanol would be different to solvation by acetonitrile and then it would certainly affect the relative stabilities of the complex ions.



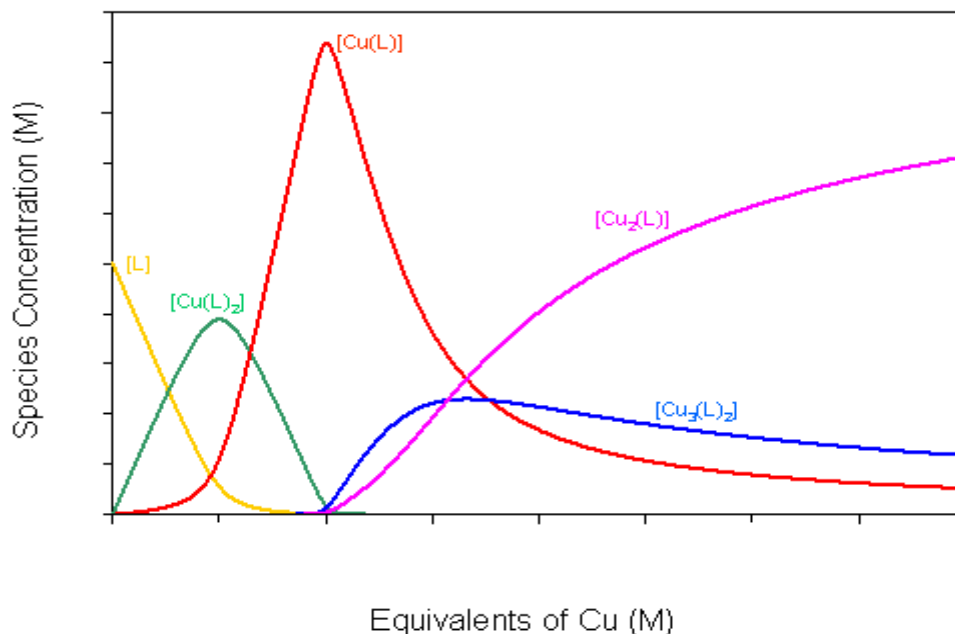


**Figure 3.19:** Relative intensities of absorption maxima linked to the ligand, bipy-aza-crown-4, and the complexes it forms with copper ion in methanol. <sup>31</sup>

So far the binding of copper ion to bipy-aza-crown-4 in acetonitrile solution has been studied by ITC and UV-Vis spectroscopy. Further studies using ESR (electron spin resonance) spectroscopy were carried out in which the copper ion was added to the bipy-aza-crown-4 ligand in acetonitrile solution and the solution was frozen at  $-150\text{ }^{\circ}\text{C}$ . The idea was that the ESR spectra of the  $\text{Cu}^{2+}$  ion might be useful in characterising the complexes formed.

### 3.3.5 - Electron Spin Resonance (ESR)

Electron spin resonance (ESR) spectroscopy is used to study paramagnetic species, which means species with unpaired electrons. As the copper ion is  $3d^9$  it has one unpaired electron, so ESR spectroscopy can be used to characterise the binding of a copper ion to a ligand.

ESR spectroscopy measures the transition between the electron spin energy levels and the dependence of this energy of the strength of an external magnetic field. The energy of the electron is measured between two states ( $\pm \frac{1}{2}$ ) and the amount of radiation absorbed is detected which is the spectral output. In ESR this spectral output is then converted into the first derivative of absorption intensity, plotted as a function of applied field. The resonance condition is given by:

$$h\nu = g\beta H,$$

where  $h$  is Planck's constant,  $\nu$  the frequency of the radiation (in the microwave range),  $\beta$  is the Bohr Magneton and  $H$  is the field strength. The parameter  $g$ , the  $g$ -factor, is a constant that is 2.0003 for a free electron and differs from this slightly for electrons associated with atoms/ions, depending on the environment.

The field experienced by the unpaired electron is affected by the local field associated with nuclei with magnetic moments. The copper nucleus has a nuclear spin quantum number of  $3/2$  so an electron associated with this nucleus exhibits an ESR spectrum split into four through hyperfine interaction. The magnitude of the hyperfine splitting is a measure of the extent the unpaired valence electron is located on the copper ion and so is sensitive to the nature of ligand bonding to the ion.

The ESR spectra reported in this thesis were recorded on frozen solutions of the copper complexes so the spectra are anisotropic. Copper ions usually exhibit axial symmetry and so, with a derivative spectrum, show two regions,

one corresponding to copper ions with their axis of symmetry parallel to the field and one with it perpendicular. The  $g$  values associated with these two regions and the hyperfine splitting constants are the parameters quoted in characterising the environment of the copper ions – that is  $g(\text{parallel})$ ,  $A(\text{parallel})$  and  $g(\text{perpendicular})$  and  $A(\text{perpendicular})$ .

It is possible to interpret ESR spectra of this type directly in terms of structural features of the complexes but, in this case, we have used the ESR spectra as a way of fingerprinting particular complexes with a view to using these fingerprint spectra to identify which of two possible complexes the copper ion is forming.

Spectra were recorded for solutions in MeCN of ligand concentrations  $5 \times 10^{-4}$  M and with progressively increased  $\text{Cu}^{2+}$ : Ligand molar ratios. Spectra were recorded at  $-150$  °C so solutions were frozen. In all cases the spectra are characteristic of tetragonally coordinated copper ion showing axial symmetry with  $g_{\text{parallel}}$  greater than 2.00 and  $g_{\text{perpendicular}}$  close to 2.00. In general, the values of  $g_{\text{parallel}}$  and  $A_{\text{parallel}}$  (hyperfine splitting) are particularly sensitive to the environment of the copper ion. In this work we hoped to characterise the copper ion complexes with bipy and with the aza-crown-4 ligands (in MeCN) and to compare those spectra with those recorded in solution of the ligand bipy-aza-crown-4 as copper ion was added.

**Figure 3.20 (a)** shows the spectrum recorded for a simple copper chloride solution in MeCN, with  $g_{\text{parallel}} = 2.19$  and  $A_{\text{parallel}} = 10.0$  mT. **Figure 3.20 (b)** shows the spectrum of copper ion in bipy solution in MeCN at a  $\text{Cu}^{2+}$ :bipy molar ratio of 0.5. This is not a very clear spectrum but a similar spectrum was recorded with  $\text{Cu}^{2+}$ :bipy molar ratios up to 1.0. Values for  $g_{\text{parallel}}$  and  $A_{\text{parallel}}$  are 2.55 and 15 mT and are taken as indications of one or other of the  $\text{Cu}^{2+}$ :bipy complexes ( $\text{Cu}(\text{bipy})^{2+}$  or  $\text{Cu}(\text{bipy})_2^{2+}$ ), although because only  $\text{Cu}(\text{bipy})_2^{2+}$  shows axial symmetry we assume it is this one. **Figure 3.20 (c)** shows the spectrum of copper ion added to excess aza-crown-4 solution in MeCN, with  $g_{\text{parallel}} = 2.19$  and  $A_{\text{parallel}} = 19.0$  mT. This spectra is assigned to the complex which a  $\text{Cu}^{2+}$  ion is bound in the middle of the aza-crown ring.

**Figure 3.20 (d)** shows the ESR spectrum of copper ion added to bipy-aza-crown-4 ligand at a  $\text{Cu}^{2+}$ : Ligand ratio of 0.5. It is a clear spectrum with  $g_{\text{parallel}} = 2.19$  and  $A_{\text{parallel}} = 18.0$  mT. The comparison between this spectrum and those of the other copper ion complexes is the key to using this ESR data. In fact, this spectrum is very similar to that of copper ion complex with the aza-crown-4 ligand and this suggests that, when reacted with bipy-aza-crown-4 ligand, copper ion first coordinates at the aza-crown ether centre. Surprisingly this is not what was found from the ITC results or from the spectral titrations. This rather unexpected result is difficult to explain. However, it is certainly possible that, because these spectras were recorded using frozen solutions, in which the complexes may have precipitated and crystallised, rather different behaviour could be seen than in solution.

As stated earlier, the crystallographic studies of  $\text{Cu}^{2+}$  complexes with the same ligand, crystallised from methanol solution show exactly the same behaviour as we observe in frozen solution described above. Complexes formed at low copper ion concentrations show the copper ion in the aza-crown site rather than the bipy site. So a reasonable interpretation of the ESR data is that the thermodynamically stable complex ions in solution and in solid state at low copper ion concentrations are different.

It would have been useful to compare the spectrum of the  $\text{Cu}^{2+}$ :bipy-aza-crown-4 to complex at low copper(II) ion concentration with spectra recorded at higher copper(II) ion concentration. Unfortunately spectra recorded at these higher copper(II) ion concentrations were very complex and impossible to interpret.

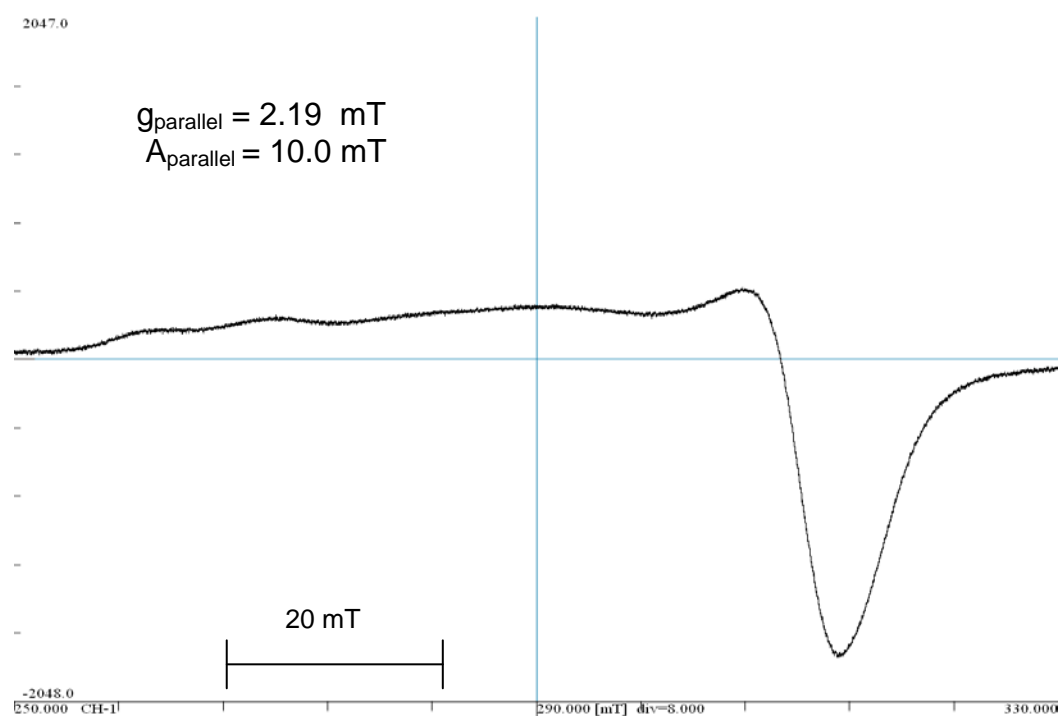


**Figure 3.20 (a):** ESR spectrum of copper chloride solution in acetonitrile at -150 °C.

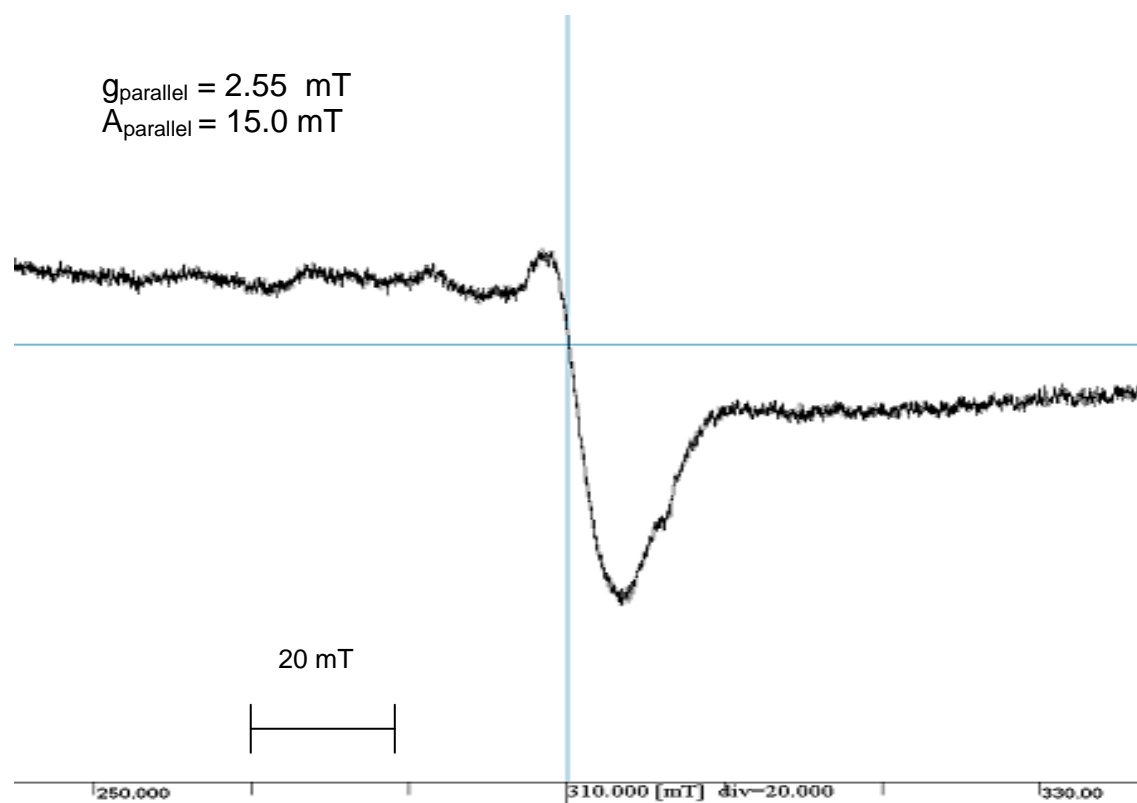


**Figure 3.20 (b):** ESR spectrum of copper chloride solution with 2,2-bipyridine solution in acetonitrile.

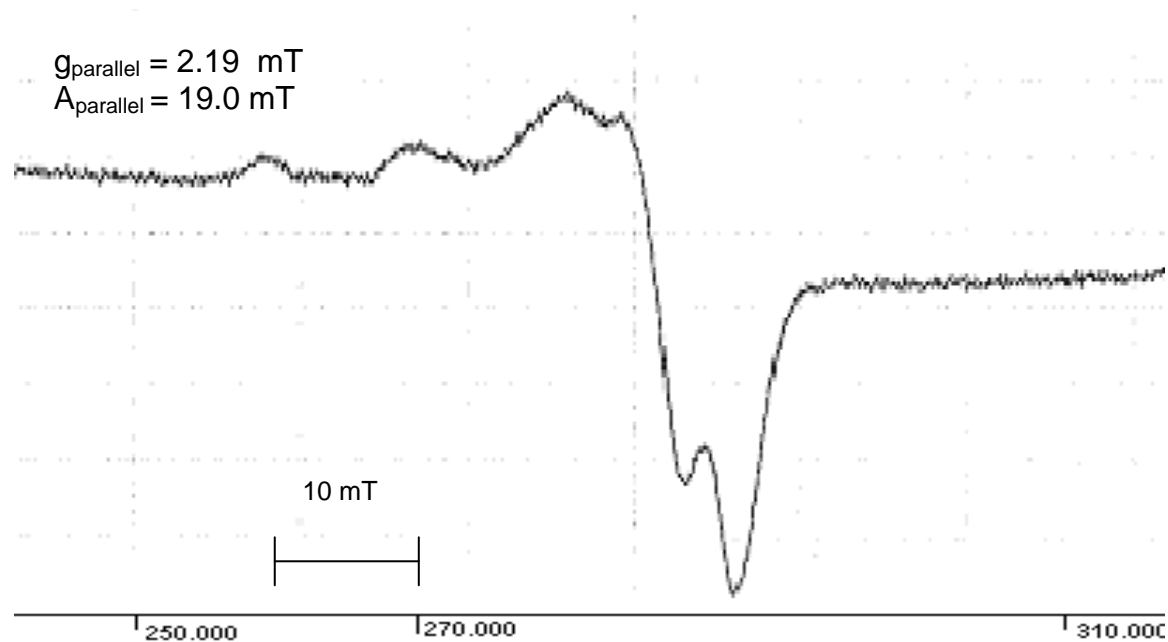


**Figure 3.20 (c):** ESR spectrum of copper chloride solution with aza-crown-4 solution in acetonitrile.

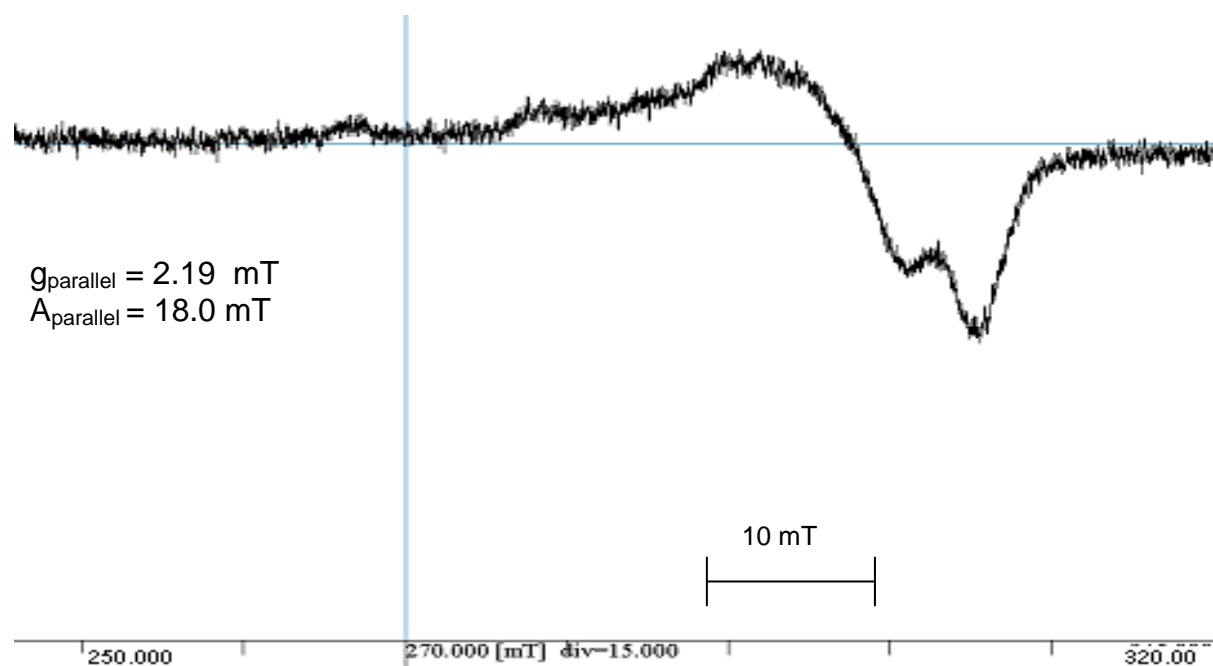


**Figure 3.20 (d):** ESR spectrum of copper chloride solution with ligand solution (bipy-aza-crown-4) when 0.5 copper ion equivalents were added in acetonitrile.

### 3.4 - Conclusion

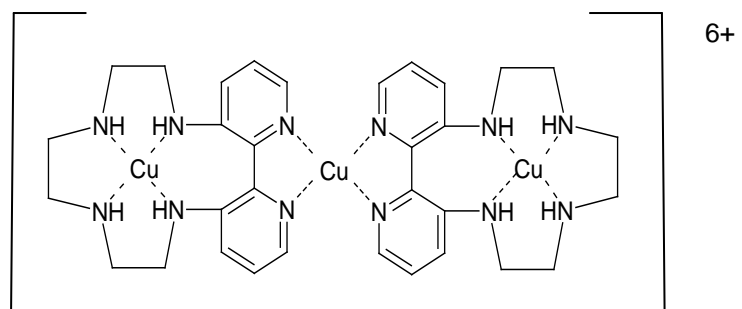
The main aim of this part of the research was to characterise the binding of copper(II) ion to bipy-aza-crown-4 ligand in acetonitrile and to compare the results with those obtained in methanol.

The ITC and spectroscopic results through addition of copper(II) ion into acetonitrile solution of bipy-aza-crown-4 ligand are in complete accord. They show that the first complex to form between  $\text{Cu}^{2+}$  ions and the ligand involves  $\text{Cu}^{2+}$  ion binding between two ligands via the bipyridine nitrogen coordination sites. After this,  $\text{Cu}^{2+}$  ions enter the aza-crown cavities to form, in the end, a  $\text{Cu}_3\text{L}_2^{6+}$  complex ion. Formally this has a 6+ charge but it is likely that  $\text{Cl}^-$  ions are also bound to the complex, reducing or negating the charge.

Parallel experiments with ESR measurements on frozen solutions taken during the titration suggest that the first site to be occupied by copper(II) ions is different, and is the site at the centre of the aza-crown group. Significantly, this is the same behaviour that is seen when  $\text{Cu}^{2+}$ /bipy-aza-crown-4 complexes are crystallised from methanol solution. The fact that different behaviour is seen using ESR (when the solutions are frozen) may be important in understanding which complexes are the most stable. It is possible that the freezing process prior to ESR measurements results in crystallisation of the complex. A tentative conclusion from this is that the thermodynamically favoured complex formed at low copper(II) ion concentration is different in the solid and solution state, in both methanol and in acetonitrile solution.

The overall conclusion is that the research has confirmed the stoichiometry of the most stable copper ion complex of bipy-aza-crown-4 ligand in acetonitrile solution is  $\text{Cu}_3\text{L}_2^{6+}$  corresponding to:

## Chapter 3.4 – Supramolecular Complexes – Conclusion



### 3.5 - References

1. Lehn, J.M, *Supramolecular Chemistry: Concepts and Perspectives*, VCH, Weinheim, **1995**.
2. Pedersen, C. J., *J. Am. Chem. Soc.*, **1967**, 89, 7017 - 7036.
3. Curry, J. D., and Busch, D. H., The Reactions of Coordinated Ligands. VII. Metal ion Control in the Synthesis of Chelate Compounds Containing Pentadentate and Sexadentate Macrocyclic Ligands, *J. Am. Chem. Soc.*, **1964**, 86,592 -594.
4. Steed, J. W., and Atwood, J. L., *Supramolecular Chemistry*, John Wiley and Sons, Chichester, **2000**.
5. Curtis, N. F., *J. Chem. Soc.*, **1964**, 2644-2650.
6. Jager, E. G., *Zeitschrift fur Chemie*, **1964**, 4, 437.
7. Curry, J. D., and Busch, D. H., The Reactions of Coordinated Ligands. VII. Metal ion Control in the Synthesis of Chelate Compounds Containing Pentadentate and Sexadentate Macrocyclic Ligands, *J. Am. Chem. Soc.*, **1964**, 86,592 -594.
8. Dietrich, B., Lehn, J. M., and Sauvage, J. P., Les Cryptates, *Tet. Lett.*, **1969**, 34, 2889 -2892.
9. Cram, D.J., *Angew. Chem. Int. Ed. Engl.*, **1986**, 25, 1039-1057.
10. Fischer, E., Einfluss der Configuration auf die Wirkung der Enzyme, *Berichte der Deutschen Chemischen Gesellschaft*, **1894**, 27, 2985 - 2993.
11. Rebek, J., Costello, T., and Wattley, R., Binding Forces and Catalysis. The Use of Bipyridyl-Metal Chelation to Enhance Reaction Rates, *J. Am. Chem. Soc.*, **1985**, 107, 7487-7493.
12. Rebek, J., Binding Forces, Equilibria, and Rates: New Models for Enzymic Catalysis, *Acc. Chem. Res.*, **1984**, 17, 258-264.
13. Rebek, J., Trend, J. E., Wattley, R. V., and Chakravorti, S., Allosteric Effects in Organic Chemistry - Site-Specific Binding, *J. Am. Chem. Soc.*, **1979**, 101, 4333-4337.
14. Koshland, D. E., Applications of a theory of enzyme specificity to protein synthesis, *Proc. Natl. Acad. Sci.*, **1958**, 44, 98 -104.

15. Pedersen, C. J., The Discovery of Crown Ethers (Noble Lecture), *Angew. Chem. Int. Ed. Engl.*, **1988**, 27, 1021 - 1027.
16. Gokel, G.W., Leevy, W.M., and Weber, M.E., *Chem. Rev*, **2004**, 104, 2723-2750.
17. Curtis, N. F., and Whimp, P. O., Some Cyclic Tetra-amines and their Metal ion Complexes. Part III. Complexes of Cobalt(III) with Hexamethyl-1,4,8,11-tetra-azacyclotetradecanes and Bidentate Ligands, *J. Chem. Soc. A*, **1966**, 867-871.
18. Whimp, P. O., and Curtis, N. F., Some Cyclic Tetra-amines and their Metal ion Complexes. Part II. Complexes of Cobalt(III) with two Isomeric Hexamethyl-1,4,8,11-tetra-azacyclotetradecanes and Monodentate Ligands, *J. Chem. Soc. A*, **1966**, 1827-1830.
19. Curtis, N. F., Some Cyclic Tetra-amines and their Metal ion Complexes. Part IV. Two Isomeric 5,7,7,12,12,14-Hexamethyl-1,4,8,11-tetra-azacyclotetradecanes, *J. Chem. Soc.*, **1967**, 1979-1980.
20. Whimp, P. O., and Curtis, N. F., Some Cyclic Tetra-amines and their Metal ion Complexes. Part V. Cobalt(III) Complexes of two Isomeric 5,7,7,12,12,14-Hexamethyl-1,4,8,11-tetra-azacyclotetradecanes, *J. Chem. Soc. A*, **1968**, 188-190.
21. Whimp, P. O., Curtis, N. F., and Bailey, M. F., Some Cyclic Tetra-amines and their Metal ion Complexes. Part VI. The Crystal Structure of Aceto-C-rac-(5,7,7,12,14,14-hexamethyl-1,4,8,11-tetra-azacyclotetradecane)nickel(II) Perchlorate, *J. Chem. Soc. A*, **1970**, 1956-1963.
22. Curtis, N. F and Reader, G. W., Some Cyclic Tetra-amines and their Metal ion Complexes. Part VII. Nickel(II) Complexes of some Tetra-aza-cyclotridecane Derivatives, *J. Chem. Soc. A*, **1971**, 1771-1777.
23. Jackels, S.C., Busch, D.H., Barefiel, E.K., Rose, N.J and Farmery, K, *Inorg. Chem*, **1972**, 11, 2893-2901.
24. Bazzicalupi, C., Bencini, A., Bianchi, A., Danesi, A., Giorgi, C., Lodeiro, C., Pina, F., Santarelli, S., and Valtancoli, B., A Zinc (II)-based receptor for ATP binding and hydrolysis, *Chem. Commun*, **2005**, 2630-2632.
25. Bazzicalupi, C., Bencini, A., Bianchi, A., Faggi, E., Giorgi, C., Matera, I., and Valtancoli, B., ATP recognition and sensing with a

- phenanthroline-containing polyammonium receptor, *Chem. Commun.* **2006**, 4087-4089.
26. Bazzicalupi, C., Bencini, A., Bianchi, A., Del Piero, S., Fornasari, P., Giorgi, C., Melchior, A., Portanova, R., Tolazzi, M. and Valtancoli, B., Co(II) and Cd(II) Complexation with two dipyridine-containing macrocyclic polyamines in water and dimethyl sulfoxide, *New. J. Chem.* **2005**, 29, 805-811.
27. Bazzicalupi, C., Bencini, A., Bianchi, A., Borsari, L., Danesi, A., Giorgi, C., Lodeiro, C., Mariani, P., Pina, F., Santarelli, S., Tamayo, A. and Valtancoli, B., Basicity and coordination properties of a new phenanthroline-based bis-macrocyclic receptor, *Dalton Trans.* **2006**, 4000-4010.
28. Bazzicalupi, C., Bencini, A., Bianchi, A., Danesi, A., Giorgi, C., Lorente, M. A. M., and Valtancoli, B., Inclusive coordination of F<sup>-</sup>, Cl<sup>-</sup> and Br<sup>-</sup> anions into macrobicyclic polyammonium receptors, *New. J. Chem.* **2006**, 30, 959-965.
29. Bazzicalupi, C., Bencini, A., Faggi, E., A. Garau, A., Giorgi, C., Lippolis, V., Perra, A., and Valtancoli, B., Encapsulation of metal cations and anions within the cavity of bis(1,4,7-triazacyclononane) receptors, *Dalton Trans.* **2006**, 1409-1418.
30. Felton, C., Synthesis and co-ordination chemistry of allosteric systems and sensors for zinc metal ions, Thesis, **2009**, University of Huddersfield.
31. Li, J.H., Wang, J.T., Hu, P., Zhang, L.Y., Chen, Z.N., Mao, Z.W., Ji, L.N., Synthesis, structure and nuclease activity of copper complexes of disubstituted 2,2-bipyridine ligands bearing ammonium groups, *Polyhedron* **27**, **2008**, 1898-1904.

# **Chapter 4 - Overall Conclusion**

The principle technique used in this thesis has been isothermal titration calorimetry (ITC). It has been used to characterise metal complexes with both biochemical and supramolecular systems.

We have used ITC to study the way  $Zn^{2+}$ ,  $Co^{2+}$  and  $Cd^{2+}$  metal ions bind to the enzyme apoBclI. Metal ions are known to be vital to the actions of this enzyme and the nature of metal binding has been studied by many techniques other than ITC. The results of the work in this thesis confirm that in general two metal ions can bind to the enzyme molecule. The interpretations of the results are consistent with the models for binding sites for these metal ions proposed by others. ITC has, however, revealed new information on the interactions between metal ions at the two binding sites, showing that, in the cases of zinc and cobalt ion, binding at the two sites is cooperative, meaning that binding occurs simultaneously at the two sites. With cadmium ion there are less obvious effects on the second binding sites when the first site is occupied. The two sites appear to react with metal ions quite separately, or in a non-cooperative manner. ITC has also shown that the metal binding process is entropy driven, at least in the case of zinc and cobalt ions. It has also provided information on how metal binding influences the  $pK_a$  of ionisable hydrogen ions on the amino acid residues involved in binding. Further work could usefully confirm some of the conclusions drawn on this aspect.

In the other part of the study, ITC has revealed new information on how copper ions bind to an example of a new class of chelating ligand in which there is more than one coordination site, bipy-aza-crown-4. This ligand has essentially two binding sites, both of which coordinate metal ions through nitrogen atoms. One site is at the centre of the aza-crown moiety and the other is based on bipyridine units on the ligand. The ITC work has been carried out in acetonitrile solvent and this fact alone is worthy of mention because virtually all reported ITC experiments to date have been carried with aqueous solutions.

The data we have collected in acetonitrile shows clearly that copper (II) ion, when added progressively to a solution of the ligand, binds first to the bipyridyl

site, bridging between two ligands. Only when these sites are fully occupied does it bind in the aza-crown site, so first forming a  $\text{CuL}_2^{2+}$  complex followed by a  $\text{Cu}_3\text{L}_2^{6+}$  complex. These assignments were supported by UV-Visible spectroscopic titrations using acetonitrile solution in which spectral end points coincided with the stoichiometries of these two complexes. ESR spectroscopy was also used to follow the nature of the  $\text{Cu}^{2+}$  environments in these  $\text{Cu}^{2+}$  titrations into ligand solution. Spectra were recorded on frozen solutions and the results suggested that the order in which  $\text{Cu}^{2+}$  enters the binding sites is different to that found through ITC and spectroscopic titrations. A possible explanation is that, in freezing the acetonitrile solution for ESR measurement, the complex ions crystallise out of the solution and the thermodynamically favoured complexes in the solid state are different to those in solution.

Indeed, this might be an explanation for why the apparent order in which the two ligand binding sites are occupied in methanol solution differs for that in acetonitrile solution. In the X-ray crystallographic studies performed on complex salts crystallised from methanol solution, evidence suggests that the aza crown ether site is the first occupied by the  $\text{Cu}^{2+}$  ions. But with the ESR studies, the result refers to *solid state complexes* rather than complex ions formation in solution. It may be the that, in the crystallised state the favoured coordination site is in the crown ether, whether crystallised from methanol or from acetonitrile, but in solution, a different site is favoured (in acetonitrile anyway).

Overall, this research has illustrated the usefulness of ITC in studying reactions in solutions, through applications to two rather different systems. The potential of the techniques, in areas much broader than the usual biochemical systems that have been the mainstay of ITC studies, has been revealed.

## **Future Work**

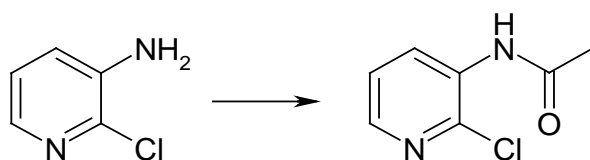
For Future work we could carry out more studies with BclI enzyme and with  $Zn^{2+}$ ,  $Co^{2+}$  and  $Cd^{2+}$  over the pH range to reduce the uncertainties in the data presented in this thesis. Also there are other enzymes for which there is uncertainty over the number of metal ions that are bound for which an ITC study might be informative.

For the supramolecular systems, as ITC has been one the first applications to be used to study metal ion complexes with synthesised ligands offering more than one binding site and in which an allosteric effect might be in operation, so with further developments of similar/type of complexes, ITC technique should be considered as a front-line technique in the study.

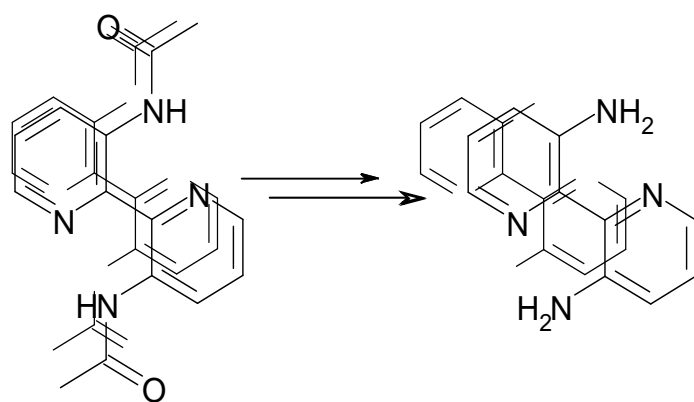
# Appendix

**Synthesis of bipy-aza-crown-4 ligand (extracted from ref 30)**

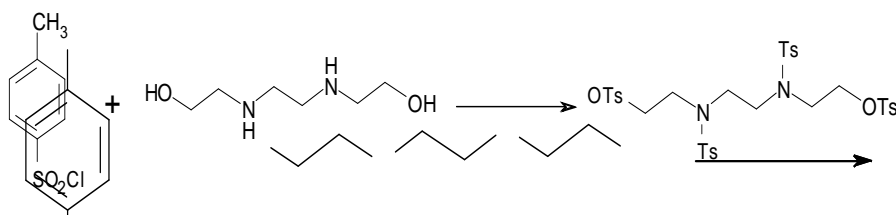
This is the detailed synthesis of bipy-aza-crown-4 taken verbatim from Cara Felton's thesis (graduated from University of Huddersfield 2009)

**3-Amino-2-chloropyridine**

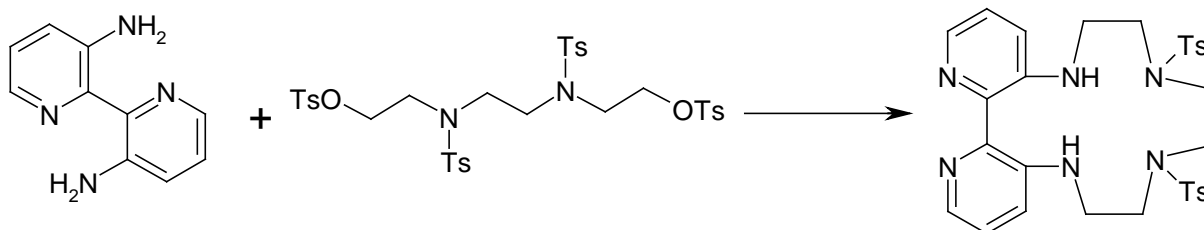
3-amino-2-chloropyridine (5 g, 0.039 mol) was dissolved in acetic anhydride under stirring, this was allowed to stir for 12 hours. The solvent was reduced by rotary evaporation, toluene added and the solvent removed again. The product was recrystallised from toluene giving a fine white crystalline powder (6.46 g, yield = 97 %). A  $^1\text{H}$  NMR was obtained and was identical to literature values.<sup>1</sup>



3,3'-Diacetylaminobipyridine (5.36 g, 0.0198 mmol) was suspended in concentrated hydrochloric acid (20 ml) and refluxed for 1 hour. Once the solution had cooled it was neutralised with concentrated ammonia solution, and the product extracted into DCM (4 x 100 ml). The solvent was removed at reduced pressure giving an iridescent yellow powder (1.85 g, yield = 50 %).  $^1\text{H}$  NMR [500 MHz,  $\text{CDCl}_3$ ] ( $\delta$ ); 8.0 (dd,  $J$  = 1.9, 3.9 Hz, 2H, -py), 7.0 (m, 4H, overlapping -py) 6.2 (s, 4H,  $-\text{NH}_2$ ).

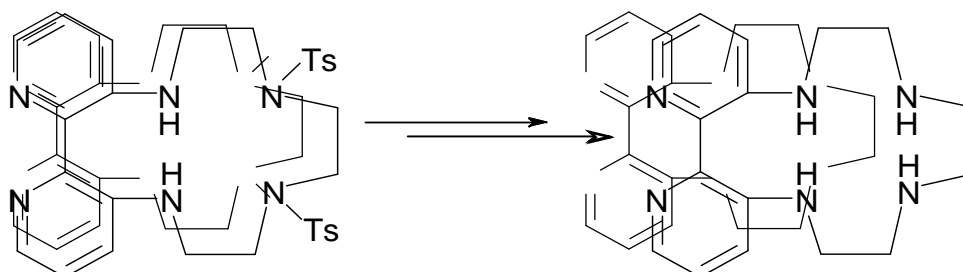


A solution of p-toluenesulfonylchloride (7.7 g, 0.04 mol) suspended in pyridine (20 ml) was added drop wise, over 2 hours to a vigorously stirred solution of N,N'-bis(2-hydroxy-ethyl) ethylene diamine (1.48 g, 0.01 mol) in pyridine (20 ml) at 0 °C. The solution was then stirred for 4 hours while the solution returned to room temperature. This was poured over ice (50 ml) and concentrated hydrochloric acid (50 ml) and chilled for 12 hours. The solution was decanted off leaving an oily yellow brown residue. The product was recrystallised from methanol giving the product as a yellow powder which was isolated by filtration (5.67 g, yield = 74 %). <sup>1</sup>H NMR [400 MHz, CDCl<sub>3</sub>], (δ); 7.8 (d, *J* = 8.3 Hz, 4H, -ph), 7.7 (d, *J* = 8.3 Hz, 8H, -ph), 7.4 (d, *J* = 8.16 Hz, 8H, -ph), 4.2 (t, *J* = 5.3 Hz, 4H, -NCH<sub>2</sub>CH<sub>2</sub>-), 3.4 (t, *J* = 4.6 Hz, 4H, -NCH<sub>2</sub>CH<sub>2</sub>O-), 3.3(s, 4H, -NCH<sub>2</sub>CH<sub>2</sub>N-), 2.5 (s, 12H, CH<sub>3</sub>).



To a solution of 3,3'-diamino-2,2'-diamine (0.5 g, 2.69 mmol) in dry THF (30 ml), at -78°C, n-butyl lithium (7.4 ml, 1.0 M solution in hexanes) was added slowly. Upon addition a yellow precipitate formed which was replaced by a red precipitate after more than half of the base was added. The reaction was allowed to warm to room temperature, after which the tetra-tosylate (2.06 g, 2.69 mmol) in THF (10 ml) was added and the resulting solution refluxed for 3 hours. The reaction was evaporated to dryness and purified by column chromatography (SiO<sub>2</sub>, 5% MeOH in DCM) giving the tosylated aza-crown as a yellow solid (0.14 g, yield = 8 %). <sup>1</sup>H NMR [400 MHz, CDCl<sub>3</sub>], (δ); 8.21 (2H, d, *J* = 4.5; pyridyl H), 7.62 (4H, d, *J* = 8.3; tsH), 7.33 (4H, d, *J* = 8.1; tsH), 7.25

(2H, dd,  $J = 7.3, 4.4$ ; pyridyl H), 7.10 (2H, d,  $J = 7.4$ ; pyridyl H), 4.76 (2H, t,  $J = 4.7$ ; pyridyl-NH), 3.8 – 2.8 (12H, m (overlapping);  $-\text{CH}_2-$ ), 2.47 (6H, s;  $-\text{CH}_3$ ).  
ESI-MS  $m/z$  607  $\text{M} + \text{H}^+$ .



The ditosylated aza crown (0.14 g, 0.23 mmol) was suspended in concentrated  $\text{H}_2\text{SO}_4$  and heated at  $100^\circ\text{C}$  for 48 hours, in a sealed vessel under an atmosphere of dinitrogen. The acidic solution was poured over ice and adjusted to 14 pH with NaOH. Extraction into DCM (4 x 100ml), followed by evaporation gave the bipyridine aza-crown as a pale yellow solid (0.031 g, yield = 45 %).

$^1\text{H}$  NMR [400 MHz,  $\text{CDCl}_3$ ], ( $\delta$ ); 8.00 (2H, t,  $J = 3$ ; pyridyl H), 7.09 (4H, d,  $J = 3$ ; pyridyl H), 4.78 (2H, t,  $J = 4.3$ ; pyridyl-NH), 3.40 (2H, m;  $-\text{CH}_2-$ ), 3.10 (2H, m;  $-\text{CH}_2-$ ), 2.70 (2H, m;  $-\text{CH}_2-$ ), 2.60 (2H, d,  $J = 9.4$ ;  $-\text{CH}_2-$ ), 2.5 (m, 2H;  $-\text{CH}_2-$ ), 2.3 (2H, d,  $J = 9.4$  Hz;  $-\text{CH}_2-$ ), terminal NH to broad to be observed. ESI-MS  $m/z$  299  $\text{M} + \text{H}^+$ .

## References

1: C.R. Rice, S. Onions, N. Vidal, J. D. Wallis, M.C. Senna, M. Pilkington and H. Stoeckli-Evans, *Eur. J. Inorg. Chem.* 2002, 1985.